Evolution of water reservoirs in the early solar system through their oxygen isotopic composition

Thesis

UNRESTRICTED

Carbon chemistry of giant impacts.

by

Jennifer Ileana Abbott

BSc. Hons. (St Andrews University) 1993

MSc. (The University of Leeds) 1995

A thesis submitted for the degree of

Doctor of Philosophy

September 1999

Planetary Sciences Research Institute

The Open University

ABSTRACT.

Impact diamonds were found in several impactites from the Ries crater, Germany including fallout and fallback (crater fill) suevites, a glass bomb, impact melt rock and shocked gneiss. These diamonds formed two distinct grain size populations: 50-300 μm apographitic, platy aggregates with surface ornamentation and etching that were observed using optical and scanning electron microscopy and 5-20 μm diamonds which displayed two different morphologies identified using transmission electron microscopy and selected area electron diffraction. These 5-20 μm grains comprised apographitic, platy grains with stacking faults, etching and graphite intergrowths together with elongate skeletal grains with preferred orientations to the individual crystallites. Thermal annealing of stacking faults and surface features was also detected.

Stepped combustion combined with static mass spectrometry to give carbon isotopic analysis of individual diamonds, graphite and acid-residues indicate that the primary carbon source is graphite. This graphite was found to be ^{13}C-depleted with respect to similar samples from the Popigai impact crater.

The admixture of presumably carbonate derived carbonaceous material is suggested to account for the ^{13}C-enriched $\delta^{13}C$ compositions encountered in whole-rock suevites known to include carbonate melts.

On the basis of morphology, mineralogical associations, diamond/graphite ratios and carbon isotopic compositions three possible formation mechanisms for impact diamonds are suggested: fast, high temperature conversion of graphite following the passage of the shock wave, a vapour phase condensation or growth within substrate minerals or an orientated stress field and the incomplete transformation of a mixture of amorphous and crystalline graphite. Further more exotic mechanisms such as intermediary carbyne phases cannot be discounted.

Impact diamonds, 1-5 μm in size, were also identified in suevite residues and a black matrix lithic breccia from the Gardnos impact crater, Norway. The carbon isotopic

compositions are in agreement with previous measurements of whole rock samples with a small ^{13}C-enriched component probably representing diamond.

ACKNOWLEDGEMENTS.

Firstly I would like to thank Colin Pillinger and Ian Gilmour for their supervision. Iain Gilmour for discussions and critical reviews of this thesis. In addition for managing to scrounge drinks off me at OU summer schools. I would also like to thank Rob Hough who contributed his time and effort reading through and commenting on this thesis.

Thanks go to PPARC for funding this research.

Grateful thanks to D. Stöffler, B. French and S. Vishnevsky who provided the samples without which this study could not have existed.

Thanks go to Judy Pillinger for sorting out various problems and necessary supplies.

Huge thanks go to Jenny Gibson and Michelle Higgins for training me to use the various carbon stable isotope mass spectrometers and especially teaching me how to deal with their occasional quirks. Thanks also to Ian Wright, Frachi and Sasha for fixing the various little quirks.

Grateful appreciation and thanks must be extended to Naomi Williams for all her help with the SEM, cathodoluminescence, TEM and dark room facilities, most especially in aligning a temperamental TEM. In addition to Gordon Imlach who must have been bemused by my grateful excitement at finding an operational dark room.

To my flatmates for the last two years Nicky Simpson and Julia Hadley thanks for putting up with me and all those late night discussions and panics. Thanks go to all the staff and regular habitués of the Cellar bar for not mentioning deadlines.

Most of all thanks to my parents for their constant support and encouragement over the last 28 years. I wont even make you read it. Thanks to my sister for providing wine and distracting nephews and Colin for catching the lobsters.

LIST OF CONTENTS.

LIST OF FIGURES.

CHAPTER 4.

CHAPTER 5.

LIST OF TABLES.

CHAPTER 5.

LIST OF EQUATIONS.

LIST OF ABBREVIATIONS.

$\delta^{13}C$	Standard delta notation.
HCl	Hydrochloric acid.
HF/HCl	Hydrofloric acid/Hydrochloric acid.
HNO_3	Nitric acid.
SEM	Scanning electron microscope.
TEM	Transmission electron microscope.
BFTEM	Brightfield transmission election microscope.
N-73	Nördlingen 1973 drill core.
NC	Samples from N-73.
OQS	Ötting quarry suevite.
OQGB	Ötting quarry glass bomb.
SBS	Seelbronn quarry suevite.
ITZ	Itzingen quarry granite.
AQG	Aumuhle quarry gneiss.
BB	Bunte Breccia.
G	Samples from Gardnos impact crater.
-P	Samples treated with perchloric acid.
-G	Graphite from sample.
-D	Diamond from sample.
IWU	Illinois Wesleyan University.

CHAPTER 1. INTRODUCTION AND BACKGROUND.

The processes and products of impact cratering through asteroid and cometary impacts have been extensively studied. Modern theories on impact cratering largely developed from work published by Shoemaker (1960, 1963) based on investigations of the Barringer Meteor crater, Arizona. Shoemaker was the first to link the geological structure of Meteor crater with cratering mechanics based on observations of the Teapot Ess nuclear explosion crater (Melosh, 1989).

Over 150 terrestrial craters have been identified to date and some of these have been extensively investigated including, Chicxulub (Hildebrand et al., 1991), Chesapeake Bay (Poag et al., 1994), Ries (Von Englehardt, 1995) and Popigai (Masaitis, 1994). Figure 1.1. shows the distribution of the known terrestrial impact craters.

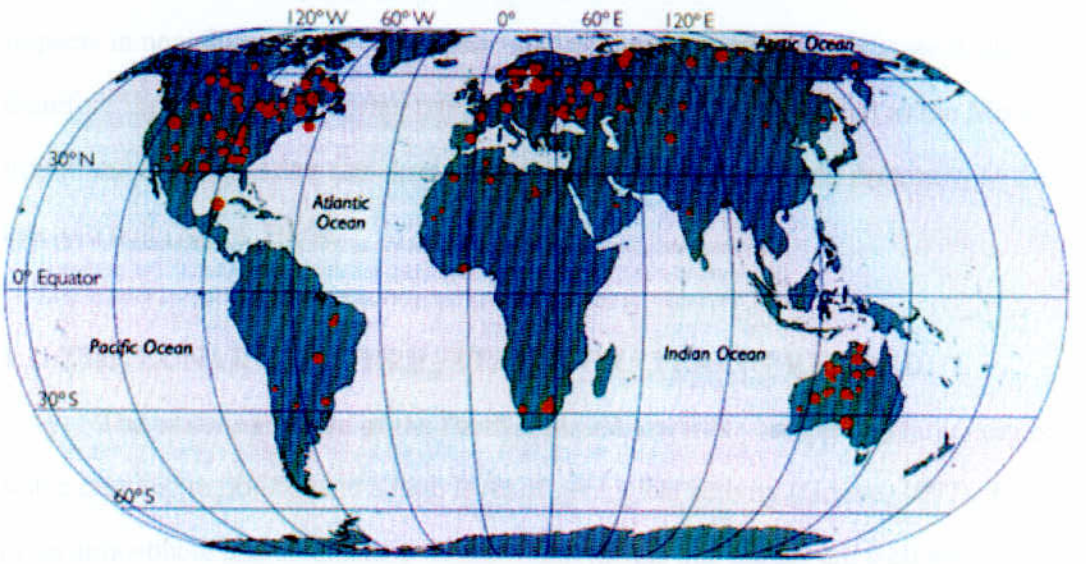

Figure 1.1. The location of known impact craters (1992 data). Illustrating bias towards North America and Australia. (Grieve and Pesonen, 1996).

The distribution is apparently concentrated in the northern hemisphere and Australia because these are regions of old stable cratons and the areas most systematically searched (Grieve and Pesonen, 1996).

Impact cratering has shaped the surface of rocky bodies in the Solar System, following the condensation of interstellar dust and planetary accretion. The surfaces of many of the planets and satellites have been extensively restructured by cratering, for example one hypothesis for the origin of the Earth and the Moon is that it was formed by the impact of a Mars-sized planetisimal with the proto-Earth, (Hartmann and Davies, 1975, Newson and Taylor, 1989). The crust on the far side of the Moon is thicker which may be related to the redistribution of crustal material by giant impacts (Jones, 1999). The high elevation of the southern hemisphere of Mars compared to the northern hemisphere has been attributed to redistribution of the crust as a result of the formation of the Hellas impact crater (Smith et al., 1999). Infalling material may have helped shape the terrestrial atmosphere by the dispersal and introduction of volatiles (Melosh, 1989). Studies of the cratering history of the Moon provide evidence of asteSoid and cometary impacts in near-Earth space back almost to the formation of the Solar system, and so therefore the terrestrial cratering rate. The proximity of a satellite such as the Moon is important as the cratering rate through the Solar System varies with proximity to the asteroid belt (Jones, 1999).

1.1. THE LUNAR AND TERRESTRIAL CRATERING RECORD.

The cratering record of the Earth is biased towards younger and larger craters on stable cratonic regions due to a high level of geological activity (Grieve, 1997). The lack of an atmosphere and weathering on the Moon means that craters are well preserved. Observations of the Moon have provided an almost complete record of the near-Earth impact history (McEwan et al., 1997). The lunar highlands are near-saturated with craters which have an average age of 3800-4300 Ma. This provides evidence for near Earth cratering from close to the formation of the solar system at 4500 to 3900 Ma, the

period of heavy bombardment and then up to the present day (Jones, 1999). Figure 1.2. illustrates the impact cratering rate for the Earth-Moon system; the peak in this cratering rate represent the period of late-heavy bombardment. The terrestrial cratering rate has been calculated as $5.6 \pm 2.8 \times 10^{-15}$ km^{-1} a^{-1} for structures over 20 km in diameter (Grieve, 1986).

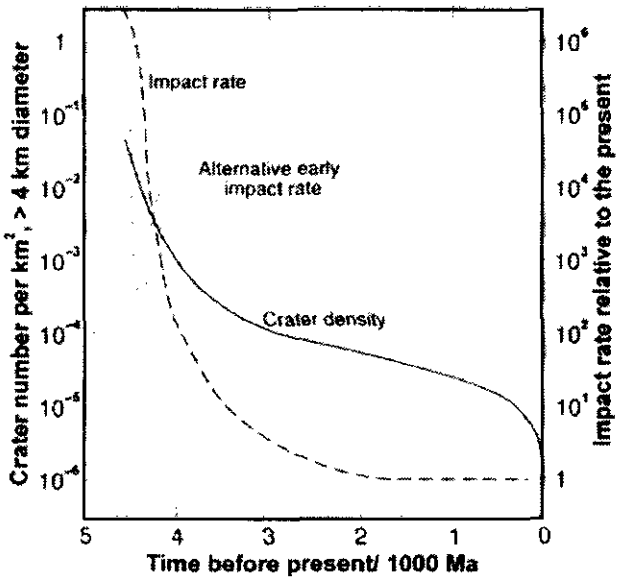

Figure 1.2. Cratering rates of the Earth-Moon system (Jones, 1999).

Impact craters have two main forms, simple and complex. Figure 1.3 shows the simple-complex transition for the Earth, Moon, Mars and Mercury. The transition between simple and complex craters has been observed to scale inversely with the gravitational acceleration of the planet (Melosh, 1989; Pike, 1988). Thus the transition occurs at 10 km on Mercury and between 2 to 4 km on the Earth when the gravitational pull of the planet results in collapse of the simple crater structure forming complex rings and domes (Melosh, 1989). Further data from the Mars Orbiter Laser Altimeter indicated that the transition occurs at 8 km ±0.5 km on Mars (Garvin and Frawley, 1998).

Simple craters are generally small in size and form bowl like depressions with little detailed structure. This type of crater is formed by high speed impact and typifies the craters found on the Moon and Mercury (Melosh, 1989).

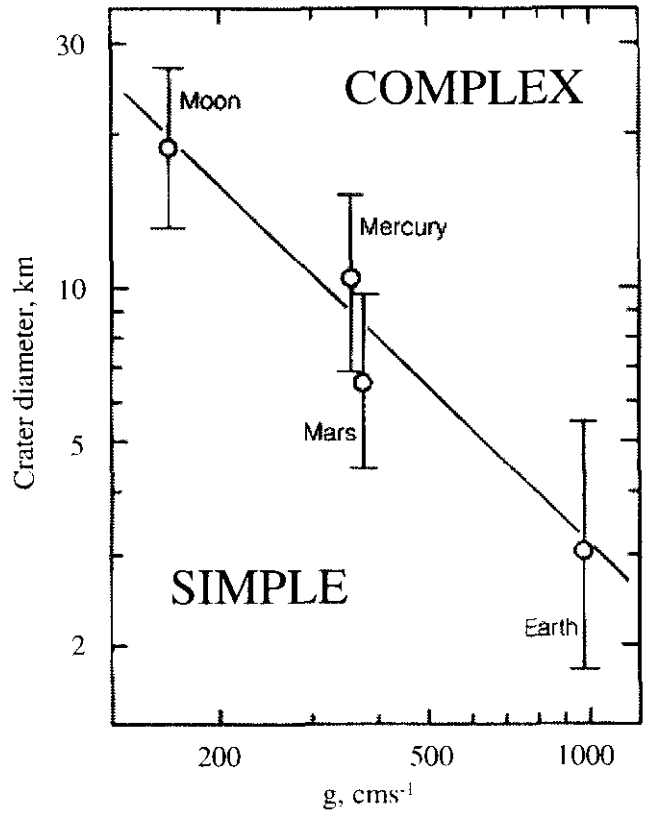

Figure 1.3. Crater diameter and gravitational acceleration (g) at the simple to complex transition on the Earth, Moon, Mercury and Mars (Melosh, 1989).

Possibly the best example of a simple terrestrial crater is the Barringer Meteor crater, Arizona, that was formed by the impact of a 3-4 x 10^6 t (45-50 m diameter) iron meteorite called Canon Diablo (Roddy and Shoemaker, 1995). Roddy and Shoemaker (1995) also suggest that the impactor originated from a collision in the main asteroid belt (0.5 by), fragmenting the Fe-Ni core of an asteroid which collided with the Earth 50,000±3000 yr ago.

Gravitational collapse produces more complex crater forms such as central uplifts, terraces and ring faults. These are illustrated by the lunar crater Theophilus a

102 km diameter crater which displays a series of terraces and central peaks up to 3 km in height, Melosh. (1989). Currently one of the largest known craters on the Earth is the Chicxulub crater which was identified using seismic exploration techniques (Hildebrand et al., 1991) and is associated with the KT boundary layers (Alvarez, 1980). Vredefort and Sudbury impact craters may be larger.

Much of the interpretation of the mechanics of cratering and crater forms has been based on astronomical observations of the Moon and other planets. Hydrocode modelling using computer simulations of impacts has been used to demonstrate the potential influences of different factors. Hydrocode simulations of Chicxulub (Pierazzo et al., 1998) have been used to model changes in the atmosphere, especially in CO_2, S and H_2O as a result of the impact and its effects on the target rocks.

1.2. ASTEROIDS AND COMETS.

The objects which create impact craters are asteroids and comets. The asteroids and comets which could impact the Earth are known as near Earth objects (NEOs), these are primarily short-term comets and asteroids. There are also less frequently encountered long-period comets. Over 400 NEOs have been identified (Lupishko and Dimartino, 1998).

Asteroids are primarily derived from the asteroid belt between Mars and Jupiter and the Edgeworth-Kuiper belt (EKB) and may emerge due to resonant phenomena (Morbidelli and Gladman, 1998). Collisional fragmentation of asteroids within the asteroid belt may also result in the ejection of material into unstable orbits and 10% of the short-period comets could be supplied by Trojan asteroid collisions (Marzari et al., 1997). Collisions within the EKB are sufficient to replenish the short term comets (Davis and Farinella, 1997).

Comets encompass the long-period comets with orbits greater than 200 years of which 1000 are known and over 180 short-period comets with orbits of less than 200 years (Jones, 1999). Long period comets appear at random and are uniformly

distributed (Weissman, 1997). The main source of short period comets is the Oort cloud where there are an estimated 10^{13} comets (Farinella and Davies, 1996). Many comets are passed from the Oort cloud by galactic perturbations through the planetary system and into Earth-crossing orbits (Napier and Clube, 1997; Valtonen et al., 1995). Comet showers may be triggered by perturbations of the Oort cloud by massive interstellar clouds (Stothers, 1998), the Solar Systems oscillation perpendicular to the galactic plane (Matese, 1995; Shoemaker, 1990) and the passage of Suns through the cloud (Weissman, 1996). From extraterrestrial ^{3}He found in pelagic limestones it has been suggested that a comet shower occurred over a 2.5 Ma period covering the formation of the Popigai (35.7 Ma) and Chesapeake Bay (35.5 Ma) impact craters (Farley et al., 1998). Periodicity in the impact cratering rate is a controversial subject with suggested increases in the cratering rate as a result of periodic variations in comet and asteroid ejection, from 30-500 Myr (Rampino, 1997; Rampino and Haggerty, 1996; Matese et al., 1995). Analysis of the known terrestrial cratering rate has not shown evidence of such events (Fernandez, 1992; Montanari, 1998).

The nature and size of the impactor, comet or asteroid has a great influence on the size of impact crater produced. Comets impact at much higher velocities than asteroids; the mean impact velocity of a long period comet is between 56-58 km s^{-1} (Weissman, 1997) whereas asteroids impact at between 17-20 km s^{-1} (Steel, 1998). The peak shock pressures generated by impactors of the same radius varies with composition in the order of iron > stony > ice (Kieffer and Simonds, 1980) as a result of density differences.

Geochemical evidence has indicated that the majority of impactors are chondritic especially in the case of large craters, suggesting a greater role for comets in large craters (Grieve and Pesonen, 1996).

1.3. EXPERIMENTAL CRATERING.

Experimentally generated craters such as those produced by nuclear explosions (Polansky and Ahrens, 1994), the NASA Ames vertical gun range (Shultz and Gault, 1982) and two-stage light gas gun (Taylor et al., 1997) have been used to calculate the pressures and temperatures produced by impacts, atmospheric effects and crater scaling relationships. These experiments operate on a variety of scales; light gas gun experiments produce small-scale craters (cm-scale) often to test materials such as samples of the LEO remote sensing platform (Taylor et al., 1997).

Shock recovery experiments have been used to calculate the pressures and temperatures required to produce the observed shock features found in quartz (Stöffler et al., 1975), quartz and feldspars (Huffman et al., 1993) and a variety of other materials (Stöffler, 1972). As well as the production of gases such as CO_2 (Martinez et al., 1995) and SO_2/SO_3 (Yang and Ahrens, 1998) from shocked rocks.

Experimental simulations of impacts have been used to determine the influence of the velocity and mass of the impactor (Giblin, 1998). Hypervelocity impact tests using simulated comet and asteroid material were performed at the Air Force Arnold Engineering Development Centre SI Range Facility, USA (Tedesci et al., 1995).

1.4. ATMOSPHERIC EFFECTS.

An asteroid of 1 km diameter has an average impact velocity of 20 km/s^{-1} with a kinetic energy (KE) of 4 x 10^{27} ergs (Jones and Kodis, 1982). A significant proportion of this energy would be deposited in the atmosphere, although the majority would be exchanged with target rocks (Jones and Kodis, 1982). Ahrens and O'Keefe (1987) investigated the interaction of a 10 km bolide with the atmosphere and calculated that 8% of its energy would exchange with the atmosphere during its passage. Following impact with the ground, vapour, melt and solid ejecta thrown from the crater would transfer an additional 40% of the energy to the atmosphere (Ahrens and O'Keefe, 1987). As the meteorite passes through the atmosphere it will punch a hole in the upper

atmosphere which is then filled with an upward inward flow field carrying vapour, melt and fragmented rock or dust (O'Keefe, 1982). This ionized gas cloud expands explosively behind a spreading curtain of ejecta forming a toroid which dissolves as it ascends (Schultz, 1982). Expansion of the vapour plume or fireball associated with the impact may result in widely distributed ejecta, for example the KT boundary clay forms a 3 cm thick globally distributed layer (Hildebrand, 1993).

Large impacts could result in the distribution of tektites and fine grained ejecta across a wide area by entrainment in the upper atmosphere. Calculations indicate that an impact the size of the KT event would only affect a column of atmosphere up to 50 km in radius and only 7% of the ejecta and vapour would escape from the upper atmosphere (Newman et al., 1999). A chondritic asteroid would need to be >250 m in diameter in order to produce a vapour plume capable of carrying material into the stratosphere (Kring et al., 1996).

Computer models of impacts have also been used to calculate the effects of vaporised target rocks on the composition of the atmosphere. Pierrazzo et al., (1998) calculate that an impact on the scale of Chicxulub would result in a maximum increase in atmospheric CO_2 of 40 % and that the most important component would be sulphur combined with water. Shock vaporisation experiments of anhydrite showed that an impact on the scale of the KT event would yield 0.5 to 2 $x10^{17}$g of SO_2 and SO_3 resulting in a model global cooling effect of 10°C (Yang and Ahrens, 1998).

1.5. SHOCK METAMORPHISM.

The shock waves produced by an impact, shock metamorphose the target rocks to varying degrees but are rapidly attenuated by distance (Simmonds et al., 1976). Shock metamorphism is the process whereby a series of irreversible changes occur in rocks and minerals subjected to pressures above their Hugoniot Elastic Limit (HEL) (Sharpton and Grieve, 1990). These include structural dislocations (kink bands, planar deformation features), shatter cones and high pressure mineral polymorphs. The type

and extent of these changes depends on the shock pressures experienced, as the degree of shock metamorphism increases with increasing pressure and temperature (P/T) conditions. The HEL represents the critical shock pressure at which a solid yields under the uniaxial strain of a plane shock wave (Stöffler, 1972), where the stress reaches a limiting value between plastic and brittle deformation. HELs vary considerably between different rock types and minerals, for example granodiorite at 4.5 Gpa (Borg, 1972), basalt at 5 Gpa (Nakazawa et al., 1997) whilst quartz may have a HEL in the range of 4.5-14.5 Gpa depending on the orientation of the crystal (Duvall and Graham, 1977).

Le Chateliers Principle states that when an external force is applied to an equilibrium system the system adjusts to minimise the effects of the force. One way in which this is accomplished is by the formation of high pressure mineral polymorphs. The formation of high pressure minerals results in a reduction in rock volume (Riedel and Karato, 1997) associated with the higher density and smaller crystal form of high pressure phases. For instance, the formation of diamond from graphite results in a 50% reduction in molar volume (Anthony, 1999) and the density of SiO_2 increases from 2.63 g/cm^3 to 2.93 g/cm^3 in coesite and 4.23 g/cm^3 in stishovite (Stöffler, 1972). Increased pressure conditions will eventually result in rock melt or vaporisation (Kieffer and Simonds, 1980; Rodonot, 1994).

The high pressure polymorphs of quartz, coesite and stishovite (Coes, 1953) have been used extensively as indicators of shock metamorphism (Melosh, 1989) and they are considered to be among the best-known indicators of shock in quartz-rich rocks (Gilmour, 1998). Coesite, which has been found around the rims of the Ries crater is formed at temperatures of 450 to 800 °C and pressures in excess of 38 kbar and stishovite at 130 kbar and >1200 °C (Deer et al., 1992). Table 1.1 summarises the shock indicator phases and associated conditions of formation.

Table 1.1. Summary of shock features and formation conditions. (After Graup, 1990).

Shock stage	Pressure (Gpa)	Post shock temperature (°C)	Shock effects	Occurrence (at the Ries crater)
V	>80	>3000	Vaporisation	-
IV	80-60	3000-1700	Complete melting of rocks	Suevite
III	60-45	1700-900	Selective fusion of quartz and feldspar glass, thermal decomposition of amphibole, pyroxene, biotite.	Suevite
II	45-35	900-300	Diaplectic glasses of quartz and feldspar. Coesite and stishovite. Deformation lamellae and kink bands.	Suevite Polymict breccia (Bunte Breccia)
I	35-10	300-100	Diaplectic crystals with planar deformation features. Planar elements and kink bands.	Suevite Polymict breccia (Bunte Breccia)
O	10-1	100-0	Fracturing of minerals. Kink bands, planar elements and shatter cones.	Suevite, Bunte Breccia, megablocks.

1.5.1. General shock effects.

The products of shock metamorphism (table 1.1) form a rough series through increasing pressure and temperature conditions. Shatter cones are a relatively low pressure feature which form conical structures generally orientated towards the centre of the crater and were first observed from the Kentland structure (Dietz, 1947; 1959). Kink bands are a common feature observed in layered minerals such as graphite, biotite and feldspars. They are most commonly reported from biotites, as the result of crystal gliding along the basal plane with external rotation of the crystal lattice (Stöffler, 1972).

Planar deformation features (PDFs) are formed with increasing shock pressures and may be observed in minerals such as quartz, micas and feldspars and were first described in quartz from the Clearwater Lake structure, Indiana, USA (McIntyre, 1962). PDFs are themselves an internal structure resulting from the shock transformation of the crystal lattice, forming sets of intersecting parallel lamellae. There are four different forms of PDF: (1) bands of dislocations, (2) lamellae with different proportions of amorphous silica, (3) brazil twin lamellae and (4) serrated ladder structure parallel

lamellae (Goltrant et al., 1992). Their formation may result from shock pressures between 15-35 Gpa (Martinez and Aginner, 1998). Goltrant et al., (1992) proposed a model where discontinuities are formed in certain structural planes by the movement of atoms towards energetically more favourable positions and predicted an increase in the density of PDFs with shock intensity. Theoretical calculations have shown that at pressures >10 Gpa the energy of the shock front is released by the nucleation of amorphous and increasingly compressible zones whose growth is driven by the propagating shock front (Goltrant et al., 1992).

Diaplectic glasses or maskelynite, i.e. glass that is formed in the solid state by shock induced melt, not melting due to temperature increases, are also used as shock indicators. Diaplectic glasses occur as shock induced solid state transformations in quartz, plagioclase and alkali-feldspars, as the reversion products of corresponding high pressure phases during pressure release (Stöffler, 1972). Under high pressures (>25 Gpa) PDF consist of superheated melt which forms diaplectic glass following quenching (Langenhorst, 1994).

High pressure mineral polymorphs have been described from a number of craters, for example the high pressure forms of quartz (i.e. coesite and stishovite) in rocks from the Ries crater (Chao, 1967), Vredefort (Martini, 1978) and Haughton (Martinez et al., 1993). The high pressure form of plagioclase (jadeite) forms at pressures >150 Gpa (Stöffler, 1972) and has been found at the Ries crater (James, 1969). Diamonds may be formed by the shock compression of carbon to high pressures and temperatures, yielding metastable diamond on quenching (Erskine and Nellis, 1991). This is discussed in greater detail in section 4.8.

1.6. CLASSIFICATION OF IMPACTITES (with particular reference to the Ries crater).

The nature and type of impactites (rocks affected by impact) which are formed by asteroid or comet impact vary according to the composition of the target rocks. The

target stratigraphy may be sedimentary, igneous, metamorphic or a combined sequence for example, sedimentary cover overlying an igneous and metamorphic basement such as the Ries (Hörz et al., 1983). Relatively dry metamorphic and crystalline basement rocks will tend to result in the formation of impact melt sheets and dikes, whilst targets composed of sedimentary rocks overlying a crystalline basement will tend to result in the formation of lithic impact breccias with glass associated with minor impact melt (Kieffer and Simmonds, 1980). The explosive expansion of vapour derived from hydrous minerals, devolatilised by high pressure and temperature conditions, and pore waters incorporated in sedimentary rocks, increases the dispersion and fragmentation of melt (Kieffer and Simmonds, 1980).

Impactites may be classified into two broad subheadings, proximal and distal with numerous sub-classifications. Figure 1.4 shows a suggested classification scheme for impactites with their location in relation to the crater (Stöffler and Grieve, 1996). Proximal deposits occur around the site of impact whereas distal deposits may occur globally, for example, the KT boundary clay or up to several 100 km from the site of impact. The Ries tektites, known as moldavites illustrate this and are found up to 400 km from the Ries crater (Bouska, 1994). There are a considerable number of different terms used in the literature to describe impactites many of which are local terminology; the suggested classification scheme was intended to simplify this terminology.

1.6.1. Proximal impactites.

Proximal impactites include cataclastic breccias, lithic impact breccias, and impact melt rocks. Cataclastic breccias are rocks which have been deformed by shearing, granulation and pervasive microfracturing by the movement of rocks relative to each other as a result of impact generated shock waves, post impact re-bound and ring faulting movements. The Nördlingen 1973 drill core in the Ries crater, Germany (Stöffler, 1977 and Chao, 1977) revealed cataclastic breccia dikes below the transient crater floor and within the fractured basement rocks (Stöffler et al., 1977).

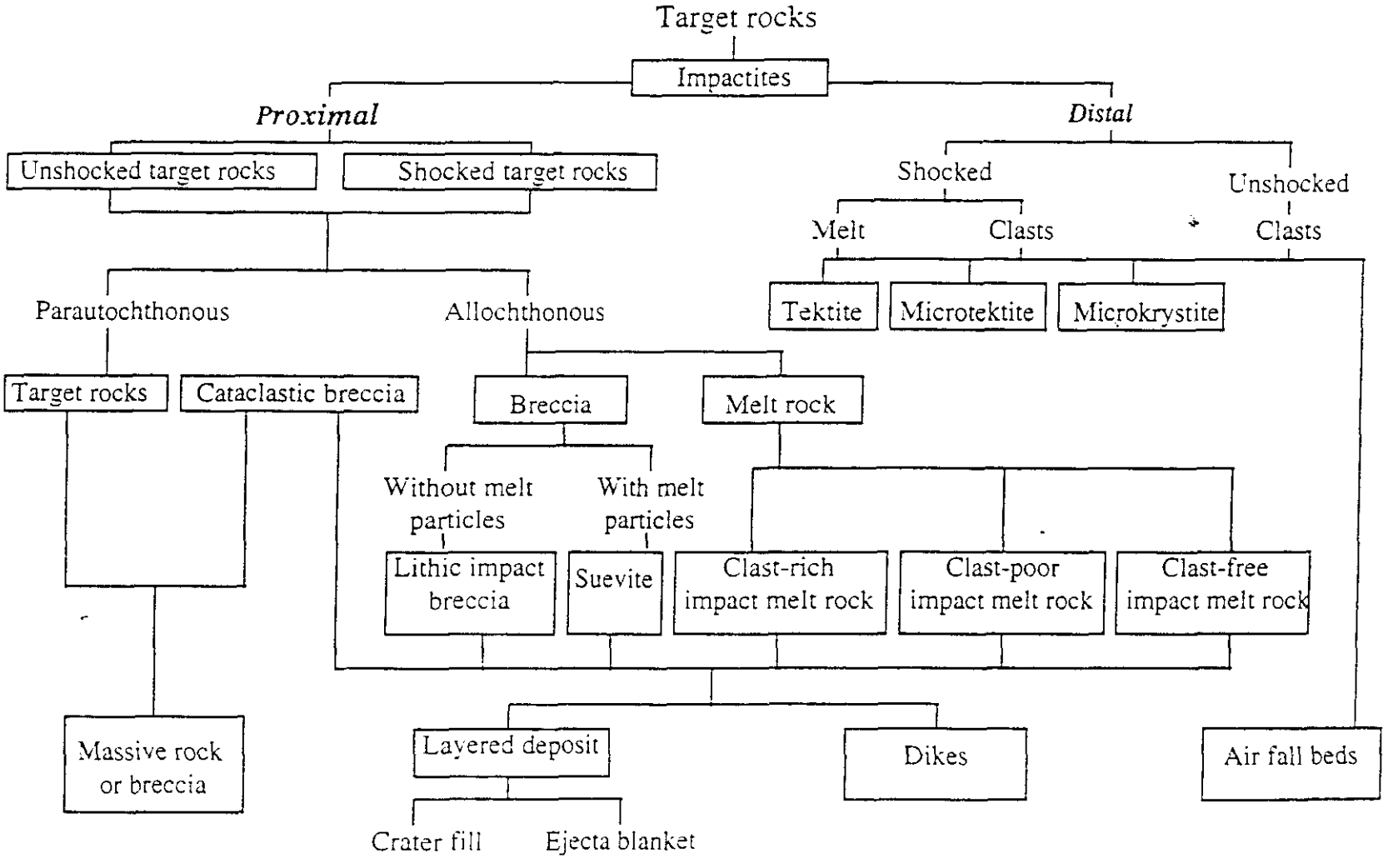

Figure 1.4. Classification of impactites from single impacts. From Stöffler and Grieve, (1996).

Similar structures were found in the 1992 drill core of the Kalkkop impact crater, Eastern Cape Province, South Africa which contains cataclastic breccias within the basement rocks (Reimold et al., 1998). As well as injection dikes of lithic impact breccias (Reimold et al., 1992).

Lithic impact breccias are breccias formed by the shock fragmentation of the target rocks but do not contain impact melt glass. An example is the Bunte Breccia from the Ries crater which is predominantly (90-95 vol%) composed of sedimentary rock fragments (Hörz et al., 1983) and was derived from the shallowest levels of the target stratigraphy (Stöffler, 1973). The lithology represents the main excavation and ejection stage during the crater formation as it comprises over 90 vol% of the total ejecta blanket (Hörz, 1982).

Suevite is a term local to the Ries crater that is used to describe a lithic impact breccia with glass. Suevites contain fragments of crystalline and sedimentary rock, variable percentages of aerodynamically formed glass bombs and fragments with a finely comminuted matrix of the same composition (Masaitis, 1994). In the case of the Ries, the rock is predominantly derived from basement rocks which underlie a thin sedimentary sequence (Hörz et al., 1983). The bulk composition of the suevite glasses is consistent with the proportions of crystalline rock clasts within the suevite, indicating that the glasses originated from the shock-fusion of a similarly composed basement (Von Englehardt, 1997). Lithic impact breccias are described from a number of other impact craters, for example Popigai (Masaitis, 1994; 1998), Ilyinets (Gurov et al., 1998), Chicxulub (Claeys et al., 1998) and Gardnos (Andersen and Burke, 1996). Lithic impact breccias may be deposited within the crater itself or form part of the ejecta blanket outside the crater structure.

Impact melt rocks may be subdivided into 3 sub-groupings on the basis of their clast content (Stöffler and Grieve, 1996). Impact melt rocks occur at the Popigai impact crater where they are termed tagamites and consist of a glassy or crystalline matrix with fragments of the target rocks and minerals (Masaitis, 1994). Large volumes of impact

melt may result in the formation of melt sheets or lenses, for example Lappajärvi (Kukkonen et al., 1992) and Sudbury (Grieve et al., 1991). Thick impact melt sheets and lenses tend to be found near the centre of impact craters although they may form discrete deposits within the ejecta blanket outside the crater cavity. Impact melt rocks from Polsingen quarry, Ries have been re-interpreted as high temperature suevites, abnormally rich in melt which recrystallized at higher temperatures than normal suevite (Von Englehardt and Graup, 1984).

All these impactites may occur as layered deposits within the crater, ejecta blanket or as dikes within the crater floor. Depending on the nature of the target stratigraphy they are all commonly polymict except in cases of single lithology targets (Stöffler and Grieve, 1996).

1.6.2. Distal impactites.

These represent the deposits which are found at some distance from the impact crater and may be subdivided into shocked melt and unshocked air fall deposits (fireball layers). Target material which has been vaporised by the impact event may be ejected to form tektites, microtektites and mikrokrystites.

Tektites are glass bodies, often with unusual forms and textures which are found in groups or strewn fields. These are defined on the basis of radiometric dating and geographical proximity (Bouska, 1994). Table 1.2. lists the principal tektite groups and fields, although there are considerable subdivisions within some of these groupings. For instance the Indochinite group includes Javanites, Philippinites, Thailandites, Billitonites and Malaysianites (Bouska, 1994).

Table 1.2. Principal tektite groups and localities.

Tektite group[1]	Location[1]	Associated crater	Age (Ma)[1]
Bediasites and Georgianites	North American Strewn Field - inc. Texas, Georgia, Cuba, Barbados, Caribbean Sea, Gulf of Mexico.	Chesapeake Bay[2]	35
Moldavites	Central European Strewn Field. S. Bohemia, S-W. Moravia.	Ries	14.7
Urengoites	Novyi Urengoi, W. Siberia.	Unknown	24
Irghizites	Zamanshin crater, N. Kazakhstan.	Zamanshin[3]	0.81 to 1.1
Ivory Coast Tektites, Ivorites	Ouelle region, Ivory Coast.	Botsumtwi[4]	1.1
Australasian Tektites	Australia and Tasmania.	Unknown	0.78
Indochinites	S-E. Asia.	Unknown	0.69
Libyan desert glass[5]	W. Desert, Egypt.	Aerial burst	29

[1]. Bouska, (1994). [2]. Poag et al. (1994). [3]. Bouska et al. (1981). [4]. Koeberl et al. (1994). [5]. Wasson and Moore, (1998).

Tektites have been the source of considerable debate with two main schools of thought, the lunar volcanic theory and the terrestrial impact theory. The lunar volcanic theory suggested that tektites are lunar volcanic glass ejected by volcanic activity (O'Keefe, 1976; 1985; 1994). This was modified with many of the textural and structural features of tektites and their association with impact events explained by volcanic ejection from small icy Moons such as Io, Callisto and Triton (Izokh, 1997).

This theory has now been largely discounted in favour of the terrestrial impact theory, where tektites are formed from impacts on Earth and represent melts of surficial, predominantly sedimentary rocks (Koeberl, 1994). The Ries moldavites have been attributed to melting and vaporisation of surficial sands by the approaching impactor on the basis of their geochemical compositions and melting experiments (Von Englehardt et al., 1987). Similar geochemical and isotopic evidence has been used to link the Chesapeake bay impact crater with the North American strewn field (Mchugh, 1998; Glass, 1998) and the Bosumtwi crater, Ghana with the Ivory Coast tektites (Taylor and Epstein, 1966; Koeberl et al., 1998). Libyan desert glass (LDGs) have a close

compositional relationship with mature sandstones from the Jurassic-Cretaceous Nubia group (Barrat et al., 1997) and may be the result of an aerial burst analogous to the Tunguska event (Wasson and Moore, 1998).

Microtektites are glassy bodies (<1mm in diameter) which occur within widely distributed layers often in deep sea sediments. Spherical, transparent and colourless microtektites with a similar composition to the North American microtektites are found in the Ocean Drilling Project (ODP) Hole 689B and represent distal ejecta from the Chesapeake Bay impact crater (Glass and Koeberl, 1999).

Microkrystites are sand-sized spherules of silicate melt which have been found associated with the KT boundary layer (Smit et al., 1992) and in a 2.54 Ga layer in the Hammersley Group, Western Australia (Simonson et al., 1998). Microkrystites are smaller than tektites/microtektites, do not show splash forms and may represent re-condensed material from the vapour cloud (Smit, 1992).

Microspherules, such as microtektites and microkrystites form widely dispersed distal deposits due to their small size which allows dispersion through the atmosphere and thus further afield from the source crater. They are commonly associated with shocked quartz and grains of spinel, e.g. in upper Eocene sediments from Massignano, Italy (Pierrard et al., 1998).

Distal deposits of diamond from the Popigai impact crater (yakutites) can be found over 400 km from the centre of the crater forming a strewn field of diamonds (Vishnevsky et al., 1997) similar to those formed by tektites.

Airfall beds are most notably described from the KT boundary (Alvarez et al., 1980). These globally distributed deposits are associated with high iridium concentrations (Alvarez et al., 1980; 1992), fragments of shocked quartz (Bohor et al., 1984), spinels (Alvarez et al., 1980) and diamond (Gilmour et al., 1992; Hough et al., 1995b). The KT boundary clay is also associated with a global soot layer from the combustion of biomass within impact generated wildfires (Wolbach et al., 1990a).

1.7. CARBON.

Carbon is unique in the number and complexity of compounds it is able to form, elemental carbon posesses 3 bonding states: sp^3, sp^2 and sp hybridisation (Kudryavtsev, 1999). Carbon can occur as (1) diamond (the sp^3 allotrope of carbon), (2) graphite (the sp^2 allotrope), (3) fullerenes (sp^2/sp^3 mixed), (4) carbynes (sp^2/sp^3 mixed and hybridized), (5) soot, (6) complex organic polymers, (7) hydrocarbons and (8) carbonate minerals. As well as carbide minerals such as silicon carbide (SiC). The crystalline structure of five of the allotropes of concern: diamond, londsdaleite, graphite, fullerenes and carbyne are illustrated in figure 1.5.

Diamonds can exist and be formed in a wide range of environments, such as meteorites, impact craters, gas-phase experimental reactions and from a wide range of carbon based source material (e.g. coal, carbynes, hydrocarbons and fullerenes). This has opened new fields of research and many questions concerning the actual formational constraints on diamond and other high-temperature or high-pressure carbon phases.

1.7.1. Diamonds in meteorites.

Diamonds were first found in ureilites such as the Novo Urei meteorite (Yerofeev and Lachinov, 1888) and Goalpara (Urey et al., 1957) as well as irons, such as Canyon Diablo (Foote, 1891), ALHA-77283 (Clarke et al., 1981) and Chuckwalla (Clarke et al., 1994). The diamond is often found in association with lonsdaleite (Hanneman, 1967; Clarke, 1994) and has been attributed to shock synthesis from graphite (Abee) or soot (Novo Urei) (Fisenko et al., 1995).

Presolar grains such as diamond and silicon carbide found in primitive meteorites are the carrier phases for anomalous noble gas signatures such as Xe-HL (Lewis et al., 1987). The formation of these grains has been attributed to shock synthesis from precursor carbon material by collisions of the parent meteorite

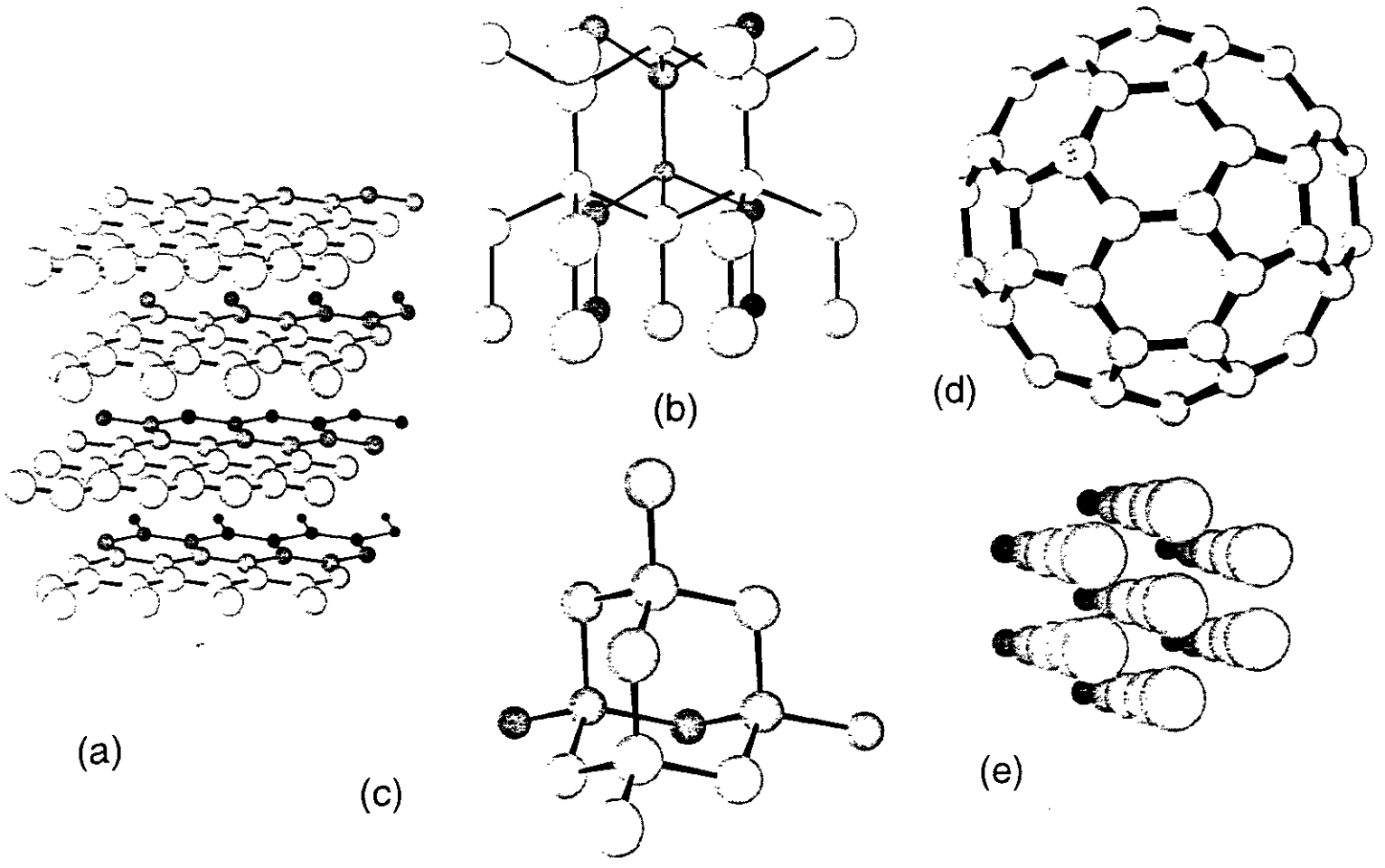

Figure 1.5. Schematic illustrations of the crystalline structure of the carbon polytypes: (a). Graphite, (b). Londsdaleite, (c). Diamond, (d). C_{60} fullerene and (e). Carbyne. Carbyne structure from Heiman, (1994).

throughout its history as well as relict presolar interstellar diamonds, which may be formed by gas-phase reactions. Comparison of microwave assisted chemical vapour deposition (MWCVD), hot filament assisted CVD (HFCVD) and shock-produced diamonds indicated that the most likely model for the formation of diamond found in ureilites was a vapour growth model (Matsuda et al., 1991; 1995).

1.7.2. Diamonds associated with impacts.

Diamonds were initially reported from the Popigai impact crater (Masaitis, 1972) and subsequently from the Ries crater (Rost et al., 1978), the KT boundary layer, (Carlisle and Braman, 1991; Gilmour et al., 1992) and a number of other European craters (Vishnevsky et al., 1997).

Diamonds in the Popigai impact crater, Siberia are found within shocked gneiss clasts in tagamites (impact melt rocks) and suevites (impact breccia with glass) (Masaitis, 1993). These diamonds display forms and characteristics suggestive of direct transformation from graphite by shock (Masaitis, 1993; 1995; Koeberl et al., 1997).

Diamonds containing lonsdaleite were reported from the Ötting and Bollstadt suevites of the Ries crater (Rost et al., 1978) as polycrystalline aggregates up to 300 μm in size. Many of the diamonds are polycrystalline aggregates showing characteristics indicative of the shock transformation of graphite similar to those from the Popigai impact crater. However, nanometre (< 6 nm) diameter diamonds in association with silicon carbide have also been reported from the Ries crater and are considered to be the result of a CVD-like formational process (Hough et al., 1995c).

The polytypes of diamond are analogous to the various polytypes of silicon carbide (SiC) and the two end-member polytypes, 3C (cubic diamond) and 2H (hexagonal lonsdaleite) are well known. A further intermediate polytype 6H has been identified in vapour deposited diamond powder, and further polytypes 4H, 8H, 15R (rhombohedral) and 21R are predicted (Spear et al., 1990). The structure of polytypes

4H, 6H, 8H, 10H, 15R and 21R have been calculated by replacing the silicon atom in SiC with carbon (Phelp et al., 1993).

Carbonado is a form of diamond which occurs as porous polycrystalline aggregates composed of single crystallites up to 250 μm in diameter. They are notably found in placer deposits in Carnot-Berberati and Ouadda-N'dele in the Central African Republic and Bahia, Brazil (Master, 1997), North Yakutia, Sayan and the North Russian platform (Kaminsky et al., 1978) and have clear crustal mineral associations (Smith and Dawson, 1985). Several theories for the formation of these aggregates have been suggested, including;

(1) impacts (Smith and Dawson, 1985) on the basis of their crustal $\delta^{13}C$ and $\delta^{14}N$ isotopic ratios (Shelkov et al., 1994; 1995),

(2) the effects of radiation on organic matter, a mechanism similar to that found to produce diamond in coal (Kaminsky et al., 1987; Ozima and Tatsumoto, 1997),

(3) high-pressure growth and sintering over a long period achieving thermal equilibrium boundary structures (Chen and Van Tendeloo, 1999)

(4) meteoritic, and formed through solar or presolar processes (Haggerty, 1996).

De et al., (1998) found a close genetic relationship between Brazilian and Central African carbonados proposing their formation within a united landmass during the late Archean. Carbonados from Brazil and Central Africa do not contain londsdaleite unlike impact diamonds but may have SiC inclusions (De et al., 1998).

1.7.3. Graphite associated with impacts.

Graphite commonly occurs in metamorphic rocks as well as carbonaceous and iron meteorites. Most natural graphite is a mixture of two different configurations, 2H hexagonal graphite and 3R rhombohedral graphite. Rhombohedral graphite may form up to 30% of the graphite structure as the individual crystals increase in size (Shi, 1996). Small-scale structural and compositional heterogeneities may be retained depending on the degree of crystallinity and maturity (Rietmeijer, 1991)

Natural graphite may be metamorphic graphite formed from regional or contact metamorphism of organic matter, or fluid-deposited graphite from carbon which has been mobilised by fluids and then reprecipitated (Luque et al., 1998). During prograde metamorphism, oxygen, hydrogen and nitrogen are released from organic matter and the residual carbon atoms become increasingly ordered (Grew, 1974; Itaya, 1981; Buseck and Huang, 1985). The nature of the precursor carbon, e.g. aromatic structures with hexagonal benzene ring structures, greatly affects the ease of graphitisation and degree of structural order attained (Buseck and Huang, 1985). Amorphous forms of carbon and carbon black are now seen to be poorly crystalline forms of graphite rather than another carbon allotrope (Kudryavstev, 1999). Anthracite and bituminous coals have been converted to graphite using simple shear at temperatures up to 900 °C and pressures of 1 Gpa indicating that strain energy provides the majority of the activation energy required for graphitisation (Bustin et al., 1995).

Graphite has been found to show low-level shock features common to other layered minerals such as biotite, for example kink bands (Stöffler, 1972). These shock structures may become preserved in impact diamonds subsequently formed by direct shock transformation (Valter, 1986).

Crystalline and poorly crystalline graphite is believed to be the main carbon source for impact diamonds found at the Popigai crater (Koeberl et al., 1997). Graphite occurs within Archean crystalline basement rocks which form part of the target area. Many of the impact diamonds recovered show inherited hexagonal platy graphitic structures (Koeberl et al., 1997).

1.7.4. Fullerenes and soot associated with impacts.

Fullerene (C_{60}) is a complex carbon molecule with the form of a truncated isohedron, which was discovered from experiments involving the laser vaporisation of graphite (Kroto et al., 1985). Pure C_{70} crystallises in cubic close-packing (c.c.p) and hexagonal close-packing (h.c.p) structures which form a series of phase transitions

corresponding to different degrees of molecular structural disorder (Van Tendeloo et al., 1993) with h.c.p and c.c.p domains separated by stacking faults (Blanc et al., 1996). These structures form a homogenous solid state polymerisation phase transformation with increased temperature (Marques et al., 1996). Kroto et al., (1985) postulated that the stability of the molecule meant that it could be a major constituent of circumstellar shells and interstellar dust. Since then fullerenes have been found in a variety of terrestrial environments.

Fullerenes have been reported in the carbon-rich mineral shungite (Buseck et al., 1992), fulgurite (Daly et al., 1993), the KT boundary layers (Heymann et al., 1994; 1996; 1998), the carbon-rich layer in the Sudbury impact crater (Becker et al., 1994) and the Permo-Triassic boundary sections (Chijiwa et al., 1999). Fullerenes and fulleranes have also been detected in meteorites such as Allende where they are considered to be the products of gas-phase reactions (Becker et al., 1994; Becker and Bunch, 1997). Fullerenes have been detected in a tiny impact crater on the Long Duration Exposure Facility (LDEF) and may have originated from a chondritic impactor or have been produced in situ by the impact (Di Brozolo et al., 1994).

There is still some controversy regarding the formation or origin of fullerene at impact sites and its relationship with the other carbon allotropes such as diamond, carbyne (chaoite) and graphite. However, a number of arguments have been proposed which include wildfires (Wolbach et al., 1990a) and the pyrolysis of meteoritic organic matter and synthesis in the impactor with the fullerene surviving the impact event (Gilmour, 1999). Kroto, (1991) showed that fullerenes can form from the incomplete combustion of organic material (trees and plants) containing unsaturated hydrocarbons. Fullerenes are synthesized experimentally by the laser vaporisation of carbon (Kroto et al., 1985; Taylor et al., 1990) and can be transformed to diamond by shock compression and rapid quenching (Sekine, 1992; Hirai et al., 1995).

Soot, 100-300 Å spherical carbon particles attached in necklace like chains (Harris and Weiner, 1985), has been reported from at least 13 KT boundary layer sites

and is used as evidence for widespread forest fires (Gilmour et al., 1989) and may be formed from the incomplete combustion of organic matter in a mechanism similar to that of C_{60} (Kroto, 1991). The carbon isotopic composition ($\delta^{13}C$ -25.8 ‰) indicates the main carbon source was terrestrial vegetation (Wolbach et al., 1990b). Soot is another form of carbon which can be experimentally transformed into diamond under conditions of high pressure (Donnet et al., 1997).

1.7.5. Carbynes associated with impacts.

The carbyne chaoite, a high temperature chain-structure polymorph of carbon, was found within graphite in fragments of shocked basement gneisses from the Ries crater (El Goresby and Donnay, 1968). Chaoite has different mineralogical characteristics to graphite and was considered to be a product of the shock transformation of graphite via a similar mechanism to diamond (El Goresby and Donnay, 1968). Carbynes are triply bonded chain allotropes of carbon stable between 2600 K and 3800 K (Whittaker, 1978).

Carbynes were subsequently found in graphite in meteorites, for example diamond-graphite aggregates in ureilites (Vdovsykin, 1972), within complex impact diamond grains containing lonsdaleite and disordered graphite from the Popigai impact crater (Vishnevsky and Palchik, 1975) and the Allende meteorite (Hayatsu et al., 1980). They are also found in terrestrial graphite from Sri Lanka and California (Whittaker, 1979) and marble from the Santa Rosa mountains, USA (Whittaker and Kintner, 1985). Although Rietmeijer (1991) reanalysed graphite from Sri Lanka and determined that the carbyne domains represented distorted pre-graphitic C-(H, O, N) material.

It has been suggested that chaoite and other carbynes may form an intermediary stage in the transformation of graphite to diamond (Whittaker, 1978; Heimann, 1994). Whittaker, (1979) proposed that the Ries chaoite may pre-date the impact, occurring naturally in graphite within the basement gneisses, although it should have been transformed to diamond. Graphite may be shock compressed to a carbyne form which

then collapses back into the diamond structure after the passage of the shock front (Heimann, 1994). Borodina et al., (1996) produced nanocrystalline cubic diamond from the shock loading of amorphous carbyne films. Further experimental evidence has indicated that shock pressures of <5 Gpa with no thermal activation can transform carbyne to diamond through the cross-linking of periodically arranged sp-hybridized short chains (Heimann, 1999).

1.8. IMPACT DIAMOND OCCURRENCES AND CHARACTERISTICS.

Diamonds have been identified and described from several impact structures to date including Popigai (Masaitis et al., 1972), Ries (Rost et al., 1978), Kara (Koeberl et al., 1990), Puchezh-Katunki (Marakushev et al., 1993), Zapadnaya (Masaitis, 1993), Ilyinets and Obolon (Gurov et al., 1995), and the K-T boundary layer (Carlisle and Braman, 1991; Gilmour et al., 1991).

Some characterisation of impact diamonds has been made; Vishnevsky et al. (1997) published a comprehensive review of impact diamonds which provides access to Russian data. Table 1.3 summarises the current data available for diamonds from the published literature.

The structural features of impact diamonds together with mineral associations indicates that there are a wide range of possible sub-classifications including paramorphs of graphite or coal formed by direct transformation, skeletal aggregates formed by etching or a restricted carbon feedstock, nano-diamonds formed by shock, explosion, vapour condensation or homogenous nucleation.

From table 1.3 a number of comparisons can be made, primarily the association of cubic diamond with lonsdaleite (which is the high pressure hexagonal polymorph of diamond that can be identified using single grain x-ray analysis). The impact diamonds themselves are commonly small (1-500 μm), porous, microcrystalline aggregates of

<6 nm-1μm crystallites. These are often coloured as a result of numerous inclusions, such as graphite (black) and nitrogen (yellow) (Valter et al., 1992) and apographitic with the preservation of the original graphite morphology (Masaitis, 1994).

Table 1.3. Summary of the characteristics of impact diamonds.

Crater	Lithology	Size/colour	Morphology	$\delta^{13}C$ (‰)	% Londs	Comments
Ries [1,2,3]	Suevite	2-300 μm grey aggregates	Large plates and skeletal aggregates with SiC	-16 to -22	yes	Intergrowths of SiC and diamond
Ries [4,5]	Glass	50-300 μm yellowish aggregates	Plates, scales, etched	-26 to -16	yes	-
Popigai [6,7,8]	Suevite	-	Aggregates, apographitic	-12 to -18 -10 to -17	5-60	Include CO_2
Popigai [9,10, 11]	Gneisses	0.1-1.5 mm yellow/grey aggregates	Aggregates	-12 to -17	5-60	-
Kara [12]	-	red/orange	Preferential orientation	-23 to -24	low	Coal as carbon source
Zapadnaya, Obolon, Illyinets [12]	Suevite	0.4-0.5 mm colourless-yellow/ black	-	-	5-10 and 40-50	-
Sudbury [13]	Onaping formation	100nm-1μm crystallites in aggregates	Friable, aggregates. corroded	-	<30%	–
Lappajärvi [13;14]	Suevite	100nm-1μm crystallites in aggregates	Tabular, aggregates	-	<30%	Primary graphite twins, strong corrosion
Tunguska [15]	Peat	15 μm	Anhedral	-25	-	$\delta^{15}N$=0 ‰
KT [16,17]	Fireball layer	6 nm-30 μm	Near cubic	-11 to -19	-	-

[1]. Hough et al. (1995a), [2]. Hough et al. (1995c), [3]. Rost et al. (1978), [4]. Abbott et al. (1996; 1998a; 1998b), [5]. Siebenschock et al. (1998). Schmitt et al. (1999). [6]. Koeberl et al. (1997), [7]. Grieve, (1994), [8]. Masaitis and Shrafranovsky, (1994), [9]. Vishnevsky et al. (1995), [10]. Shelkov et al. (1998). [11]. Masaitis et al., (1998). [12]. Ezersky, 1982; Gurov et al. (1995) [13]. Langenhorst et al. (1998). [14]. Langenhorst et al. (1999). [15]. Hough et al.,(1995d), [16]. Hough et al. (1995b; 1997). [17]. Gilmour et al. (1992).

Figure 1.6 illustrates the range in the carbon isotopic composition of these diamonds, the main feature is the wide range of values obtained.

The isotopic composition of the diamonds vary within and between localities depending on the nature of the precursor carbon, e.g. diamonds from both Kara and

Tunguska are isotopically lighter than those from the KT fireball layer as the carbon sources are different. The diamonds from Kara have been ascribed an origin from coal in the basement rocks vaporised by the impact (Ezersky, 1982; 1986). The source of carbon in Tunguska was not directly identified, although poorly crystalline

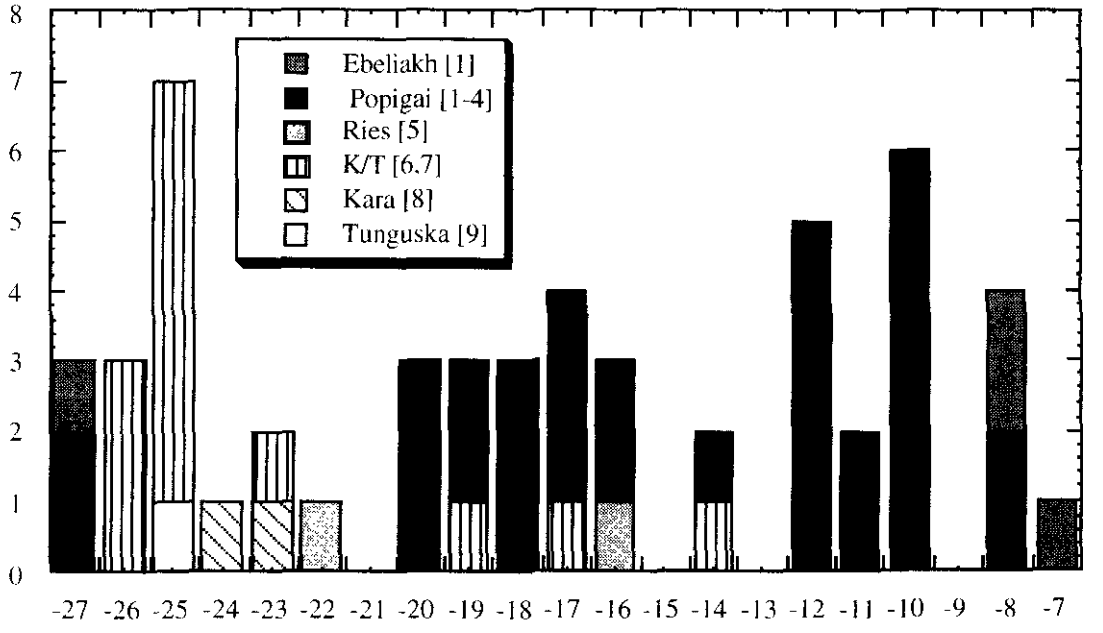

Figure 1.6. Summary of impact diamond $\delta^{13}C$ compositions.

[1]. Shelkov (1997) [2]. Koeberl et al. (1997) [3]. Grieve (1994) [4]. Masaitis and Shrafranovsky, (1994) [5]. Hough et al. (1995c) [6]. Hough et al. (1997) [7]. Gilmour et al. (1992) [8]. Vishnevsky et al., (1995) [9]. Hough et al. (1995d)

graphite or amorphous carbon is the most likely source (R. Hough, Pers. Comm.). Nano-diamonds (< 6 nm) from the KT fireball layer may be derived from graphite known to exist in samples of the Chicxulub drill core (V. L. Sharpton (1997), Pers. Comm.), with a possible contribution from end-member mixing with carbonates which form a significant proportion of the Chicxulub target stratigraphy (Sharpton et al., 1996). The Ries diamonds are similarly suggested to be the result of mixing between carbonate rock and basement graphite material (Hough et al., 1995c).

Diamonds from the Popigai crater have apographitic morphologies with inherited graphite twinning (Masaitis, 1995; Koeberl, 1997) and are perhaps the best examples of direct graphite-diamond transformation. It has however, been suggested

that carbynes may form an intermediary phase during this transformation (Whittaker, 1967; Heimann, 1998). Alternatively the variation may indicate the heterogeneous nature of the source material,. Note that the carbon stable isotopic composition of metamorphic graphite is highly heterogeneous in composition. Graphite is formed from the progressive metamorphism of organic matter and thus initially inherits its stable isotopic composition. During prograde metamorphism the degree of crystalline maturity in the graphite increases and is associated with a carbon fractionation of around 3‰ (Scheele and Hoefs, 1992) due to isotopic equilibrium with carbonate minerals during metamorphism (Arneth et al., 1985). Further graphite heterogeneity may be the result of changes in fluid compositions (Duke and Rumble, 1983).

Clearly characterisation of the carbon isotopic composition of potential local source lithologies and the shocked fragments incorporated in the suevite host rock is required in order to attempt to constrain both the source lithologies and formational mechanisms.

1.9. STABLE CARBON ISOTOPES.

Stable carbon isotope ratios are used extensively to characterise and constrain carbon sources and to some extent formational processes.

The stable isotopic ratio of carbon, ^{12}C (98.89%) and ^{13}C (1.11%) is determined by measuring the ratio of $^{13}C/^{12}C$. Results are presented using the standard delta notation (δ) as,

Equation 1.1 $$\delta\,^{13}C = \left(\frac{(^{13}C/^{12}C)\text{sample} - (^{13}C/^{12}C)\text{ standard}}{^{13}C/^{12}C\text{ standard}} \right) \times 10^{3}\ ‰$$

Standard normalisation is commonly to the Pee Dee Belemite (PDB) standard, with laboratory standards normalised against this. Thus a sample with $\delta^{13}C = -17‰$ is depleted in ^{13}C by 1.7% relative to the PDB standard.

For the stable isotopes, such as $^{13}C^{12}C$, $^{18}O^{16}O$ their chemical properties are determined by their atomic number, thus isotopic ratio differences and variations are due to mass differences and so vibrational energy of the atoms. This is especially important in the light elements where the ratio of the mass differences are higher and thus variations in the isotopes more likely to be apparent (table 1.4).

Table 1.4. Mass differences for light stable isotopes.

Isotopes	Mass difference
$^{1}H/^{2}H$	1/2
$^{12}C/^{13}C$	1/12
$^{14}N/^{15}N$	1/14
$^{16}O/^{18}O$	2/16

Fractionation is caused by any process inducing the isotopic ratios in different phases or regions to differ. These processes include equilibrium fractionation, non-equilibrium chemical processes and physical processes.

For equilibrium fractionation, the fractionation factor (α) can be calculated theoretically, however due to uncertainty in much of the thermodynamic data, this is generally impractical and the values are determined experimentally, or by calculations based on natural systems which are assumed to be in equilibrium. The size of the fractionation factor (α) at specific pressure and temperature conditions (P/T) determines the degree of fractionation possible in a given process or reaction. Although the effects of pressure (β factor - reduced isotopic partition function) on equilibrium isotopic fractionation is small, it does produce isotopic shifts at high pressure and theoretically graphite will be enriched in ^{13}C compared to diamond under equivalent P/T conditions (Polyakov and Kharlashina, 1994).

Non-equilibrium chemical processes are commonly kinetically driven, when an equilibrium is not maintained. The strength of bonds in compounds will vary due to molecular vibrations; for example, the ^{12}C-O bond is weaker than the ^{13}C-O bond due to

the higher energy of the lighter isotope, therefore in kinetic processes ^{12}C will be fractionated from ^{13}C which will be concentrated in the residue. Thus, chemical processes such as biological activity can fractionate ^{12}C from ^{13}C, for example organic matter is usually depleted in ^{13}C with negative delta values, relative to the dissolved carbonate (mainly HCO^{3-}) in the oceans which has a $\delta^{13}C$ value of ~ 0‰. Photosynthesis concentrates ^{12}C in organic matter and depending on the biological pathway employed, organic carbon is in general depleted in ^{13}C compared to oxidised carbon or carbonates. The observed isotopic heterogeneity of graphite has been attributed to changes in fluid compositions with time (Duke and Rumble, 1983), heterogeneity in the original precursor carbon (with isotopic equilibrium being achieved alongside crystalline maturity) (Buseck and Huang, 1985), or variable crystalline maturity and isotopic equilibrium with metamorphic decarbonation of carbonate minerals (Arneth et al., 1985). It has been observed that the values of $\delta^{13}C$ in associated schists and marbles in the Panamint Mountains, California, was controlled by the relative proportions of calcite and graphite (Bergfeld et al., 1996).

Physical processes such as vapour-liquid fractionation will depend on the difference in vapour pressure between the lighter and heavier isotopes. Incomplete rapid evaporation or volatilisation may enrich the vapour in ^{12}C leaving a ^{13}C-rich residue. Detailed mineralogical studies of shocked carbonate bearing impactites from the Haughton crater, Canada indicated that decarbonation outgassing of CO_2 occurred in the centre of the crater and a significant proportion of this back-reacted with reactive residual oxides (CaO and MgO) to provide an associated carbon fractionation (Martinez et al., 1994). Shocked calcite at the Ries is believed to have formed under both reducing and oxidised conditions from CO_2, O_2 and Ca within a vapour plume (Miura, 1995).

1.10. SUGGESTED FORMATION MECHANISMS.

A number of mechanisms have been proposed for the formation of the diamond associated with impact processes. The initial mechanism which satisfies a lot of the

textural and structural evidence from impact diamond samples is a mechanism of direct transformation (Masaitis, 1995). Subsequently a CVD-like vapour phase mechanism was proposed to account for an observed association with silicon carbide and fine-grained textural features (Hough et al., 1995c). Experimental synthesis of diamonds has produced additional suggestions regarding the exact mechanisms of transformation. These are outlined briefly within this section and discussed in greater depth in subsequent chapters.

Apographitic, hexagonal and platy diamond structures, which have been observed in many impact diamond examples (Vishnevsky, 1997), are used as evidence for the direct shock transformation of graphite to diamond. The mechanism for the transformation of minerals to their high pressure phases involves the formation of a denser more compact crystalline form in order to minimise the high shock pressures experienced during the impact event. There are a number of different mechanisms proposed for this transformation (De Carli, 1967; De Carli and Jamieson, 1961; De Carli, 1998; Chomenko et al., 1975) operating over a variety of pressure and temperature conditions. Carbynes have been suggested as an intermediate phase in the shock transformation of graphite to diamond (Whittaker, 1978; Heimann, 1998). In addition fullerenes (Epanchintsev et al., 1995; 1997), soot (Donnet et al., 1997; KohseHoinghaus, 1998) and hydrocarbons (Matsumoto et al., 1982) can be transformed to diamond experimentally.

The observed association of impact diamond with silicon carbide, both as intergrowths and separate crystals from the Ries crater suevites together with their fine-grained and skeletal structures led to the suggestion of a chemical vapour deposition (CVD) like mechanism (Hough et al., 1995c). CVD methods for the growth of synthetic diamond involve the nucleation and condensation of diamond from an ionised gas feedstock containing the required elements. Techniques which employ a silica substrate produce diamond associated with silicon carbide (Stammler et al., 1997). As the carbon is deposited it reacts with silica atoms evaporated from the substrate (≤1000 °C)

forming silicon carbide, as the amount of carbon increases relative to silica, diamond is formed. The skeletal, fine-grained structures of the impact diamonds found associated with silicon carbide indicated that they may have formed as a result of rapid condensation and growth within a vapour phase (Hough et al., 1995c) or from a limited carbon source as observed in natural diamonds (Shafranovsky, 1964). Langenhorst et al. (1999) suggest that extensive corrosion and etching might result in the formation of skeletal structures in diamond formed by the shock transformation of graphite.

The mechanisms and conditions of impact diamond formation, whether via direct transformation or a CVD-like mechanism, will be closely linked to the physical and chemical conditions created by the impact event. Shock ejection and vaporisation of the target rocks is expected to produce an upwardly expanding cloud of vaporised rock, dust and fragments of shocked rocks and minerals (O'Keefe, 1982). The temperature and pressure of this cloud or fireball would be highly heterogeneous and change depending on the degree of adiabatic pressure-release, following escape from the transient crater and the amount of cold, admixed fragments. The proportions of ionized plasma in the vapour cloud may be highly complex due to the interactions of jetting, entrained fragments and internal shear-heating of the projectile and target (Schultz and Gault, 1979). The fireball could provide the necessary feedstock elements for CVD with the combustion of carbon leading to the formation of increasingly reduced chemical conditions and possibly an undersaturation in carbon. Localised areas of the plume may even be hot enough for the formation of plasma-like hot ionised gas. Laboratory experiments generating hypervelocity impact produced plasmas indicated temperatures of 4500 K and charged particle densities of 10^9 to 10^{10} ions/cm^{-2} with low angle impacts producing enhanced vaporisation and self-luminous ionized clouds (Crawford and Schultz, 1991).

1.11. OBJECTIVES.

This work initially focused on samples from the Ries crater, Germany, which was chosen because of good exposures of the different impact lithologies. The samples were fallout suevites (polymict impact breccia with glass), fallback suevite, impact melt rock, lithic impact breccia, shocked granite and basement rocks. Previous work on the Ries crater investigated mineralogical, compositional and structural characteristics and has been used to delimit the impact processes, dynamics and extent of shock (Von Englehardt et al., 1997). Thus, a detailed investigation of the carbon isotopic composition of the target lithologies, impactites and individual mineral components such as diamond, graphite and silicon carbide, has been undertaken with the aim of correlating the compositions of the source rocks with diamonds found in the fallout suevite.

The initial stages involved prolonged acid demineralisation of the whole-rock samples to obtain resistant residues. Morphological characterisation of the residue minerals was undertaken using microscope techniques, such as scanning electron microscopy (SEM) and transmission electron microscopy (TEM) in order to identify the minerals present (zircon, graphite, diamond, silicon carbide etc.). This electron microscopy study also provided textural and structural evidence for possible shock related deformation of the minerals, for example stacking faults and twinning. Impact diamonds were detected in and isolated from acid-demineralised residues of several samples, such as fallback suevite, gneiss and impact melt rock which had not previously been studied in this manner.

The whole-rock samples were analysed for bulk carbon stable isotopic compositions using dynamic mass spectrometry in order to characterise the isotopic composition of the Ries impact rocks from around the crater. This was accompanied by a detailed investigation into the isotopic composition of the resistant residue components using stepped combustion combined with high resolution static mass spectrometry.

A second study involved samples from the Gardnos impact crater, Norway. Small samples of impactites and target rocks from the crater were acid demineralised using a microwave assisted reaction system (MARS5™). The residues were analysed using TEM in order to characterise the composition of the carbon within the rocks. Graphite was identified in a number of samples and diamond in suevite and black matrix lithic impact breccia. Further samples were prepared for solvent extraction and gas chromatography mass spectrometry.

CHAPTER 2: PETROGRAPHIC DESCRIPTIONS AND EXPERIMENTAL TECHNIQUES.

2.1. INTRODUCTION.

This chapter contains descriptions of the samples which were selected for analysis and their petrography, followed by details of the experimental techniques employed. These techniques aimed to investigate the mineralogical and isotopic composition of carbon in the whole-rocks, extracted lithic fragments and individual minerals. The samples and localities used are described below.

Whole-rock samples, extracted lithological fragments, glass and samples from the Nördlingen 1973 drill core (N-73) (Stöffler, 1977; Chao, 1977) were analysed for their carbon stable isotopic compositions. The samples were susequently acid demineralised to leave a resistant residue in order to separate individual carbonaceous components. These demineralised samples (herein called residues) were analysed for their carbon stable isotopic compositions as were extracted single grains of diamond and graphite. The residues were studied at various stages throughout the demineralisation using a petrological microscope, scanning electron microscope (SEM) and transmission electron microscope (TEM).

A suite of samples from the Gardnos crater were demineralised using a microwave accelerated reaction system Mars5™ (CEM Corporation). Following this, amorphous and graphitic carbon was removed using chromic and perchloric acids and the samples analysed using TEM and stepped combustion combined with static mass spectrometry. Additional samples of graphite from the Lappajärvi impact crater were analysed using static mass spectrometry combined with stepped combustion for carbon stable isotopes.

The acid-demineralisation procedures have been developed over a number of years at the University of Chicago (Lewis et al., 1975; Lewis et al., 1987; Amari et al., 1990) and within the Planetary Sciences Research Institute (Russell et al., 1990;

Gilmour et al., 1992). The method is capable of producing very clean residues of highly resistant materials such as diamond and silicon carbide, through the removal of less resistant carbonates and silicates. The procedure is described in detail in section 2.3.

2.2. RIES CRATER SAMPLE DESCRIPTIONS [48°51'N, 10°29'E].

The samples from the Ries crater are representative of the different impact lithologies present, including highly shocked impact breccias, lithic impact breccias (Bunte Breccia) and variably shocked crystalline basement material. The sample localities are illustrated in section 3.1.

Eleven individual samples were studied (table 2.1)

Table 2.1 Ries samples and localities.

Sample	Locality	Sample type	Sample abbreviation
Fallout suevite	Otting quarry	Lithic impact breccia with glass	OQS
Fallout suevite	Seelbronn quarry	Lithic impact breccia with glass	SBS
Part of a glass bomb	Otting quarry	Impact melt glass	OQGB
Bunte Breccia	Aumühle quarry	Lithic impact breccia	BB
Impact melt rock	Polsingen quarry	High temperature suevite	PIMR
Gneiss	Aumühle quarry	Gneiss	AQG
Unshocked ejected granite	Itzingen quarry	Friable granite	ITZ
Fallback suevite	Nördlingen drill core 1973 (N-73) (343, 20 m).	Lithic impact breccia with glass	NC343
Fallback suevite	N-73 (384, 07-14 m)	Lithic impact breccia with glass	NC384
Fallback suevite	N-73 (494, 64-86 m)	Lithic impact breccia with glass	NC494
Basement	N-73 (1059, 10-25 m)	Unshocked crystalline basement	NC1059

The N-73 material was provided by Professor D. Stöffler, Institut für Mineralogie, Berlin and the fallout samples provided by Professor D. Stöffler and Dr. R. Hough, PSRI, Milton Keynes. The terms suevite and Bunte Breccia are local Ries terms for lithologies better described respectively as a polymict impact breccia with glass and a lithic impact breccia which does not contain melt particles. Suggested

terminology to encompass the wide range of local impactite terms (Stöffler and Grieve, 1996) was discussed in section 1.6.

The samples and localities described below comprise of a range of impact lithologies from around the crater itself. Descriptions of the localities and lithologies are derived from Chao, (1978). Detailed descriptions of the various impact lithologies may be found in Hörz et al. (1983), Von Englehardt, (1990), Von Englehardt et al. (1995) and Von Englehardt, (1997).

2.2.1 Ötting quarry, fallout suevite (OQS).

The Ötting quarry is a relatively large outcrop (24 m thick) of suevite (impact breccia with glass) to the north east of the inner crater rim and is underlain by Malm limestone and Bunte Breccia. The exposure in the quarry comprises of fresh unweathered suevite containing vesiculated glass bombs and basement rock fragments exhibiting all stages of shock metamorphism. Samples from OQS were used to date the impact event, to 14.8 ± 0.7 ma using $^{40}Ar/^{40}K$ (Gentner et al., 1963) and to 15.0 ± 0.1 ma using $^{40}Ar/^{40}Ar$ (Staudacher et al., 1982).

In hand specimen the sample is a large block, approximately 40 by 22 cm in size with a greenish grey/white groundmass of altered glass with fragments of rock and minerals. Figure 2.1. is a photograph of a cut block of suevite from the Ötting quarry and shows glass and lithic fragments within a fine-grained grey matrix. The groundmass is most likely chloritized and composed of clay minerals such as montmorillonite replacing altered glass as described by Von Englehardt (1997). The sample includes two large elongated black glass bombs, the largest of which is about 15 cm in length and has a highly irregular upper margin in comparison to the smooth lower margin (figure 2.2).

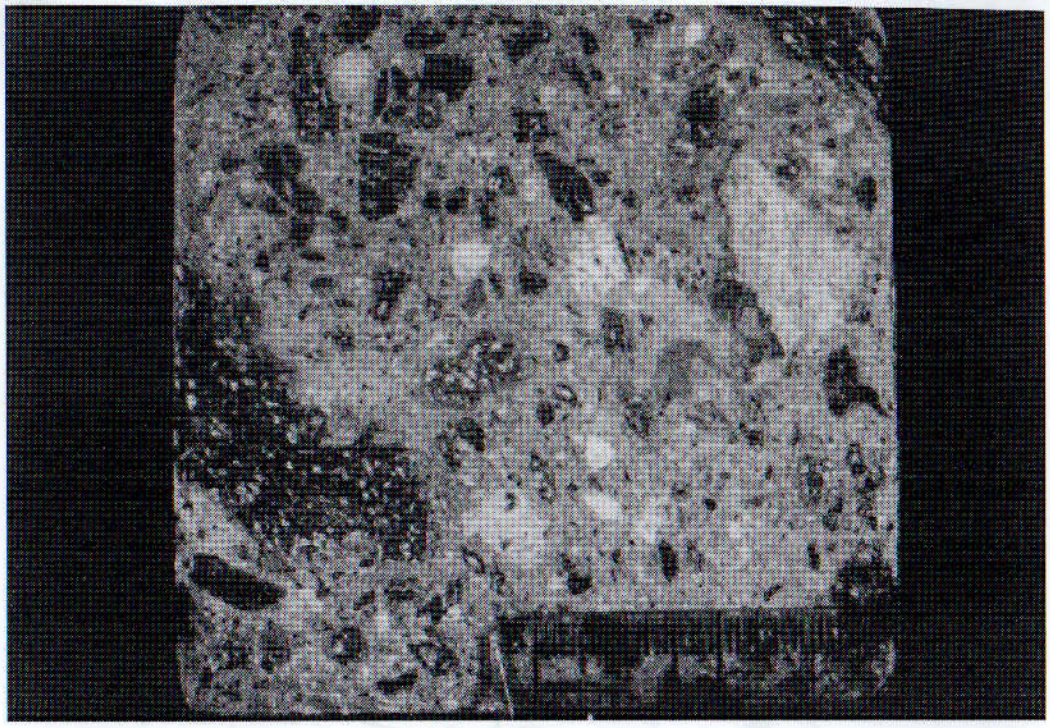

Figure 2.1. Photograph of a 7.5 cm by 7.5 cm cutblock of suevite from OQS. Scale shown by cm scale ruler in the bottom right corner.

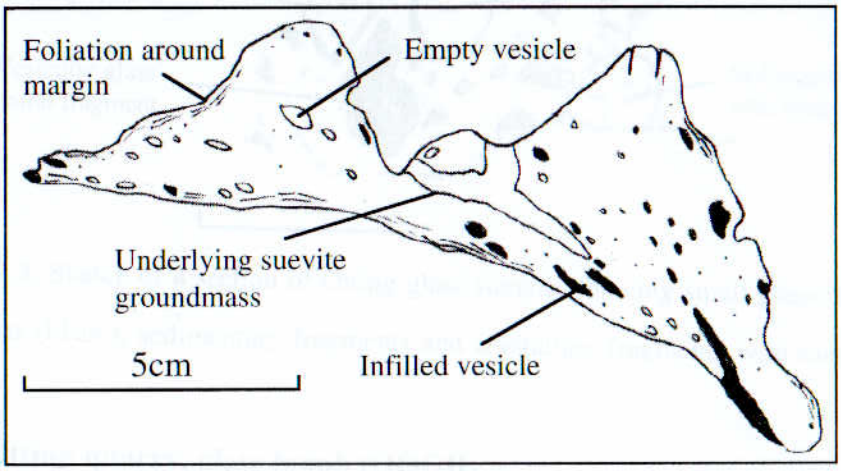

Figure 2.2. Sketch of a glass bomb within OQS groundmass. Showing empty and infilled vesicles, foliation of small vesicles and glass around fine grained margin and irregular structure.

The form of this bomb is reminiscent of the bowl shaped glass bodies described by Von Englehardt et al. (1995). Inclusions and vesicles within the glass appear to follow the finer grained margins of the bomb and indicate exsolution of a gas phase due

to pressure release and cooling (Von Englehardt et al., 1995). The number of vesicles varies from about 5 to 60 vol% in different glass fragments and bombs and may be filled with secondary mineralisations such as chalcedony, montmorillonite, calcite or zeolites (Von Englehardt et al., 1995). Chilling of the glass as it was ejected results in the formation of finer grained chilled margins.

The groundmass contains many smaller glass fragments which are often vesicular and as with the larger bombs these vesicles may be filled with secondary mineralisation. Some lithoclast fragments have visible glass rims, this is illustrated in figure 2.3.

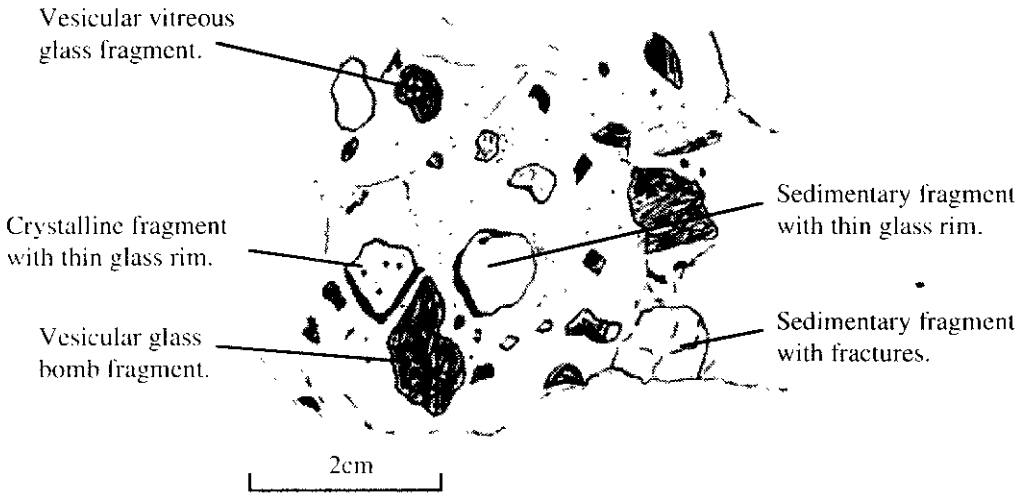

Figure 2.3. Sketch of a section of Ötting glass suevite, showing small glass bomb fragments (black), sedimentary fragments and crystalline fragments with thin glass rims.

2.2.2. Ötting quarry, glass bomb (OQGB).

The primary glass sample used was a part of the largest glass bomb yet recovered from the Ötting quarry (by D. Stöffler). The original sample was approximately 30 cm in length and composed of black, highly vesicular vitreous glass. These vesicles were mainly devoid of infilling mineralisation. Examination in thin section revealed a streaky layered internal structure with numerous inclusions of crystalline fragments and vesicles (figure 2.4). The brown coloration of schlieren reflects increased concentrations of iron, magnesium and calcium or water oxidation

(Von Englehardt et al., 1995). The bomb is illustrated in figure 2.5 which is a photograph of part of the sample showing a ropy-like texture and the irregular surface coating of the suevite groundmass.

Figure 2.4. Photomicrograph of Ötting quarry impact melt glass. Showing streaky layered structure, inclusions of crystalline material and vesicles. Magnification x5. (Field of view 20 mm).

Figure 2.5. Photograph of part of a 7 by 6 cm glass bomb from the OQS. Scale shown by cm scale ruler in the bottom right corner.

2.2.3. Seelbronn quarry (Aufhausen), fallout suevite (SBS).

The Seelbronn quarry (also known as Aufhausen) is a smaller suevite quarry to the south east of the inner crater rim, possibly sampling a different part of the basement during formation.

In hand specimen this sample is approximately 10 x 20 cm in size and comprised of two layers. One layer is composed of very fine grained, light grey material containing mica, small crystal fragments and small lithoclastic fragments. Whilst the other layer is coarser in texture, containing a higher percentage of glass and lithoclastic fragments. Very little groundmass is discernible. The colour is a dark grey dominated by black glass fragments. The suevite contains several rock fragments, approximately half of which are crystalline although highly altered and fine grained, the other fragments appear to be highly altered sedimentary fragments. The degree of alteration and clay mineralisation in these samples makes the exact lithological composition of the fragments difficult to determine.

The impact melt glass inclusions are dark and almost black in colour with a slightly vitreous lustre although only small fragments are present (0.5 to 2 cm) compared to the larger bombs within the OQS sample.

2.2.4. Auhmüle quarry, Bunte Breccia (BB).

The Auhmüle quarry locality consists of Bunte Breccia underlying fallout suevite and is located at the northern crater rim. Bunte breccia is a term used to describe the Bunte Trümermasser deposits which form a near continuous ejecta sheet around the crater (Chao et al., 1978). This polymict lithic impact breccia is composed of primarily sedimentary derived fragments and unconsolidated local material (Von Englehardt, 1990).

The sample is illustrated in figure 2.6 which shows the fine grained layering. In hand specimen the sample is a highly friable black, fine grained rock. The sample has a clear foliation or bedding on a very fine scale with a vitreous sheen to the surfaces. Although the Bünte Breccia is predominantly a massive deposit, localised lineation textures may be found along contacts (Hörz et al., 1983). The fine grained matrix also

includes small fragments of sedimentary rock, which are the same blue-black colour as the groundmass and so hard to distinguish. These were detected when the sample was ground for acid demineralisation.

Figure 2.6. Photograph of BB (2.5 cm by 1.5 cm)from Aumühle quarry. Scale given by mm divisions on ruler in the bottom right corner.

2.2.5. Polsingen quarry, impact melt breccia (PIMR).

Polsingen quarry is located to the east of the crater and comprises of a red impact melt breccia. The breccia has a fine grained matrix consisting of glass containing crystalline rock fragments, the red colour is the result of hematite alteration within the rock (Chao et al., 1978). The locality was re-interpreted as a high temperature suevite, abnormally rich in melt which recrystallized at higher temperatures than normal suevite (Von Englehardt and Graup, 1984).

Figure 2.7 is a photograph of the hand specimen showing the red oxidised colour, a number of lithic fragments and the vesicular glassy texture of the groundmass. In hand specimen the sample has a fine grained red-grey matrix with a vesicular or

pitted texture, it includes several large lithoclastic fragments which are highly altered and either rounded or very irregular in form. The matrix is distinct from that of the suevite samples in that it is composed of glass rather than polymict fragments of glass, rock and minerals. The distinct greenish colour amongst the red matrix may represent chloritisation of the sample.

Figure 2.7. Photograph of PIMR (5.5 by 4.2 cm). Scale given by ruler in bottom right corner.

2.2.6. Itzingen quarry, granite (ITZ).

The quarry at Itzingen is a sand/gravel pit exploiting variably shocked, highly altered and friable granitic material, which was ejected from the crater during the impact event. The basement below the target area originally comprised of Variscan granitic intrusions overlying a deeply inclined Pre-Variscan gneiss complex underlying a thin sedimentary cover (Graup, 1978).

The sample is illustrated in figure 2.8 and in hand specimen the rock is friable, coarse-medium grained and composed of quartz, pink and white feldspar with mica and

black opaque minerals. The larger white feldspar crystals contain mica and/or opaque inclusions.

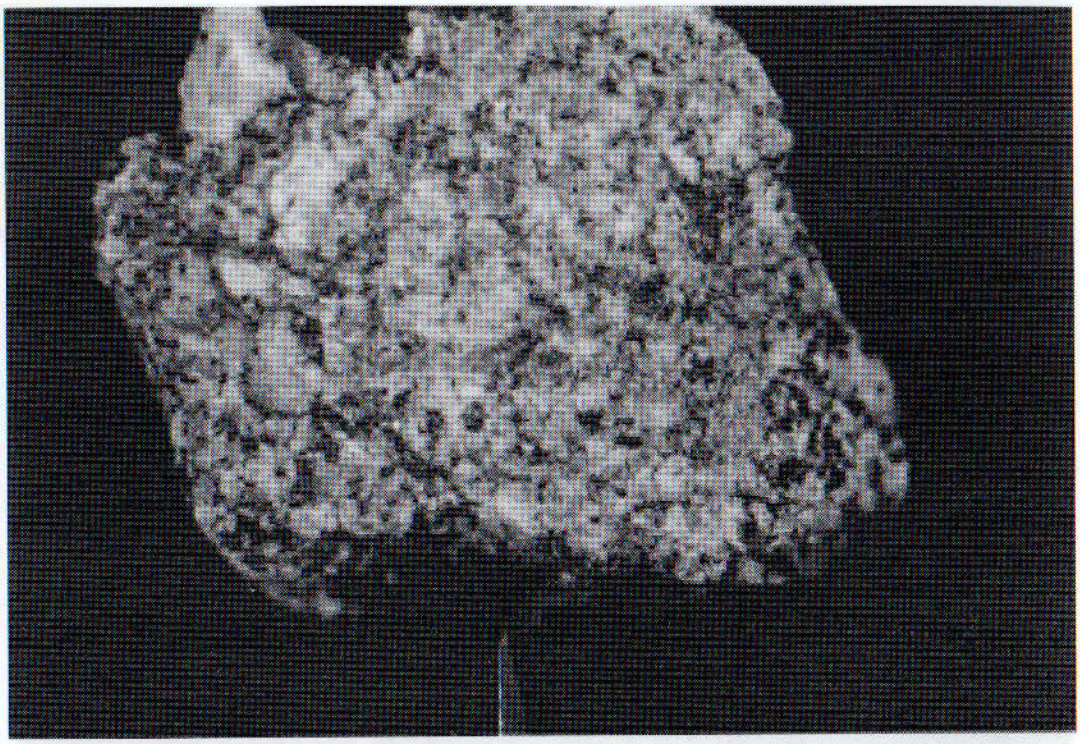

Figure 2.8. Photograph of granite from ITZ (3.5 by 3 cm). Scale given by cm scale ruler in the bottom right corner.

2.3. NÖRDLINGEN 1973 DRILL CORE.

Three drill cores have been placed in the Ries crater area, these include Deiningen, Nördlingen 1973 and an industrial hole (1001). The Nördlingen 1973 drill core has been described by a number of authors (Burberger, 1974; Jankowski, 1977; Stöffler, 1977); Stahle and Ottemann, 1977) and much of the work is summarised in Von Englehardt and Graup, (1984). The core was located approximately 4 km north east of Nördlingen and this location was selected on the basis of geophysical evidence to be halfway between the inner crater ring and the outer crater ring (Chao, 1977). The drill core reached a depth of 1206 m, approximately 600 m into the crystalline basement. The specimen descriptions below are based on hand specimen examination of the core material samples.

2.3.1. Brecciated crystalline basement 1059, 10-25 m depth (NC1059).

This segment of core is a relatively fresh, medium to fine grained crystalline rock. The dominant colour is a pink-red and the sample probably represents shocked granite, comprising of areas of fine grained brecciation and coarser areas with a surrounding textural lineation. The photograph of the sample (figure 2.9) illustrates the fine grained nature of the sample.

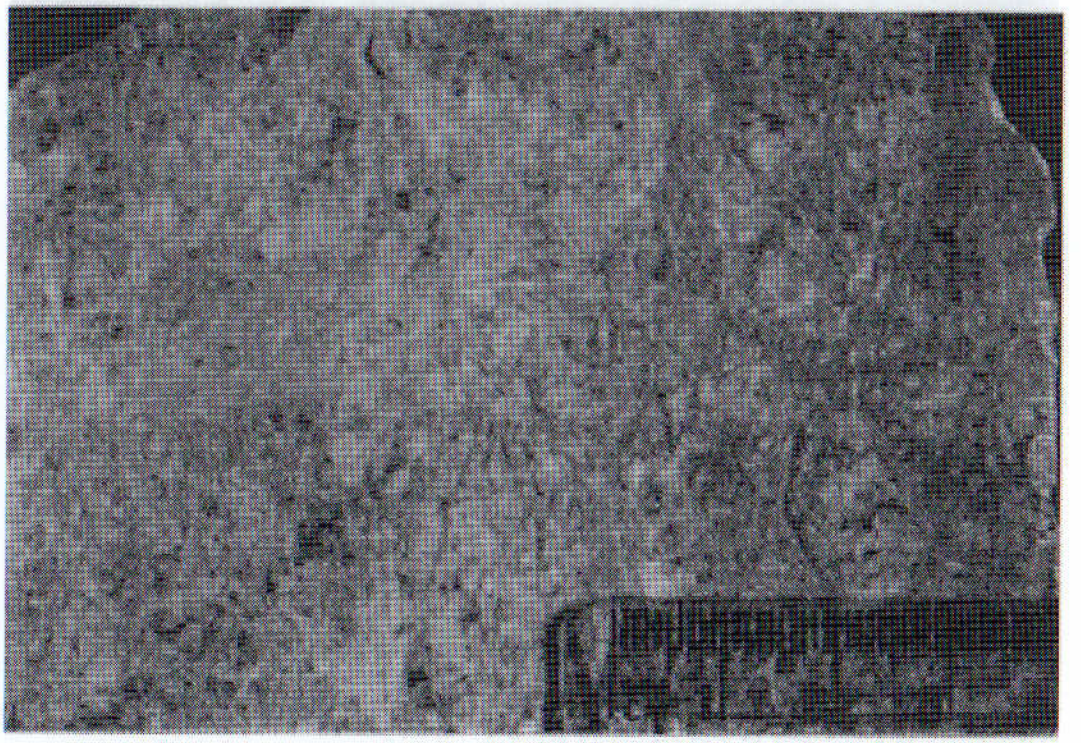

Figure 2.9. Photograph of brecciated basement NC1059 (10 by 6 cm). Scale given by cm scale ruler in the bottom right hand corner.

2.3.2. Suevite 494, 64-86 m depth (NC494).

This sample has a red-brown colour in comparison to the Seelbronn suevite or Ötting suevite which are both grey in colour, possibly related to variatioins in the extent of weathering oxidation and iron content. The sample is cross cut by a large elongated, pitted and vesicular glass bomb with a lineation of inclusions along its margins. The bomb comprises about 10 vol% of the total sample. Lithic inclusions comprise of 2 to 3

cm fragments of target material, one of which has a visible thin glass rim. The groundmass includes approximately 40 vol% of small (20 to 60 mm) crystalline fragments and altered glass. The photograph (figure 2.10) shows an elongate glass bomb amid the red-brown groundmass which contains numerous angular lithic fragments.

Figure 2.10. Photograph of suevite NC494. (8 x 3 cm).

2.3.3. Suevite 384, 07-14 m depth (NC384).

This sample had a similar orange-red-brown colour as above. The majority of the sample was composed of highly devitrified and altered glass fragments, although a few may be altered sedimentary fragments and no black vitreous glass was evident. The sample was vesicular and included crystalline basement rock fragments which were relatively fresh and about 0.5 to 1 cm in size or smaller. Figure 2.11 is a photograph of the sample showing altered glass or lithic fragments as well as other less altered lithic fragments amid the fine grained groundmass.

Figure 2.11. Photograph of suevite NC384 (7 by 5 cm. scale given by cm scale ruler in the bottom right hand corner.

2.3.4. Suevite 343, 20 m depth (NC384).

This is a relatively small section of core compared to the other samples which is similar to the suevites described above but less porous or friable. The sample includes a large (3-4 cm) fragment of crystalline material (possibly gneiss) with a glass rim. Smaller crystalline basement fragments and devitrified glass are also present. One small (20 to 30 mm) fragment is similar to the brecciated crystalline basement sample described in 2.2.6 and thus probably represents granite. Figure 2.12 shows the sample with numerous altered and pitted fragments which may be altered glass or lithics. A single large lithic fragment can be seen at the top of the sample.

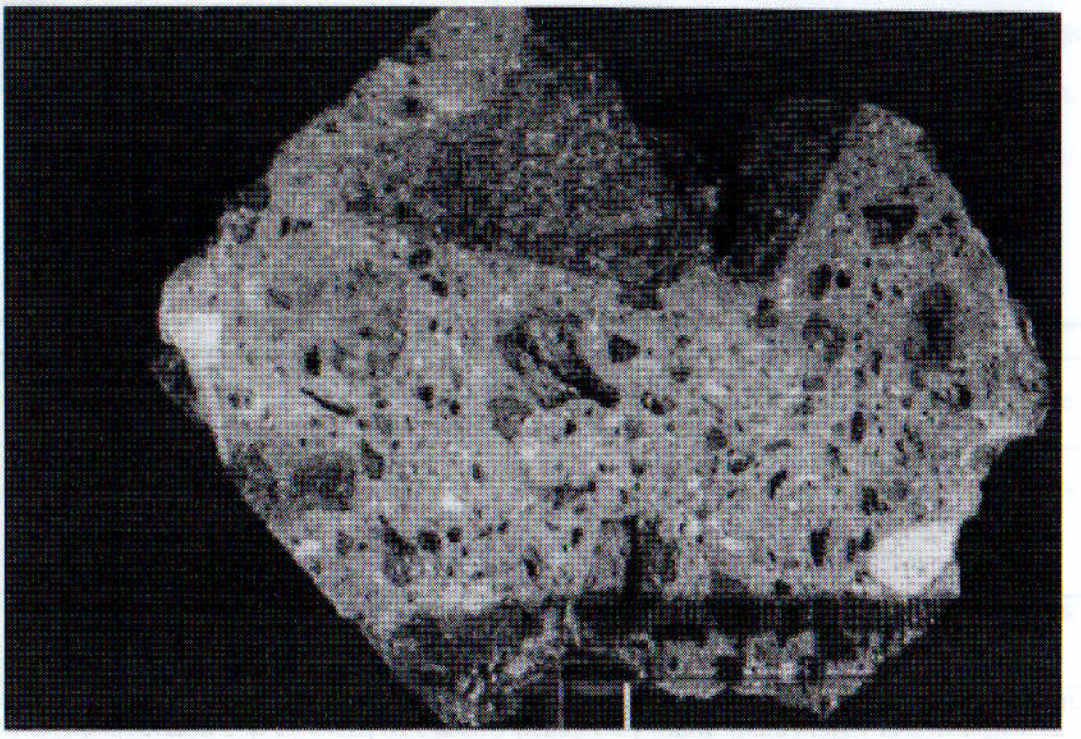

Figure 2.12. Photograph of suevite NC343 (11 by 9.5 cm). Scale given by cm scale ruler in the bottom right hand corner.

2.4. GARDNOS AND LAPPAJÄRVI IMPACT CRATERS.

2.4.1. Gardnos impact structure. [60°40'N 9°00'E].

Located 125 km north-west of Oslo, Norway the Gardnos impact structure is approximately 4.5 km in diameter and was formed on a crystalline metamorphic amphibolite facies target (French et al., 1996; 1997) which may have been overlain by shales. The target rocks comprise of granites, granitic gneisses with minor amphibolite, metagabbros and quartzite. Impactites consist of fractured and blackened quartzites, lithic breccias and melt bearing breccias (French et al., 1992).

High pressure carbon phases such as diamond have yet to be detected in the Gardnos impactites or shocked target material. The impactites do however, show anomalously high carbon contents in excess of those present in the target rocks. The carbon stable isotopic composition of the impactites and target rocks ranges from $\delta^{13}C$ values of -28.1 to -31.5 ‰ (French et al., 1997).

A selection of whole-rock samples of impact breccia and suggested shale target material from the Gardnos impact structure, Norway were provided by Dr. B. French, Smithsonian Institute (USA). The eight samples provided are detailed in table 2.2.

Table 2.2. Gardnos samples and characteristics.

Sample	Number	Locality	Characteristics
Lithic breccia (subcrater rocks)	120	Dokkelvi River, Tunnel Dump.	Granitic gneiss inclusions up to several cm in size in black massive matrix.
Basement rocks (quartzites, shocked, fractured, black and carbon-bearing)	129	Dokkelvi River, Tunnel Dump	Highly fractured, with clasts of darkened quartzite in dense massive black matrix.
Melt bearing suevite breccias	133	Dokkelvi River, above suevite /basement contact	Typical dark green suevite breccia with black glassy inclusions (fladen).
Melt bearing suevite breccias	137	Flatdalselvi River, 1m above contact suevite/basement	Dense dark green suevite with some mafic inclusions.
Black shales	164	Fagernes-Bjorgo highway, 5 km E of Bjorgo	Alum shale (Cambr-Ordovician). Crumpled black shale below overthrust Proterozoic quartzite.
Black shales	169	Road cut 2 km S of Biri, W side Lake Mjosa.	Biri shale (Proterozoic) Dark black fissile shale, highly folded and contorted. Assoc. Biri limestone and limestone breccia
Black matrix lithic breccia	178	NE Dokkelvi River	Non-typical , contains numerous quartz clasts, rare black clasts in very dense black matrix
Melt matrix impact melt breccias	179	Dokkelvi River	Typical, massive dense green rock with scattered clasts up to 2-4 cm, in aphanitic matrix with greasy lustre.

2.4.2. Lappajärvi impact crater.

The lake Lappajärvi impact crater, western Finland is a 23 km diameter 80 Ma elongated basin within Proterozoic gneisses and acid-intermediate rocks overlain by Quaternary sediments (Langenhorst et al., 1999). The structure of the crater and impactites hves been extensively investigated using geophysical techniques and a number of boreholes (Pipping and Lehtinen, 1992; Elo et al., 1992). The impactites present include large volumes of impact melt (Henkel and Pesonen, 1992), impact melt breccias (Kärnäite) and suevite breccias (Pipping and Lehtinen, 1992). Diamonds from

the suevites and impact melt rocks have a tabular form and surface striations inherited from precursor graphite (Langenhorst et al., 1998; 1999).

Samples of isolated impact diamonds and graphites from the Lappajärvi impact crater were provided by Professor S. Vishnevsky. Russian Academy of Sciences. The samples consisted of alkali fusion extracted diamonds and graphite residues from which individual diamonds and graphite grains were selected and analysed for carbon stable isotopes.

2.5. SAMPLE CRUSHING AND PREPARATION.

Crushing of the samples prior to acid digestion was required in order to increase the surface area of the samples, and thus facilitate faster dissolution of the minerals. The samples were crushed manually, to eliminate the possibility of contamination by grinding powders (carbides) common in the rock crushing labs. All the samples for the acid digestion were crushed manually and only samples for whole-rock XRF and bulk carbon isotopic analysis were crushed mechanically and ground to a very fine powder (10 gm), using an agate tema barrel.

2.6. ACID DEMINERALISATION.

Three different acid demineralisation techniques were employed:
(1) conventional demineralisation using a series of increasingly corrosive acids, (2) a microwave assisted demineralisation system and (3) high pressure and temperature bombs. Each method has its merits and tackles different problems associated with the demineralisation of heterogeneous samples. Conventional demineralisation is prolonged compared to microwave dissolution but much larger samples can be processed. The microwave process involves considerable cleaning of the sample vessels as does the high pressure bomb technique.

2.6.1. Conventional acid demineralisation.

The acid demineralised residues were prepared following the schematic illustrated in figure 2.13. The procedures for the preparation of solutions are described in appendix 1.

Figure 2.13. Summary of acid demineralisation stages. Duration of steps depends on the nature of the individual sample.

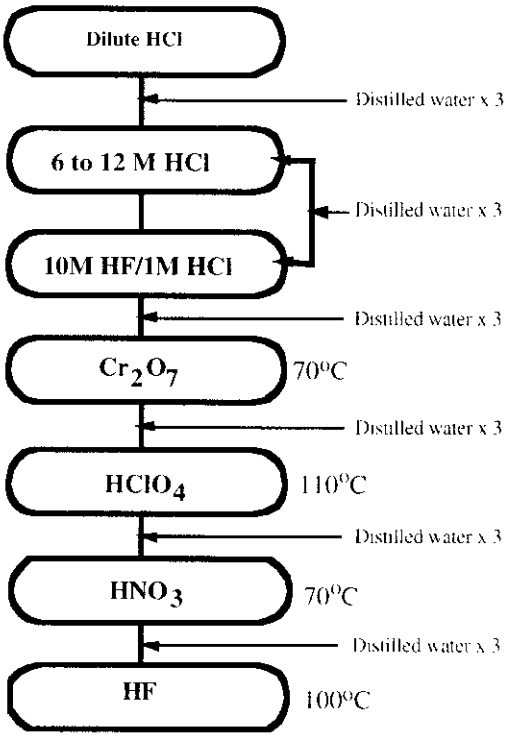

The technique separates resistant phases such as diamond and silicon carbide from other minerals within the samples although resistant zircon and metal silicates require considerable acid treatment for removal. The acid dissolution involves increasingly concentrated applications of hydrochloric acid (HCl) to remove carbonates, hydrofluoric / hydrochloric acid 10:1 to remove silicates, HCl to remove neo-formed fluorides, chromic acid ($Cr_2O_7^{2-}$) to remove organic carbon and fuming perchloric acid ($HClO_4$) to remove graphitic carbon. To illustrate the prolonged nature of the digestions appendix 2 summarises the procedure for a glass sample.

The initial stage of the acid digestion involved covering the samples with dilute HCl in 300 ml teflon bombs. This often resulted in a strong reaction producing CO_2 gas. Suevite samples were more likely to display strong reactions than crystalline or glassy materials because of the higher proportions of carbonate minerals in the rock. The acid reacts rapidly, progressing through yellow-orange and finally a dark orange-red colour indicating reaction of the acid with minerals within the sample. After the sample ceased to react appreciably, increasingly concentrated HCl was used (up to 12 M) at 100 °C. When the sample appeared free of carbonates, disaggregated and showed no reaction to HCl the next stage was started.

Using a mixture of 10 M HF and 1 M HCl dissolves silicates within the samples and further disaggregates the residue. The production of neo-formed fluorides (insoluble fluorides formed from the reaction of HF with carbonates) may be avoided by extensive HCl application prior to this stage, yet usually some fluoride formation is unavoidable and these are removed using repeated cycles of concentrated HCl and heat. The formation of fluorides was particularly problematic in fallout suevite samples compared to the glass and core samples, due to differences in their carbonate contents.

Non-crystalline and organic carbon is removed from the samples using chromic acid at 70-100 °C. Oxidation of carbon in the sample results in the chromic acid changing from orange to a blue or black colour.

Perchloric acid is used to remove crystalline graphite, by fuming the samples at 100-110 °C until the samples are white-grey. Perchloric acid is a strong oxidising agent that requires a wash down fume cupboard facility.

The application of concentrated hydrofluoric acid (48 %) to the samples is a final stage to remove resistant zircon crystals. Samples were heated to 120-150 °C on a hot-plate in 15 ml teflon bombs for several weeks.

Analysis of the Seelbronn suevite residues under the SEM indicated the persistence of zircon and some metal silicates, representing etched mineral residues. Removal of metal silicates was achieved using hot concentrated nitric acid at 70-100 °C

for several days. Nitric acid reacted strongly with the samples, visibly reducing the dark colour and amount of metal silicates. This was confirmed using the SEM.

At several stages through the digestion technique the residues were weighed in order to attempt to calculate the percentage of diamond in the original samples (table 2.3).

Table 2.3. Residue weights and percentage of original sample weight.

Sample	Original weight (g)	Residue weight (g)	% of sample remaining
Otting glass bomb 1	149.75	0.0026	0.00389
Otting glass bomb 2	59.30	0.0027	0.00161
Seelbronn suevite 1	100.53	0.0151	0.0152
Seelbronn suevite 2	94.80	0.0109	0.0103
Nördlingen core 494	162.08	0.0308	0.0499

2.6.2. Microwave assisted dissolution.

The microwave accelerated reaction system MARS 5™ (CEM Corporation) allows the treatment of samples at high temperature and pressure. The dissolution system uses microwave energy to heat samples because water and acids rapidly absorb microwave energy and the elevated temperatures cause rapid dissolution of the samples. The system comprises of a 1200 W microwave, microwave transparent high pressure/temperature acid-resistant teflon bombs with explosion proof kevlar jackets, and a control vessel with a sapphire thermowell. The system can accommodate 12 vessels at a time with a maximum of 3 to 4 g of sample per vessel.

The vessels must be clean, dry and free of particulate matter prior to use as drops of liquid or particles will absorb microwave energy, resulting in localised heating and possible damage to the vessels. For similar reasons, acids such as concentrated sulphuric or phosphoric acids cannot be used as they will heat beyond the melting point of the vessels. The samples are covered with approximately 12 ml of HF/ HCl (10:1) to remove silicates and 5 ml of HCl to remove carbonates and neo-formed fluorides.

The microwave is computer controlled with the temperature and pressure of the samples constantly monitored through the control vessel and displayed on the computer. Individual cycles are programmed into the control panel or a pre-programmed cycle is used.

The protocol used for the Gardnos samples involved gentle heating for 5 minutes to 100 Psi and 100 °C to create a good seal on the vessels. Then 5 minutes to the maximum pressure and temperature for digestion (300 Psi and 200 °C) which was maintained for 10 minutes before cooling to <50 Psi and <60 °C. A further 1-2 days in HF/HCl removed all silicates and zircons.

The main problems associated with the microwave digestion technique are the formation of fluorides and cleaning the vessels after use. Fluorides and organic carbon material clings to the inside and base of the bombs although the addition of nitric acid to the samples can reduce this problem. The bombs are cleaned by scrubbing and prolonged sonication at 50 °C in a water bath. The bombs can then be rinsed with distilled H_2O and dried prior to use.

2.6.3. High pressure bombs.

Six samples were treated with a mixture of concentrated HF and nitric acid (HNO_3) in high pressure bombs at 180 °C for 1-2 weeks. This technique proved highly effective in increasing the rate of removal and digestion of resistant zircon grains although similar results were obtained from microwave digestion. The size of the bombs meant that only small samples could be accommodated and so would not be suitable for processing large amounts of rock.

2.6.4. Additional sample preparation techniques.

A number of the samples contained a high proportion of zircon grains with two morphologies, highly birefringant crystals and cloudy polycrystalline grains. As shock formed and shock deformed zircons have been reported by Bohr et al. (1993), it was decided to replicate a zircon etching technique to look for planar deformation features

(PDFs). Etching of zircon using a hot concentrated alkali such as sodium hydroxide (NaOH) should preferentially attack PDF and cracks within the grains.

Heated sonication using a water bath was attempted in order to speed the dissolution of neo-formed fluorides. This generally resulted in drawing out organic carbon matterial from within the sample and coating the insides of the bombs, which proved very difficult to remove. It was decided that prolonged exposure to hot HCl was the best solution for neo-formed fluorites.

2.7. CARBON STABLE ISOTOPIC ANALYSES.

The samples were analysed for carbon stable isotopes as bulk whole rock samples, extracted lithic fragments, acid demineralised samples as well as single diamonds, graphite and silicon carbide picked from the residues. Mass spectrometry analyses were performed using two systems; a static mass spectrometer for high resolution stepped combustion analyses (Wright and Pillinger, 1989; Prosser et al., 1990) and a SIRA dynamic mass spectrometer for bulk carbon analyses.

Bulk carbon stable isotope measurements were made on whole-rock samples and extracted lithic and glass fragments prior to demineralisation. Following demineralisation stepped combustion analyses were performed on the residues as well as selected diamond, graphite and silicon carbide grains.

2.7.1. Whole-rock carbon stable isotopic analyses.

The samples were weighed into 2x3 mm quartz buckets in a clean room and covered with baked copper oxide (CuO) powder to supply oxygen for the combustion of carbon in the samples. The CuO powder and buckets were pre-baked at 1000 °C overnight to reduce the carbon blank. The 2x3 mm buckets and samples are then placed in 4x6 mm quartz buckets and sealed using a blow torch whilst at a vacuum pressure of at least 10^{-5} torr. These were then heated at 1000 °C for 10-12 hours.

The gases produced by the combustion process (mainly CO_2) were cracked into an evacuated glass extraction line for the cryogenic separation and collection of CO_2.

frozen to approximately -196 °C on to a cold finger using a dewar of liquid nitrogen (LN_2) with non-condensable gases pumped away. The CO_2 was released using a dewar of pentane slush at -135 °C and measured on a capacitance manometer baritron and the carbon yield calculated. The samples were then transferred to a SIRA dynamic mass spectrometry system. (Appendix 4).

2.7.2. Stepped combustion carbon analyses.

Stepped combustion analyses were initially performed using the semi-automated static mass spectrometer system MS86 which uses a SIRA 24 analyser (Wright and Pillinger, 1989; Prosser et al., 1990). Samples of graphite, diamond and bulk samples of acid-resistant residues were analysed. Stepped combustion enables detailed analyses, contaminant removal and selective combustion of different carbonaceous materials (Wright and Pillinger, 1989). Combustion of a sample through a series of increasing temperature steps, ranging in increments from 100 or 200 °C down to 10 °C steps, depending on the resolution required, enables highly detailed analysis of separate components.

Samples were loaded into platinum buckets pre-baked at 1000 °C, weighed and transferred to the MS86 extraction system for analysis and evacuated (10^{-6} to 10^{-7} torr) before the analyses start.

The glass line furnace is cooled to 200 °C and the CuO to 650 °C for 10 minutes to resorb the released oxygen then to 450 °C to reduce the carbon blank, the overnight blank is then pumped away. CuO wire is used to provide oxygen for the combustion of carbon in the samples. Reference gas samples are also run to check the mass spectrometer precision before the sample is loaded.

The evolved gases from each temperature step (30 minute duration) are purified cryogenically using liquid nitrogen and transferred to the mass spectrometer capacitance manometer with the release of CO_2 monitored by the computer. The system measures 20 points on the release profile and if they are all within 1 % the gas is isolated from the glass line. The gas is then frozen down on a cryotrap at approximately -196 °C for 10

minutes, before non- condensable gases are pumped away. Once the mass of gas has been calculated, the system selects one of 6 sequences for splitting the gas to a suitable mass (2-4 ng) for the mass spectrometer. After the sample has been run the system automatically selects an appropriate bleed time for the continual bleed reference gas and runs this through the mass spectrometer, this is followed by a second aliquot of reference gas to fine tune the mass balance and the results calculated and tabulated.

There are two reference gas systems used, the first operates on a continual bleed system, with low levels of gas bleeding continuously from the reference bulb with a $\delta^{13}C$ -39 ‰. This enables the gas to be collected for a calculated period of time to accumulate enough to balance the sample mass before release to the mass spectrometer. The second reference gas operates on a fixed system and is used to check the isotopic composition of the first reference gas. This has a carbon isotopic composition of $\delta^{13}C$ = +0.71 ‰.

Carbonate standards are run to check the precision of the mass spectrometer. The standard PSU3 uses a single tiny grain of the powdered carbonate with an expected $\delta^{13}C$ of -3.45 ‰ and the main gas release is at 600-700 °C.

Furnace blanks and overnight blanks are taken from the furnace after cooling of the CuO, the blank is generally around 1 ng of carbon and $\delta^{13}C$ = -25 ‰. The isotopic composition of the blank is generally not measured only the mass of CO_2 evolved to ensure a low level of carbon contamination. Blanks are reduced by cycling the CuO at 600 to 950 °C to combust carbon species (Wright and Pillinger, 1989), prebaking the platinum buckets and maintaining the glass line vacuum. (Appendix 5).

2.8. OPTICAL AND ELECTRON MICROSCOPY.

The samples from the Ries crater were studied at several stages through the acid demineralisation treatments, using optical and a scanning electron microscopy (SEM). This enabled the progress of the demineralisation to be monitored and changes in the chemistry and mineralogy of the sample to be noted. Further into the demineralisation

procedure, the samples become clean enough and disaggregated enough to allow analysis using transmission electron microscope (TEM) techniques.

The three microscope techniques (optical, SEM and TEM) have their own advantages and disadvantages. Each technique provides a different view of the samples, for example the SEM provides elemental and morphological data whilst the TEM provides mineralogical and structural information. This is relatively simplified as the two techniques provide images of the samples in distinctly different ways and different scales of magnification revealing further detail.

2.8.1. Petrological microscope.

Optical analysis of the samples enabled the selection of small diamond grains and a photographic record of the samples progress through the acid demineralisation stages, providing a quick, simple way to check the composition of the samples and the structure of the grains within the residues. In addition a visual record of the diamonds found within the samples is important if they are subsequently combusted for isotopic analysis.

The microscope used was a Zeiss (D-7082) Universal Microscope with magnifications from x 5 to x 40, capable of transmitted and reflected light and a MC100 camera attachment. Photographs of the samples or individual grains within the samples were taken using the MC100 camera attachment loaded with tungsten filament Kodak gold slide film.

The residues were analysed at several stages throughout the acid dissolution process in order to note changes in the composition and morphology of the residual grains. The initial analysis of the samples followed the silicate digestion stage (HF/HCl), this proved difficult as the samples contained contamination from fluoride salts and amorphous organic material and were thus difficult to observe. Far better results were found when the samples were studied under the optical microscope after the fuming perchloric ($HClO_4$), chromic and advanced HF/HCl stages, when organic material and fluorides were eliminated. Thus samples were checked under the

petrological microscope following the acid treatment stages for clarity, in that they were free of amorphous acid salts and for large diamonds (50-100 um). If the samples appeared contamination-free they were stored in the glass petri-dishes ready for electron microscope analysis. The samples were cleaned of acid residues or salts by repeated washes with distilled H_2O. This was necessary as not only is the presence of acid salts within the sample hazardous to health (moisture from skin contact could produce HF acid) but fluoride and chloride salts could become volatilised under the electron beam and damage the equipment. Analysis of the samples under the petrological microscope also becomes difficult if the sample is full of acid salts.

2.8.2 Scanning Electron Microscope (SEM).

The SEM was located in the Material Science electron microscopy suite at the Open University and comprised a Jeol JSM-820i with a Kevex Delta 4 system and a quantum detector for energy dispersive x-ray spectroscopy (EDS) and elemental analysis of the samples. Scanning electron microscopes form an image of the sample in a cathode ray-tube synchronised with an electron probe as it scans the surface of the sample (Rochow and Rochow, 1978). Interaction of electrons with the sample, produces x-rays, characteristic of the displacement of shell electrons in the sample atoms. Thus the energy released is unique for each atomic number and therefore, unique to each element (Lawes, 1987. This is substantiated by ensuring all the characteristic lines of an element are matched with those generated by EDS. EDS can then be used to detail the elemental composition of grains within a sample or variations in composition within individual grains, and based on these a tentative suggestion of the mineralogical composition of the grain can be presented.

Samples of the residues were loaded onto carbon sticky tabs on aluminium Cambridge-type studs by pressing the stud gently onto the sample in a glass petri dish. The carbon tabs are readily dissolved in acetone and so an individual sample can be retrieved, this is important for small residues and when individual diamonds were studied.

Unfortunately the SEM and EDS system can only elemental data on the grains studied and not a mineralogical or crystallographic identification. Although grains with relatively simple compositions such as zircon and rutile can be tentatively identified. Figure 2.14. shows an example of an EDS scan for a mineral identified as zircon.

Some elemental percentages can be obtained using standards but this is not quantified. Thus, samples were mainly imaged using the SEM and carbon grains studied for their morphology.

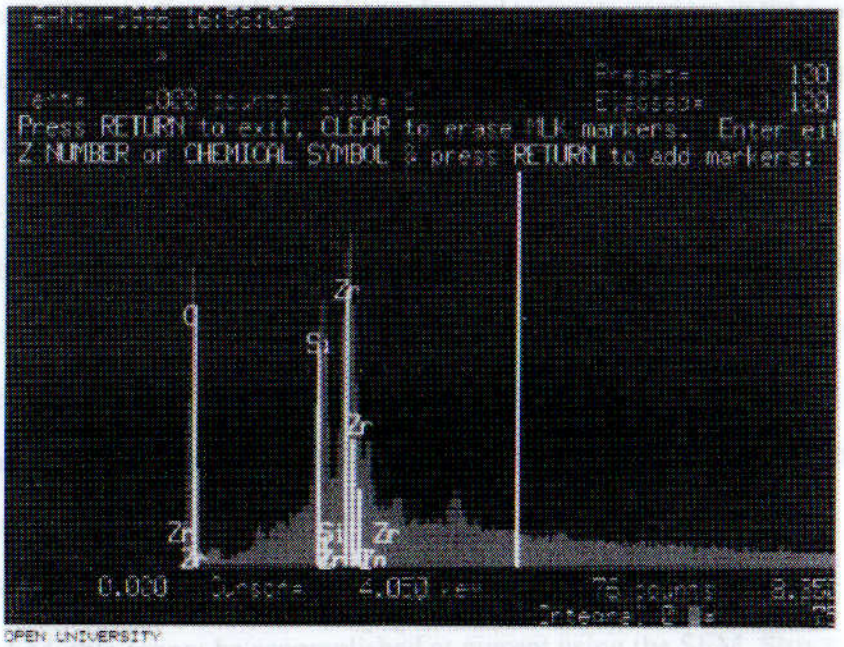

Figure 2.14. EDS scan showing spectrum emission lines for Zr, Si and O. Unlabled bar represents the cursor.

For certain analyses where the sample was insulating, charging of the sample made observation difficult but could be reduced in three ways.

(1) Using a carbon or gold coating, e.g. with the zircon samples when looking for structural features. The coating materials used are chosen based on their good conduction, chemical inertness, good secondary electron emission, small grain size and ease of production (Lawes, 1987). The problem with carbon- or gold-coating is that the coating cannot be removed.

(2) Charging can also be reduced by using a lower accelerating voltage, although this can decrease resolution and detail of the image.

(3) Using the back scattered detector but back scatter secondary electrons may only provide an image if the insulating layer is small enough that electrons can penetrate to an underlying conducting layer (Rochow and Rochow, 1978).

The diamond analysed using SEM (figures 3.4a and 3.9a-b) was studied using back scatter and cathodoluminescence, due to charging of the sample.

Cathodoluminesce is a technique which is commonly employed to study natural and synthetic diamonds. An electron beam is used to excite carriers in the sample and the subsequent recombination processes give rise to intrinsic and extrinsic luminescence effects. These emissions are however, limited to the surface layers of the sample due to the restricted penetration depth of the electron beam (Clark et al., 1996). The luminescence observed has a strong dependence on temperature, diamond growth sectors and electron beam density (Clark et al., 1996). The cathodoluminescene technique available was performed at room temperature, producing images in black and white. The images show features and structures in the diamond sample which are not apparent under normal SEM imaging or backscatter electron imaging.

For the purposes of this study there are 3 carbon polymorphs to be distinguished: this cannot be accomplished at present using the SEM. Structural detail of the crystal lattice is required which is obtained using selected area electron diffraction patterns (SAED) from a transmission electron microscope (TEM).

Although the SEM is unable to distinguish between the carbon allotropes of concern namely diamond, graphite and SiC it is able to provide detailed images of the morphology structures and textures observed in the grains. The SEM however is unable to provide crystallographic evidence such as a diffraction pattern to identify the different polymorphs. The use of electron back scattered diffraction (EBSD) is unfeasible as the mineral grains do not have a flat surface (R. Hough, Pers. Comm.), nor are they suitable for producing polished sections.

2.8.3. Transmission Electron Microscopy (TEM).

Detailed observation of the samples and mineralogical identification of the carbon phases was achieved using a Jeol 2000FX microscope with a Kevex Detector Delta 4 system and Quantum detector for EDS analysis, in the electron microscopy suite at the OU. The TEM allowed the analysis of much finer material and resolution at a much smaller scale, plus selected area electron diffraction (SAED) allows the mineralogical identification of phases. The TEM provides an image from electrons which pass through the sample and is projected onto a florescent screen, thus the thickness of the samples is vitally important.

A sample of the individual residues were loaded onto copper grids coated with a holey carbon film as a suspension in water or isopropanol using a disposable glass pipette. The grid was loaded into the TEM in a single tilt sample holder.

Carbon grains or grains with interesting morphologies were analysed using EDS and identified from their elemental composition and SAED diffraction patterns. Identified grains were photographed along with sufficient SAED diffraction patterns.

Measurement of the SAED patterns using the negatives provides confirmation of the composition of the grains on the basis of the spacing between spots and rings in the pattern. The different carbon polymorphs and silicon carbide have different characteristic d-spacings (listed in table 2.4).

Table 2.4. Characteristic d-spacing for carbon polymorphs and silicon carbide (SiC).

Polymorph	Radius (mm)	d-spacing Angstrom (A)
Graphite	5.99	3.35
Diamond	9.74	2.06
Londsdaleite	9.24	2.17
Carbyne	44.87	0.447
a-SiC	7.99	2.51
ß-SiC	7.96	2.52

An equation using the camera constant is used to calculate the d-spacing in angstroms (Equation 2.1).

Equation 2.1. (2.006/R) = d-spacing (Å)

R = radius in mm. 2.006 = camera constant.

The camera constant is obtained for each TEM using standards. To index ring patterns the diameter of the rings is measured and converted to the interplanar d-spacing using the camera constant then the values are compared to the standard values of the substance concerned (Andrews et al., 1971).

SAED patterns may be hard to interpretate as it has been found that flakes of sheet silicate minerals and quartz may combine with graphite to give carbyne d-spacings (Smith and Buseck, 1981; 1982). However experiments by Gilkes and Pillinger (1999) indicated that distinct carbyne diffractions can be obtained. SAED patterns can be used to confirm the identification of a grain on the basis of structural information and to characterise further structural features namely twinning, polycrystallinity, stacking faults and layering.

Images of the samples and pictures of the diffraction patterns are essential records of the analysis of the sample. Photomicrographs are obtained under vacuum on preloaded P8005 Agfa 23D56 6.5x9 cm film.

For TEM analysis sample grains need to be of a certain thickness, to enable the electron beam to penetrate the sample. Thick samples can be electron thinned to slowly strip away layers of the crystal structure and thin the sample. Alternatively the edges of grains can be analysed although this introduces the problem of selectivity.

The use of the TEM in examining shocked material, reveals many more features than previously described at much finer scale. More numerous PDF can be detected using the TEM rather than conventional optical microscopy (Goltrant et al., 1992). The full list of TEM and SAED is contained in appendix 3.

CHAPTER 3. IMPACT DIAMONDS IN THE RIES CRATER I: REGIONAL AND LITHOLOGICAL DISTRIBUTIONS IN FALLOUT IMPACTITES.

3.1. INTRODUCTION.

One of the main aims of this thesis is to investigate variations in the morphology, isotopic composition, type and amount of carbon within the Ries crater impactites. Each suevite from the Ries crater is characterised by a particular abundance pattern of crystalline rock types and shock metamorphism stages (Graup, 1981). With this in mind, samples of the impactites from different sites around the Ries crater were selected and demineralised as detailed in section 2.6. This included two fallout suevite breccias (lithic impact breccia with glass) from the Seelbronn and Ötting quarries which lie on opposite sides of the crater (figure 3.1). This could reveal variations in carbon stable isotopic compositions and degree of shock due to sampling of different parts of a heterogeneous basement. Further samples of impact melt glass, impact melt rock, lithic impact breccia (Bunte Breccia), shocked granite and shocked gneiss were also prepared and analysed. Samples from the Nördlingen core 1973 (N-73) are referred to where appropriate but are mainly discussed in chapter 4.

The carbon content of whole-rock samples from around the Ries crater, can be used to trace lithologies containing the most carbonaceous material, that in turn may have contributed to the formation of impact diamonds. This carbon may be graphite as in Popigai (Masaitis, 1995), coal as in Kara (Ezersky, 1982; 1986), carbynes (El Goresy and Donnay, 1968; Whittaker, 1978 and Heimann, 1994), a combination of graphite and carbonates (Hough et al., 1995c) or amorphous and organic carbon. Separated fractions of glass and lithological fragments were extracted from these impactites wherever possible and their carbon contents and stable isotopic compositions determined. Further carbon stable isotopic measurements were made for acid-demineralised residues of the Ries samples as well as extracted graphite and diamond grains.

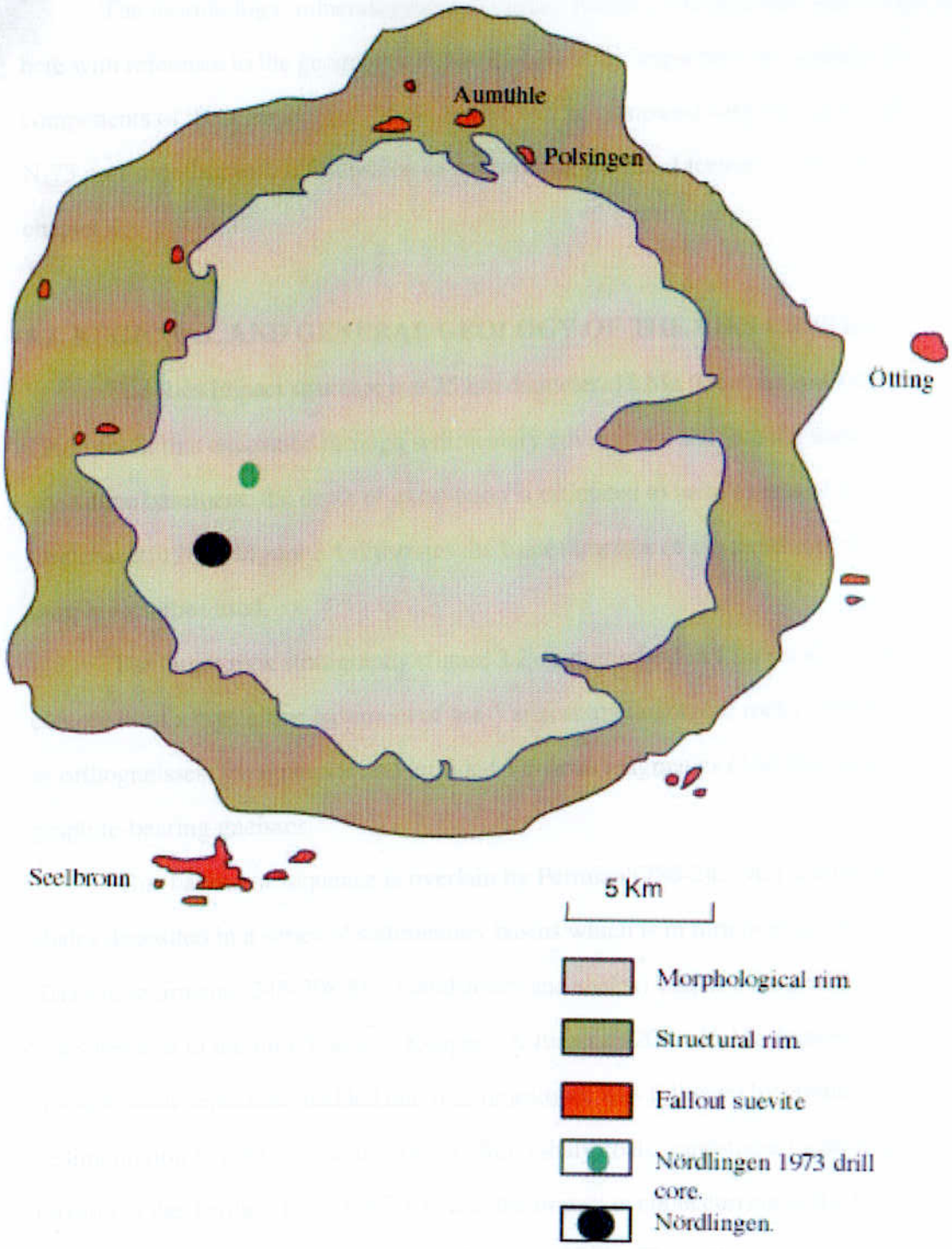

Figure 3.1. Schematic map of the Ries crater showing sample localities, Nördlingen and Nördlingen drill core 1973.

Scanning and transmission electron microscope techniques (SEM and TEM) were employed to study the morphological and crystal structures of the grains within the residues.

The morphology, mineralogical and carbon isotopic compositions are discussed here with reference to the geographical distribution of the impactites and individual components of these impactites. These results will be compared with those from the N-73 core together with a discussion of the possible diamond formation mechanisms in chapter 4.

3.2. REGIONAL AND GENERAL GEOLOGY OF THE RIES CRATER.

The Ries impact structure is a 25 km diameter, 15 Ma (Gentner and Wagner, 1969) crater that excavated through sedimentary cover rocks and into the underlying crystalline basement: the depth of excavation is estimated to be in excess of 4 km (Von Englehardt, 1984). Figure 3.1 illustrates the basic structure of the crater and shows the sample localities used.

The target rock stratigraphy (figure 3.2), summarised in Chao et al. (1978) comprises of a crystalline basement of pre-Variscan metamorphic rocks (350 Ma) such as orthogneisses, paragneisses and intruded Variscan magmatics (330 Ma) including graphite-bearing gneisses.

This basement sequence is overlain by Permian (286-245 Ma) sandstones and shales deposited in a series of sedimentary basins which is in turn overlain by terrestrial Triassic sediments (245-208 Ma) (sandstones and shales) with a widespread marine transgression in the mid-Triassic (Keuper). A Jurassic (208-146 Ma) marine transgression depositing bedded and reef limestones was followed by continental sedimentation in the Cretaceous (146-65 Ma) (shaly coals, sandstones) with widespread erosion in the Tertiary period (65-1.8) and the impact event occurring in the Higher Tortonian, around 15 Ma (Gentner and Wagner, 1969). The crater was subsequently filled with fresh water lacustrine sediments, carbonates and sulphur-rich shales until the mid-Miocene. During the Quaternary period, uplift and erosion led to the exposure of the impact lithologies around the crater rim and formation of the present day topography.

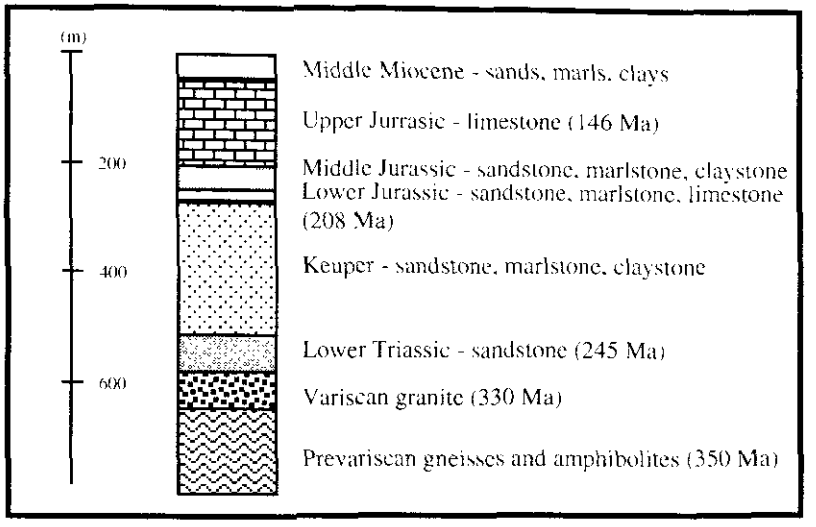

Figure 3.2. Pre-impact stratigraphy of the Ries crater area. Adapted from Von Englehardt (1990).

The impact lithologies are varied but three main divisions may be identified on the basis of the lithological fragments they contain as well as the degree of shock metamorphism. Extensive work has been carried out on the impact deposits and has been summarised in a review by Von Englehardt, (1997).

3.2.1. Moldavite tektites.

Tektites from the Ries are preserved as the Central European strewn field and found up to 350 km from the Ries crater. These glassy, lustrous and often bright green samples have been shaped by their passage through the atmosphere and subsequent fragmentation as well as alteration within the host sediments (Bouska, 1994). They are believed to have formed from surficial Miocene sands transformed to glass by the fore shock-wave of the Ries impact (Von Englehardt et al., 1987; Meisel, 1997). The tektites commonly have etched and ornamented surface structures which have been attributed to intense hot plasma attack for between 1-3 seconds during their formation (David, 1972). Subsequently, experimental and field evidence has shown that pyramidal surface structures may be formed by alkaline conditions in clay-rich sediments and pitting by acid conditions in sandy gravel deposits (Bouska, 1994). A demineralised sample of a 4

g piece of Moldavite glass failed to reveal any acid resistant mineral inclusions such as zircon, diamond or graphite (R. M. Hough, Pers. Comm.).

3.2.2. Bunte Breccia (Lithic impact breccia).

The Bunte Breccia (Bunte Trümmermassen) is a lithic impact breccia which comprises > 90 vol% of all the impact deposits at the Ries crater (Hörz, 1982) and forms a near continuous curtain of ejecta underlying the patchy suevite deposits (Chao et al., 1978). The breccia is 90-95 vol% sedimentary in composition but includes fragments of all the rock types in the Ries stratigraphic column (Hörz et al., 1983). The sedimentary fragments show no signs of shock, indicating that the sedimentary column was not affected by shock pressures > 10 Gpa (Von Englehardt, 1990).

3.2.3. Suevite (Polymict impact breccia with glass).

Approximately 92 suevite localities have been identified in and around the Ries crater area and were described in detail by Chao et al. (1978). The suevites exhibit all degrees of shock metamorphism; glass drop spherules in the groundmass give 600 °C thermoremnant temperatures with an initial freezing at 2000 °C. This attests to high temperature deposition conditions (Graup, 1981). High pressure mineral phases such as coesite and stishovite, along with shock deformation features such as deformation lamellae, kinkbands and planar deformation features, indicate shock pressures ≤ 35-45 Gpa (Graup, 1990). The impact glass in the suevite is attributed to the shock fusion of gneisses at pressures in excess of 60-80 Gpa (Von Englehardt, 1997). The suevite may be divided into fallout suevite, deposited in isolated areas up to 10 km beyond the crater rim (Von Englehardt et al., 1995) and fallback suevite which fills the crater cavity. Fallback suevite is distinct from fallout suevite in that it contains less glass (under 5 % compared to 15 vol%) and no aerodynamically shaped bombs just smaller isometrically shaped bodies (Stöffler et al., 1977).

3.3. OCCURRENCE AND DISTRIBUTION OF DIAMOND AND GRAPHITE IN IMPACT PRODUCED ROCKS OF THE RIES CRATER.

Diamonds were identified in suevite and glass samples from the Ötting and Seelbronn quarries (Abbott et al., 1996) as individual grains observed within the residues using optical microscopy and on a finer scale using transmission electron microscopy (TEM). Diamonds were also found in shocked gneiss from the Aumühle quarry and in an impact melt rock/suevite from the Polsingen quarry. Diamonds were not detected in a residue from the Bunte Breccia sample. Table 3.1 lists the grains (graphite, diamond, rutile and silicates) found in the samples throughout the analyses.

Table 3.1. Composition of grains from SEM and TEM analysis of acid resistant residues.

Sample	SEM	TEM
	Composition	Composition
OQGB	Zircon, Al-Fe-Mg-silicates, rutile graphite, diamond.	Graphite and diamond
OQS	n/a	Graphite and diamond
SBS	Zircon, Al-Fe-Mg-silicates, rutile, Cr-Fe-Mg-spinel, graphite.	Graphite and diamond
PIMR	n/a	Graphite and diamond
AQG	n/a	Graphite and diamond
BB	n/a	Graphite and rutile

The general structure of the underlying basement rocks was extrapolated by Graup (1981) and is shown in figure 3.3. This illustrates how the basement composition and structure vary across the target area, indicating that there may be detectable differences in the abundance and form of diamonds within the impactites depending on which lithologies they are primarily derived from. Radial variation in the distribution of diamonds has been identified at the Popigai crater (Masaitis, 1998) but has yet to be identified at the Ries (Schmitt et al., 1999).

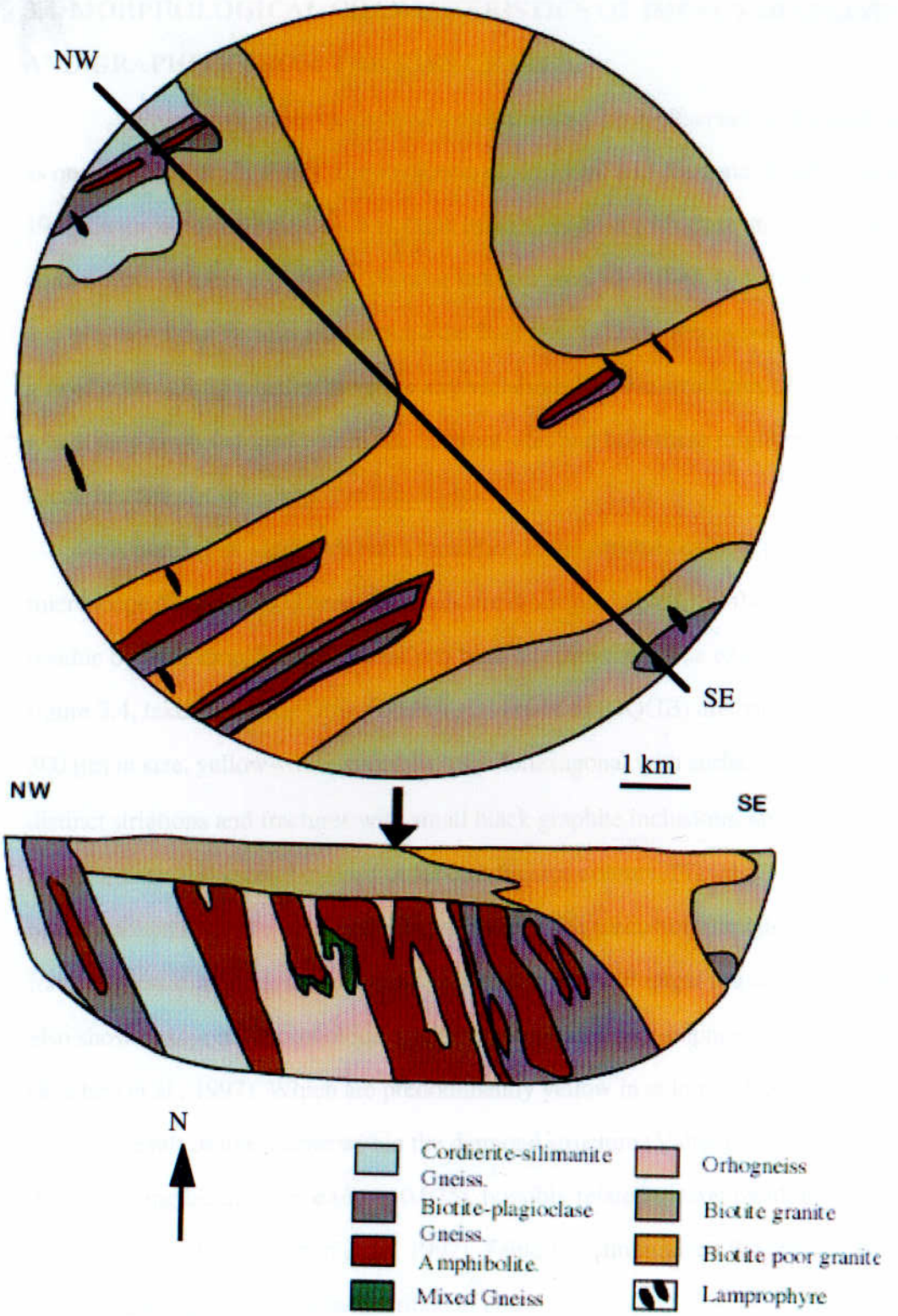

Figure 3.3. Structure and lithology of the pre-impact basement, Ries crater (After Graup, 1978).

3.4. MORPHOLOGICAL CHARACTERISTICS OF IMPACT DIAMONDS AND GRAPHITE FROM THE RIES CRATER.

A wide range of shock-derived structures have been observed in minerals such as quartz (Horn et al., 1981), zircon (Kamo et al., 1996) and diamond (Koeberl et al., 1997) in impact lithologies, such as lithic impact breccias with glass and individual components of these e.g. gneiss. Similar features were identified in diamonds, zircon and graphite from various sites around the Ries crater. These were observed with the aim of determining whether there are any variations in these structures or the degree to which they are developed within the different sites and how these might relate to the shock histories of the respective lithologies.

A number of diamonds were identified in the residues using a petrological microscope (figure 3.4). These diamonds are distinguishable from the rest of the residue by their morphology, colour and high birefringence. The examples shown in figure 3.4, taken from the Ötting quarry glass residue (OQGB) are between 150 and 300 μm in size, yellow-white in colour, pseudohexagonal with surface cross-hatching, distinct striations and fractures with small black graphite inclusions, strong birefringence and second to third order interference colours. Figure 3.4a. shows rotation of the stacked layers relative to the basal plane of the precursor graphite structure. The form of these diamonds mirrors those reported from the Popigai impact crater which also show hexagonal morphologies, lamellar structures and graphite flake inclusions (Koeberl et al., 1997). Which are predominantly yellow in colour, a feature considered to be the result of lonsdaleite within the diamond structure (Valter et al., 1992) and display strong birefringence (up to 0.025), possibly related to strain within the crystalline structure (Koeberl et al., 1997). Table 1.3. summarised the characteristics of many of the impact diamonds described to date.

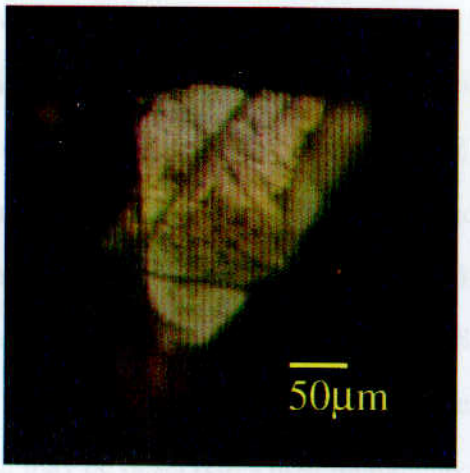

(a) Plane polars.

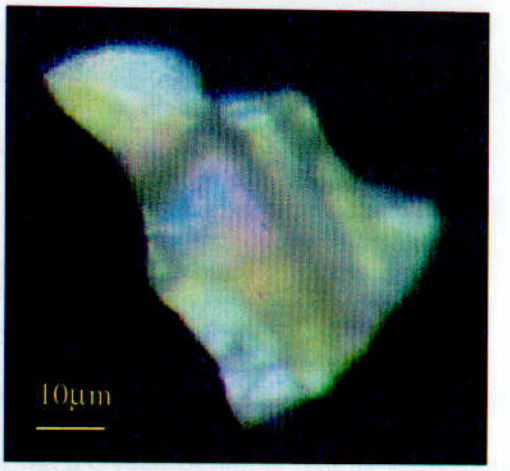

(b) Crossed-polars.

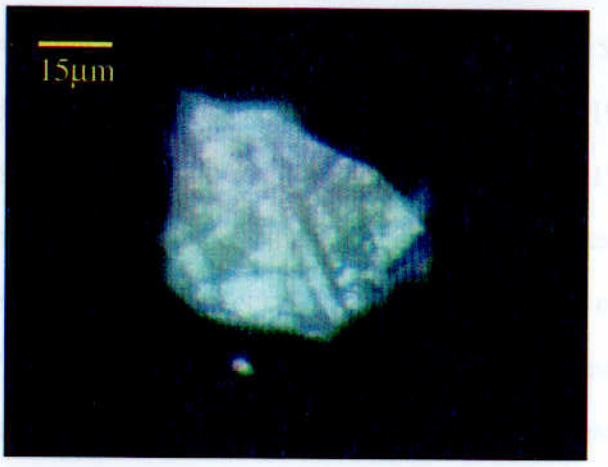

(c) Crossed polars

Figure 3.4. Optical microscope photomicrographs of diamonds from OQGB residues. (a) Yellow-white triangular layered diamond (plane polars). Surface shows linear cross-hatching features. (b) Layered white diamond (crossed-polars). (c) Layered white diamond (plane-polars). Surface shows parallel linear hatching.

Structural defects in minerals related to the passage of shock waves during an impact event have characteristic forms. Shock produced impact diamonds are considered to be unequivocal indicators of past impact events (Langenhorst et al., 1999). Microscope investigations of these impact diamonds can show structural and morphological characteristics indicative of shock (e.g. kink bands) or vapour phase formation mechanisms. Lesser degrees of shock may induce crystallographic dislocations in minerals such as kink bands, mechanical twins and deformation bands

known as extinction bands (Stöffler, 1972). Shock metamorphism of graphite in the elastic wave may result in the formation of kink bands, parallel to graphite [0001] and planar fractures parallel to graphite [1120] prior to the transformation to diamond during shock-front propagation (Valter and Yerjomenko, 1996). This has been used to explain inherited features seen in diamond-lonsdaleite paramorphs from Popigai, Zapadnaya, Terny and Ilyinets (Valter, 1986; Valter and Yerjomenko, 1996).

The images shown in the subsequent sections illustrate the variety of structures which may be observed. These include layering, a crystallographic feature of graphite which may be preserved in shock derived diamonds, linear features, etching and pitting, skeletal grains, polycrystalline grains, twinning and stacking faults. Some of these features have been described from other impact craters (Rost et al., 1978; Hough et al., 1995c; Masaitis, 1994; Koeberl et al., 1997 and Langenhorst et al., 1999) and are compared with features observed in this study. The observed features and their variation throughout the crater are discussed (sections 3.4) and subsequently compared with the results from the N-73 drill core in chapter 4. These observations combined with mineralogical associations and shock metamorphism histories are used to suggest which mechanisms of impact diamond formation might account for the known features.

3.4.1. Layered grains (≤5 - 300 μm).

Many of the carbon grains observed under the SEM showed clear layered structures which were observed both parallel and perpendicular to the c-axis of graphite. The side view of a sample from the Seelbronn quarry residue (figure 3.5) shows three primary layers and within these a number of less distinct finer layers. These features may be an artefact of slight compositional changes within certain layers, changes in the degree of crystallinity or orientation of the plates. Small-scale chemical and structural heterogeneities such as rotational layer disorder can persist in graphite depending on the degree of crystallinity and maturity (Rietmeijer, 1991). This is due to the gradual release of oxygen, hydrogen and nitrogen from organic matter during graphitisation (Grew, 1974; Itaya, 1981; Buseck and Huang, 1985).

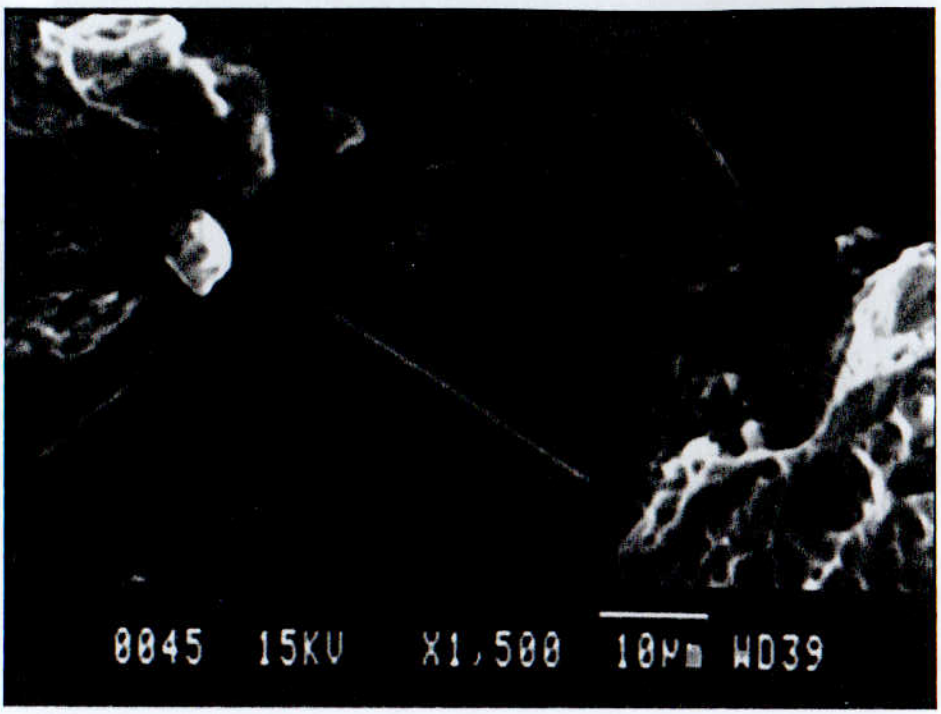

Figure 3.5. Scanning electron microscope image of a layered carbon grain from the SBS residue. The image shows 3 clear primary layers marked by high relief, with finer secondary layers. [x1,500, 15 kV].

Layered structures show a number of forms, simple layering as shown in figure 3.5 or more complex layering as illustrated by grains in the OQGB residue (figures 3.6a-b). These layers appear to be graphitic but are disturbed and curled, a form reminiscent of partially combusted carbon material such as wood or paper, the sample also shows the additional feature of two sets of linear decoration (discussed in section 3.3.2).

Planar graphitic fragments believed to exist in carbon vapours curl up in order to minimise dangling bonds resulting in the formation of fullerenes (Zhang et al., 1986) when exposed to high temperatures in the order of > 4000 K (Robertson et al., 1992; Ugarte, 1992). So these curled layers (figure 3.6a) may reflect a less extreme reaction of the carbon material to elevated temperatures, 800-1200 K (Robertson et al., 1992) insufficient to result in the combustion, melting or vapourisation of graphite (≤ 4000 K).

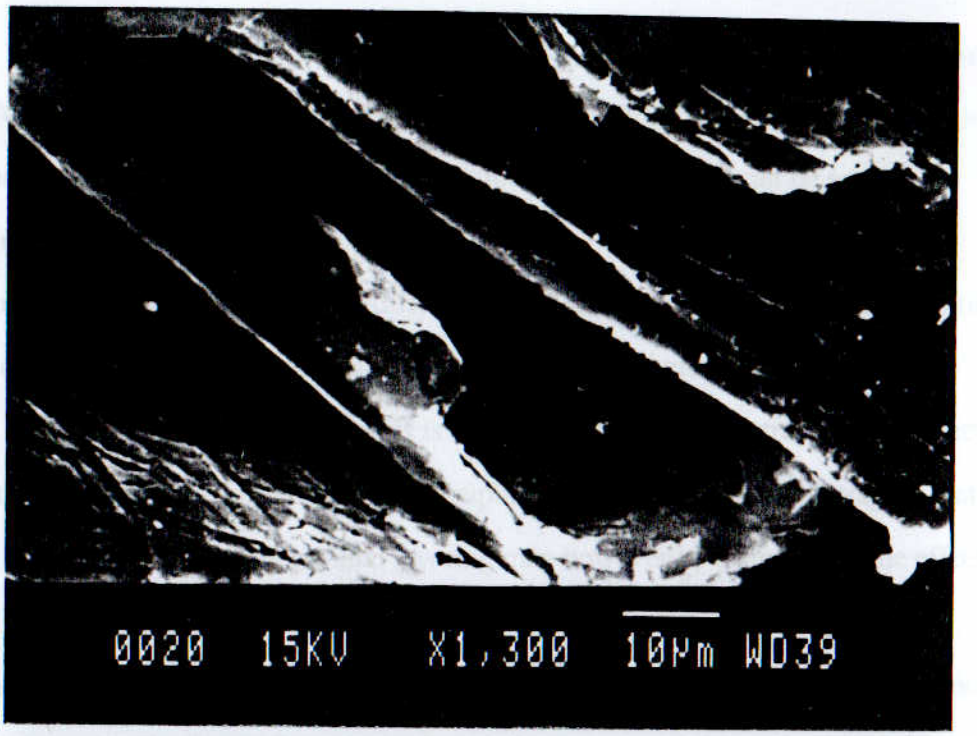

(a)

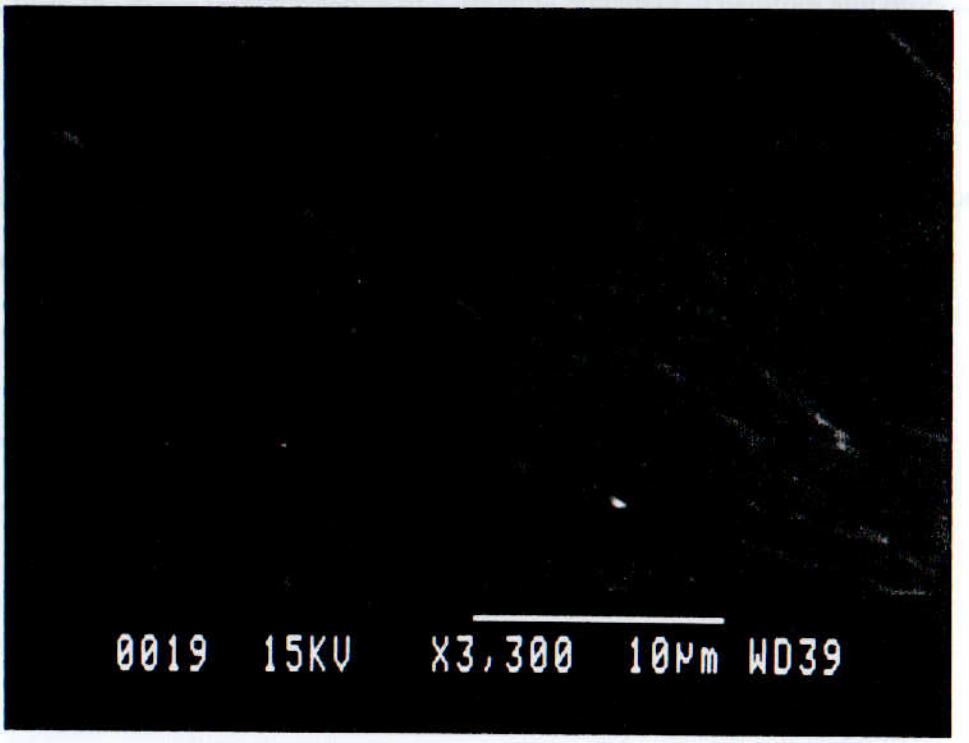

(b)

Figure 3.6. (a) Scanning electron microscope image of a carbon grain from the Ötting glass bomb residue with two sets of planar features at 60°. [x1,300, 15 kV]. (b) High magnification scanning electron microscope image of surface planar features on a layered carbon grain from the Ötting quarry glass bomb residue. [x3, 300, 15 kV].

Layered structures were observed at a much finer scale using the TEM. Figure 3.7. shows a very elongate (10-15 μm), narrow (1-1.5 μm) diamond from the gneiss residue from the Aumühle quarry with a number of layers which can be seen at the margins with numerous short black parallel stacking fault lamellae. Many of the diamonds found show a number of different plates on the SAED patterns representing individual overlying layers with stacking rotation or misorientation.

The layering in these diamonds is a relict crystallographic structure inherited from the precursor graphite. Layering in graphite is an intrinsic crystallographic feature of the mineral, this simple horizontal layering may however be distorted by the effects of a low degree of shock metamorphism. The obvious preservation of this graphitic structure along with hexagonal and planar structures strongly suggest that the diamond results from the direct transformation of a graphite precursor. Therefore any proposed diamond formation mechanism for crystals with these morphologies must preserve the pre-existing crystal structure yet allow recrystallisation as polycrystalline diamond. This excludes mechanisms involving a liquid or gaseous phase with the growth of diamond from a carbon feedstock or via diffusion, but requires rearrangement of the carbon bonds.

Figure 3.7. Bright field transmission electron microscope (BFTEM) image of an elongate, layered diamond from the Aumühle quarry gneiss. [x10 k, 200 kV, scalebar 500 nm].

3.4.2. Linear orientation features in layered and skeletal grains (≤ 5-300 μm).

These have a number of forms, from narrow parallel to sub-parallel lines, cross-hatched parallel to sub-parallel lines, ridges and fractures. Figure 3.6a-b shows close-up images of two sets of continuous linear planar features intersecting at 60° on the surface of a layered carbon crystal from the Ötting quarry glass residue. Figure 3.8b shows a diamond grain from the Seelbronn quarry suevite residue under the SEM, the sample shows clear layering and a linear surface ornamentation along the long axis of the grain. Linear structures have also been observed in the skeletal diamonds (section 3.4.4) from the Seelbronn suevite (figure 3.13a-b), where the individual crystallites within the diamond appear to show a linear orientation along the long axis of the sample. This can often be seen on SAED patterns as a streaking of the individual spots.

(a)

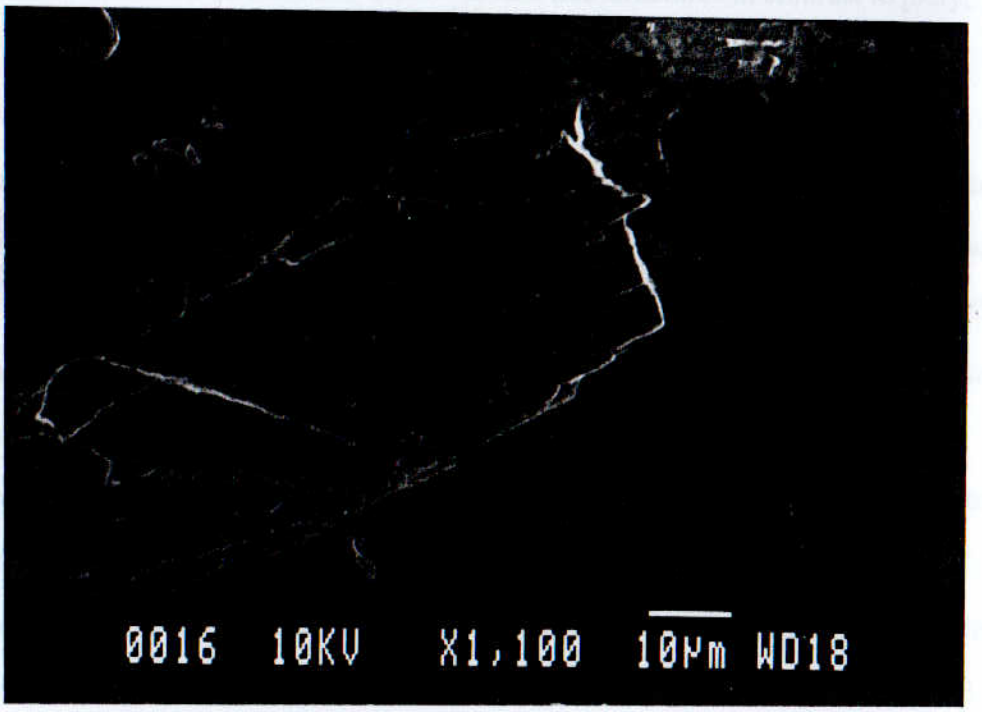

(b)

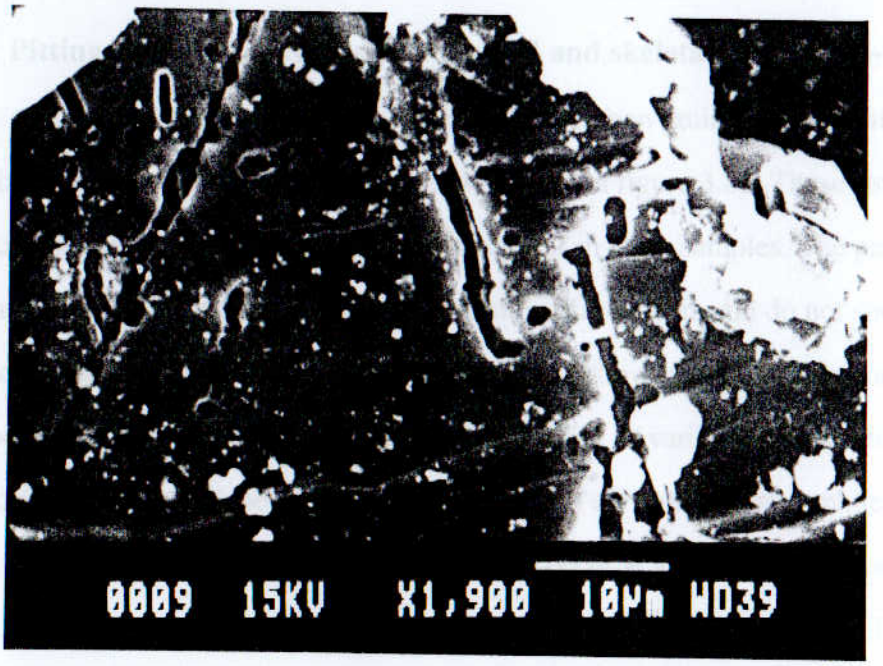

Figure 3.8. (a) SEM image of a carbon grain from the Seelbronn quarry suevite residue showing linear surface textures orientated along the long axis and needle like projections. [x1,100, 10 kV]. (b) SEM image of etching and pitting of a layered carbon grain from the Ötting quarry glass bomb residue. Elongate etch pits are visible on subsurface layers of the grain. [x1,900, 15 kV].

Skeletal diamonds form narrow needle like structures in contrast to platy, layered structures. Skeletal diamonds do not show clear layered or apographitic structures rather they are composed of numerous individual crystallites (≤ 1 μm) forming fine grained needle-like structures. Many of the blocky diamonds also show faint linear structures representing individual crystallites with preferred orientations.

The features may represent palimpsest or relict features (Valter et al., 1992) inherited from the precursor carbon or PDFs akin to those documented in shocked quartz and zircons (McIntyre, 1962; Goltrant et al., 1992; Bohor et al., 1993) or. Inherited palimpsest structures suggest a mechanism involving direct transformation without the destruction of the pre-existing structure. In contrast linear structures representing the preferred orientation of crystallites may have been formed as a direct result of the formation mechanism. This is discussed in further detail in section 3.4.4. with reference to skeletal structures which show strong preferred orientations.

3.4.3. Pitting and etching features in layered and skeletal grains (≤ 5-300 μm).

A form of etching which was observed in a carbon grain from the Ötting quarry glass bomb residue under the SEM, is shown below in figure 3.8b. These structures are distinct from any seen in the planar graphitic grains in other samples. The pits can be seen not only in the surface layer but also in subsurface layers and do not show the same orientation throughout. Rather, they appear to follow varying orientations which may be related to the orientation of the particular plane or variations in the structural or compositional nature of the sample e.g. the degree of crystallinity or graphite maturity.

Surface etching of the samples appears to occur at all scales, from coarse structures (5-20 μm) which follow fractures, to nanometre scale structures (10-50 nm). Surface etching pits on diamond can be observed in the examples shown in figures 3.9a-b. The diamond from the Ötting quarry glass bomb (OQGB-D1) was white-yellow in colour under the optical microscope. 300 μm in size and triangular with pitting and fractures on two scales. Etched fractures cut across the layered structure of the sample and at a higher magnification small etching pits were observed which sometimes formed

in linear trails across the surface of the grain. The cathodoluminescence image (figure 3.9b) showed no zonation just faint structural differences and areas of graphite. The etching structures are similar to those seen in a diamond from the Seelbronn quarry suevite (figure 3.10a) which shows linear features along the long axis of the grain, layering and a linear trail of ovoid etching pits beneath a remnant of another layer which were not parallel to the axial foliation. Suggesting the preferential etching of a structural weakness that is not parallel to the preferred orientation of the crystallites and is not visible under the SEM.

A high magnification image of OQGB-D1 (figure 3.10b) illustrates not only the fine linear etching structures but also irregular surface etching pits a few nm in diameter, which give the sample a granular texture. Very fine-scaled (5-20 nm) etching on the OQGB-D1 sample is illustrated below in figure 3.11a. The figure shows an area from the bottom centre of the sample which has a granular texture, where etching may reveal polycrystallinity in the diamond (removing individual crystallites) or the removal of re-graphitisation features. Similar corrosion and etching was reported for diamonds from Lappäjarvi which show surface structures attributed to the removal of individual crystallites (Langenhorst et al., 1999). However OQGB-D1 was extracted from the residue following the HCl/HF stages alone and had not been exposed to chromic or fuming perchloric acid which would remove graphite coatings. Thus the structures are more likely to be the result of etching, for example by hot alkali gases such as OH-, Na and K (Vishnevsky and Raitala, 1999), silicate melts (Langenhorst et al., 1999) or the removal of regraphitisation coatings formed during the impact. Therefore it is considered that they do not represent features attributable to the acid digestion process itself.

(a)

(b)

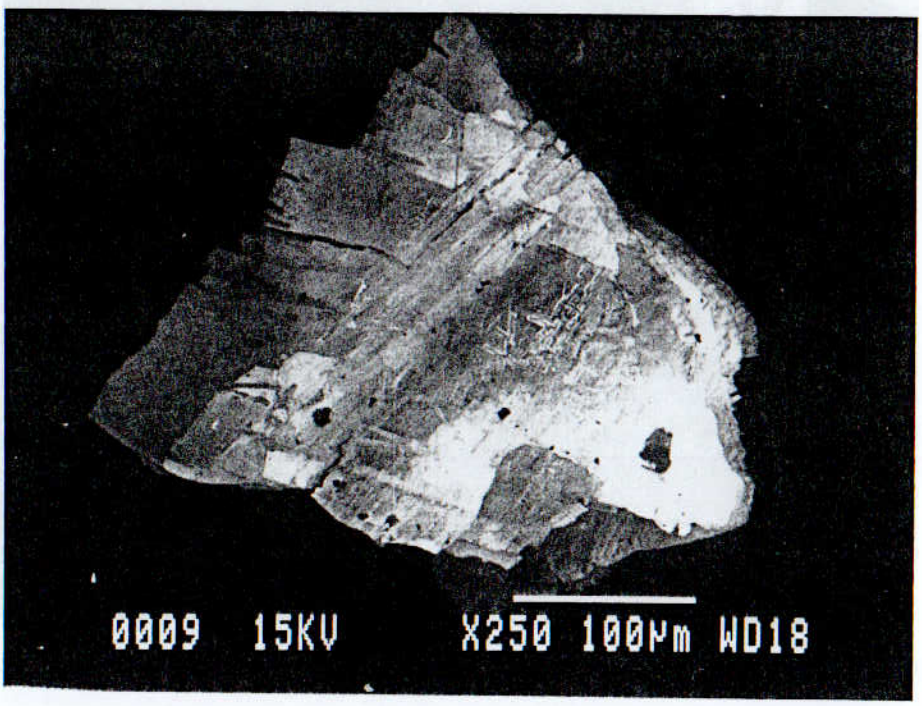

Figure 3.9. (a) SEM backscattered electron image of a layered diamond extracted from the Ötting quarry glass bomb (OQGB-D1) showing clear layering and surface etching. [x250, 15 kV]. (b) SEM cathodoluminescence image OQGB-D1 showing individual layers and dark areas representing graphitic inclusions or remnant twins. [x250, 15 kV].

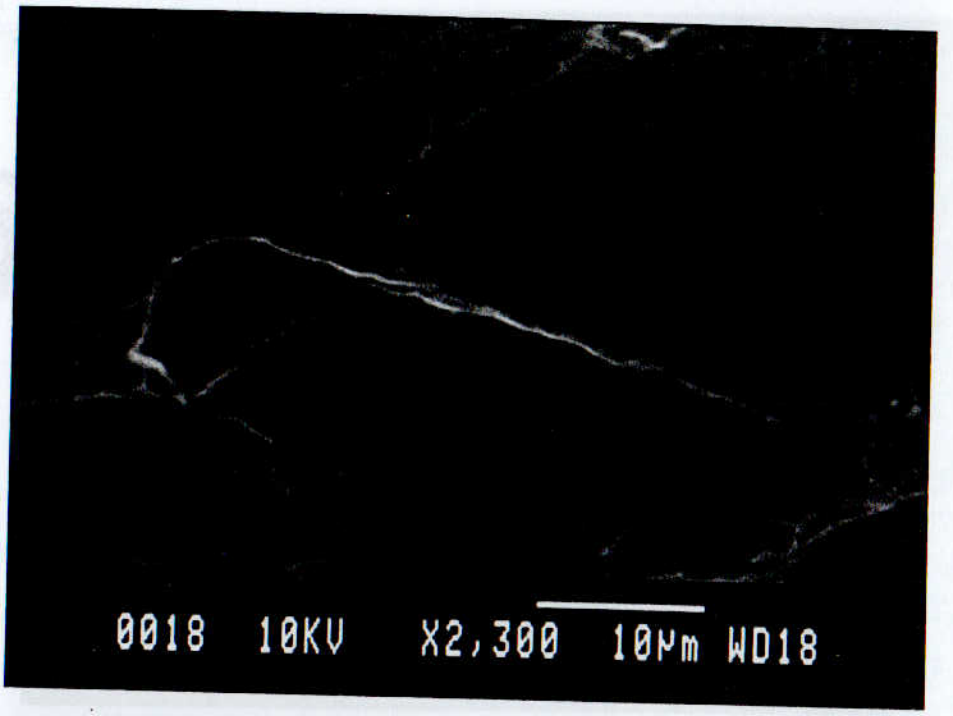

(a)

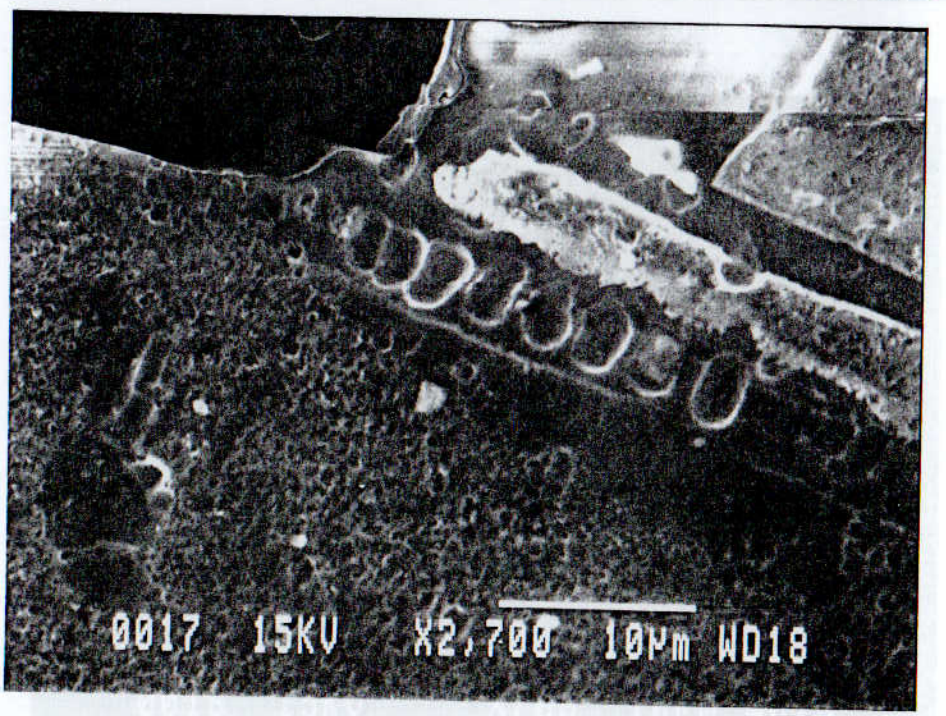

(b)

Figure 3.10. (a) High magnification SEM image of elongate carbon grain from the SBS residue showing surface lineation, layering and etch pits. The etch pits follow a linear trend across the main linear feature. [x2,300, 10 kV]. (b) SEM backscattered electron image of OQGB-D1 showing linearly distributed etch pits and finer scale surface etching features. [x2,700, 15 kV].

(a)

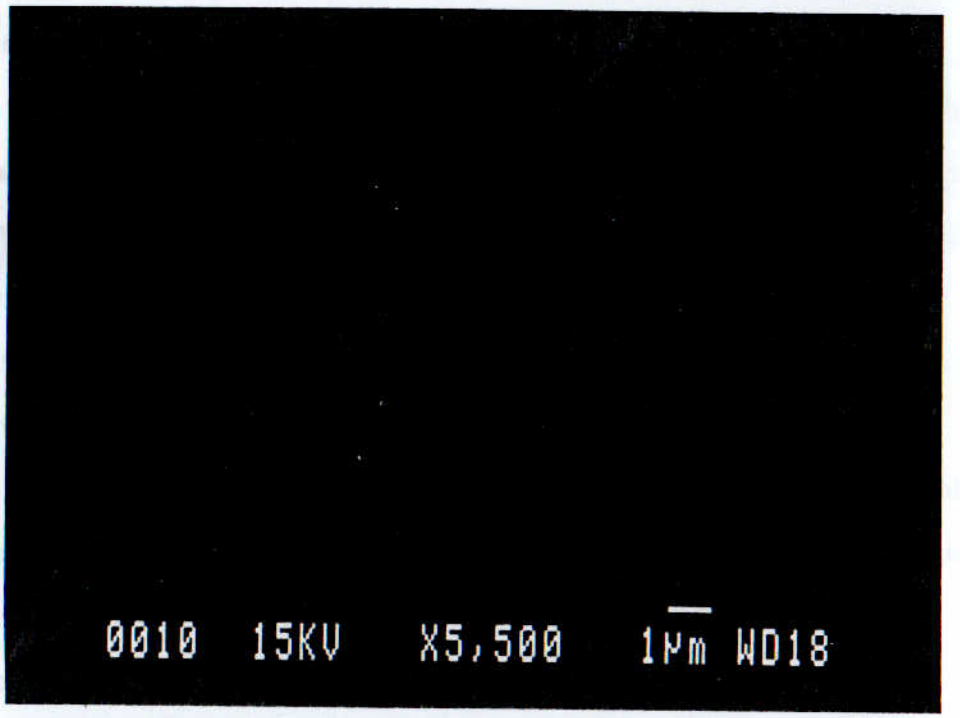

(b)

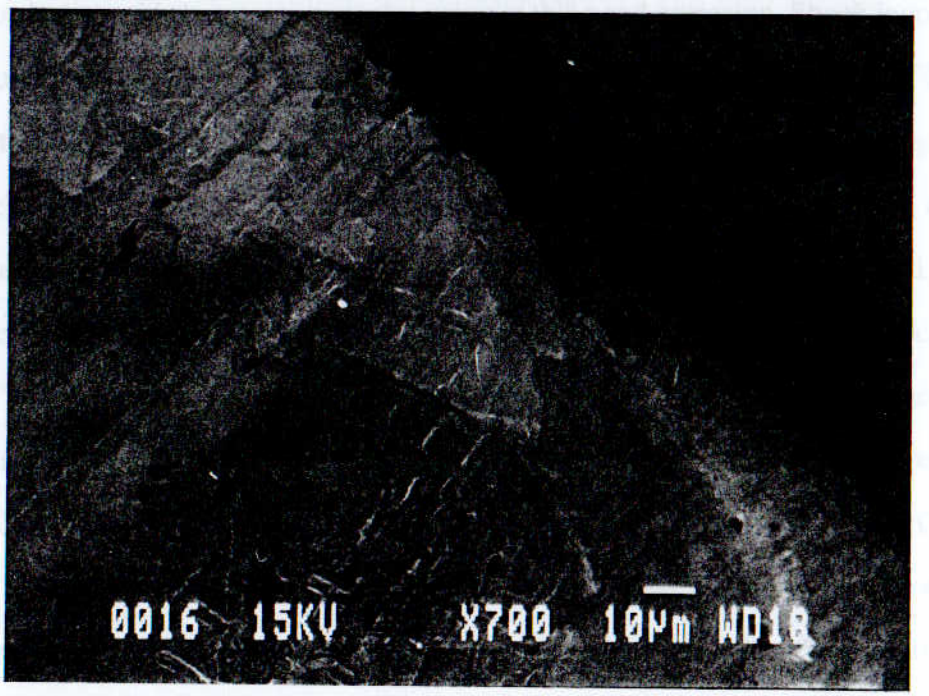

Figure 3.11. (a) SEM backscattered electron image of surface etching features on OQGB-D1. [x5,500, 15 kV]. (b) Cathodoluminescence SEM image OQGB-D1 showing linear cross-cutting surface etch pits and needle like etched margins on several layers. [x700, 15 kV].

The surface structures shown in figure 3.11b are similar to the features seen in figures 3.9a-b.

Figure 3.12a shows an etched and corroded blocky diamond with a strong sub-parallel linear trend across the grain. These linear structures may represent stacking faults or ridges of diamond crystallites in preferred orientation. This may represent etching of an apographitic diamond (Langenhorst et al., 1999) or the incomplete transformation of a mixture of graphitic and poorly graphitic amorphous carbon to graphite.

Pitting features may be the result of etching through oxidation and partial combustion of carbon during or after diamond formation by highly charged ionised gases within the impact fireball (Vishnevsky and Raitala, 1999). Post-formation graphitisation, when temperatures remain high (≤ 2000 K) following diamond formation, or preferential etching of material along structural planes or less crystalline areas during acid treatments may also cause etching and corrosion. Shock induced disruption of the crystal lattice in isolated areas may result in the formation of less crystalline areas, which would be more susceptible to impact associated etching or acid attack. Diamond is extremely inert and not affected by any acids or chemicals, except those which act as oxidising agents at high temperatures, ≤ 700-1300 K (Field, 1992) which is well in excess of the temperatures used during the acid digestion process (30-120 °C). As noted previously the diamond (OQGB-D1) showing etching structures (figure 3.9-3.11) was not exposed to chromic or perchloric acid or temperatures > 30-60 °C. Other samples which show etching were exposed to perchloric acid (120°C) and may show some reaction to ionised acid (H_3O^+) in solution which can remove small diamond particles from diamond films by reaction with surface H^+ (Gi et al., 1995). Perchloric acid will remove amorphous carbon and poorly graphitic carbon and reveal graphitisation etching structures.

Figure 3.12. BFTEM image of an etched blocky diamond from the Ötting quarry suevite. [x20 k, 200 kV, scalebar 200 nm].

This may indicate that the diamond is a product of the incomplete transformation of graphite or incomplete secondary graphitisation of diamond. Etching features do not on their own provide evidence for the mechanisms of transformation but may highlight other structural features that do, (for example, preferred orientations in crystallites within a larger polycrystalline sample, which suggests orientated growth due to nucleation in an orientated stress field, see section 3.4.5).

3.4.4. Skeletal grains (≤ 5-15 μm).

Skeletal diamond structures were observed in many of the samples in this study. The example shown in figures 3.13a-b from the Seelbronn suevite appears to be composed predominantly of cubic diamond although small areas near the tips of the needles also show graphite diffraction maxima (inset SAED). Similar skeletal structures were observed in the OQSR (figure 3.14a-b) and in diamond and diamond/SiC intergrowths (Hough et al., 1995c).

The inset SAED patterns support the interpretation of the features seen in the bright-field images. The patterns show polycrystalline ring patterns and a linear orientation to the smeared spots, representative of a preferred orientation to the crystallites or crystal defects such as stacking faults. This is evident in the linear skeletal structure along the long axis of the grain with the needle like projections following this orientation.

The needle-like structures are extremely delicate in appearance and may be as fine as a few nm in diameter. Figure 3.15a illustrates this with an image of a fine grained 1-5 nm elongate needle protrusion from a larger (2-5 μm) diamond grain from the OQGBR. A further example from the Seelbronn suevite (figure 3.15b)

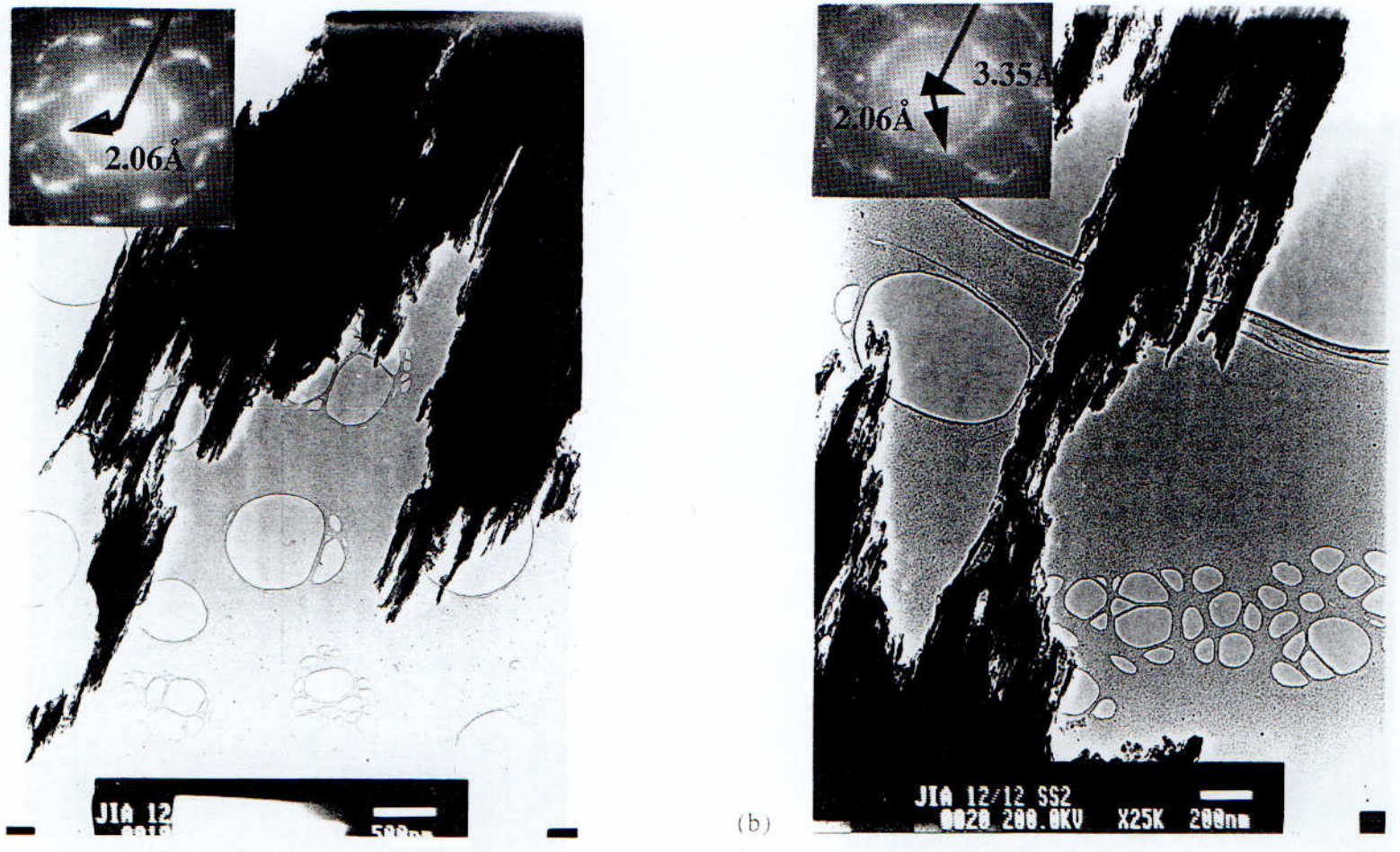

(a) (b)

Figure 3.13. (a) BFTEM image showing skeletal polycrystalline diamond from the SBS, with marked linear orientation of crystallites along the long axis of the grain. Inset SAED shows diamond at 2.06 Å. [x25 k, 200 kV, scale bar 500 nm]. (b) BFTEM image showing same sample with needle like structure, distinct linear orientation of individual crystallites along the long axis. Inset SAED shows diamond at 2.06 Å and graphite at 3.35 Å. [x25 k, 200 kV, scale bar 200 nm].

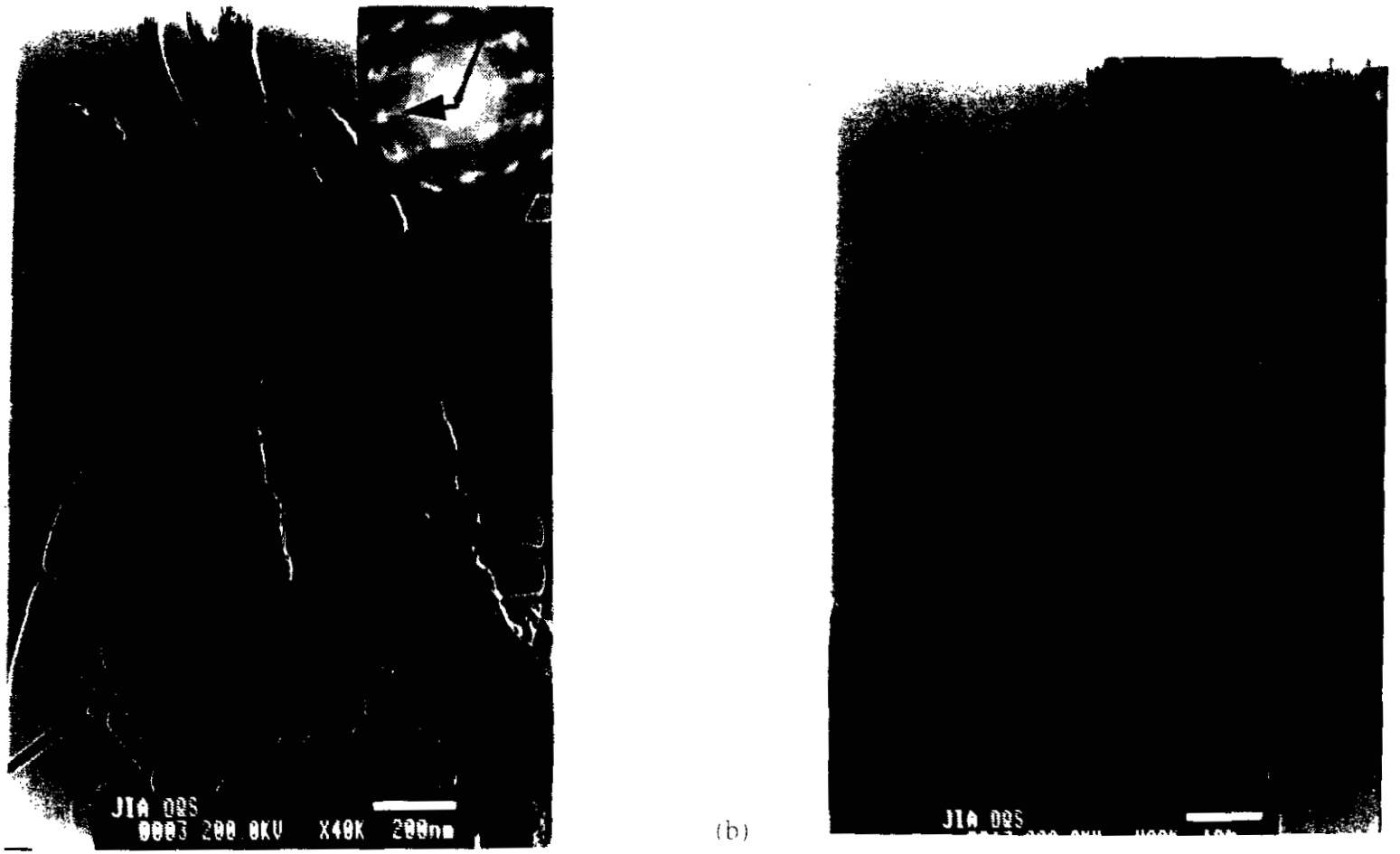

Figure 3.14. (a) BFTEM image of skeletal and etched diamond from the Ötting quarry suevite. Inset SAED shows diamond 2.06 Å. [x 40 k, 200 kV, scalebar 200 nm]. (b) High magnification BFTEM image. [x 80 K, 200 KV, scalebar 100 nm].

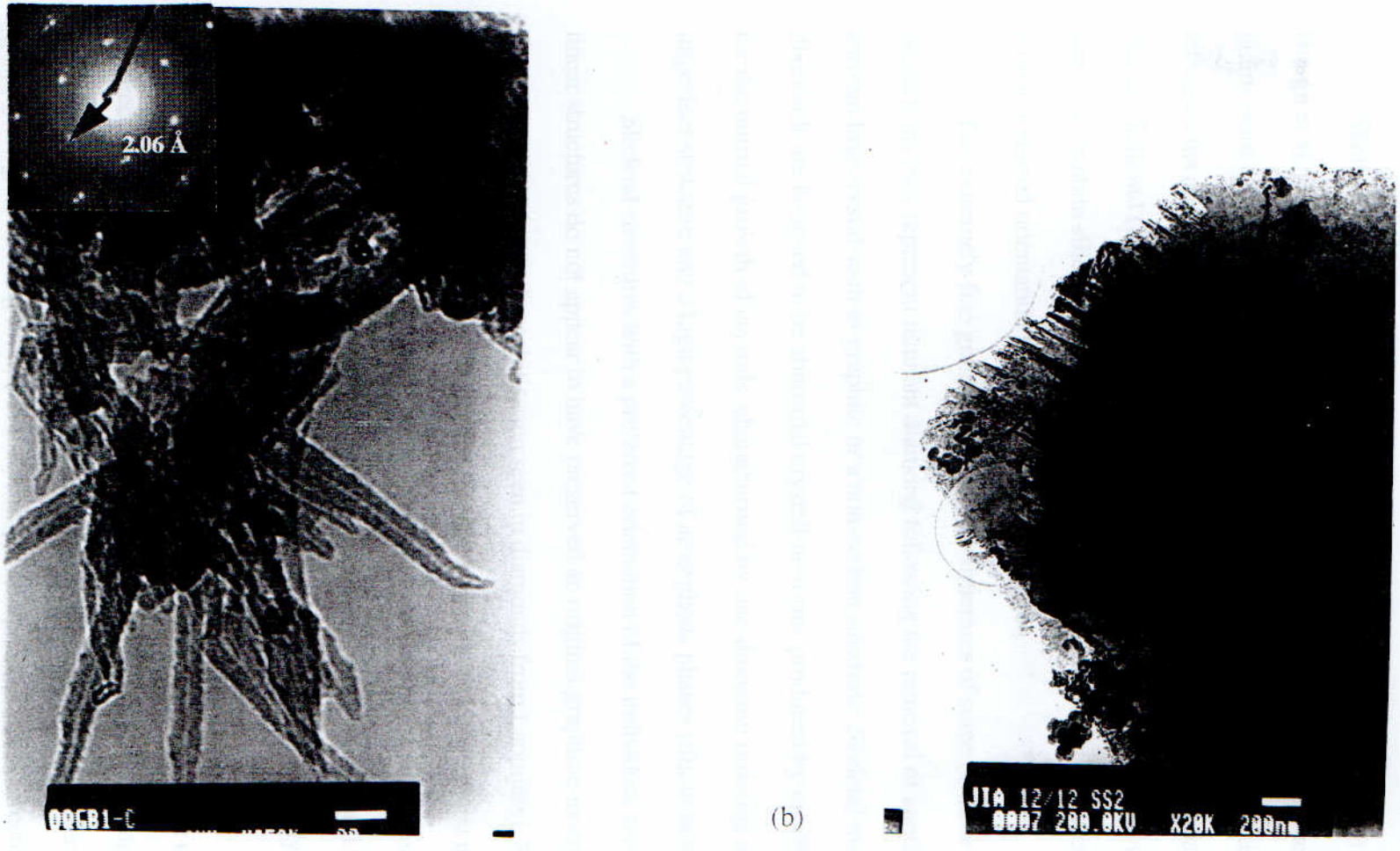

Figure 3.15. (a) BFTEM image of skeletal diamond from the Ötting quarry glass bomb. [x 80 k, 200 kV, scalebar 20 nm]. (b) BFTEM image of diamond from the Seelbronn quarry suevite with needle-like skeletal margins highlighting the linear orientation of crystallites. [x 20 k, 200 kV, sclaebar 200nm].

shows a series of 20 nm skeletal needles along the edge of a much larger (3-6 μm) grain.

Skeletal structures were observed in impact produced diamond and described by Hough et al. (1995b) from the study of very fine grained crystals under the TEM. These grains were found associated with diamond, silicon carbide and diamond/silicon carbide intergrowths and used to propose a CVD like mechanism for the formation of skeletal impact diamond (Hough et al., 1995b). The examples shown in this thesis did not appear to contain silicon carbide. The structures were predominantly polycrystalline with a preferred orientation to the individual crystallites.

The extremely fine grained and delicate structures of some of these needle-like projections may represent remnant diamond following the removal of another surrounding crystal such as graphite or a non-carbon substrate. Skeletal mantle-derived diamonds are believed to be abnormal crystalline forms produced by insufficient carbon for the normal growth of crystals, characterised by one-direction ordering along [111], imperfect structure and a high percentage of amorphous phases (Shafranovsky, 1964).

Skeletal structures with a preferred orientation of the individual crystallites or linear structures do not appear to have preserved an original graphitic morphology. Extensive corrosion and graphitisation seen in diamonds from Lappijärvi, Finland was suggested as an explanation for skeletal diamond structures (Langenhorst et al., 1999). Yet there are distinct structural differences between apographitic and skeletal diamonds. Etched and corroded apographitic diamonds were seen (chapter 4) but still preserve remnant graphitic structures. The skeletal diamonds described in this study and by Hough et al. (1995b) display no apographitic structures.

Therefore the mechanism of transformation appears to involve the destruction of the precursor phase structure and the growth of individual crystallites along a dominant axis which may represent the direction of minimum pressure (Kerschhofer et al., 1998) with crystal growth being limited in the principal compressive stress direction. The transformation of a mixture of graphitic and poorly graphitic carbon could produce skeletal diamond from the transformation of graphitic carbon alone. From the skeletal

textures of some very fine grained diamond crystals observed in the Ries crater samples (Hough et al., 1995b) it has been suggested that this form of impact diamond may be due to very rapid growth from feedstock ions in a plasma or within the structure of other minerals (Dr. R. Hough, Pers. Comm.) using pre-existing grain surfaces as a substrate. Fine grained Skeletal crystal structures can be formed by shock. Rapid growth textures with fine grained radiating structures have been observed for vapour generated SiC formed by conically converging shock-wave techniques (Yamada and Tobisawa, 1990). The structure of these crystals is very similar to that shown in a diamond from the OGGBR (figure 3.15a) and does not appear to be the result of etching

Another possibility that should be considered is that these skeletal structures may have formed as a result of the acid digestion process itself either through the removal of a substrate mineral or the clustering together of nano-crystalline diamond. Although these structures are very delicate and fine grained they appear to be robust and as such it is hard to suggest a mechanism, such as surface charging by which nano-crystallites could adhere to each other with sufficient strength to retain their structure during SEM and TEM investigations. This indicates that the primary mechanism involved is one of growth from a carbon feedstock with multiple nucleation sites forming diamonds which have not inherited any of the structural characteristics of the precursor carbon. Alternatively, as with the polycrystalline grains described in section 3.4.5. these structures may have formed from the nucleation of individual diamond crystallites within the precursor structure. Experimentally shock synthesised diamonds are predominantly small, polycrystalline and do not preserve the structure of the precursor carbon phase (De Carli, 1995).

3.4.5. Polycrystalline grains (≤ 5-300 μm).

The majority of impact diamonds are polycrystalline with individual grains up to 0.2-1 cm in size and composed of individual crystallites 0.1-5 μm in diameter (Masaitis, 1998). Rarely single crystal diamonds are also reported (Gurov et al., 1995). Individual nano-diamonds from Chicxulub are ≤ 6 nm in diameter (Gilmour et al., 1992). The

diamonds seen in this study ranged in size from ≤ 5-300 μm and were exclusively polycrystalline, no single crystal diamonds were detected.

The texture is akin to the granular polycrystalline texture described for shock zircons in section 3.4. The sample illustrated in figures 3.13a-b is a polycrystalline diamond from the Seelbronn suevite residue, the diamond has a clear linear orientation along the long axis with needle like projections and structures. The SAED pattern shows a polycrystalline ring structure and streaking along the diamond 2.06 Å spots. This streaking may be the result of microtwins in the structure of the diamond (unresolvable at these magnifications) or stacking faults. Surface textures on a very fine scale (<1 μm) observed using the SEM (figure 3.11) may represent the surface expression of polycrystalline structure.

Polycrystalline diamonds have been described by Langenhorst et al. (1996) as aggregates commonly found in tagamites (impact melt breccias) from Popigai and suevites from Ries, formed of 1 μm crystallites containing numerous stacking faults parallel to the (110) crystallographic plane. Langenhorst et al. (1996) suggest that diamonds with these morphologies may have formed by a CVD-like process as described by Hough et al. (1995b). Koeberl et al. (1997) found that all impact diamonds from Popigai are polycrystalline with an annealed thin film surface attributed to a period of high temperature during formation. The properties of diamond from the Popigai impact crater are dependent on their high density of crystalline defects (Masaitis, 1998). The properties of nano-diamonds have been considered experimentally by Saha et al. (1998) who found significantly different structural, physical and chemical properties including strain, distortion, roughness and dislocations. Thus, polycrystalline diamonds may hold proportionally higher degrees of crystalline dislocations and defects in the form of stacking faults. These defects can provide contributions to the required activation energy which can enhance the growth kinetics of the new phases such as graphite (Green, 1992).

Polycrystallinity may represent the replacement of precursor graphite by nano-diamonds crystallising rapidly from numerous nucleation sites, such as stacking faults

within the graphite structure during phase transformation. A similar mechanism is proposed for the high pressure phase transformation of olivine (Kerschhofer et al., 1998). Alternative mechanisms may include the rapid crystallisation of diamond nuclei from feedstock gases via a CVD-like process (Hough et al., 1995c) or the shock comminution of precursor graphite prior to the graphite-diamond transformation resulting in inherited polycrystalline textures (Vishnevsky et al., 1997). The structure of flattened volume xenomorphic impact diamonds from Popigai has been attributed to mosaic fragmentation of graphite during shock wave transformation (Vishnevsky et al., 1997). Progressive comminution of pre-graphitic carbon subjected to experimental shock pressures up to 59.6 Gpa, produced characteristic polycrystalline ring patterns (Rietmeijer, 1995). Polycrystalline diamonds take three main forms; (1) apographitic platy diamonds preserving a graphite morphology, (2) volume xenomorphic grains with sugary textures and blocky structures and (3) skeletal diamonds with a preferred orientation and no obvious inherited graphitic structures. These structures indicate that the transformation mechanism may involve a vapour or liquid phase and the destruction of the pre-cursor carbon structure or the direct transformation of communited graphite to diamond preserving the pre-existing graphite structure as well as a polycrystalline shock induced structure.

In addition the preservation of polycrystallinity and structural defects such as stacking faults indicates that the diamonds were quenched and did not experience a period of high temperature ($\geq$ 2000 K) sufficient to anneal these defects or induce graphitisation.

3.4.6. Diamond/graphite intergrowths.

Shock produced diamonds may contain graphite as inclusions, flakes or surface coatings. The black colour of some of the diamonds from the Popigai impact crater has been attributed to an impurity of graphite (Valter et al., 1992). This is an important feature with reference both to the structures observed in shock and impact produced diamonds, the possible formation mechanisms and post formation processes.

Many of the SAED patterns for diamonds found in the impactites show characteristic graphite spots (3.35 Å) and commonly areas of the samples will show predominantly cubic diamond SAED patterns with isolated areas of graphite (figure 3.13b). Studies of graphite maturity have shown that SAED patterns can be used to distinguish between poorly crystalline and highly crystalline graphite (Buseck and Huang, 1985). The sample shown (figure 3.13b) show strong diamond diffractions with faint residual graphite which appears to be crystalline (i.e spots appear in the SAED rather than faint or diffuse ring patterns). Buseck and Huang, (1985) showed that as graphite maturity increases, electron diffraction patterns show increasing numbers of rings, decreased diffuseness and in well crystallised graphite, discrete spots. The SAED pattern (figure 3.13b) shows diamond and graphite with streaking of the diamond spots through the (111) spots indicating a polycrystalline texture with a preferred orientation to the crystallites. Following perchloric acid treatment many of the samples revealed detailed skeletal structures where graphite may have been removed. Skeletal structures were not seen in the diamond from the Aumühle gneiss residue which revealed predominantly elongate layered structures, with thick, short stacking faults and poor resolution of detail (figure 3.7a-b).

Diamond/graphite intergrowths may be the result of two processes, post shock graphitisation of diamond or the incomplete transformation of graphite to diamond. Shock produced diamond from the martensitic transformation of graphite by shock compression of the crystal lattice from a sp^2 to sp^3 configuration is only stable at the high pressures (30 to 50 GPa) at which it was formed, rapid pressure loss combined with elevated temperatures results in regraphitisation (Donnet et al., 1997). Thus, impact diamonds are metastable after the passage of the shock front. Rapid cooling or quenching of impact produced lithologies enables the metastable preservation of diamond (Masaitis, 1998). This requires cooling to $\leq$ 1000 K (De Carli, 1995) and will be discussed in section 4.6.3.

3.4.7. Stacking faults.

Stacking faults appear as distinct dark lamellae under the TEM. Figure 3.16a-b shows examples of these structures from the OQGBR and PIMR. The inset SAED pattern (figure 3.16a) gives a clear diamond reflection. The second example (figure 3.16b) shows stacking faults in a diamond composed of numerous layers from the Polsingen quarry. At the margins of the crystals, short, black and cross-hatched stacking fault lamellae of variable orientation can be seen. Polsingen quarry was originally seen as an impact melt rock, which was reinterpreted as an abnormally melt-rich, high temperature suevite, which cooled over a longer period and recrystallized at higher temperatures than normal suevite (Von Englehardt and Graup, 1984). Diamonds in this locality are therefore likely to be extensively re-graphitised or etched. Stacking faults were also observed in diamond from the Aumühle quarry gneiss (figure 3.7a-b). The best developed stacking faults were seen in samples from the OQGB, although some examples were found in the SBS residue.

Two forms of stacking faults could be distinguished in the demineralised samples and may appear in the same crystal.

(1) Very densely distributed, narrow black lamellae with variable sub-parallel orientations and cross-hatching. Predominantly observed in the Ötting quarry glass and Seelbronn suevite.

(2) Sparsely distributed, short, thick black lamellae with near constant sub-parallel orientations and some cross-hatching, may be wavy in form and were predominantly observed in Aumühle gneiss, Seelbronn suevite and Polsingen high temperature suevite.

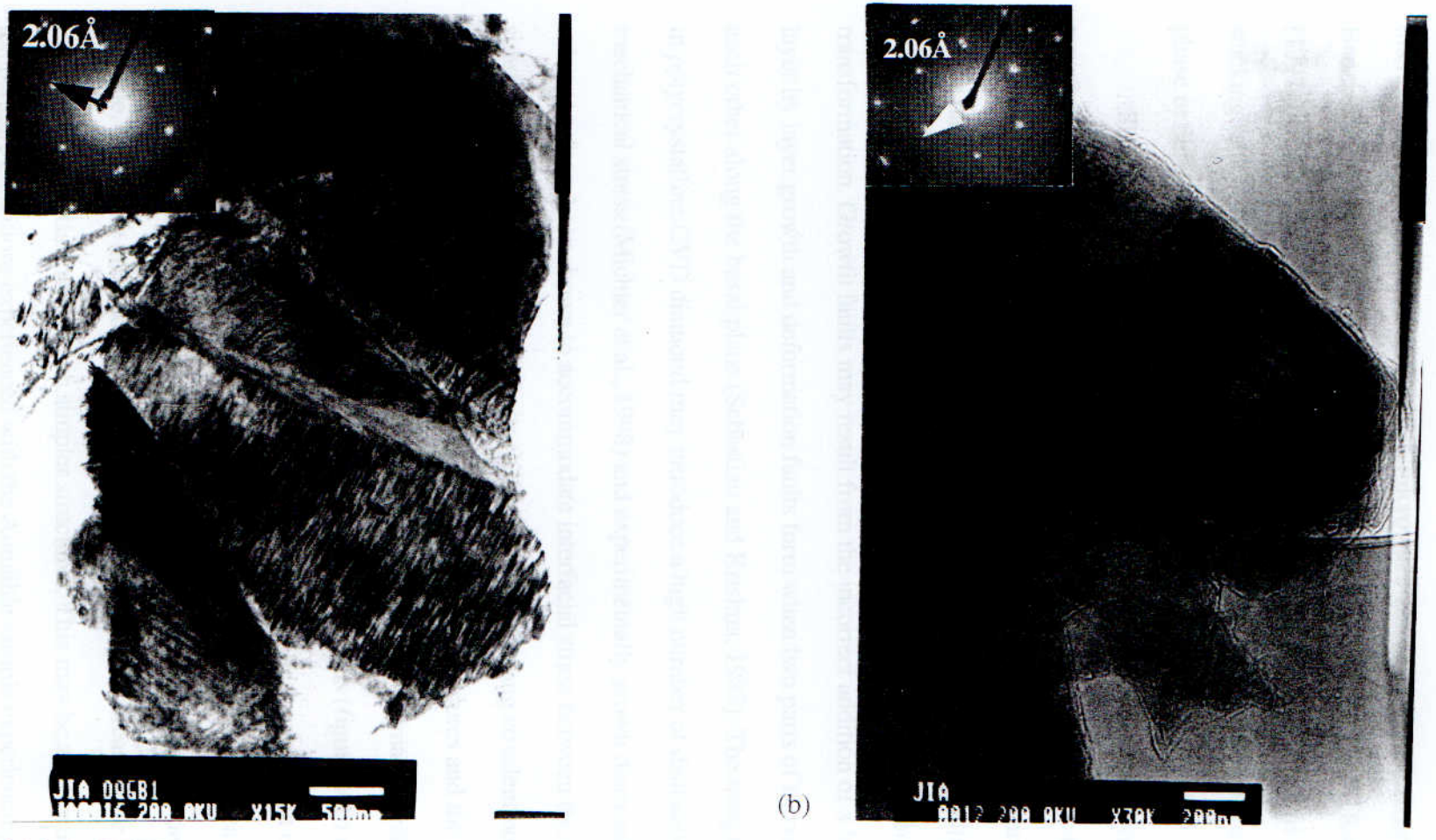

Figure 3.16. (a) BFTEM image of dense stacking fault features in diamond crystal from the Ötting quarry glass bomb. Inset SAED shows diamond 2.06 Å. [x 15 k, 200 kV, scalebar 500 nm]. (b) BFTEM image of stacking faults in a diamond grain from the Polsingen quarry impact melt rock. Inset SAED shows diamond 2.06 Å [x 60 k, 200 kV, sclaebar 200 nm].

Stacking fault features have been described in a number of diamonds from other impact craters, such as Popigai (Koeberl et al., 1997) and in experimentally grown diamond thin films (Nistor et al., 1997), microwave-assisted CVD (Badzian and Badzian, 1996) and shock transformation diamonds (Yusa et al., 1998). Koeberl et al. (1997) described lamellar structures in the Popigai diamonds which could represent stacking faults or microtwins within an intergrowth of a cubic phase with a lamellar phase or defect.

Stacking faults may occur in crystals during growth, deformation or phase transformations where they form a break in the normal stacking sequence (Sebastian and Krishna, 1987). Shock deformation induced stacking faults may occur in graphite on the basal planes due to the weak (Van der Waals-type) interlayer bonding (Kelly and Groves, 1970). These may be inherited by diamonds formed by subsequent shock transformation. Growth faults may result from the incorrect addition of a layer during layer by layer growth and deformation faults form when two parts of a crystal slip past each other along the basal plane (Sebastian and Krishna, 1987). The merging of grains in polycrystalline CVD diamond may introduce a high number of dislocations and mechanical stress (Michler et al., 1998) and experimentally grown diamond on substrates have been shown to accommodate interfacial stress between the diamond and substrate by twins and stacking faults (Kim, 1997). The strong covalent bonding of diamond atoms renders dislocations immobile at low temperatures and the faults advance along low energy crystallographic planes following thermal activation (Kelly and Groves, 1970). Stacking faults in apographitic diamonds (figure 16b) may represent inherited, deformation or growth structures. High resolution transmission electron microscope (HRTEM) analysis is required in order to distinguish between these different forms of stacking faults. The extent to which these features are developed is variable, e.g. figure 16a shows well defined stacking faults whereas figure 3.7a-b from the Aumühle gneiss shows much simpler structures. This may be a reflection of the temperature conditions experienced with the Aumühle sample experiencing post deposition annealing. Alternatively the mechanism of diamond formation may be

reflected in the density of stacking fault structures developed, if the density of defects in polycrystalline vapour growth diamond exceeds that in shock transformed diamond.

Stacking faults within a mineral may be a result of shock displacing the normal crystal lattice in order to accommodate passage of the shock front, with large numbers of stacking faults forming behind the shock front (Pujols and Boisard, 1970). This is akin to a mechanism described for the formation of amorphous silica layers in PDF in quartz which have been attributed to the crystallographic structure of the mineral adjusting to accommodate the passage of the shock front (Goltrant et al., 1992). Similar mechanisms may help explain the formation of stacking fault structures in impact diamonds. The variation in the orientation of stacking faults in figure 3.16a suggests that if these structures are shock propagated then the direction of principal stress was variable. The impact shock wave is highly heterogeneous as it passes through a target material which is variable in its properties and composed of multiple intersecting surfaces. This results in highly variable peak shock conditions from the interaction of the shock wave with phase or grain boundaries and free surfaces (Stöffler, 1972). Thus individual crystals have their own specific pressure and temperature histories dependent on their textural relationship to adjacent crystals. PDFs have been shown to show a strong relation to the orientation of the shock propagation relative to the crystal orientation (Stöffler, 1972) as the Hugoniot elastic limit (HEL) of quartz varies depending on the orientation (Duvall and Graham, 1977).

Alternatively variations in the orientation of these features may represent either different diamond plates or layers, each with a different orientation relative to rotation between connected layers (Koeberl et al., 1997).

Stacking faults appear to indicate either the adjustment of the crystal lattice to the shock wave during direct transformation to diamond (hence representing sites of nucleation for the daughter polytype), or they may be growth structures formed during the nucleation and growth of diamond from a gaseous or liquid carbon feedstock. Pre-existing or shock-propagated stacking faults and other defects in the precursor carbon phase may increase diamond formation and subsequent growth by contributing to the

required activation energy, thus reducing the transformation temperature (Salje, 1985) or also by assisting diffusion (Morris, 1980). Detailed HRTEM studies of these structures may be able to evaluate the type of stacking faults involved and hence which mechanisms may be the most likely.

3.4.8. Twinning.

Microtwinning is a common feature in impact diamonds; these may be inherited features, for example, graphite twins or formed by shock. Diamonds from Popigai show thin lamellae which could represent stacking faults or microtwins (Koeberl et al., 1997). Detailed examination of microtwins requires the use of high resolution transmission electron microscopy (HRTEM).

The diffraction patterns of many of the samples show double reflections indicating more than one diamond plate or twinning.

Twinning in diamond may be either growth twins, for example contact and penetration twins or deformation twins. Growth twins form readily during diamond growth as a simple rotation around the bond direction from the usual staggered diamond configuration to a lonsdaleite configuration (Tamor and Everson, 1994). During CVD, growth chemistry can be fine-tuned in order to minimise twin formation (Tamor and Everson, 1994) suggesting that natural vapour deposition might be characterised by a wide range of twin morphologies. Deformation twins on diamond [111] have been described following plastic deformation at room temperature (Mao et al., 1979). During phase transformations twinning may accommodate the interfacial stress between the parent and daughter phases (Bales and Gooding, 1991). Thus, depending on the nature of the twins (as determined using HRTEM) the mechanism or mechanisms of transformation may be more easily indicated.

3.4.9. Summary of diamond occurrence, structures and morphology.

The amount of diamond that was observed in the samples varied (section 4.6.2); in general the suevite and glass samples yielded significant amounts when studied under the TEM. The Polsingen and Aumühle samples contained considerably less diamond and a limited range of morphological features. Table 3.2. summarises the features that were observed and their predominance in the samples. An arbitrary scale was used in order to assign a weighting to the individual features observed in the residues. Features which were primarily observed occurred in up to 80 % of the grains analysed, commonly observed features in up to 50 % and occasionally observed structures in up to 10 % of the grains.

Table 3.2 Summary of features observed in diamonds from ejected impactites from the Ries crater.

Sample	Stacking faults	Poly-crystalline	Layered	Twinning	Skeletal	Etched	z
Otting quarry glass bomb	√√√	√√	√√	√	√√√	√	30
Otting quarry suevite	√√√	√√	√	√	√√	√	30
Seelbronn Suevite	√√√	√√	√	√√	√√√	√	20
Polsingen impact melt rock	√√	–	√	–	–	–	2
Aumühle gneiss	√√	√	√√	–	–	–	2

√ = Occasionally observed, √ √ - commonly observed, √√√ - Primarily observed.
- = Feature not detected.
z = Estimated number of diamond samples observed using optical and TEM microscopy.

The structures which have been described and discussed provide some evidence for the necessary requirements of a diamond formation mechanism. The most obvious is inherited layering and hexagonal forms which suggest a direct transformation mechanism rather than a liquid or vapour phase mechanism. Table 3.3 summarises the requirements of transformational mechanisms on the basis of the observed structures and their interpretations.

This is discussed in greater detail in section 4.7 where the evidence derived from the morphological and isotopic characteristics of the fallout and fallback lithologies is compared with the mineralogical associations and the various transformation mechanisms which have been proposed.

Table 3.3. Transformation mechanism requirements for observed structures.

Structure	**Primary structure**	**Secondary structure**	**Mechanism requirements**
Stacking faults	X	X	Direct transformation or growth
Poly - crystalline	X	X	Direct transformation or growth.
Layered	X		Direct non-destructive transformation
Twinning	X	X	Direct transformation or growth
Skeletal		X	Growth structure or partial transformation
Etched		X	Partial transformation, re-graphitisation or exposure to hot reactive gases

The only obviously primary structure is graphitic layering. Stacking faults, polycrystallinity and twinning may be inherited primary structures or secondary structures. Detailed high resolution transmission electron microscopy (HRTEM) is required in order to distinguish these structures. Skeletal and etched structures are both secondary features formed either by the mechanism of formation or corrosion of the diamonds.

3.5. SHOCK FEATURES IN ZIRCONS.

Shock features in zircons have been described by Bohor et al. (1993) and a rough sequence of structures was established according to the degree of shock (table 3.4). Shock features in zircons have many similarities to those exhibited by shocked quartz such as PDFs and zircon is considered to be more suitable for the detection of shock features in older eroded impact structures due to its resistance to weathering (Kamo et al., 1996). Experimental shocking of zircons (Reimold et al., 1998) provides

some numerical constraints on the conditions required to produce the observed series of shock features (table 3.4). The zircon samples analysed were extracted from the PIMR which has been reinterpreted as an anomalously melt-rich high temperature suevite (Von Englehardt and Graup, 1984).

Table 3.4. Shock features and experimentally derived shock conditions in zircon. [1]. Bohor et al. (1993). [2]. Reimold et al. (1998).

Stage	Shock feature - natural zircons [1]	Shock feature - experimental shock [2]	Experimental Shock pressure (GPa)[2]
I	PDF	Pervasive microcleavage and dense dislocation patterns	20
II	PDF/Granular texture	Scheelite structure phase with PDF in relict areas, PDF {320} orientation	40
III	Granular (polycrystalline texture)	Scheelite structure phase, PDF formed in zircon at shock front	60

3.5.1. Sample preparation and results.

Cloudy and clear zircon crystals were collected and etched with a solution of NaOH at ca. 70 °C for 1.5-2 hours following the procedure outlined in Bohor et al. (1993) then observed under the SEM. The samples were gold coated in order to allow observation of the surface features without surface charging problems.

The zircons were predominantly euhedral with occasional fractures and areas with a granular material texture. Figure 3.17a shows an irregularly formed crystal with etched and broken margins; the fractures crossing the grain are not linear and appear to radiate from the base of the grain. The second example (figure 3.17b) is a large euhedral crystal amid much smaller zircon crystals. This also shows non linear fractures and cracks with areas where the smooth surface of the grain has been removed revealing a granular interior. This granular texture may indicate polycrystallinity and therefore be a shock effect, which is supported by the milky white textures seen under the petrological

microscope. Two smooth pits in the crystal surface may represent crystal defects (shown at high magnification in figure 3.18).

These zircon samples do not appear to show the distinctive shock features observed by Bohor et al. (1993) and Kamo et al. (1996), although fracturing of the crystals may represent a low degree of shock alteration (<10 Gpa). Irregular fractures are observed over a wide range of shock pressures and at pressures below that of the HEL they may be the only residual effect apparent (Stöffler, 1972). The zircons do show granular internal structures indicating shock pressures of 40-60 Gpa, although this is at odds with the lack of planar surface features. One possibility is that the crystal surfaces have been annealed obliterating these features, requiring temperatures close to the melting point of zircon (≤ 2550 °C) which corresponds to shock pressures in the range 60-80 Gpa. This temperature may have been less due to the polycrystalline structure which has a greater surface area and might therefore require lower temperatures to induce surface melting. The reinterpretation of the PIMR as a high temperature suevite is in agreement with the suggestion of annealed surface films. Annealed surface films have also been observed in diamonds from the Popigai impact crater (Koeberl et al., 1997).

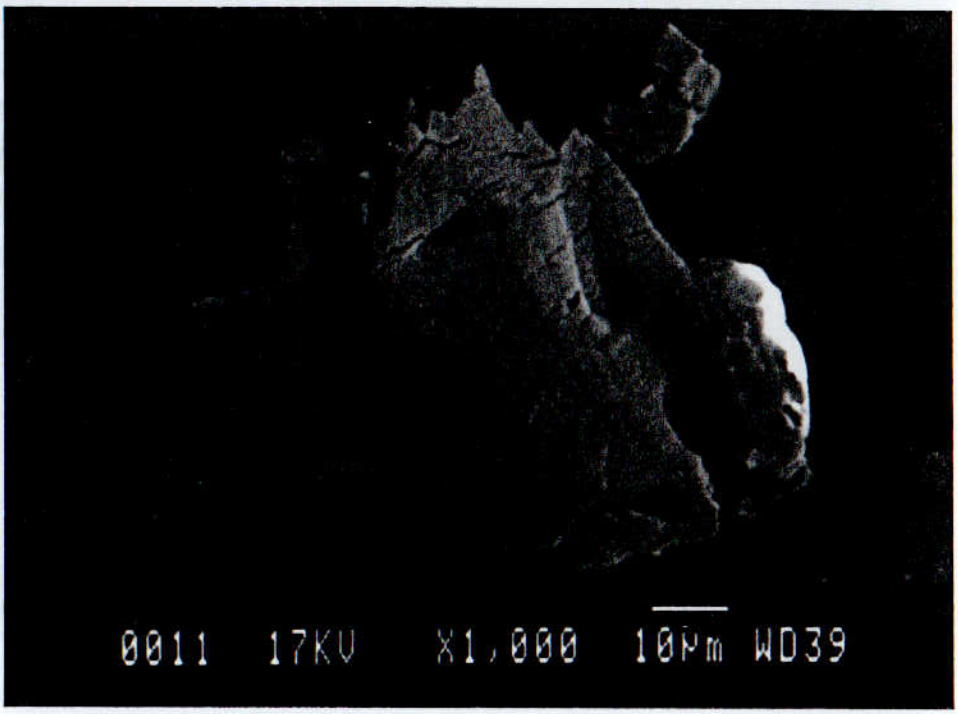

(a)

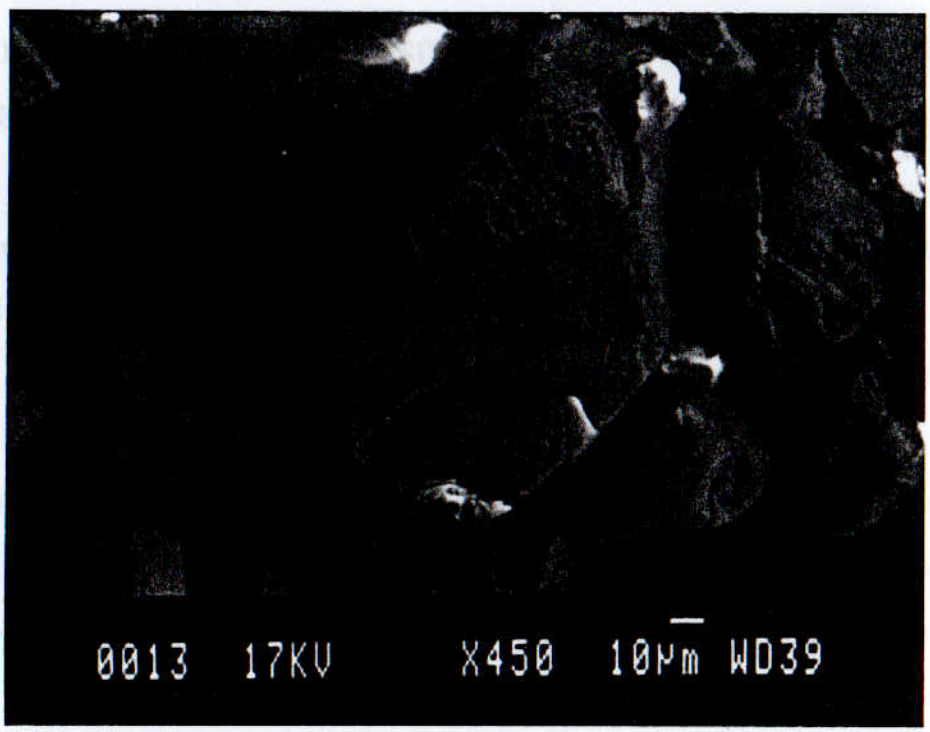

(b)

Figure 3.17. (a) Gold coated SEM image of zircon from PIMR showing linear fractures and crumbled margins. [x1,000, 17 kV]. (b) Large grain from same sample showing surface pitting and crystal defects. [x450, 17 kV].

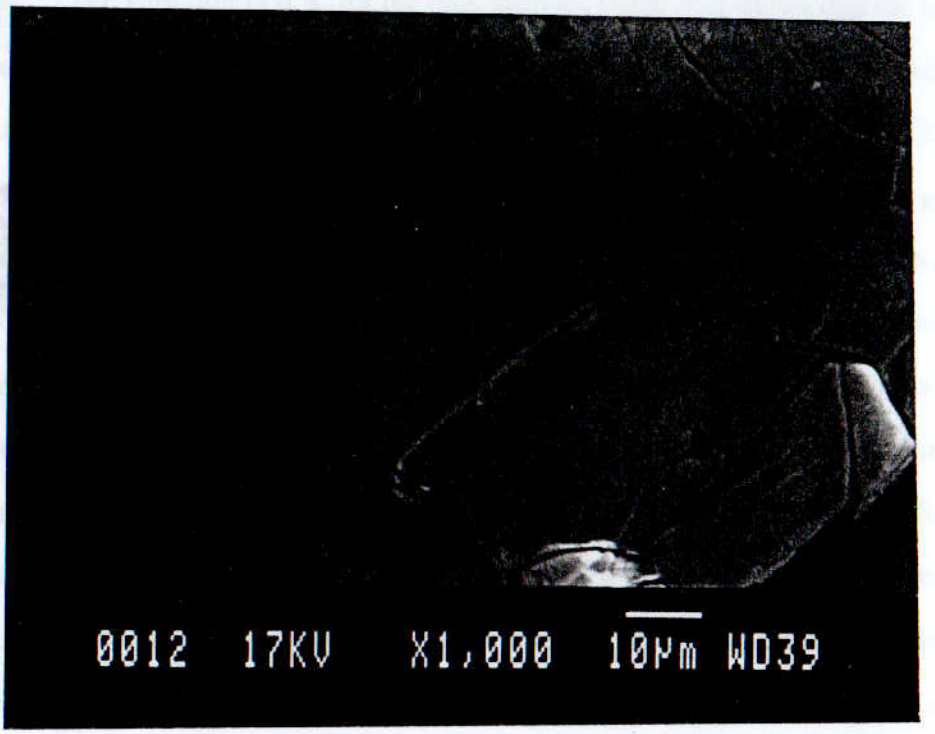

Figure 3.18. High magnification SEM image of zircon grain from the Polsingen quarry impact melt rock showing crystal defects and fractures. [x2,000, 17 kV].

3.6. STABLE ISOTOPIC COMPOSITION OF CARBON IN RIES IMPACT ROCKS.

Bulk carbon stable isotope analyses of a variety of samples from the Ries crater were made with the intention of constraining the composition of the carbonaceous material and thus indicate possible carbon sources for diamond.

The samples analysed comprised fallout suevites, a glass bomb, Bunte Breccia, variably shocked granite and 3 fall-back suevite samples from the N-73 core, plus basement material from the core. In addition samples of glass and lithic fragments (sedimentary and crystalline) were isolated from the matrix of the fallout suevites using a geological hammer and chisel and analysed separately. It should be noted that not all of the samples analysed were eventually found to contain diamond and these samples were analysed purely in order to characterise the stable carbon isotopic composition of the target rocks and impact lithologies and provide comparison with those samples which were diamond-bearing (section 3.3/4.3).

The variation in $\delta^{13}C$ for the bulk samples (table 3.5) shows that the fallout suevites are enriched in ^{13}C relative to graphite, indicating the incorporation of more oxidised forms of carbon such as carbonate. The fallback suevites are less ^{13}C-enriched indicating a higher proportion of basement-derived reduced carbon, such as graphite. By comparison the Itzingen quarry sample is depleted in ^{13}C and has a low carbon content possibly indicating the presence of a graphite component. This will be discussed in further detail in section 3.8.2. The Itzingen quarry represents an ejected mass of variably shocked and altered granite derived from the shallow levels of the Ries basement, which forms a minor component in ejected glass and suevite (Stöffler, 1977). The Seelbronn suevite samples yielded ^{13}C-enriched isotopic ratios with a high carbon content possibly indicating a greater carbonate component. This is in agreement with hand specimen investigations of the lithic fragment populations within the impactites, which show the fallout suevites contain more sedimentary material and the fallback suevites more basement material relative to the proportions of each in the target (Stöffler, 1977).

Table 3.5. Whole-rock bulk carbon isotope compositions, Ries crater.

Samples	$\delta^{13}C_{(PDB)}$	$\pm\sigma$	Carbon content (wt %)
Otting Quarry Suevite	-11.90	0.039	1.57
Seelbronn Quarry Suevite	-7.89	0.023	3.88
Nördlingen Core 1059	-13.99	0.022	0.12
Nördlingen Core 494	-18.23	0.016	0.13
Nördlingen Core 384	-13.94	0.019	0.43
Nördlingen Core 343	-15.39	0.020	0.41
Itzingen Quarry	-25.03	0.017	0.02
Bunte Breccia	-10.07	0.020	1.89

3.6.1. Ötting quarry suevite samples.

Bulk carbon analyses for samples of whole-rock, glass and lithic fragments from the Ötting quarry suevite are shown in table 3.6 and indicate that the rock is a mixture of ^{13}C-enriched lithic material (possibly sandstone, marl, chalk or limestone in composition) and ^{13}C-depleted basement material and glass fragments.

The samples of the large glass bomb (OQGB) from the Ötting quarry (as opposed to small glass fragments extracted from the suevite) are highly ^{13}C-depleted and associated with lower carbon contents. This may be due to the non-bomb extracted glass fragments containing a higher proportion of groundmass contamination or alternatively more admixed carbonate-derived material indicating, heterogeneous carbon stable isotopes in melt glass. However, chemical analyses of tektites (moldavites) and glass bombs and fragments from the Ries crater has shown that their compositions are homogenous indicating rapid comprehensive mixing (Von Englehardt, 1972; See et al., 1998). Intuitively this would suggest that the isotopic compositions might also be homogeneous and well-mixed.

Table 3.6. Bulk carbon isotopes, Ötting quarry suevite.

Samples	Type	$\delta^{13}C_{(PDB)}$	$\pm\sigma$	Carbon content (wt%)
Whole-rock	Suevite	-11.90	0.039	1.57
Glass	Bomb	-28.07	0.015	0.04
Glass	Bomb	-27.91	0.017	0.02
Glass	Fragment	-15.11	0.013	0.15
Glass	Fragment	-15.10	0.031	0.12
Glass	Fragment	-12.27	0.012	0.41
Glass	Fragment	-13.14	0.015	0.32
Lithic	Basement	-20.95	0.082	0.37
Lithic	sedimentary	-11.85	0.017	4.07
Lithic	Sedimentary	-11.53	0.010	1.15
Lithic	Sedimentary	-10.45	0.014	3.51

Lithic fragments extracted from the suevite show a range of isotopic compositions and carbon contents. Three of these samples were sedimentary in composition (chalky and fine grained), and the other appeared to be crystalline in hand specimen and had a much more ^{13}C-depleted isotopic composition compared to the other lithic fragments and was probably a fragment of basement rock.

3.6.2. Seelbronn quarry suevite.

In comparison with the samples from the Ötting quarry suevite, the Seelbronn suevite is enriched in ^{13}C (table 3.7).

Table 3.7. Bulk carbon isotopes, Seelbronn quarry suevite.

Samples	Type	$\delta^{13}C_{(PDB)}$	$\pm\sigma$	% Carbon
Whole rock	Suevite	-7.89	0.020	3.88
Whole rock	Suevite	-7.75	0.023	3.63
Glass	Fragment	-10.62	0.020	0.72
Lithic	Sedimentary	-8.19	0.012	0.29
Lithic	Sedimentary	1.95	0.010	2.49
Lithic	Sedimentary	2.38	0.015	2.94
Lithic	Basement	-9.20	0.008	2.94

The whole-rock $\delta^{13}C$ compositions are ^{13}C-enriched in comparison with the the Ötting quarry whole-rock samples, this may be due to the ^{13}C-enriched sedimentary fragments (- 8.1 to 2.4 ‰) compared with the fragments from the Ötting quarry (-10.5 to -11.9 ‰). This may suggest that the rock was derived from a shallower level in the target area introducing a greater proportion of sedimentary and carbonate lithologies and a lower proportion of basement material and associated reduced carbon. Graphite is formed from chemically reduced organic carbon material, which is usually depleted in ^{13}C producing negative $\delta^{13}C$ values ($\delta^{13}C$ = -30 to -20 ‰). Whereas chemically oxidised carbonate material is generally enriched in ^{13}C. This was discussed in section 1.9. The carbon stable isotopic composition indicates a greater carbonate component enriching the rock in ^{13}C, this correlates with recent observations of primary carbonate

impact melt within suevites located to the south and south-west of the Ries crater (Graup, 1999). The Seelbronn quarry was located to the south-west of the crater compared to the Ötting quarry which lies to the north-east (Map 3.1) and yielded only a single example of carbonate melt (Graup, 1999). Post-impact processes e.g within the subsequent crater lake may have complicated the $\delta^{13}C$ compositions through the formation of secondary carbonate cements.

3.7. CARBON STABLE ISOTOPIC COMPOSITIONS OF RESIDUES.

Stepped combustion analyses have been used extensively to provide detailed information about the stable carbon isotopes $^{12}C/^{13}C$ of carbonates, demineralised residues and individual diamonds (Wright and Pillinger, 1989; Prosser et al., 1990). The use of incremental temperature steps enable the differentiation of the carbon allotropes and even grain size variations between samples (e.g. Ash et al., 1987). The technique used was described in detail in section 2.7.2.

The primary mechanism proposed for the formation of impact diamonds from the Ries and Popigai craters is a direct shock transformation from graphite derived from basement gneisses (Masaitis, 1995). In order to relate the isotopic compositions of samples from the Ries crater, such as diamonds (Hough et al., 1995c; Abbott et al., 1996; 1998a; 1998b and this study) and silicon carbide (Hough et al., 1995c) to this basement derived graphite, samples of graphite were also extracted from the residues. Isotopic studies of graphite from Popigai (Masaitis et al., 1990; Shelkov, 1997), Lappajärvi and the Ries (this thesis) indicates that graphite has a highly diverse carbon isotopic composition (section 3.7.2), therefore diamonds of varying carbon isotopic composition may have formed from a graphite feedstock.

3.7.1. Stepped combustion analyses of acid residues.

Although attempts were made to extract diamond and graphite grains from the acid-demineralised residues this often proved difficult and bulk analyses were performed using a small random selection of grains. The samples were composed of

diamond with minor graphite as deduced by the TEM observations. Zircon may also have been present although these were not detected by the TEM and would reduce the overall carbon yield. Zircons tend to cluster towards the edges of the TEM grids and become charged by the electron beam.

Results from the stepped combustion of a sample from the OQS residue are shown in figure 3.19. The carbon yield per °C (ppm/°C) is plotted along the left hand side of the graph as a histogram and the $\delta^{13}C$ values along the right hand side of the graph as a line with error bars. The OQS residue shows a single carbon release at 700 °C with a $\delta^{13}C$ of -22 ‰ which most likely represents the combustion of diamond. The total carbon yield was 27.6 wt % with the peak release representing 85.3 % of this. This sample was not found to contain SiC. It has been shown (Ash et al., 1990) that the combustion temperatures of diamond are dependent on the grain size due to variations in the surface area, with 1mm diameter diamonds combusting at around 800-850 °C and 1-10 nm diamond at 500 °C. In samples composed of a distribution of different grain sizes the exothermic combustion of diamond may result in the combustion of larger crystallites at lower temperatures. Russell (1992) showed that for mixed grain size fractions the combustion of smaller crystallites promoted the lower temperature combustion of the coarser grained fraction. As these residues may contain a mixture of diamond grain sizes the maximum temperature at which they combust may not be a wholly reliable indicator of the maximum grain size due to co-combustion processes.

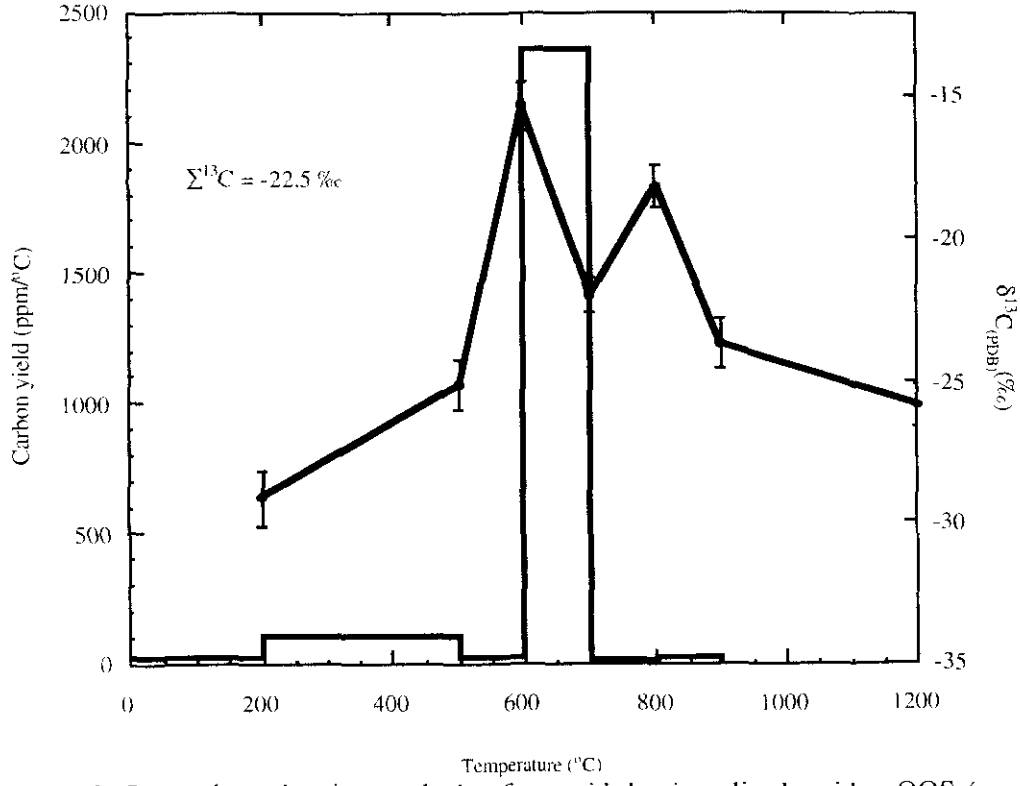

Figure 3.19. Stepped combustion analysis of an acid-demineralised residue OQS (sample weight = 24.2 µg). $\Sigma\ \delta^{13}C$ = -22.5 ‰ and Σ carbon yield = 27.6 wt%.

The residue from SBS (figure 3.20) shows a gradual increase in carbon yield from 600 °C to a peak at 800 °C and subsequent sharp decease in yield. The total carbon yield was 96.9 wt % with the peak yields (750 - 900 °C) representing 92.8 % of this. Carbon yields below 450 -500 °C have a $\delta^{13}C$ from -25 to -26 ‰ representative of organic contamination most probably from sample handling. The carbon stable isotopic is relatively stable (-16.8 to -17.2 ‰) across the peak yield temperatures, representing a plateau. The experiment reveals the combustion of either variably sized diamond crystallites or the gradual combustion of a relatively large diamond.

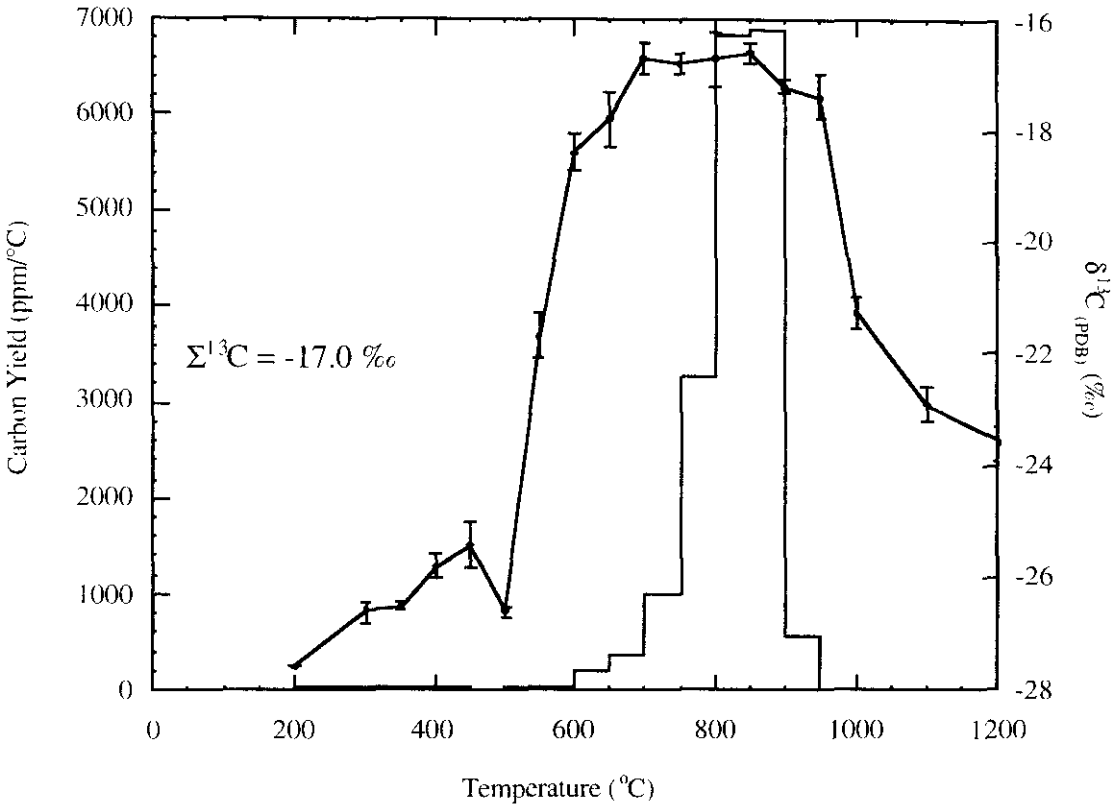

Figure 3.20. Stepped combustion analysis of an acid-demineralised SBS (sample weight = 2µg). $\Sigma\ \delta^{13}C$ = -17.0 ‰. Σ carbon yield = 96.9 wt %.

3.7.2. Graphite carbon stable isotopic compositions.

The carbon isotopic compositions of a number of graphite grains were measured using static mass spectrometry combined with stepped combustion. This allows a comparison of these compositions with those of the impact diamonds, silicon carbide (Hough et al., 1995c) and whole rock samples. The two examples in figures 3.21a-b were black grains with a graphite (hexagonal, platy) morphology extracted from acid-demineralised residues prior to the perchloric acid stage. These two stepped combustion profiles for graphite (figures 3.21a-b) show yields at temperatures expected for graphitic carbon.

Figure 3.21 shows a graphite analysis from the Seelbronn quarry suevite residues (SBS). The peak combustion yield occurs at 500-600 °C with a $\delta^{13}C$ of -19.9 ‰. The SBS graphite (figure 3.21) has a total carbon yield of 68.4 wt % with the peak release representing 82.4 % of this. The $\delta^{13}C$ of the low-temperature and high-

temperature carbon releases range from -31.7 to -24.1 ‰ whilst the peak release at 550-600 °C has a $\delta^{13}C$ of -19.0 ‰.

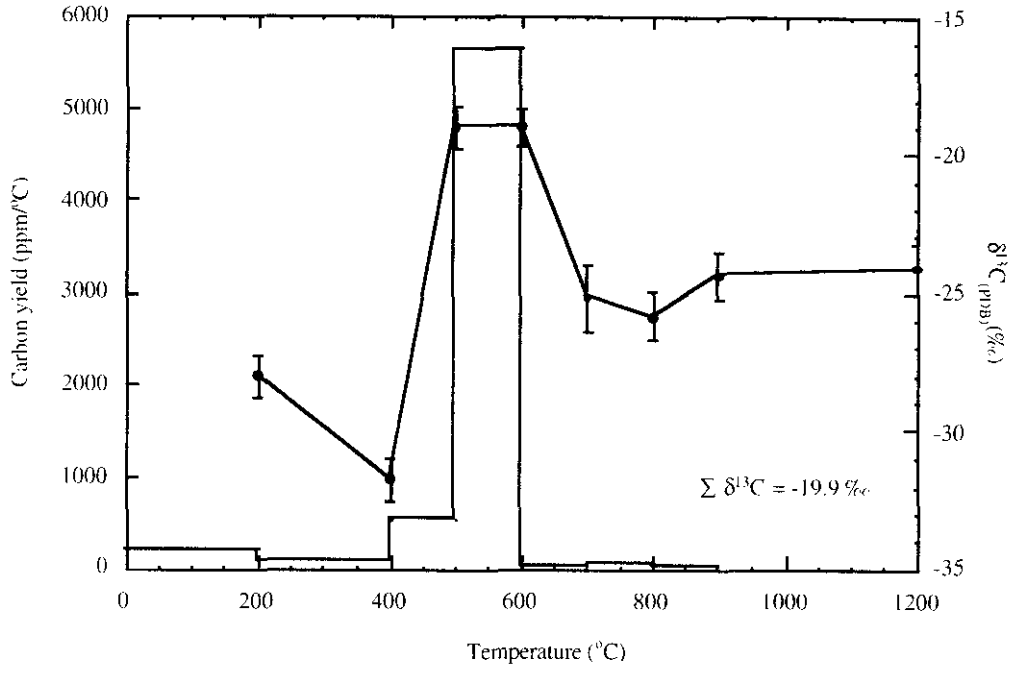

Figure 3.21. Stepped combustion analyses of graphite extracted from the acid-demineralised residue of the SBS (sample weight = 2 µg). $\Sigma\ \delta^{13}C$ = -19.9 ‰ and Σ carbon yield = 68.4 wt%.

The following example (figure 3.22) shows a stepped combustion plot for a fragment of crystalline graphite from the OQGB residue. This sample was extracted from the residue following sample disagregation by concentrated HCl but prior to the HF/HCl, chromic or perchloric acid stages. The main carbon yield is at 700°C and represents 88 % of the total carbon yield (50.4 wt%). The carbon stable isotopic composition is as expected for graphite ($\delta^{13}C$ -29 to -19 ‰) and the high temperature of combustion may relate to the size of the graphite fragment (weight) or degree of crystallinity.

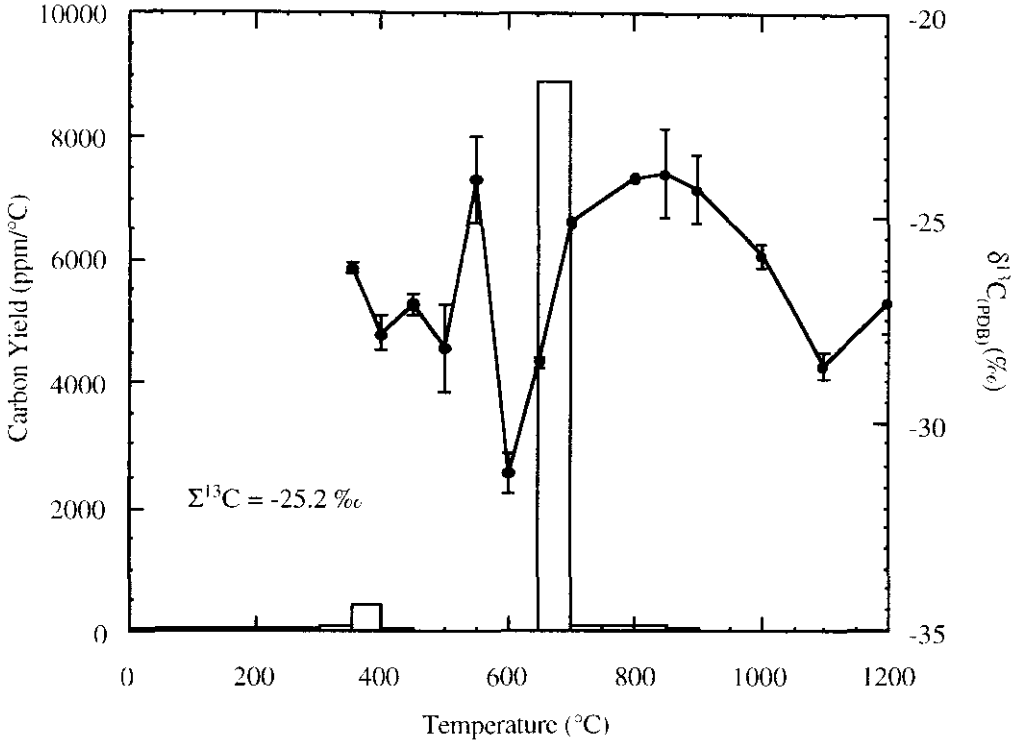

Figure 3.22. Stepped combustion analysis of graphite extracted from the acid-demineralised residue of OQGB (sample weight = 18.4 μg). $\sum \delta^{13}C$ = -25.2 ‰ and carbon yield 50.4 wt%.

The release of carbon at a single 50 °C temperature step indicates that the combustion of the sample was rapid and complete once activated. This suggests that the graphite may have been shielded by a heat annealed surface layer allowing rapid combustion when temperatures sufficient to remove this film were obtained. An annealed surface would probably represent a lower surface area therefore, requiring higher temperatures in order to combust compared to a polycrystalline sample composed of ≥ 1μm crystallites. Annealed surfaces have generally been described in diamond samples rather than graphite. It is debateable whether graphite grains could form annealed surfaces.

The $\delta^{13}C$ composition of the two samples range from -19.9 ‰ in the SBS to -25.2 ‰ in the OQGB. This may reflect the heterogeneous nature of the basement graphite composition, alternatively some graphitic carbon within the samples may represent re-graphitised impact produced diamonds. If impact diamonds are not rapidly

quenched to ≤1000°C they are rapidly regraphitised (De Carli, 1995) this is also observed in vapour deposited diamond. This would incorporate any carbon stable isotopic components derived from the mixing of graphite and carbonate sources as suggested by Hough et al. (1995b) producing graphite enriched in ^{13}C.

The stable carbon isotopic composition of graphite depends on the isotopic composition of the precursor organic matter and the extent of fractionation during metamorphism. Several mechanisms may fractionate graphite during metamorphism including approximately 3 ‰ due to the removal of ^{12}C from the dehydrogenation loss of CH_4 (Peters et al., 1981a; 1981b). Also high temperature exchange between organic matter and sedimentary carbonates associated with the release of ^{13}C-rich CO_2 during decarbonation (Valley and O'Neil, 1981) with a Δ(cc-gr) of up to 3.3 and 7.1 ‰ (Arneth et al., 1985). Calcite-graphite exchange fractionation may account for an isotopic shift from ~ -23 to -28 ‰ in unmetamorphosed to greenschist facies rocks to approximately -2 to -12 ‰ in amphibolite facies rocks and -2 to -5 ‰ in granulite facies rocks (Arneth et al., 1985).

The graphite analyses (figure 3.23) from both Shelkov, (1997) and Masaitis et al. (1990) are for samples from the Popigai crater, Russia, indicating that in comparison the graphite from the Ries crater basement rocks is depleted in ^{13}C. The analysis of graphite from the Lappajärvi impact crater is also enriched in ^{13}C compared to the graphite from the Ries. These variations may reflect different organic matter sources, metamorphic basement assemblages and different metamorphic histories between the two target areas. This will have an affect on the isotopic composition of any diamonds derived from these graphite sources.

The results (figure 3.23) indicate that the stable carbon isotopic composition of graphite is heterogeneous, this variation is likely to be much wider with a larger scale of analyses. The compositional range of graphite in nature ranges from -30 to -20 ‰ when derived from organic material, to -1 to -3 ‰ when equilibrated with carbonate-bearing rocks (Scheele and Hoefs, 1992; Arneth et al., 1985), this indicates that a vapourised carbonate component may not be required to produce the ^{13}C-enriched isotopic

compositions suggested for vapour growth impact diamonds (Hough et al., 1995c). Although, this depends on the isotopic composition of the graphite in the basement and the range seen here is predominantly ^{13}C-depleted.

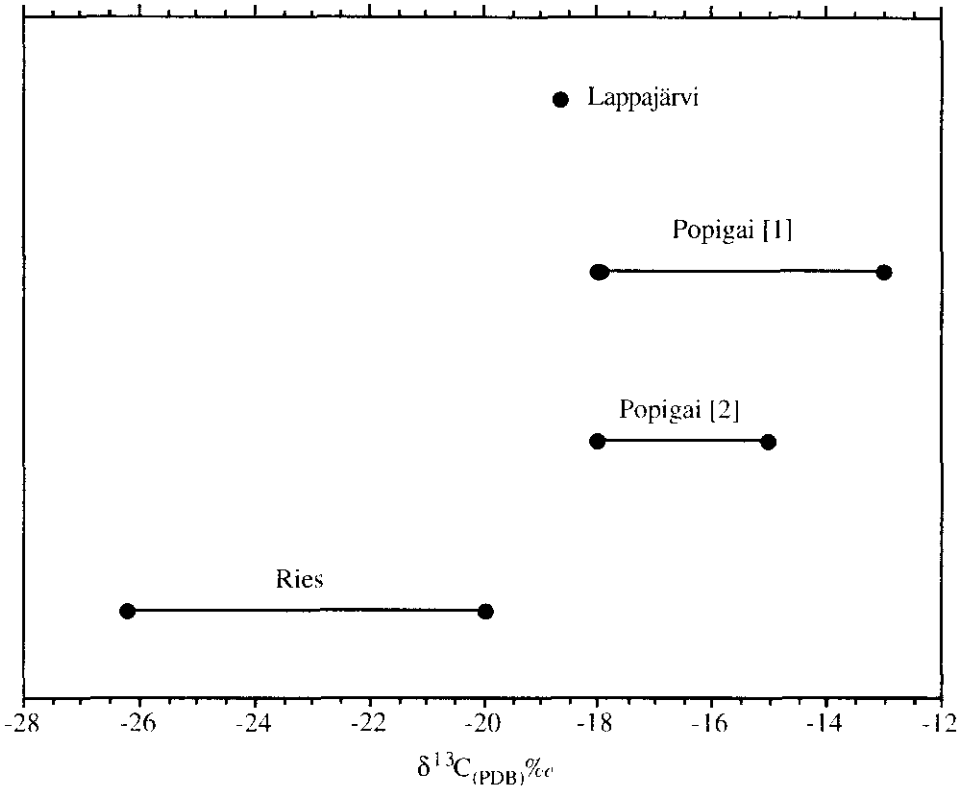

Figure 3.23. Comparison of graphite stable carbon isotopic compositions from Lappajärvi and Ries (this study), with Popigai [1]. Masaitis et al. (1990); [2]. Shelkov (1997).

3.7.3. Diamond carbon stable isotopic compositions.

A polycrystalline diamond picked from the acid-demineralised residue of the OQGB (figure 3.4b) was step combusted to establish its carbon release profile and carbon stable isotopic composition (figure 3.24). The peak carbon yields represent 86.1 % of the total carbon yield. The plot shows a clear carbon release from 700-900 °C with a peak at 800 to 850 °C, representing the combustion of the main body of the diamond with little to no carbon release after 900 °C. The carbon stable isotopic

composition was stable across the main carbon yield, varying from $\delta^{13}C$ of -26.4 to -26.7 ‰. The size of the crystal (50 μm) results in a relatively high temperature release.

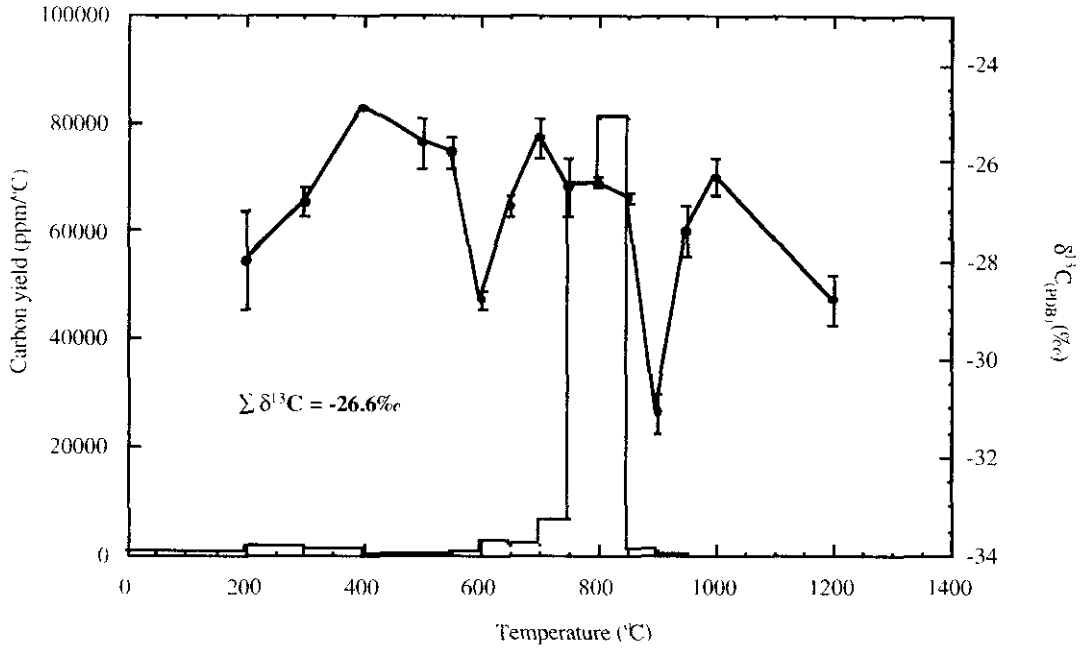

Figure 3.24. Stepped combustion analysis of diamond from the OQGBR (sample weight = 2 μg). Σ $\delta^{13}C$ = -26.6 ‰. Σ carbon yield = 87.1 wt%.

3.7.4. Silicon carbide.

Although silicon carbide was observed in one of the demineralised residues, isolation of individual crystals or a concentrate proved impossible. A sample of OQS containing blue and green silicon carbide from previous Ries crater studies (Hough et al., 1995c) were provided by Dr. R. Hough. The stepped combustion plot for the sample is shown in figure 3.25. The sample appears to be a mixture of diamond, silicon carbide and a low temperature amorphous yield. The silicon carbide crystal itself begins to combust at the 1300 °C temperature step and is probably only partially combusted. The limited temperature range of the furnace limits the duration at which the sample can be held at 1300°C. Individual temperature steps are normally 30 minutes in duration but the 1300 °C step was extended to 60 minutes. The average carbon isotopic composition

of the sample was -24.2 ‰ and the silicon carbide had a $\delta^{13}C$ of -27.5 ‰. The low temperature steps probably represent graphite and diamond.

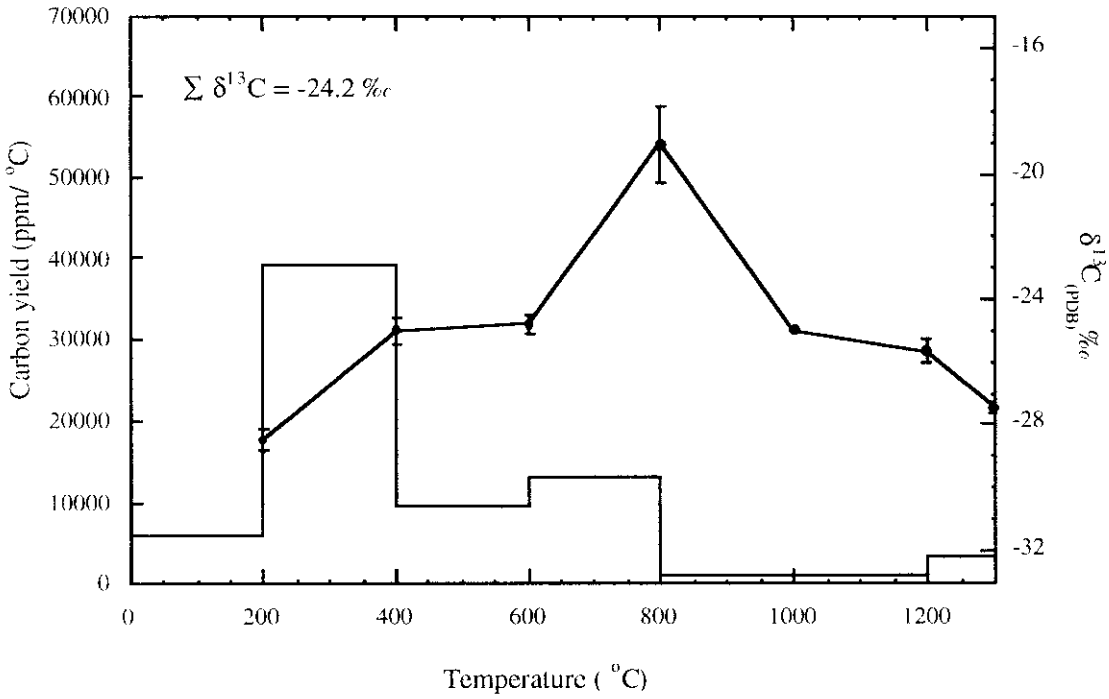

Figure 3.25. Stepped combustion analysis for an acid-demineralised residue OQS containing <50 µm silicon carbide crystals (sample weight = 2 µg). Σ $\delta^{13}C$ = -24.2 ‰. Σ carbon yield = 70.8 wt%.

The composition of the residue and SiC release is in keeping with the overall composition of the Ötting quarry residue and graphite within the Ries crater impactites. Indicating that the carbon source for SiC formation may also be graphite as suggested for the impact diamonds. The mechanisms for SiC formation are discussed in detail in chapter 4.

3.8. SUMMARY AND CONCLUSIONS.

The evidence presented here from the study of the morphological structure and carbon stable isotopic composition of the Ries crater fallout impactites is discussed below. This information is discussed in greater detail in chapter 4 where comparison will be made with the fallback impactites and shock metamorphism data in order to combine this with the carbon phase diagram, known carbon polymorphs and suggested diamond formation mechanisms.

3.8.1. Morphology and structures.

The morphological structures described in this chapter may be seen in shock-produced diamonds (Vishnevsky et al., 1997; Koeberl et al., 1997) and to some extent other minerals, such as zircon (Bohor et al., 1993) and quartz (Stöffler, 1977).

Under the TEM the samples displayed many of the characteristic features of impact diamonds such as dense distributions of stacking faults in multiple orientations, twinning, polycrystallinity, layering, etching and linear surface ornamentations. The combination of the various formation mechanisms for stacking faults, twinning and polycrystallinity may allow some interpretation of the conditions required in terms of shock pressures and temperatures during and post impact and also the precursor carbon material itself.

Many of the impact diamonds show etched features which may lie along fractures, planar dislocations or areas of other intergrown minerals removed by acid treatments. Holes of variable size and density were observed on some diamonds from the Ries crater described by Rost et al. (1978) and attributed to solution, other diamonds in their study did not show these features. The removal of graphite intergrown within diamond by fuming perchloric acid oxidation may result in the formation of skeletal structures, fissures and fractures. Finely detailed surface structures such as pitting, observed at high magnification on the surface of diamond under the SEM may be the result of etching of the diamond by silicate melts (Langenhorst et al., 1999) or reactive gases (Vishnevsky and Raitala, 1998) or the removal of secondary graphitisation coats.

The environment of formation and the presence of a highly ionised vapour of silicate rock, combined with highly reducing conditions could result in hot gas phase reactions dissolving and etching the diamond surfaces.

The majority of impact diamonds are considered to be formed from the direct transformation of graphite (Masaitis, 1972; Langenhorst et al., 1999). This is based on their inherited textures, isotopic compositions and the prevalence of graphite in the target rocks. The preservation of inherited features can include crystal form, twins, growth and aggregates of the primary graphite (Valter and Yerjomenko, 1996). Some impact diamonds, termed Togorites are considered to have formed from the direct transformation of coal, most notably from the Kara impact crater, Russia (Ezersky, 1982; 1986). The resulting diamonds are porous, black-brown in colour and show palimpsest biogenic textures (Grieve and Masaitis, 1994). The mechanism for this direct transformation is debated and several potential formation paths have been proposed, these are discussed in chapter 4.

The majority of impact diamonds are polycrystalline (Koeberl et al., 1997), although two single crystal diamonds were described from Czechoslovakian impact deposits by Gurov et al. (1995). Polycrystalline grains are formed from numerous individual ≤ 1 μm crystallites, which gives a granular texture when observed under high magnification using the TEM. These crystallites are described as being irregular to rounded in form, although they may be elongated (Langenhorst and Masaitis, 1996) which may give rise to the reported preferred orientation of many polycrystalline diamond aggregates (Vishnevsky et al., 1995). Nano-diamonds ≤ 6 nm were found in K/T boundary layers (Gilmour et al., 1992) and could represent individual crystallites found in polycrystalline diamonds. The origin of the polycrystalline texture may be a result of the shock transformation, with the nucleation of numerous individual crystallites (Kerschhofer et al., 1998) or an inherited pre-shock structure. Experimental shock studies in natural graphitic carbon revealed progressive comminution in response to shock pressure up to 59.6 Gpa (Rietmeijer, 1995). Similar results were reported by Zhuck et al. (1997) with crystallite sizes of the order 0.1 to 1 μm. Therefore,

polycrystallinity from the comminution of samples may be an inherited pre-transformation shock effect similar to shock-produced kink bands observed in diamond formed from graphite (Valter and Yerjomenko, 1996).

Comparison of polycrystalline structures associated with preferred orientation of crystallites and high stacking fault and dislocation densities in diamonds may be made during experimental shock-induced polymorphic transformations in olivine (Kerschhofer et al., 1998). The results suggest that in larger crystals (60 μm) the polymorphic transformation may occur by intracrystalline nucleation of the high pressure phase at the intersection of stacking faults and dislocations. Smaller grains (<10-20 μm) appear to form by nucleation on the grain boundaries (Rubie and Champness. 1987; Boland and Lieberman, 1983). Interaction of these two mechanisms may result in the formation of polycrystalline aggregates of the high pressure polymorph with a possible preferred orientation of the crystallites as a result of the principal compressive stress direction (Kerschhofer et al., 1998). Strong preferred orientations are seen in diamond, lonsdaleite and graphite in the ALHA77283 and Canon Diablo meteorites (Clarke et al., 1981). This olivine phase transformation mechanism is not martensitic but suggests ways in which structural characteristics such as preferred orientations and high stacking fault densities may be explained. The shock transformation of poorly crystalline and amorphous carbon material within an orientated stress field could result in the formation of loosely aggregated diamonds and skeletal structures where only the graphitic carbon is transformed.

The effect of stacking faults on the selected area electron diffraction pattern (SAED) of diamond obtained by TEM has been used as one possible explanation for the commonly reported presence of lonsdaleite, with stacking faults considered as internal surface interfaces, related to the energy difference between hexagonal and cubic diamond structures (Stoneham, 1992). The existence of lonsdaleite is controversial, although many authors state that the presence of hexagonal (lonsdaleite) and cubic diamond is a necessary feature to prove a shock origin for diamonds found in shock produced lithologies (e.g. Valter, 1996). Lonsdaleite is determined by single grain x-ray

analyses which measure the bulk strain and are low resolution (mm to μm) in comparison to TEM and SAED studies (nm to μm). High resolution transmission electron microscopy (HRTEM) is required in order to distinguish the nature of the stacking faults. A correlation may be seen between the presence of extensive stacking fault features in individual nanometre sized diamond crystallites and the occurrence of lonsdaleite. Diamonds transformed from graphite by laser-heated diamond anvil cell techniques contain numerous stacking faults and the lack of lonsdaleite in the SAED patterns was used to suggest that the stacking faults were not present due to lonsdaleite (Yusa et al., 1998). The percentage of lonsdaleite with the cubic phase of diamond has been observed to decrease with increasing crystallite size (Valter and Yerjomenko, 1996), this is interpreted as the result of increased duration of the quasistatic phase of pressure behind the shock wave which is greater for larger impact craters. Thus, a higher percentage of lonsdaleite may be observed in diamonds from smaller impact craters. Lonsdaleite can only be made from highly ordered crystalline graphite (De Carli, 1995) suggesting that the degree of graphite maturity in the target rocks may also be important.

Solid state structural phase transformations involve a change in the stacking sequence of layers without altering the structure of the layers. SiC phase transformations may commence with the random insertion of stacking faults (Sebastian and Krishna, 1984). The irregular insertion of stacking faults may occur 2-3 layers apart and nucleate randomly (Fujita and Ueda, 1972), as the transformation progresses the reflections of the second phase predominate and the first phase fades out. The end product is disordered, containing numerous faults because as the second phase grows the various nucleation sites meet at faulted interfaces (Sebastian and Krishna, 1984). This might be expected to produce a mixture of different polytypes within single grains. SiC polytypes of several types were observed in fine grained skeletal aggregates (Hough et al., 1995c) and this is also indicated by recent Raman studies (Dr. R. Hough, Pers. Comm.). Thus a correlation may be seen between the predominance of stacking faults in impact diamonds and the formation of the high pressure polymorph. These

stacking faults and/or defects may be heat annealed or graphitised (1000-2000 K) during post formation processes depending on the conditions experienced. The presence of different diamond polytypes other than 3C (cubic diamond) and 2 H (lonsdaleite) within defect-rich impact diamonds has not been confirmed.

To conclude, the features observed in impact diamonds are intrinsic structural and crystallographic defects. These may be inherited from a precursor material such as graphite or formed as a direct result of shock wave interaction with the new diamond crystal lattice. Shock deformation of graphite prior to the formation of diamond has been detected as a relict feature in impact diamond itself (Valter and Yerjomenko, 1996). In combination these structures can pinpoint some of the features of the shock transformation of carbon material such as graphite, coal or amorphous carbon to diamond. The controversy between a primarily shock transformation of carbon material to diamond or a contribution from vapour condensation and growth of diamond is hard to resolve. The evidence suggests that larger diamond grains found within impact lithologies are formed by the transformation of carbon to diamond in the solid state, whilst skeletal, polycrystalline diamonds may have formed via another process such as CVD. Several mechanisms have been suggested for this and are discussed in chapter 4.

3.8.2. Carbon stable isotopes.

The bulk carbon isotopic analyses of the OQS and SBS and individual components within these impactites support geochemical evidence previously used to suggest the formation of glass in suevites from the vapourisation of a mixed gneiss complex up to 1 km below the Ries crater target area (Von Englehardt, 1995).

Thus, the carbon isotopic composition of the suevites represent a mixture of predominantly basement-derived graphite and shallow level sedimentary rock-derived carbonate. Carbonate-rich rocks occur within the sedimentary cover sequences (figure 3.2) which overlie the target area, including over 350 m of limestones and marls of the Jurassic Upper Malm (Chao et al., 1978). The variation in the whole-rock carbon stable isotopic composition of the various Ries crater localities sampled is shown in figure

3.26. The $\delta^{13}C$ composition of the glass bomb from the Ötting quarry suevite (- 28.1 to -27.9 ‰) indicates a predominantly and possibly exclusively, derivation from basement material containing graphite with little or no admixture of sedimentary carbon.

Figure 3.26 illustrates how the Seelbronn suevite and its individual components are enriched in ^{13}C compared to the Ötting quarry suevite and its components. The correlation between carbon contents and $\delta^{13}C$ is illustrated in figure 3.27.

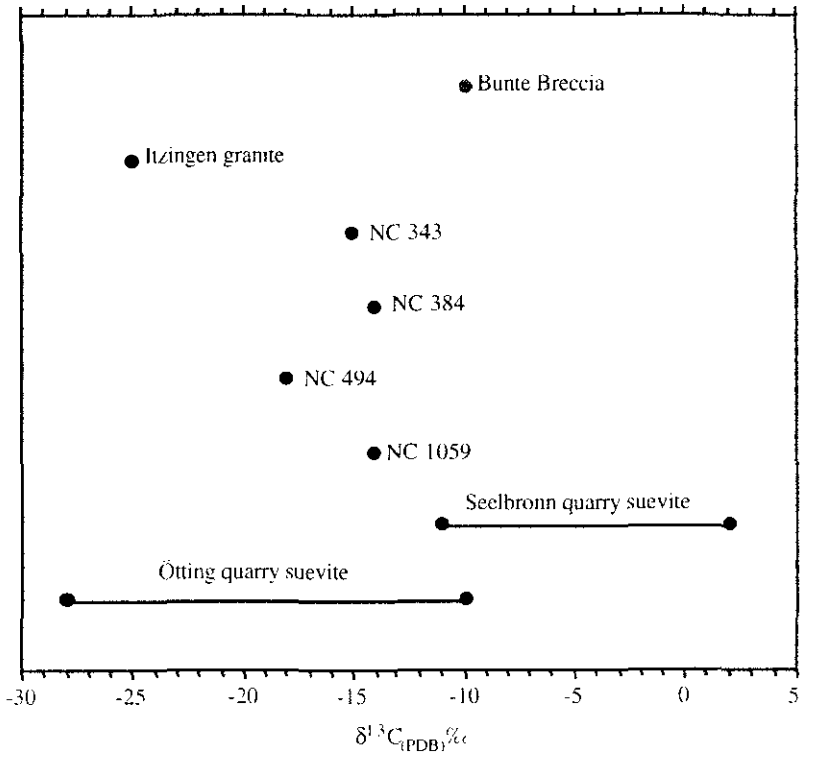

Figure 3.26. whole-rock carbon stable isotopic composition of Ries crater samples including extracted glass and lithic fragments.

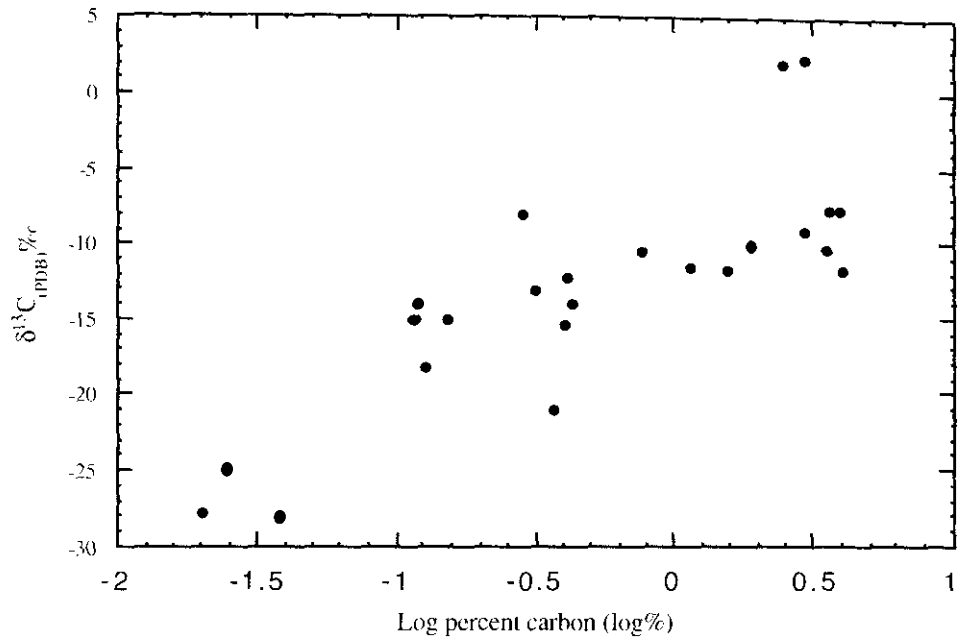

Figure 3.27. Plot of $\delta^{13}C$ versus carbon content (log wt% C) for the whole-rock samples (OQS, SBS, ITZ, PIMR, BB and extracted glass and lithic fragments).

The correlation between increasing carbon content and ^{13}C-enrichment in these samples can be accounted for by increased carbonate contents. The ^{13}C-depleted low carbon content samples are the glass bomb samples, and the $\delta^{13}C$ compositions correlate well with the $\delta^{13}C$ composition of graphite from the Ries samples (-27 to -20 ‰) suggesting that the carbon content of these samples is of graphitic origin.

The $\delta^{13}C$ variations between suevite localities may be indicative of a different lithological sample suite for the sedimentary and crystalline fragments within the suevite representing either a different part of the basement (figure 3.3) or a different stratigraphical level. This enrichment in ^{13}C relative to the basement component may indicate an enrichment in carbonate. The chemical compositions of various suevites supports this as the reported CaO wt % of the Seelbronn suevite is 4.09 compared to 2.97 wt % in the Ötting suevite (Von Englehardt and Graup, 1984). Petrographic examination of suevites from around the Ries crater has indicated an increased proportion of primary carbonate melt within the suevites concentrated to the southwest and east of the crater (Graup, 1999). The source of this carbonate is believed to be the

Malm limestone present only in the south and east of the target area at the time of impact, with the exception of isolated outliers to the north (Graup, 1999). The distribution of this carbonate melt component within the suevites corroborates the evidence which can be drawn from the carbon stable isotopic compositions. This is complicated by the presence of up to 40-50 % of crystalline calcite (Graup, 1999) within the suevite groundmass formed by post-impact hydrothermal deposition or cementing (Von Englehardt et al., 1995). This would introduce a ^{13}C enrichment depending on the proportions of calcite cement within the whole rocks analysed and lithic fragments. Analyses of acid-demineralised residues (e.g. Seelbronn) where calcite has been removed by HCl indicate that a ^{13}C- enrichment persists which cannot be accounted for by post-impact calcite cements.

Although the $\delta^{13}C$ of the Ötting quarry glass is depleted in ^{13}C compared to the graphite and basement material analysed, it is possible that incomplete combustion of graphite and carbon during the impact explosion and crater plume formation, may have caused further enrichment of ^{13}C in any residual carbon. The glass is formed from the condensation of vapourised or melted basement rocks shocked to 60-80 Gpa. These may have experienced some degree of evaporation and condensation related to kinetic isotopic fractionation with ^{12}C being concentrated in the vapour phase following evaporation/vapourisation and thus in the glass condensate. During CVD-like deposition of diamond, graphite and diamond may preferentially incorporate ^{12}C and ^{13}C respectively due to the formation of ^{12}C-graphite from $^{12}CH_4$ leaving a $^{13}CH_4$ residue to form H-CH_4 and ^{13}C-diamond (Ash, 1990).

The isotopic composition of graphite within the suevites and the target area basement rocks supports the idea that large (30-≥300 μm) impact diamonds formed through the shock transformation of graphite to diamond.

3.8.3. Mechanisms for transformation.

Comparison between the morphological, structural and stable carbon isotopic compositions of the diamond and graphite from the Ries crater impactites will be made

in chapter 4. A consideration of the potential transformation mechanisms suggested by experimental diamond production, structural characteristics and carbon phase associations will also be presented.

CHAPTER 4. IMPACT DIAMONDS IN THE RIES CRATER II. AN INVESTIGATION OF THE NÖRDLINGEN 1973 CORE: WITH COMPARISON TO FALLOUT IMPACTITES AND A DISCUSSION OF THE MECHANISMS OF DIAMOND FORMATION.

4.1. INTRODUCTION.

A number of impact craters have been investigated using drill cores, e.g. Chicxulub (Hildebrand et al., 1991), Lappajärvi (Kukkonen et al., 1992), Ilyinets (Gurov et al., 1998), Gardnos (Naterstad and Dons, 1994) and Ries (Stöffler et al., 1977; Chao, 1977). Three cores have been drilled in the Ries crater area: Deiningen drill hole, an industrial hole 1001 and Nördlingen 1973 (N-73). This study used samples from the Nördlingen 1973 (N-73) core.

The N-73 core was located approximately 4 km NE of the town of Nördlingen (section 3.1), the site was selected to lie halfway between the inner crater ring and outer crater rings on the basis of geophysical evidence (Chao, 1977). The drill core reached a depth of 1206 m, penetrating through shallow level crater lake sediments, layered suevites and crystalline material before reaching the basement gneiss from 602 m to 1206 m. For a detailed description of the drill core see Burberger, (1974); Jankowski, (1977); Stöffler et al. (1977) and Stahle and Ottemann, (1977). The drill core not only provided samples of the impactites and basement rocks but also a considerable amount of geophysical data which has been used to interpret the deep structure of the crater (Pohl, 1977). These measurements included electrical resistivity, neutron porosity index, bulk density and gamma radiation (Pohl et al., 1977).

The results from analyses of the core samples are discussed separately from the other Ries samples because the study is the first of its kind to undertake detailed carbon isotopic analyses of these samples. The structure and lithologies of the N-73 drill core are discussed first in order to place the samples in context (section 4.1.1), this is followed by a detailed discussion of the morphology and structure of the diamond found in some samples (Abbott et al., 1998b). The distribution of these structures (e.g.

stacking faults, polycrystallinity, etching and layering) within the Ries crater samples will also be discussed. The isotopic composition of the core samples is then discussed with a comparison of these samples with those described in chapter 3. This is followed with an evaluation of possible formation mechanisms proposed, with reference to the observed structures, carbon stable isotopic compositions, carbon polymorphs and diamond concentrations.

4.1.1. Lithology of Nördlingen 1973 core.

The core, illustrated in figure 4.1 can be separated into three basic units comprising post-impact Miocene lacustrine sediments (263-314 m), fallback suevite (polymict impact breccia with glass) (331-602 m) and fractured, brecciated basement rocks (602-1206 m). The fallback suevites (table 4.1.) may be further subdivided into a graded unit (314-331 m), high temperature suevite (331- 525 m) and low temperature suevite (525-602 m) (Chao, 1977). Remnant magnetisation carried by magnetite in the high temperature suevite indicates cooling from >600 °C, whereas in the low temperature suevite, temperatures below 250 °C are indicated by maghemite (Pohl, 1977). Melted rutile and magnetite indicate that formation temperatures were in the range of 1100-1800 °C (Stahle and Ottemann, 1977) with glass from within the suevites indicating peak shock pressures of 60-80 Gpa and temperatures > 2000 °C.

The proportions of the different rock fragments within the suevites varies with depth. The core suevites contain mainly lithic fragments derived from the basement gneiss complex and very few sedimentary rock fragments from the upper 700 m of the pre-impact target stratigraphy (Stöffler, 1977). Suevite and dike breccias in the core are strongly deficient in limestone from the upper part of the pre-impact stratigraphy, whereas the fallout suevite and especially the Bunte breccia has an excess of limestone (Stöffler, 1977). This is supported by the carbon stable isotope data presented in this thesis (see 3.5/4.5).

Figure 4.1. Schematic illustration of drill core Nördlingen 1973. After Chao, (1977).

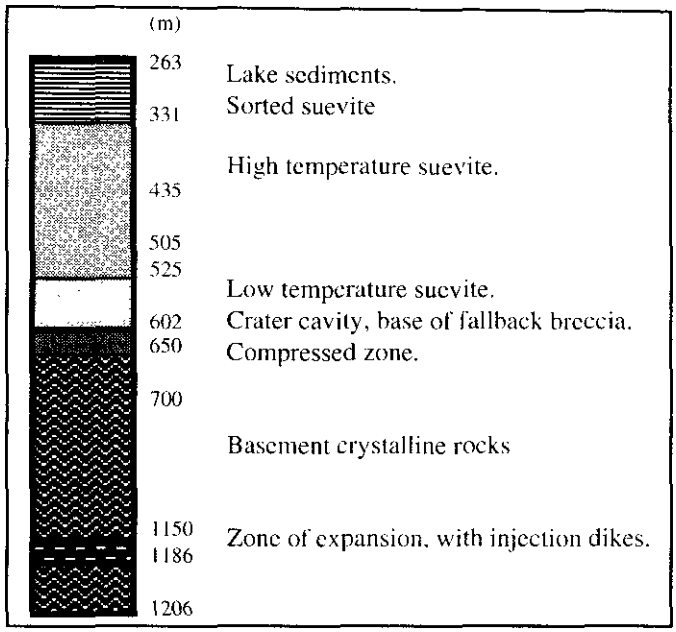

Table 4.1. Classification of Nördlingen 1973 drill core (N-73) suevites.

Unit	Depth (m)	Characteristics
I	314-331	Graded unit fine grained, near glass free upper layer (314-323 m) with mica flakes in horizontal orientation and a lower glass rich coarse grained layer (323-331m) (Jankowski, 1977).
II	331-525	Suevite with strong magnetisation (Pohl, 1974) containing some large blocks of basement rocks. High temperature suevite (Chao, 1977).
III	525-602	Suevite with very low magnetisation and a low glass content. Low temperature suevite (Chao, 1977).

4.1.2. Shock metamorphism in N-73.

The N-73 core provides a near continuous profile through the fallback suevites and crystalline rocks to a depth of 1206 m. The degree of shock metamorphism throughout the core was found to vary with depth as well as within individual subdivisions of the crater suevite and basement (Stöffler et al., 1977; Von Englehardt and Graup, 1977). Each suevite from the Ries crater was found to be characterised by a particular abundance pattern of crystalline rock types and shock metamorphism stages (Graup, 1981). The fallback suevites contained much less material of the high shock

stages with the crystalline rock fragments showing lower degrees of shock (5-15 Gpa) compared to the fallout suevites (30-60 Gpa) (Stahle and Ottemann, 1977).

Diagnostic shock features in the core samples include intergranular microfractures in quartz and hornblende, kink bands in chlorite and biotite, twin lamellae in calcite and mechanical twins in plagioclase (Chao and El Goresy, 1977), shatter cones, shocked quartz (Stöffler et al., 1977) and high pressure mineral polymorphs such as diamond (Abbott et al., 1998b and Schmitt et al., 1999).

The occurrence of some of the reported shock structures were found to decrease with depth. The proportion of the total quartz which is shocked decreases with depth in the suevite below 380 m (Stöffler, 1977). The intensity of shatter cone fractures also decreases with depth and these are associated with small striated shear joints from outward movement due to the passage of shock waves in the upper part and by dykes which may show schlieren indicating lateral movement (Von Huttner, 1977). There is also a decrease in the intensity of deformation from 506-667 m and from 667-1206 m where all rocks show level 0 metamorphism, indicating shock pressures < 10 Gpa, decreasing to 1 Gpa at 1206 m (Von Englehardt and Graup, 1977). Variations in the occurrence of these features have been used to determine the structure of the buried impactites (Stöffler, 1977).

The amount and form of melt glass within the fallback suevite differs quite significantly from that in the fallout suevites. Fallback suevites lacks aerodynamically shaped bombs and the glass is comprised of small irregular fragments (Von Englehardt and Graup, 1984). Within the fallback suevites the percentage of glass decreases from 15-67 vol% in the upper sections to 0-40 vol% from 380-525 m, with no glass apparent below 525 m (Stöffler, 1977). There is no direct decrease with depth as the graded unit (unit I) comprises a near glass-free upper layer, with a glass-rich lower layer (Von Englehardt and Graup, 1984). The overall glass content is estimated to be 28 vol% in fallout suevites and 2-16 vol% in fallback suevites (Von Englehardt and Graup, 1977). The lower glass content may be due to the formation of zeolites, analcite and montmorillonite at the expense of glass (Stahle and Ottemann, 1977).

4.1.3. Structure and geophysical properties of N-73.

Measurements of the geophysical properties of the N-73 profile revealed a low variation in seismic velocity, absorption, electrical resistivity, density and porosity within the suevites but a high degree of variation within the crystalline basement (Pohl, 1977). The results indicated that brecciation extends to a depth of 5-6 km and 20 km in diameter, although the degree of fracturing may also decrease with depth (Pohl, 1977).

The suevite within the crater (figure 4.2) is not believed to have been emplaced as a single unit, rather that emplacement occurred in several stages (Stöffler, 1977). The unit I suevite (314-331 m) coarsens with depth indicating that the material settled back into the crater cavity from the impact ejecta cloud (Jankowski, 1977). The underlying suevite, unit II (331-525 m), has been interpreted as a fallback formation and partially slumped from the crater rim. Unit III (525-602 m) is intercalated with basement rocks and is interpreted as a ground surge into a fractured and disrupted basement. The floor of the transient crater at 505-602 m is disrupted by intercalations of suevite and the lower basement and cut by dike breccias (Stöffler, 1977). The present crater form results from the collapse of a transient crater of 2-2.5 km depth followed by uplift of the basement due to rebound and rim faulting after the excavation stage (Stöffler, 1977).

The crystalline basement (table 4.2) revealed a number of features which can be used to interpret the core samples and crater structure. The basement from 602 to 1206 m is a complex structure containing dyke breccias of shocked material, suevite and allochothonous basement layers. The crystalline sequence in the core profile is not autochthonous but is composed of a series of disconnected slices where the rocks now located below 670 m slid down from near the original crater rim underneath more highly shocked rocks (Von Englehardt and Graup, 1977).

Table 4.2. Classification of N-73 drill core fallback suevite and crystalline basement. (From Stöffler, 1977 and Jankowski, 1977). (! = indicates samples found to contain diamond).

Unit	Depth (m)	Samples (R. Schmitt, Pers.Comm.)	Samples (this study)	Characteristics
Suevite				
I	314-331	*	* !	Coarsens with depth suggesting fallback from ejecta.
II	331-525	* * * * *		Suevite above 378 m (variable melt content) material slumped from the inner crystalline ring.
			** !	Suevite below 378 m probably represents a fallback formation (melt content decreases with depth.
III	525-602	* * * *		Intercalated with basement rocks, interpreted as a ground surge into a fractured and disrupted basement.
Crystalline basement				
I	505-670	* !		Moderately shocked (160 kbar) with shatter cones. Cut by suevite in upper part (505-602 m and 642 m) and dike breccias with compositions similar to melt poor suevite.
II	670-790	*		Low shock metamorphism (>50 kbar). Increased intensity of shatter cones cut by carbonate rich dike breccias. Moderately shocked granite (762-775 m) allochothonous relative to country rocks.
III	790-890	* * * *		Low shock metamorphism with polymict and carbonate bearing dike breccias.
IV	890-1070	* *	*	Weak shock effects only in biotite. Fine grained dike breccias, less polymict with a distinct laminated texture including shocked quartz.
V	1070-1190	* * *		Weak shock effects only in biotite. Dike breccias with a high ratio of quartz to feldspar and no shocked quartz. Extreme concentration of dikes within granitic intercalation (1133-1190 m).
VI	1191-			Different lithology (migmatic augen gneisses). No dike breccia.

4.2. HAND SPECIMEN DESCRIPTIONS.

The samples of core were provided by Professor D. Stöffler and comprise three suevites from the 343 m (slumped material), 384 m (fallback), 494 m (fallback) sections and a basement rock from the 1059 m section. These suevites all fall within the second unit of the core from 331 to 525 m depth, which makes them "high temperature suevite with strong magnetisation and including some large blocks of basement material" (Stöffler et al., 1977).

The four core samples each 10 cm diameter and 10 to 15 cm in length having been cut in half parallel to the core axis to form semi-circular cross sections (i.e. 400 to 700 g in weight). A high degree of alteration such as clay mineralisation and oxidation in the samples made the identification of small fragments within the groundmass difficult, often only the freshest fragments could be identified. This was previously observed by Stahle and Ottemann, (1977) who reported that the glasses in crater suevite were almost completely decomposed or transformed into secondary minerals. The samples were all highly resistant to fracturing and far less friable than the quarry suevites, indicating that they were fresher and less weathered compared to the fallout suevite samples. The samples were described in detail in chapter 2 and are summarised in table 4.3.

Table 4.3. Summary of characteristics of the N-73 core samples for this study.

Sample type	Depth (M)	Sample no	Sample characteristics
Suevite- high temperature[1] (Slumped[2])	343, 20	NC343	Fragment of gneiss with glass rim within groundmass, possible granite fragment.
Suevite- high temperature[1] (Slumped[2])	384, 07-14	NC384	Red-brown colour, high percentage of altered fragments, fresh crystalline fragments <0.5-1 cm.
Suevite- high temperature[1] (Fallback[2])	494, 64-86	NC494	Brown colour, single elongated vesicular glass fragment, 1-2 cm lithic fragments, red alteration.
Basement rock	1059, 10-25	NC1059	Medium-fine grained, pink-red crystalline rock. Fine grained brecciated areas.

[1] Chao, (1977), [2] Stöffler, (1977).

4.3. OCCURRENCE AND DISTRIBUTION OF IMPACT DIAMONDS AND GRAPHITE IN IMPACT PRODUCED ROCKS AND SHOCKED BASEMENT MATERIAL.

Acid demineralised residues of the samples were produced following the procedures described section 2.6. The chemical and mineralogical compositions of the residues were comparable to those of the fallout suevite samples analysed (table 4.4). Scanning electron microscope analyses of the residues revealed that the core suevites contain zircon ($ZrSiO_4$), rutile (TiO_2) and graphitic carbon. Transmission electron microscope analysis of the residues identified graphite and diamond (Abbott et al., 1998b) similar to that previously found in fallout suevites (Rost et al., 1978; Hough et al., 1995c) and glass (Abbott et al., 1996; Siebenschock et al., 1998). Diamonds were not detected in the basement sample NC1059. As mentioned, these suevite samples are from within the high temperature suevite formation, the implications of this for the preservation of shock formed diamonds is discussed in section 4.6.1. Differences in the

isotopic composition and the morphological structure of the diamonds found within these samples are the subject of the discussions to follow.

Table 4.4. Composition of acid resistant residue, N-73 samples.

Sample	Composition	
	SEM	TEM
NC343	Zircon, rutile, graphitic carbon	diamond, graphite, zircon
NC384	Zircon, rutile, Al-silicates, graphitic carbon	diamond, graphite.
NC494	Zircon, rutile Al-silicates, graphitic carbon.	diamond, graphite.
NC1059	Zircon, rutile Al-silicates.	-

Under the optical microscope the residues were composed of visible zircon crystals together with black carbon clusters or flakes and in samples 343 and 384 in particular several small diamonds (50-100 μm). The NC494 sample contained a higher proportion of dark coloured material in comparison to the other two core suevite samples with a higher proportion of rutile (TiO_2) and aluminium silicates. This is comparable to the composition of the Seelbronn quarry fall out suevite residue.

4.4. MORPHOLOGICAL CHARACTERISTICS OF DIAMONDS AND GRAPHITE IN IMPACT PRODUCED ROCKS AND SHOCKED BASEMENT.

The core samples contained two allotropes of carbon, namely graphite and diamond. The features exhibited by these minerals were similar to those observed in grains from the fallout suevite residues. These features included stacking faults, layering, skeletal needle-like features, twinning and etching. In addition, blocky grains were also apparent and even best observed in the core sample residues. Layering is most likely an inherited feature from the precursor carbon material (Masaitis, 1972, 1994 and section 3. 4.1), whereas skeletal, blocky and etched features may be related to the

precursor material, conditions of formation or post impact effects. Stacking faults may be inherited structures or a result of the conditions of formation, variations in the degree of shock, variations in the degree of structural ordering or formed at polytype or compositional boundaries.

4.4.1. Layering.

The carbon observed in the samples under the scanning electron microscope (SEM) was generally of two forms, platy layered crystals and twisted fractured crystals with surface lineations. These are illustrated in figures 4.2a-b. The example shown in figure 4.2a is an irregular rounded grain from NC384 which was approximately 150 μm in diameter, platy in plan view and ornamented with linear surface features. These are picked out by the high relief of smaller crystals sticking to the surface (most likely zircons). Figure 4.2a illustrates a carbon grain amid smaller zircon crystals from NC494. The grain appears to be twisted and fractured and shows distinct linear structures along the long axis, which are ropy and irregular in texture. Figures 4.3a-b show two examples of layered crystals from NC343, with at least 11 clear layers along the length of the crystal. Each layer shows stacking faults in varying orientations. The layers also vary in thickness although they average about 1μm thick, and some appear to grade into others. Figure 4.3b shows a close-up of this layering. Figure 4.4b shows a layered grain from NC343, the layers are similar to those shown in figure 4.3a-b but show variable thickness and orientations indicating offset of the original graphitic layering.

(a)

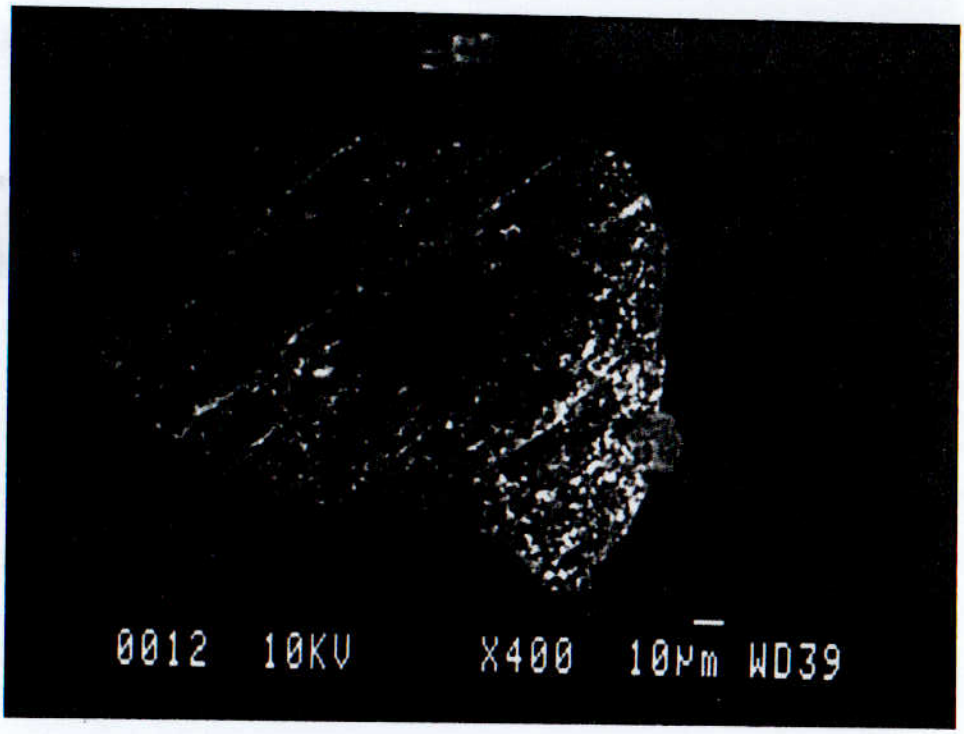

(b)

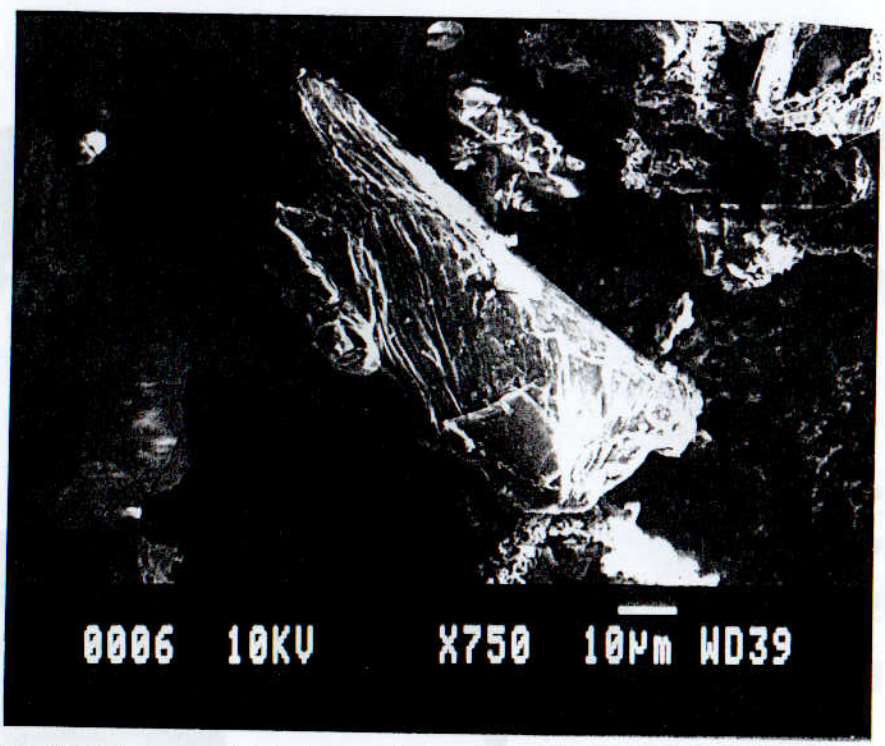

Figure 4.2. SEM images of (a) platy carbon grain from NC384 with surface lineation features highlighted by small zircon crystals. [x 400, 10 kV]. (b) carbon grain from NC494 showing surface lineation. [x 750, 10 kV].

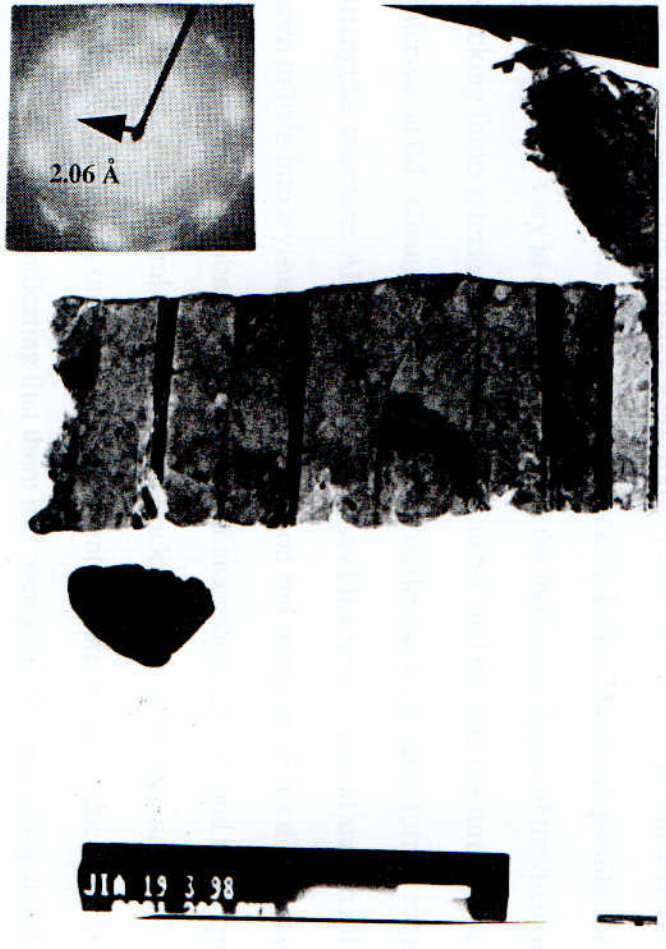

(a)

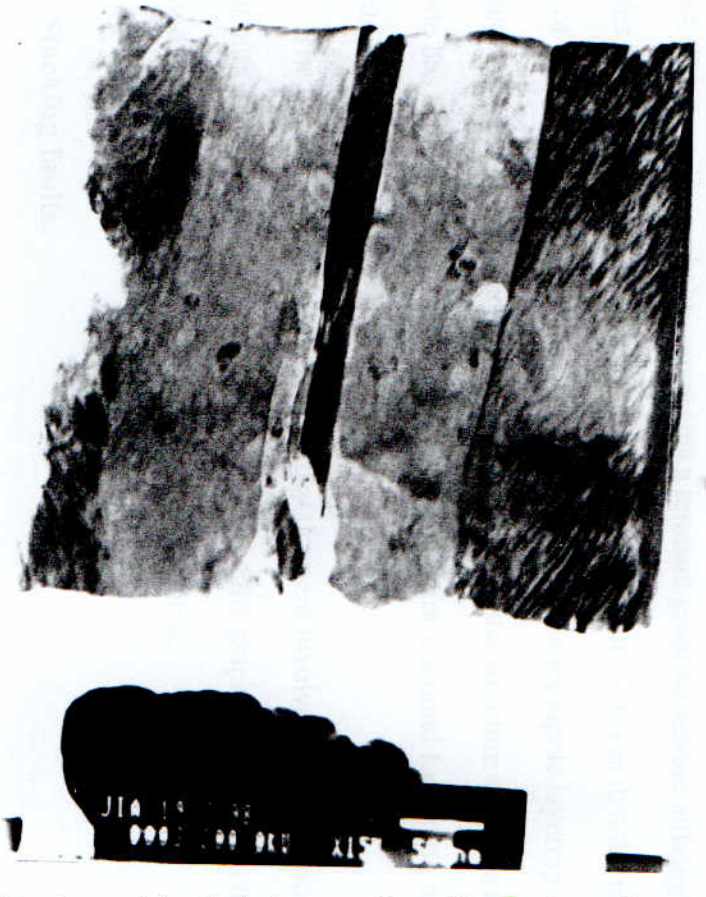

(b)

Figure 4.3. (a) BFTEM image of layered grain from NC343 showing 12 layers with alternate stacking fault features. Inset SAED shows diamond 2.06 Å [x 6k, 200 kV, scalebar 1µm]. (b) High magnification image of diamond from NC343. [x 15 k, 200 kV, scalebar 500 nm].

Layering appears to be most well developed within the diamond samples from NC384. This layering probably represents a remnant graphite feature although, the samples which are cut across the layers are unusual (figure 4.4a) in that the primary plane of weakness would be expected to follow the crystallographic layering. The existence of these layers indicates that the original crystal structure of the precursor graphite has been preserved and that the mechanism for diamond formation must take this into account.

The most likely mechanism is one that does not involve the destruction of the crystal lattice but rather the direct transformation of the graphite structure to that of diamond whilst preserving palimpsest graphite structures.

4.4.2. Stacking faults.

As the examples shown in figures 4.3a-b illustrated, stacking faults are a common feature of the diamonds found in these suevite residues. Figures 4.5a-b show these features at a higher magnification revealing greater detail of the structures. The samples are both finely layered diamonds from NC384.

The example in figure 4.4b from NC384 shows several thin diamond plates or layers with several overlapping sets of stacking faults. These sub-parallel dark lamellae can be seen to vary in orientation between the individual layers of the diamond. The stacking faults intersect at an angle of about 60° and 90° and fractures in the sample intersect at 60°. Changes in the orientation of the stacking faults form a roughly triangular structure. Alternatively at the base of the image vertical stacking faults can be seen to fade into a visually amorphous region and reappear with a diagonal orientation. This amorphous region is not composed of amorphous carbon and may represent a region where structural features such as stacking faults have been annealed. This structure is bound on one side by an apparent fracture, possibly due to the removal of associated graphite indicating that there had been graphitisation along structural defects. The inset selected area electron diffraction (SAED) pattern shows a cubic diamond structure with diffuse rings indicating polycrystallinity.

(a) (b)

Figure 4.4. (a) BFTEM image of layered diamond from NC343. [x 80 k, 200 kV, scalebar 1 μm]. (b) BFTEM image of a layered and fractured diamond from NC384 showing extensive stacking fault features and fractures at 60°. [x 20 k, 200 kV, scalebar 200 nm].

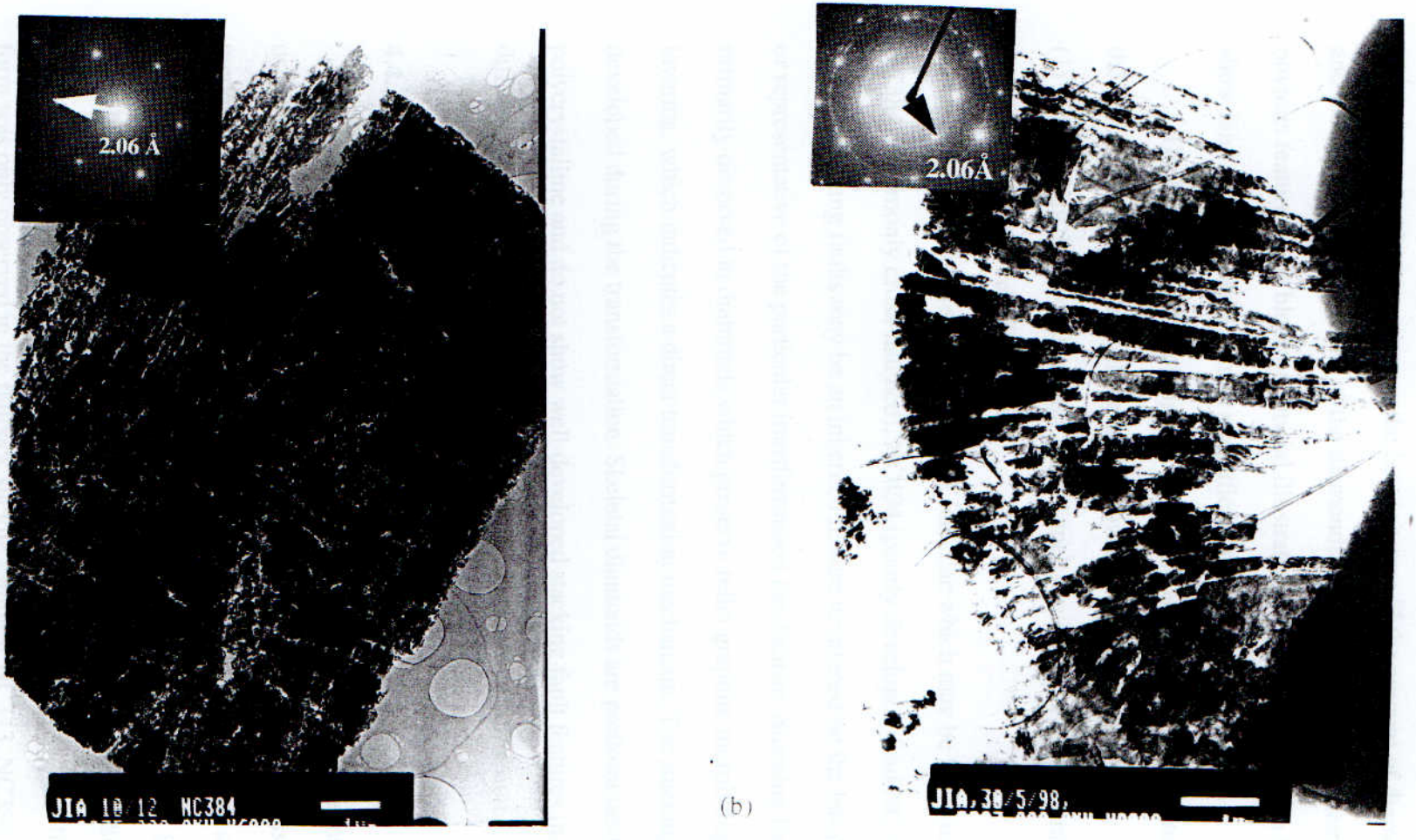

(a) (b)

Figure 4.5. (a) BFTEM image of a blocky fractured diamond from NC494 showing skeletal etched structure at the top of the grain and faint stacking fault features below the opaque area. Inset SAED shows diamond 2.06 Å.[x 6 k, 200 kV, scalebar 1 μm]. (b) BFTEM image of skeletal etched diamond grain from NC384. Inset SAED shows diamond 2.06 Å. [x 8 k, 200 kV, scalebar 1 μm].

Again the stacking faults appear to be most well developed in samples from NC384. The NC384 sample was the best in terms of the amount of diamond present and the clarity of the structure of the diamonds, the other samples contained less obvious features. The blocky diamond illustrated in figures 4.6a-b from NC494 does show faint stacking faults at high magnification.

The formation of stacking faults was discussed in detail in chapter 3 and as in the fallout impactites the stacking faults show two morphologies:

(1) very densely distributed, narrow black lamellae with variable sub-parallel orientations and cross-hatching; seen in NC384.

(2) sparsely distributed, short, thick black lamellae which may be wavy in form. Seen in NC384 (commonly cross-hatched), NC494 (poorly developed) and NC343.

Stacking faults may be an inherited feature developed on the basal graphite plane or representative of the particular transformation mechanism. Stacking faults are primarily observed in diamonds which preserve relict graphite morphologies such as layering, which indicates a direct transformation mechanism. The stacking faults may be developed during the transformation. Skeletal diamonds are predominantly polycrystalline and do not show well-developed stacking fault features indicating a difference in their formational mechanism and conditions of formation.

4.4.3. Etching.

Blocky crystals which were identified as diamond and graphite intergrowths using the thinner margins of the grains (in order to obtain SAED patterns) were found predominantly in NC494. These are distinct from the skeletal diamonds seen in the fall-out suevites (OQS and SBS) in that their morphology suggests remnant graphitic structure. The example shown in figure 4.5a is representative of several grains which were seen in this sample. These are blocky grains with areas of etching, this blocky form was only observed in the fallback suevite samples(NC343, NC384 and NC494). The sample shown in figure 4.5a is a euhedral grain from NC494 with areas of etching and stacking faults visible at the top of the image. The image shows an irregular surface

structure with a distinct linear ornamentation running across the image parallel to the main trend seen in the lower magnification image. These may represent ridges of crystallites with preferred orientations similar to those seen in skeletal diamond (figures 3.13a-b and 3.14a-b). The small grain size of the crystallites makes this difficult to determine. Further treatment of the samples using fuming perchloric acid revealed the skeletal fine grained structures shown in figure 4.5b. The sample (NC384) has a sub-parallel linear trend to the etching or skeletal structure, possibly highlighting areas where intergrown graphite has been removed by the oxidation with fuming perchloric acid.

The diamonds in the fall-back suevite samples were found to be larger and thicker than the examples extracted from the other Ries residues. The approximate thickness of the grains can be determined from optical microscope observations and the appearance of the diamond plates under TEM. Thick grains (figure 4.5a) are distinct from thinner samples (figure 4.4b) although this is generally in the order of a few μm. This may be an artefact of the extent of the acid digestion process, in that intergrown graphite or poorly crystalline diamond aggregates are still in coherent structures within the fall-back suevites. Alternatively diamonds formed from the shock transformation of coal are described as porous and blocky in structure, (Ezersky, 1982; 1986) indicating that the nature of the precursor carbon material can have a strong influence on the diamond form. Thus, it is possible that these blocky diamonds may have formed from less crystalline graphite or have been etched by the action of hot alkali gases (Vishnevsky and Raitala, 1998). This indicates that the blocky structure could be a true feature of the diamond formation process and a residual feature of the precursor material.

4.4.4. Skeletal form.

Skeletal needle-like structures were observed in diamonds from NC384 (figure 4.6). Previous analyses during this study had shown blocky morphologies with associated graphite and cubic diamond on the SAED patterns. Following further perchloric acid treatment the graphite was completely removed leaving the structures

shown in figure 4.5b. The elongate skeletal diamonds which were found in the fallout suevite samples from the Ötting and Seelbronn quarries were not observed in the NC-73 fallback suevite samples. This is unlikely to represent a feature of the acid digestion process as all the samples were treated in the same way. This is therefore, as discussed in chapter 3 more likely to represent an etching feature during diamond formation or growth of the diamond crystallites within a directional pressure field and in conditions of limited carbon saturation. The skeletal structure shown in figure 4.5b contrasts strongly with the skeletal structures described in section 3.4.4. The grain in figure 4.5b appears to be etched and corroded along remnant graphitic layering. The skeletal polycrystalline diamonds (figures 3.13-3.14a-b) do not show remnant apographitic structures suggesting that they were not formed by extensive corrosion and etching of shock transformed diamond as suggested by Langenhorst et al. (1999).

4.4.5. Twinning.

Streaking of the spots on SAED patterns, which is thought to be characteristic of twinning, was not frequently seen in the diamonds from the core samples. Samples NC343 and NC384 did show some double reflection SAED patterns indicating reflections from twinned crystals. Figures 4.3a-b shows SAED patterns for an elongate layered diamond crystal; the diffraction spots indicate that the sample was polycrystalline, with double reflections (streaking through the spots indicates the possibility of twinning). These may be inherited features - for example diamonds from Popigai show graphitic twins (Koeberl et al., 1997) - or they may be growth or deformation structures.

The twinning in these diamonds (NC343 and NC384) may be either growth twins, such as contact and penetration twins or deformation twins. As mentioned in chapter 3 growth twins form readily during diamond growth and natural vapour deposition might be characterised by a wide range of twin morphologies. Deformation twins on diamond (111) have been described following plastic deformation at room temperature (Mao et al., 1979). During phase transformations twinning may

accommodate the interfacial stress between the parent and daughter phases (Bales and Gooding, 1991). In the case of the diamonds from the Ries the transformation would be from graphite to cubic diamond.

Detailed examination of microtwins requires the use of high resolution transmission electron microscopy (HRTEM) which indicate whether the structures are a result of shock transformation or growth from a vapour phase. Daulton et al. (1996) compared structures in nano-diamond from meteorites, CVD and detonation products, determining that the ratio of different twin structures, dislocations and the presence of londsdaleite could indicate the transformation mechanism to be either martensitic or homoepitaxial growth. Table 4.5. Summarises the criteria they used and their conclusions.

Table 4.5. Nano-diamond microstructures [from Daulton et al., 1996].

Structure	**Detonation**	**CVD**	**Meteoritic**
Dominant MT	linear	non-linear	slightly non linear
Linear MT/non-linear MT	2.72	0.36	0.87
Star-twins/twins	0.04	0.23	0.09
Interpretation	*Anisotropic growth*	*Isotropic growth*	*Isotropic growth*
Twins/single crystal	2.48	1.28	1.25
Interpretation	Fast growth rate		
Dislocations	Present	Not observed	Not observed
Interpretation	Martensitic process	Homoepitaxial growth	Homoepitaxial growth
Polymorphs	Lonsdaleite	Possibly Lonsdaleite	Lonsdaleite
approximate size	<78 Å	<12 Å	<17 Å

MT = Multiple twin.

Detailed high resolution transmission electron microscope (HRTEM) studies of nano-diamonds from the Allende and Murchison meteorites (Daulton et al., 1996) indicated that there are significant differences between the structures formed by shock synthesis compared to vapour deposition (Table 4.5). Shock-produced diamonds were

dominated by anisotropic, rapid growth rate features produced by solidification or transformation behind a planar shock front (Daulton et al., 1996). CVD-produced diamonds on the other hand showed structures characteristic of isotropic growth conditions. Linear multiple twins and dislocations indicate fast martensitic anisotropic growth whereas CVD growth structures are predominantly isotopic and non-linear with a higher ratio of single crystal structures and fewer dislocations.

In the case of meteorite impact this situation is further complicated by the fact that CVD processes will be dominated by shock-induced vapourisation producing a combination of shock and vapour phase structures. The pressure and temperature conditions as well as the degree of carbon saturation will be highly variable suggesting the formation of many different structures in vapour deposited diamond, e.g. Tamor and Everson, (1994) suggest that natural vapour deposition might be characterised by a wide range of twin morphologies.

4.4.6. Summary of diamond occurrence, structures and morphology.

The diamond concentration observed in the suevite samples from the NC-73 drill core was approximately the same as that seen in the Seelbronn and Ötting suevites. The concentrations were calculated using stepped combustion carbon yields and are discussed in section 4.6.2. Previous investigations of 25 NC-73 samples (shown in figure 4.2) has suggested that there is significantly less diamond within the fallback suevites compared to the fallout samples (Schmitt et al., 1999) although the fallback suevite units investigated here were not included within that study.

The development of structural features within the diamonds studied was variable (table 4.6). The weightings for the individual features were allocated as described in chapter 3. Diamonds from NC494 were coarse, blocky and graphitic and did not show well developed stacking faults, layering or skeletal features suggesting thermal annealing. Diamonds from NC343 and NC384 clearly displayed multiple layering, stacking faults and polycrystallinity. Skeletal elongate structures as seen in the fallout suevites were only observed in diamonds from NC384.

Table 4.6. *Summary of features observed in diamonds from N-73, Ries crater.*

Samples	Stacking faults	Poly-crystalline	Layered	Twinning	Skeletal	Etched	z
NC343	√√√	√√	√√√	√√	–	–	23
NC384	√√√	√√	√√	√	√√	–	20
NC494	√	–	√	–	–	√√√	15

√ = Occasionally observed, √ √ - commonly observed, √√√ - Primarily observed.
- = Feature not detected.
z = Estimated number of diamonds observed.

These structures (e.g. stacking faults and twinnning) may indicate the requirements for the diamond formation mechanisms. It has been suggested that impact diamonds are mainly formed from the martensitic transformation of precursor carbon such as graphite (Masaitis, 1994) or coal (Ezersky, 1992; 1986) or through a CVD mechanism from a carbon feedstock possibly derived from graphite and carbonates (Hough et al., 1995c). Studies of the structural characteristics of CVD and detonation produced diamonds with meteoritic diamonds indicated that the nature of structures such as twinning and defects could indicate which mechanism of formation was the most likely (Daulton et al., 1996). Similarly the structures described in chapters 3 and 4 may indicate which mechanism or combination of mechanisms is required. This will be discussed in section 4.7 with reference to the shock pressures and temperatures experienced and the other carbon polymorphs present at the Ries crater.

4.4.7. COMPARISON OF THE DISTRIBUTION AND FREQUENCY OF STRUCTURAL AND MORPHOLOGICAL FEATURES FROM A VARIETY OF RIES CRATER IMPACTITES.

A wide variety of structural and morphological features can be identified in impact diamonds including stacking faults, twinning, polycrystallinity, layering, skeletal structures and etching. The possible causes and occurrences of these structures were

discussed in sections 3.3 for the fallout impactites and 4.3 for the fallback impactites. From the relative frequency in which these features were observed and the extent to which they are developed in the various samples an arbitrary weighting may be applied (tables 3.2 and 4.6). To illustrate this diamond grais from the OQS exhibited a wide range of features which varied in their predominance, e.g. there were more stacking faults than layering. In comparison diamonds from the NC494 suevite showed few features such as stacking faults and had mainly etched and blocky features. The distributions and frequency of features being observed is also dependent on the amount of diamond available for observation. The suevite samples provided the most diamond grains per TEM grid, averaging 15 to 40 grains and the Polsingen and Aumühle samples yielded far less, averaging only 1-5 grains.

The relative distributions of these features (stacking faults, twinning, polycrystallinity, layering. skeletal and etching) between the samples is illustrated in figure 4.6 by showing barcharts of the features for each locality and the location of the localities around the Ries crater. The two suevite samples, Ötting and Seelbronn may be compared quite closely as they comprise similar lithologies. The PIMR represents a mass of anomalously high-temperature suevite which cooled and recrystallised over a longer period of time (Von Englehardt and Graup, 1984) and it is perhaps to be expected that relatively few impact diamonds were detected in the residues and that these samples showed relatively few structural features. This may represent high temperature annealing or graphitisation. Similarly the AQG represents a variable shocked ejected mass of basement material in which diamond has been tentatively identified. further analysis of this sample is required to confirm this as only a single grain was detected.

The fallout and fallback suevites may be compared with more confidence as a large selection of grains were available for analysis under the TEM in each of these samples following perchloric acid treatments. Diamond samples with clear layering were detected in the NC384 and were comparable to those observed in the fallout suevites. There does not appear to a be a variation with depth in the features seen in the fallback suevites. As described in section 4.2. the structure of the suevite deposits within the

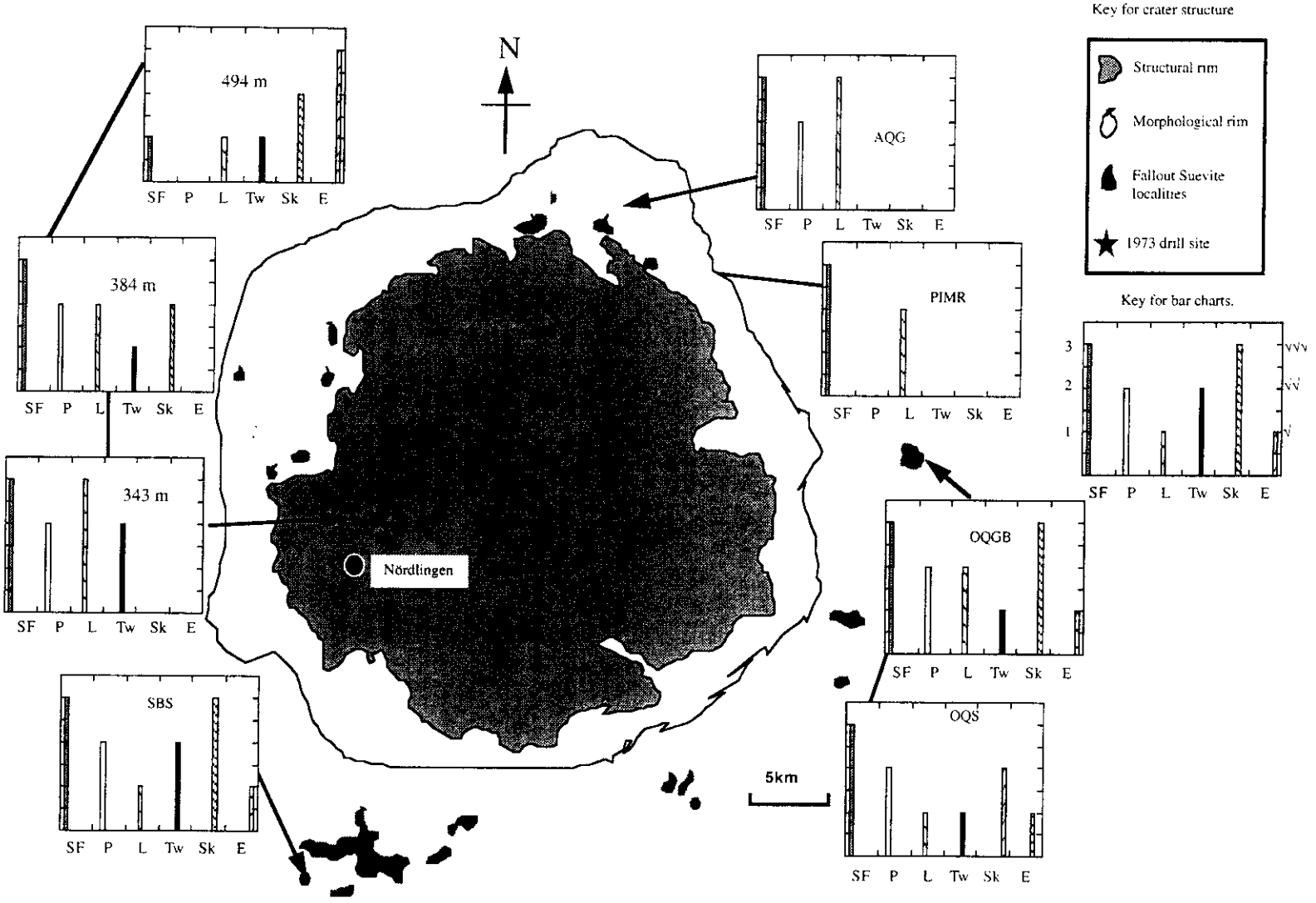

Figure 4.6. Schematic illustration of the state of preservation, distribution and frequency of structural and morphological features in impact diamonds from a variety of Ries crater impactites. Values taken from figures 3.2 and 4.6. SF = stacking faults; P = polycrystalline; L = layering; Tw = twinning; Sk = skeletal; E = etched.

crater is not straight-forward, but complicated by the intermingling of fallback units and slumped units (table 4.3). NC494 represents fallback material whilst NC384 and NC343 probably represent slumped material from the inner crater ring (Stöffler, 1977). Thus the two slumped suevites may have more in common with fallout suevite than the fallback section. This is not directly apparent from the distribution of structural features (figure 4.6) although NC494 appears to show a limited range of features which may indicate thermal annealing of structures such as stacking faults and twinning.

4.5. CARBON ISOTOPIC COMPOSITION OF DIAMONDS AND GRAPHITE FROM THE NÖRDLINGEN 1973 CORE.

The samples were analysed for bulk carbon stable isotopic values and for detailed isotopic profiles using stepped combustion combined with static mass spectrometry. These analyses were all performed as described in chapter 2.

4.5.1. Bulk carbon isotopic analyses.

Bulk carbon analyses of the four core samples, were performed using bulk combustion and a static mass spectrometry system. The results are summarised below in table 4.7. and appear to show no discernible trend with depth, e.g. as a result of different carbon sources from different depths in the pre-impact target stratigraphy.

Table 4.7. Summary of bulk carbon isotopic measurements of N-73.

Sample	Type	$\delta^{13}C_{(PDB)}$	$\pm\sigma$	% Carbon
NC343	Suevite	-15.4	0.020	0.41
NC384	Suevite	-13.9	0.021	0.43
NC494	Suevite	-18.3	0.013	0.13
NC1059	Basement	-13.9	0.018	0.12

The fall-out impactites show a reversed stratigraphy with material derived from depth (suevites) overlying material derived from shallow levels (Bunte Breccia). The lack of a trend with depth is hardly surprising considering the limited number of

samples available, the complexity of shock metamorphism and the structure of the basement itself. The isotopic values encompass a relatively narrow range from $\delta^{13}C$ = -13.9 to -18.2 ‰ and are all from whole-rock samples of core suevites and basement rock.

Interestingly the basement rock sample from NC1059 had a light carbon stable isotopic composition compared to NC494 and NC343, similar to that of the core suevite 384 m and a low carbon content that is similar to that of the 494 m section. Separate analyses of lithic fragments and glass fragments from these samples was not possible due to the highly competent nature of the samples.

4.5.2. Stepped combustion carbon isotopic analyses.

Acid demineralised residues of the core samples were analysed as bulk samples (a small random selection of grains) and as individual grains of diamond and graphite picked from the residues (prior to the perchloric acid stage). Wherever possible diamond grains identified in the residues were extracted and stored in clean dry glass petri-dishes for subsequent stable isotopic analysis.

The selection of grains was necessarily random due to the small size of the grains within the residues even under the optical microscope (50-300 μm). The composition of the residue at this stage had been confirmed as diamond using the TEM with minor zircon and highly crystalline graphite. Diamond, silicon carbide and highly crystalline graphite are the only carbonaceous phases likely to survive the acid digestion procedures. Figure 4.7 illustrates the stepped combustion profile of a selection of random grains from NC384R.

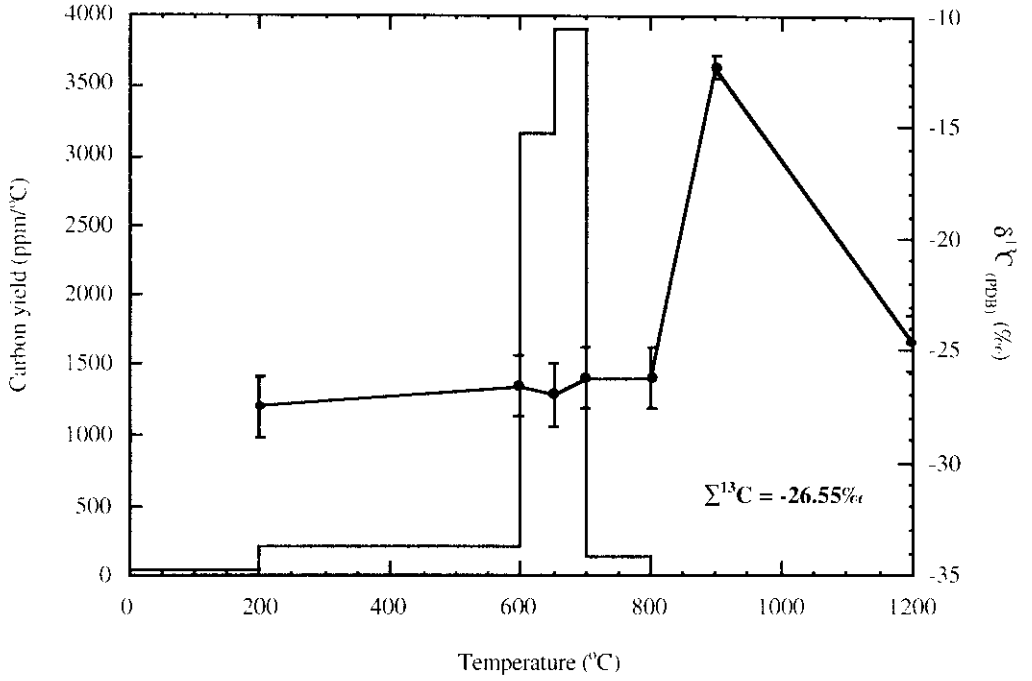

Figure 4.7. Stepped combustion analysis of acid demineralised residue from NC343 (sample weight = 20 µg). $\Sigma\ \delta^{13}C$ = -26.6 ‰ and Σ carbon yield = 88.3 wt %.

Carbon contamination from handling of the sample or platinum bucket is removed by a 200 °C cleaning step prior to the stepped combustion. The total carbon yield was 88.3 wt % and the peak yield corresponds to 70.6 % of this. The sample shows a main carbon release at 600 °C with only carbon blank releases above 700 °C. The average carbon isotopic composition for the sample is –26,55 ‰.

The carbon stable isotopic composition of the other two crater suevite samples from the N-73, are shown in figures 4.8 and 4.9.

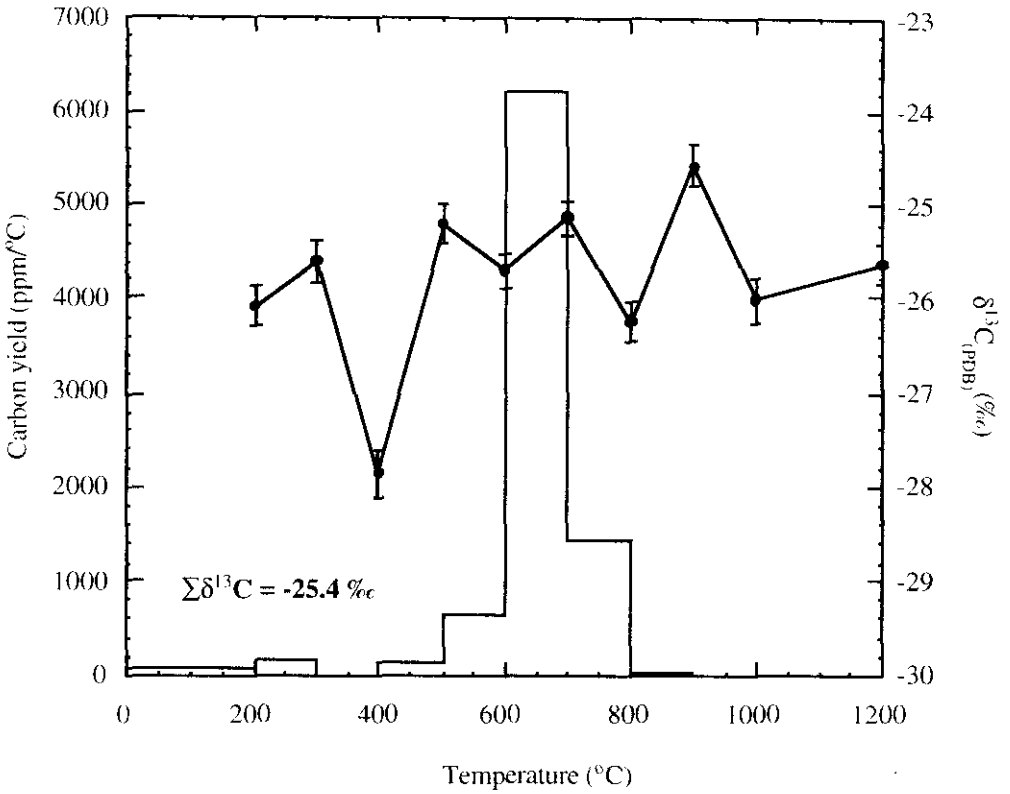

Figure 4.8. Stepped combustion analysis of acid demineralised residue NC384 (sample weight 6.4 μg). $\Sigma\ \delta^{13}C$ = -25.4 ‰ and Σ carbon yield = 45.5 wt %.

Figure 4.8. shows a single carbon release at 600 °C and 700 °C that probably represents fine grained diamond in the NC343 m residue. The total carbon yield was 45.5 wt % with the peak yield representing 77.6 % of this. The total carbon isotopic composition $\delta^{13}C = -26.6$ ‰, which does not vary across most of the stepped combustion, although the 700 °C yield is slightly enriched in ^{13}C. This value closely matches the other isotopic analyses for the core samples, with the exception of the sample from the 494 m section which is discussed below.

The second example (figure 4.9) is from the NC494 and has a more complicated stepped combustion profile. The profile shows two separate carbon releases with the first release at 600 °C probably representing the combustion of graphite or fine grained diamond and comprises 16.2 % of the total yield of 50.3 wt %. A further release at 800 to 1000 °C represent coarser grained diamond or silicon carbide, comprising of 81 % of

the yield. The isotopic composition of the sample varies quite markedly with temperature ranging from $\delta^{13}C$ = -19.2 ‰ at 600 °C, -22 ‰ at 800 °C, -12 ‰ at 900 °C and -17.9 ‰ at 1000 °C, with an average carbon isotopic composition of –17.9 ‰. The M-shaped isotopic profile is characteristic of many other diamond bearing residues e.g. Ötting quarry suevite residue (Hough et al., 1995c) and residues from the Brownie Butte fireball layer, Berwind canyon ejecta layer and Mimbral Ir-rich layer (Hough, 1996).

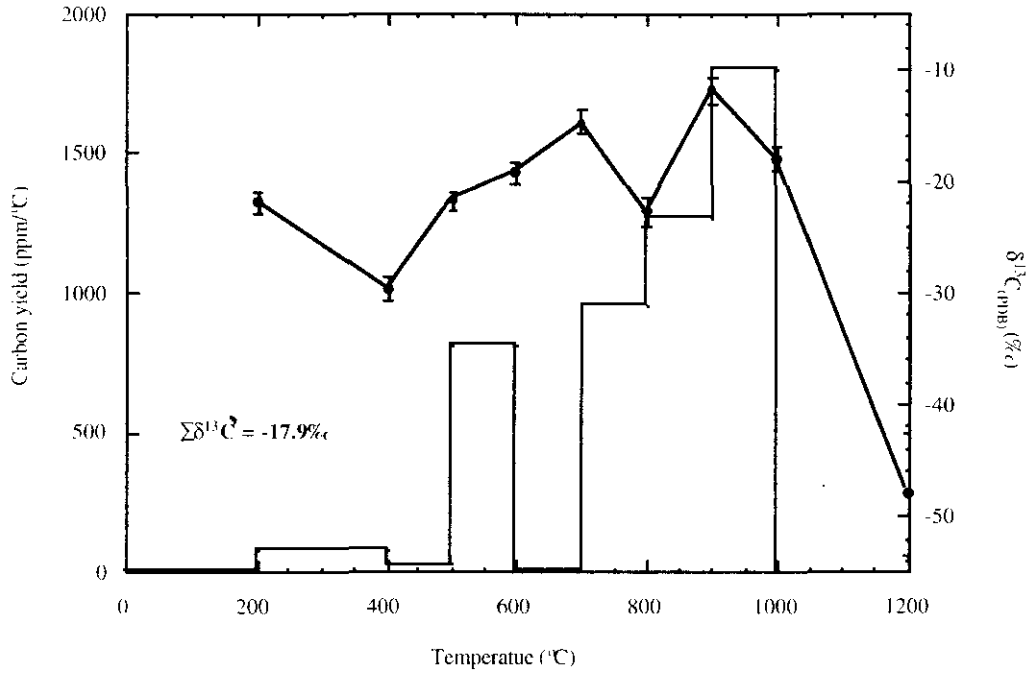

Figure 4.9. Stepped combustion analysis of acid demineralised residue from NC494 (sample weight = 4.6 µg). $\Sigma\ \delta^{13}C$ = -17.9 ‰ and Σ carbon yield = 50.3 wt %.

The $\delta^{13}C$ (-17.9 ‰) of the NC494 residue contrasts with the other analyses and compares most closely with the SBS samples and implies that different carbon sources or a single carbon source with heterogeneous stable carbon isotopes may have contributed to the sample compositions. Fall-back suevites contain less sedimentary material than the fall-out suevites (Stöffler, 1977), but the ^{13}C-enriched carbon stable isotopic compositions of the SBS and NC494 residues suggest the admixture of carbonates.

The variation in carbon yields and $\delta^{13}C$ of NC 494R (figure 4.9) indicates either a multiple phase combustion within a single release or the combustion of a single phase (diamond) with varying grain sizes. The low temperature yield (600 °C) may represent graphite as it combusts more readily than diamond although the isotopic composition $\delta^{13}C$ of -19.2 ‰ is relatively enriched in ^{13}C compared to the average composition of graphite. The high temperature yields may represent the combustion of diamond with silicon carbide with the exothermic combustion of diamond allowing the SiC to combust at lower temperatures than expected. SiC may be expected to combust at temperatures outside the range of the furnaces at approximately 1350 °C, although this is again dependent on grain size (e.g. Russell, 1992). Co-combustion with diamond may allow lower temperature combustion.

4.5.3. Graphite.

Samples of graphite were extracted from the residues wherever possible prior to the chromic and fuming perchloric acid treatment stages. These samples may in fact be graphite and diamond mixtures as examination under the TEM indicated that many of the graphite grains were in actual fact intergrowths of diamond and graphite. The grains were black under the optical microscope and were chosen with the least number of additional grains attached, for example many of the black grains appeared to be coated by clusters of zircons and or diamond.

These two stepped combustion profiles are both samples of 100-200 µm graphite extracted from the NC494 m section residues. Figure 4.10 has a total carbon yield of 18 wt % with the peak yield representing 91.4 % of this. This low carbon yield indicates that the sample was not very pure and may have contained zircon or other non-carbonaceous components. The second example (figure 4.11) has a peak yield of 70.7 %, with high carbon yield below 400 °C representing organic contamination or amorphous carbon. Both profiles show clear carbon releases at 500-600 °C, and comparable total isotopic compositions of – 26.2 to -25.4 ‰ representing the $\delta^{13}C$ of graphite in this residue. The isotopic composition of graphite from the core samples

also compares well with the composition from similar samples extracted from the fallout suevite samples. These features and those of the other core samples will be discussed in section 4.6.1.

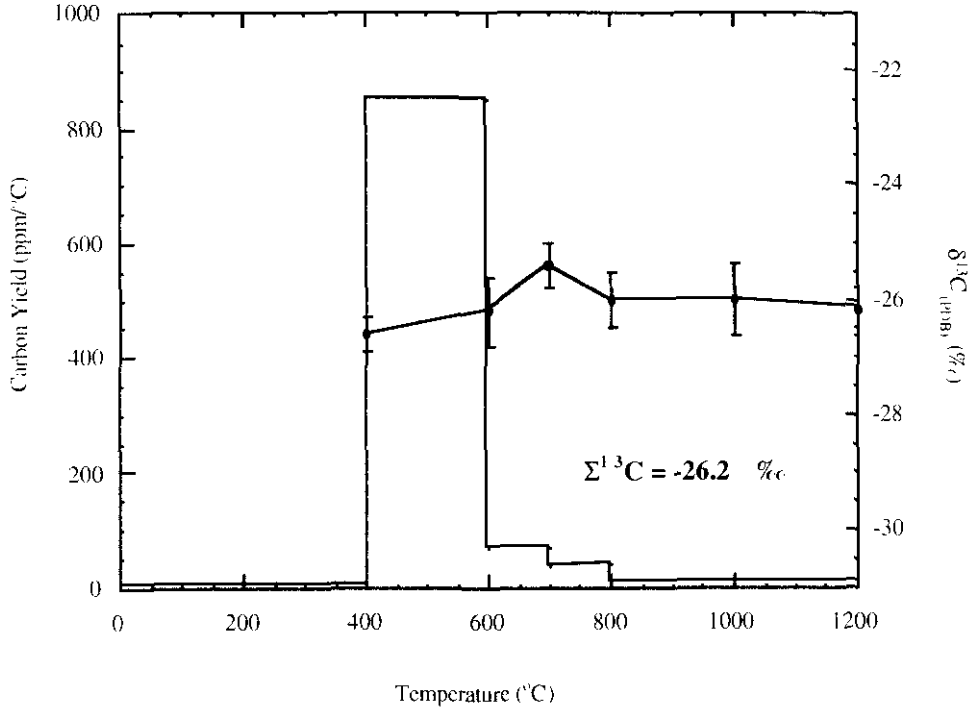

Figure 4.10. Stepped combustion analysis of a graphite grain from NC494 (sample weight = 68 μg). $\Sigma\ \delta^{13}C$ = -26.2 ‰ and Σ carbon yield = 18 wt %.

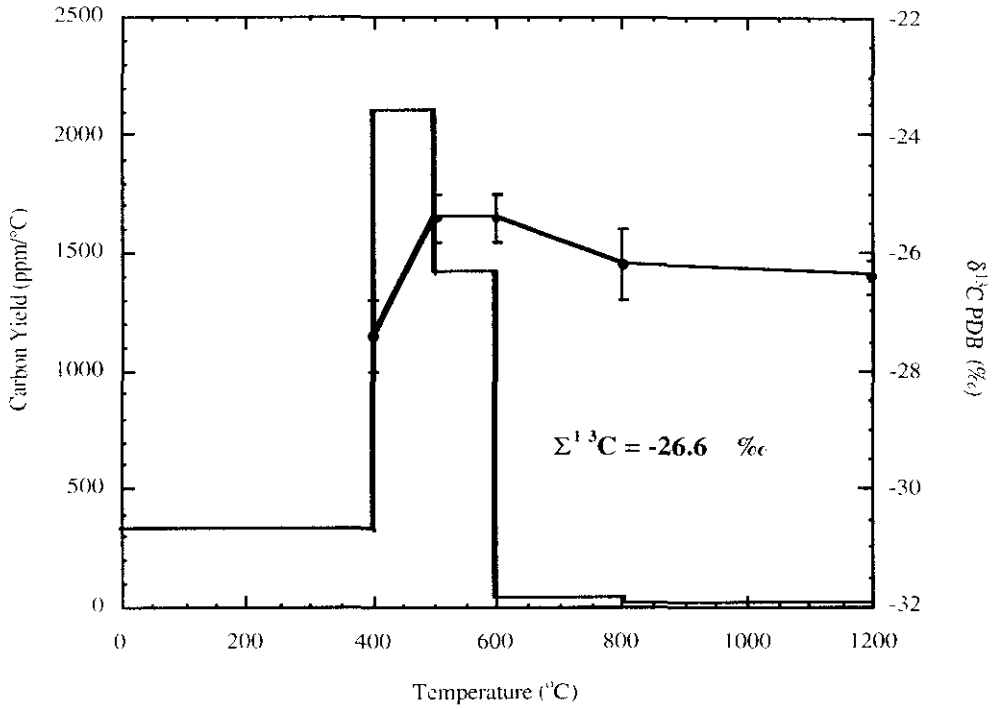

Figure 4.11. Stepped combustion analysis of a graphite grain from NC494 (sample weight = 21 μg). $\sum \delta^{13}C$ = -26.6 ‰ and $\sum$ carbon yield = 49.4 wt %.

The samples (figures 4.10 and 4.11) combusted within the temperature range at which graphite is typically combusted (from 400-500 °C). The low carbon yields suggest that the grains identifed as graphite (using optical microscopy) from the NC494 residue were not pure. The carbon yields from 500-800 °C may represent the combustion of diamond-graphite intergrowths. The grain size of these intergrowths within the sample would control the temperature of combustion. Thus the grain size of the sample is obviously important and the separation of nano-diamond scale grains from graphite becomes problematic as these fine-grained diamonds will combust at much lower temperatures, approximately 500 to 600 °C.

4.5.4. Diamond.

Although, all of the crater suevites were found to contain diamond when observed under the optical and transmission electron microscopes, these diamonds were

very small (50-150 μm). Attempts were made to pick out diamond grains from the residues for isotopic analysis. Several diamonds were transferred from the residues to clean dry glass petri-dishes but from here it proved difficult to transfer a sample to a platinum bucket for isotopic analysis. However, a single small diamond (ca. 125 μm) grain from NC384 was successfully extracted and loaded for stepped combustion (figure 4.12). This diamond had the form of a half-crystal with a pseudo-hexagonal platy structure.

The isotopic composition of the sample as given by the values from the main carbon peaks is very even and the average $\delta^{13}C$ = -26.9 ‰. The high temperature release (700-900 °C) comprises 92 % of the total yield, and the low temperature release (625-675 °C) only 3 %. The carbon appears to be released in two stages, the smaller earlier release at 675 °C could be attributed to the combustion of a thin skin layer on the diamond, with total diamond combustion by 800 °C. Thin amorphous film coatings on polycrystalline diamonds were described on impact diamonds from the Popigai impact crater (Koeberl et al., 1997), these were attributed to a brief exposure to a high temperature environment. Similar structures were observed in shocked zircons from high temperature suevites (section 3.5). This could also be attributed to the change in step size from 50 to 100 °C above 700 °C.

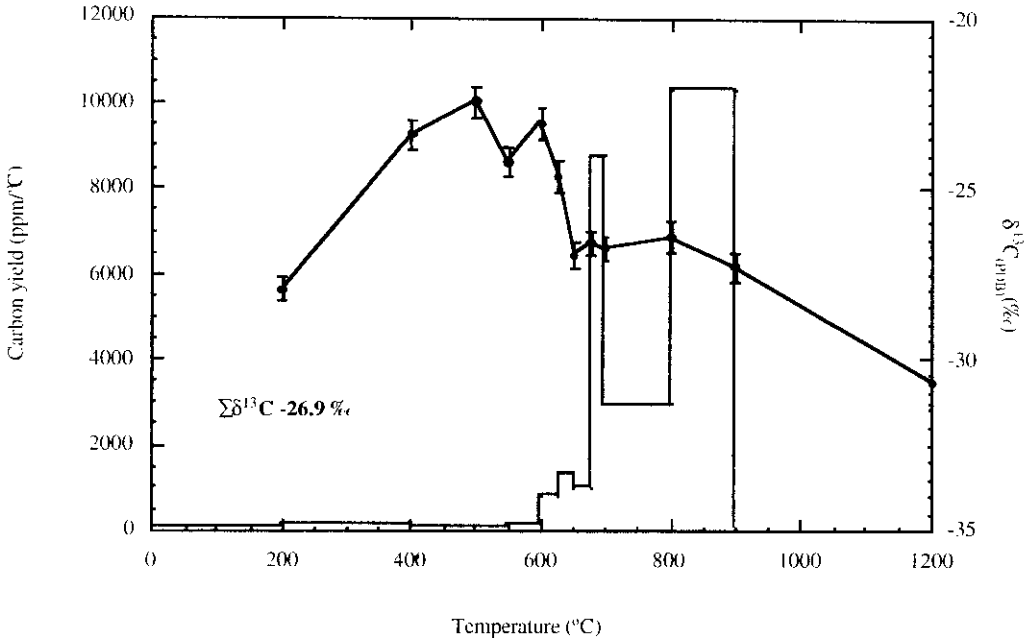

Figure 4.12. Stepped combustion plot for a diamond from NC384 residue (sample weight = 4 μg). $\sum \delta^{13}C$ = -26.9 ‰ and $\sum$ carbon yield = 100 wt %.

The carbon isotopic composition (26.9 ‰) of the diamond from NC384 compares well with the diamond from the OQGB residue (-26.6 ‰) (figure 3.24). The values also closely match those obtained for samples of graphite from the Ries samples (- 25.2 to -26.6 ‰) with the exception of graphite from the Seelbronn suevite (-19.9 ‰) and contrast with previously published values for acid-demineralised Ries crater samples which had a reported $\delta^{13}C$ of -16 to -17 ‰ and were mixtures of diamond and silicon carbide (Hough et al., 1995c).

4.6. COMPARISON OF CORE SUEVITE (FALLBACK SUEVITE) WITH FALLOUT SUEVITE SAMPLES.

Variations in lithology and shock stages between fallout and fallback suevites have been described in detail within the literature (Chao et al., 1977; Stöffler, 1977; Stahle and Ottemann, 1977). From the studies described above and in previous chapters there are a number of features that contrast the two types of suevite with each other. This is additionally complicated by the fact that the fallback suevite is partially composed of

material which slumped in from the inner crater ring (Stöffler, 1977). Nevertheless the fallout suevite appears to have been formed from material excavated from shallower levels of the target area and contains a higher percentage of sedimentary material and granite from the shallower stratigraphic levels.

4.6.1. Stable isotopic composition of fallout and fallback suevites.

The variation in the stable carbon isotopic composition of the NCsamples is illustrated in figure 4.13. This shows the structure of the core, based on data from Stöffler et al. (1977), bulk whole-rock $\delta^{13}C$ isotopic compositions and the carbon contents. The samples show no clear trend with depth, which is to be expected given the limited sample size. There is a reverse correlation of the $\delta^{13}C$ with the carbon contents. The higher carbon content is associated with ^{13}C-depleted isotopic values. The basement sample (NC1059) has a less ^{13}C-depleted carbon isotopic signature than might be expected (- 13.9 ‰), this is likely to be the result of heterogeneity within the structure of the basement. The lower parts of the core and basement of the crater is known to be composed of allochthonous layers which slumped inwards filling the original transitory crater cavity (Von Englehardt and Graup, 1977). This transient crater is calculated to have been 12-13 km wide and up to 2, 800 m deep (Von Englehardt et al., 1995). Detailed analyses of the structure of the N-73 drill core and the Ries crater impact lithologies indicates that the fallout lithologies formed from specific levels of the shocked basement, forming a reverse stratigraphy (Stöffler, 1973).

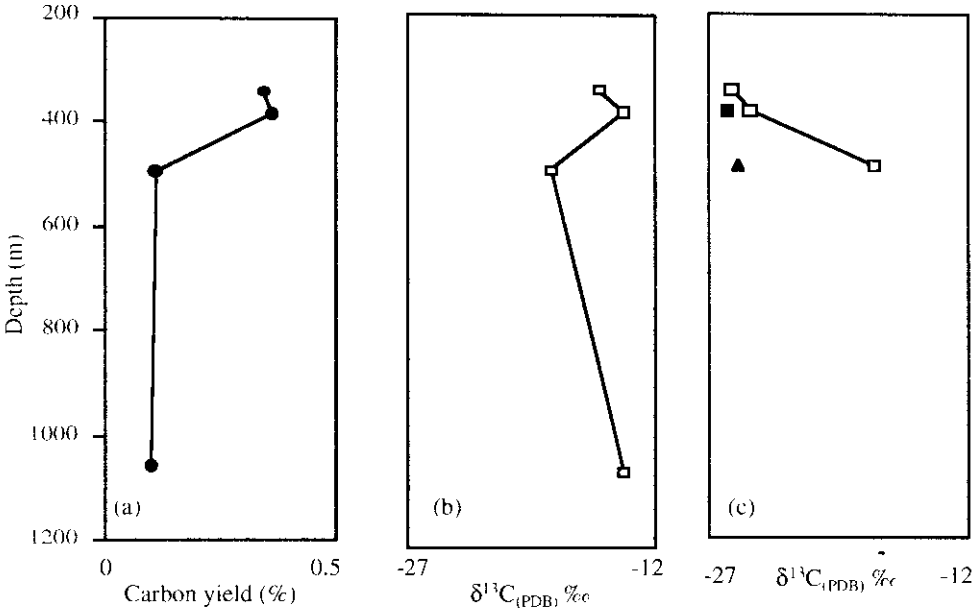

(a) whole-rock carbon yield (%) with depth.
(b) whole-rock $\delta^{13}C$ with depth.
(c) $\delta^{13}C$ of acid-demineralised residues, graphite (triangle) and diamond (square) with depth.

Figure 4.13. Carbon contents (%) and stable carbon isotopic values with depth for N-73 whole-rocks, residues and extracted diamond and graphite samples.

The range of $\delta^{13}C$ in diamond from the Ries crater impactites is from -16 to -27 ‰ (Hough et al., 1995c and this study) indicating either heterogeneity in the composition of the source carbon, or isotopic fractionation during diamond formation. Direct transformation from graphite to diamond should not result in isotopic fractionation unless the transformation is <100 % and diffusion can occur. Investigations of the isotopic fractionation between hydrocarbon gas and CVD generated diamonds has shown an isotopic fractionation of 2-3 ‰ (Derjaguin and Fedoseev, 1994) which is insufficient to produce the observed range in compositions. Isotopic exchange between graphite and carbonate minerals during the metamorphic evolution of the basement target rocks could generate the observed heterogeneity in the isotopic composition of the parent graphite (-13 to -26) (figure 3.23) and therefore, in any diamonds derived from this source. The carbon isotopic composition of graphite from the Ries crater reported in this thesis ranged from -26 to -19 ‰ , suggesting that

differences in the composition of the graphite and graphite precursor carbonaceous material is the main factor involved.

4.6.2. Diamond abundances within Ries crater impactites.

Fallback suevite appears to contain as much diamond as the fallout suevite material, the estimated amount of diamond within these impactites is shown in table 4.8. These estimated concentrations are subject to errors due to sample losses during the acid demineralisation process as well as weighing errors, hence values should be taken as general limits. The concentrations were calculated from the carbon yield from acid demineralised residues and the known weight of the residues.

Table 4.8. Estimated diamond concentrations in Ries crater impactites.

Sample	Diamond yield (ppm)	Reference
OQS	0.59	This thesis
SBS	0.85	This thesis
NC494	1.14	This thesis
NC384	1.52	This thesis
Otting quarry suevite	1-2	Hough et al. (1995c)
Fallout suevites	0.06-0.7	Schmitt et al. (1999)

The diamond concentrations determined herein range from 0.6 to 1.5 ppm which correlates with the concentrations determined by Hough et al. (1995c). Diamond abundances between 0.06 and 0.7 ppm were found by Schmitt et al. (1999) for fallout suevites from the Ries crater with concentrations in the fallback suevite estimated to be much lower. They analysed 25 samples from the N-73 drill core and only detected diamond in a glass poor sample from 568,30-60 m depth (R. Schmitt, Pers. Comm.). This suggests that there may be considerable heterogeneity in the abundance of

diamond within the core suevites due to differences in source carbon concentrations, shock histories and most importantly thermal histories. The diamonds from the NC494 and PIMR residues show evidence of thermal annealing implying longer periods at higher temperatures than the other suevite samples. This may also reduce the abundance of diamond in the residues by allowing greater graphitisation and so destruction of diamond.

The impact diamonds are predominantly found in suevites and the individual components of suevite such as glass (Rost et al., 1978; Abbott et al., 1996; Siebenschock et al., 1998) and crystalline fragments (El Goresy et al., 1999; Schmitt et al., 1999). Impact melt glasses may contain variable proportions of crystalline rock fragments (Stöffler and Grieve, 1996). Thus the diamonds within Polsingen may have originated from within crystalline fragments embedded in a fine-grained crystalline matrix (Von Englehardt and Graup, 1984). Impact diamonds have been found in-situ within shocked gneiss fragments from both the Popigai and Ries impact craters (Masaitis, 1994; El Goresy et al., 1999). Schmitt et al. (1999) suggest that the main carrier of diamond in the Ries crater are glass bombs with the source for the diamonds being graphite bearing gneisses. The higher concentration of crystalline material within the fall-back suevites suggests that these lithologies should contain equivalent or greater amounts of diamond. The lower concentrations of glass within the fall-back suevites has been attributed to replacement by zeolites, analcite and montmorillonite (Stahle and Ottemann, 1977) and the original abundance of glass within the fall-out suevites is difficult to calculate. The secondary minerals are all relatively low temperature (<500°C) and formed under conditions in which diamond should survive (section 4.6.3).

Aside from the different populations of impact diamond within the Ries crater, the data described in the previous sections indicates several points. Firstly that the diamonds in the fallback suevites (NC343, 384 and 494) are similar in structure and morphology to those detected in fallout suevite samples. Secondly, that the stable carbon isotopic composition of diamond from the core samples is comparable to those from the fallout suevites.

Using the diamond concentrations calculated above (table 4.8) and an estimated graphite concentration it is possible to calculate ratios of graphite to diamond transformation ratios. The lower limit on the concentration of graphite within the impactites may be taken from figure 4.14 using the average $\delta^{13}C$ of the ^{13}C-depleted graphite samples analysed (-26 ‰) and the intersection with the carbon concentrations. An alternative value can be taken using the $\delta^{13}C$ composition of graphite from the Seelbronn quarry (-19.9 ‰).

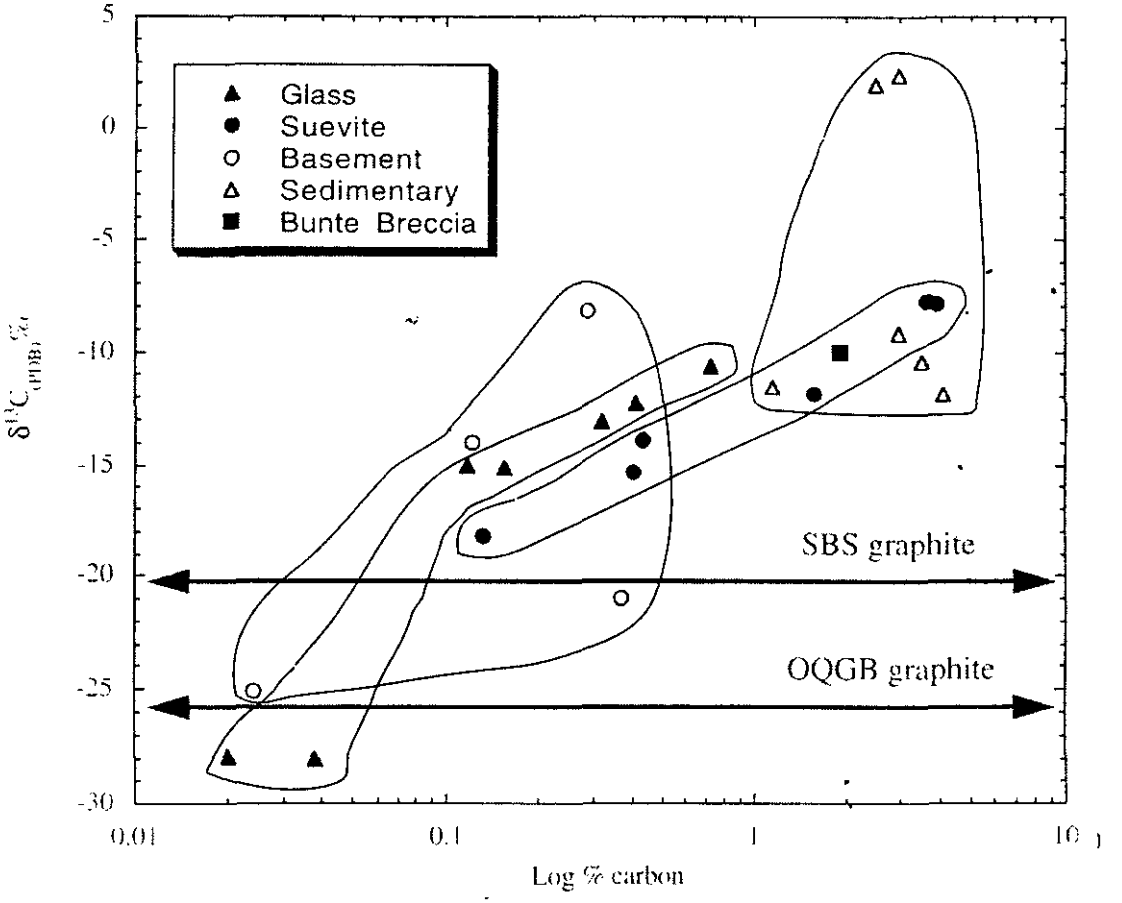

Figure 4.14. Carbon concentrations (log %) for whole-rock Ries crater impactites and individual components (appendix 4) versus carbon stable isotopic composition (‰).

The OQS graphite composition yields an approximate value of 200-830 ppm. Using the heavier composition given for the SBS graphite ($\delta^{13}C$ -19.9 ‰) a graphite concentration of approximately 500-1667 ppm is estimated. Using the estimated

diamond concentrations of 0.6-2 ppm (table 4.6), the ratio of graphite to diamond can be calculated as between 500:1 for 500 ppm of graphite and 1000:1 for 1000 ppm of graphite.

There are obvious uncertainties in the concentration of diamond and graphite within these impactites due to weighing errors as well as heterogeneity within the impactites. The values do indicate that the degree of transformation from graphite to diamond may be highly variable and that the majority of graphite does not transform to diamond. This suggests that the average temperatures and pressures experienced are insufficient for complete transformation and that localised conditions may be important. The distribution of shock indicator structures and minerals which have been used to characterise the shock history of the Ries crater impactites also highlights this heterogeneity (Stöffler, 1972; Stöffler et al., 1977). This is discussed in further detail in section 4.6.3.

It is interesting to note that the initial calculations of a graphite diamond ratio (500:1) coincides with the ratio calculated for the transformation of carbyne to diamond due to slow reaction rates (Whittaker, 1978). The carbyne chaoite was identified within shocked graphite in the basement gneisses at the Ries crater (El Goresby and Donnay, 1968). The possible relationship between graphite, diamond and carbyne is discussed in greater detail in section 4.8.2.

The fields delimited for individual components (suevite, glass, basement material, sedimentary fragments and Bunte Breccia) on figure 4.14 show mixing from ^{13}C-enriched sedimentary material with high carbon contents and ^{13}C-depleted glass and basement samples with low carbon contents. This supports the hypothesis that the isotopic compositions of the suevites and diamonds might be derived from a vapourised graphite bearing basement with variable amounts of ^{13}C-enriched sedimentary carbonate. The BB, which is known to be composed of primarily sedimentary derived fragments (Von Englehardt, 1990) lies within the sedimentary fragment field.

4.6.3. Heterogeneity of shock stage distribution, diamond morphologies and associated P/T conditions within Ries crater impactites.

It has been determined that each suevite is characterised by a particular abundance pattern of crystalline rock types and a distinct frequency distribution of shock metamorphic stages (Von Englehardt and Graup, 1984). The variation in the distribution of crystalline and sedimentary rock fragments between the different impactites and the variation in the shock stages experienced by these different target lithologies can be seen in table 4.9. This illustrates the heterogeneity present in the impactites and in the distribution of shock metamorphic conditions experienced. This heterogeneity may explain the high ratio observed between relict graphite and impact diamonds (presumed here to be derived from this graphite) present at the Ries crater.

The high pressure/temperature polymorphs and shock structures within the Ries crater impactites that have been used to determine the shock stages and conditions experienced are shown in table 4.10. This illustrates how the structures and minerals within the lithologies preserve different shock histories. The rocks form combinations of different shock stages in different proportions. The volumes of crystalline and sedimentary material affected by different shock stages is shown in table 4.11.

The distribution in shock stages shows that sedimentary material was not shocked above 45-60 Gpa and the majority was shocked at < 10 Gpa. Crystalline material experienced all stages of shock up to > 100 Gpa although again the majority was shocked to < 10 Gpa. This low shock material is predominantly located within the Bunte Breccia and lithic impact breccias. The amount of graphite-bearing crystalline rock shocked to conditions sufficient to produce diamond is limited. Only small volumes of carbonate rock would have been vapourised and available for incorporation into diamond feedstocks as suggested by Hough et al. (1995c). The presence of catalysts, e.g. carbonates, may reduce the pressures and temperatures at which diamond can form (Burns and Davies, 1992).

The observed heterogeneity in the ratio of graphite to diamond transformation as well as the distribution of shock indicator phases and structures suggests that the target

Table 4.9. Distribution of glass, crystalline clasts, sedimentary clasts and shock pressures and temperatures within the Ries crater impactites studied.

Impactite	Locality	% glass	Shock stage and P/T (Gpa/°C)	% crystalline	Shock stage and P/T	% sedimentary	Shock stage and P/T
Bunte breccia				<0.15 clasts >1 cm	< II, 35-45 Gpa	60-80	0, <10 Gpa
Fallout suevite		30-50 groundmass 16 coarse fraction	> 80 Gpa, > 2000 °C Deposition ~ 750 °C	2- 10 (54 % metamorphic)	0-IV, <10-100 Gpa	Coarse fraction 0.2 - 0.5	Limestone temp 550-900 °C
	Otting	17.9	> 80 Gpa, > 2000 °C	2.5	0 - VI	1 - 2	
	Seelbronn (Aufhausen)	13-18	> 80 Gpa, > 2000 °C	2-4		0.2	
	Polsingen	Abnormally rich in melt	> 80 Gpa, > 2000 °C High temperature deposition				
Fallback suevite		28	> 80 Gpa > 2000 °C	gneiss 42 amphibolite 14.5 granitic 12.5	5 - 15 Gpa	0.2	
	Graded unit (314-331 m)	15 - 67	> 80 Gpa > 2000 °C	68		0.2	
	High temperature suevite (331-525 m)	40 - 0	> 80 Gpa > 2000 °C Deposition >600 °C	68		0.2	
	Low temperature suevite (525-602 m)	0		100			

Data compiled from Stöffler et al., (1977), Stöffler, (1978), Von Englehardt, (1990), Von Englehardt et al., (1995).

Table 4.10. Characteristic shock features and shock produced minerals within Ries crater impactites.

Mineral/structure	Pressure (Gpa)	Temperature (°C)	Shock stage	Reference
Shatter cones	1-10 Gpa	100 °C		Stöffler (1972); Stöffler et al. (1977)
Kink bands	10-45 Gpa	100-300 °C		Stöffler 1972; Stöffler et al. (1977)
PDF	15-35 Gpa	200-300 °C	I	Stöffler (1972); Stöffler et al. (1977)
Coesite	30-50 Gpa	450-800 °C	I-II	Shoemaker and Chao (1961); Chao (1967)
Stishovite	15-40 Gpa	1200 °C	I-II	Shoemaker and Chao (1961); Chao (1967)
Diaplectic glass	25-35 Gpa	1200-1500 °C	II-III	Stöffler (1972); Stöffler et al. (1977)
Jadeite (plagioclase)	>150 Gpa		V	James (1969)
Silicate melt	100	2500 °C	IV	Grieve et al. (1996)
$CaCO_3$ melt	>42 Gpa		I-II	Graup (1999)

Table 4.11. Estimated volumes of crystalline and sedimentary rock clasts exhibiting each shock stage.

Shock stage	Shock pressure (Gpa)	Crystalline (km^3)	Sedimentary (km^3)	Total (km^3)
V	>100	3.54	0	3.54
IV	100-60	1.54	0	1.54
III	60-45	1.03	0.02	1.05
II	45-35	1.28	0.03	1.31
I	35-10	11.4	0.12	11.52
O	<10	51.0	67.5	118.5

From Von Englehardt and Graup, (1984).

rocks were themselves shocked heterogeneously. There are distinct gradations to the degree of shock experienced by the target rocks according to their proximity to the point of impact (Von Englehardt and Graup, 1984). This is illustrated by figure 4.15 which shows isobars for the shock front and the zones of decreasing shock effects.

In addition it has been suggested that highly variable peak shock pressures and temperatures may be generated by pre-existing heterogeneity and variable structure within the target rocks (Stöffler, 1977). The interaction of shock waves with grain boundaries, pore spaces, fractures and faults may cause localised hot-spots and areas of elevated pressure and/or temperature. It has been suggested by De Carli, (1967; 1979; 1995) that diamond may be formed in hot spots; observations of diamond found in-situ within shocked graphites at the Ries crater have been attributed to this mechanism (El Goresy et al., 1999). This is discussed in greater detail in section 4.8.

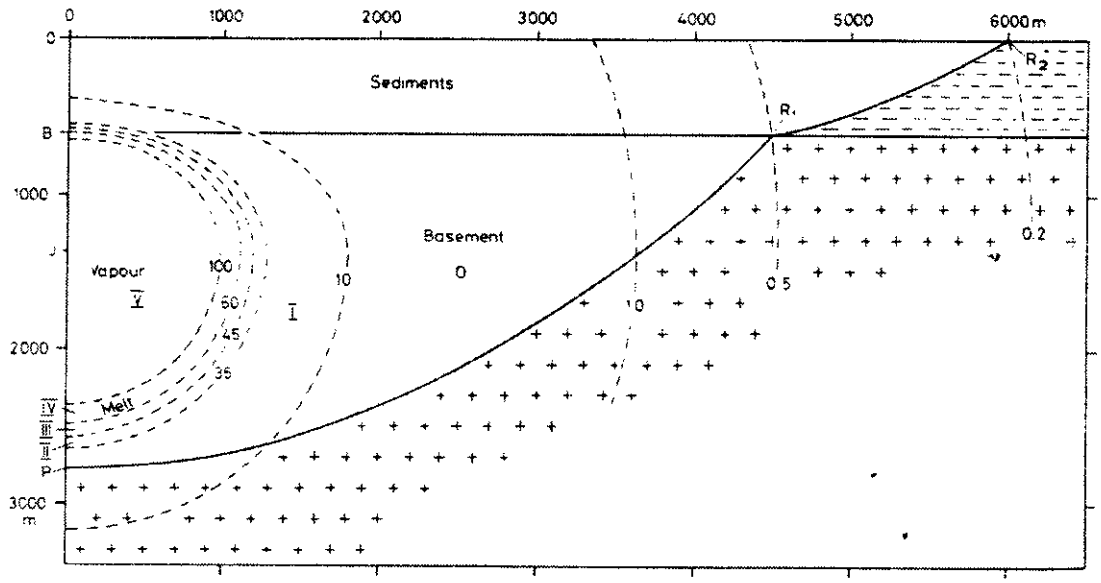

Figure 4.15. Deep burst model of the formation of the Ries crater. OR2 is the crater radius at surface, BR1 the radius at basement/sediment boundary, OJ the penetration depth of the projectile and OP the maximum depth of the crater. Dashed lines represent isobars (Gpa) with zones of decreasing shock effects (V-O). [From Von Englehardt and Graup, 1984).

4.6.4. Preservation of diamond in fallout and fallback suevites.

Impact diamonds are primarily believed to be present predominantly within basement gneiss and derived from graphite (Masaitis, 1994 and El Goresy, 1999). Diamonds have also been found within impact glass (Rost et al., 1978; Abbott et al., 1996; Siebenschock et al., 1998; Schmitt et al., 1999). This glass is primarily derived from vapourised and melted basement gneiss (Von Englehardt and Graup, 1984) at temperatures between 1300 to >3000 °C (Von Englehardt , 1997). It should be noted that the glass may contain small fragments of highly shocked but un-melted crystalline rock which may in turn contain diamond. The low concentration of gneiss fragments within the glass (< 0.1 wt%) suggests that the concentration of diamond in these fragments would be anomalously high in order to account for the observed abundance of diamond in the glass (~ <1 ppm). The amount of crystalline fragments within the glass is difficult to determine due to post deposition secondary mineralisation. This suggests that the impact diamonds are located within the glass itself and not exclusively within crystalline fragments.

Glass fragments and bombs found within the fallout suevite were brittle at the time of their deposition indicating a rapid decrease in temperature due to pressure release from 80 Gpa (Von Englehardt and Graup, 1984). This may have aided in the preservation of the diamonds due to quench cooling. Apatite and sphene fission track annealing indicate minimum temperatures in excess of 500 °C in the Ötting quarry suevite and 250 °C for the core suevites (Pohl, 1977). The diamonds found in the N-73 core during this study were obtained from samples of high temperature suevite, so called because of >600 °C thermoremenant magnetisation temperatures (Pohl, 1977).

The concentration of impact diamonds in tagamites and suevite from the Popigai crater, Russia have been found to vary radially from the centre of the crater depending on the original concentration of precursor graphite, superimposed shock zonation and the character of ejection (Masaitis, 1998). Further heterogeneities in the concentration of diamond were linked to the extent of melt contamination by cooler clasts and fragments resulting in localised quench cooling (Masaits, 1998). The mixing

of cold unshocked fragments into melt can rapidly decrease the temperature and cause local to total quenching which may occur in less than 100 seconds (Kieffer and Simonds, 1980). No distribution trends have yet been identified in the Ries impactites (Schmitt et al., 1999 and this study).

Many of the impact diamonds found during this study and those described in the literature show evidence of corrosion and etching (Rost et al., 1978; Masaitis, 1998) and diamonds from the Popigai impact crater show etched honeycombed textures, graphite coatings and dissolution and corrosion patterns (Masaitis, 1998). The extraction technique used to obtain the Popigai diamonds is an exothermic alkali fusion technique involving temperatures >833 K. This is significantly greater than the temperatures employed to demineralised the samples described in this study (section 2.6) and may result in etching and corrosion of the diamonds. In addition post formation graphitisation or hot alkali gases such as OH-, Na and K in high temperature ($\leq$ 2000 °C) impact melt (Vishnevsky and Raitala, 1998) may produce etched features. The impact diamonds from the Ries were frequently found to have graphite coatings.

Experimental calculations of the graphitisation of diamond indicate that the complete conversion to graphite requires 1 Ma at 12, 273 K or 1 Ga at 1273 K (Pearson et al., 1995). Although extremely rapid graphitisation can also occur. Within an impact event the graphitisation of diamond may be expected to follow that observed in experimental shock transformation experiments which require the immediate quenching of products in order to obtain diamond (Bogdanov et al., 1995; Epanchintsev, 1995; Hirai et al., 1995). Similarly in CVD diamond synthesis quenching may be required to prevent reverse graphitisation (Rao et al., 1995). Explosion synthesised nano-diamonds comprise a diamond core within a graphite shell, the result of regraphitisation when pressure drops sharply but temperatures remain high (Donnet et al., 1997). Diamond is rapidly transformed to graphite at temperatures $\geq$ 1000 K in the presence of free oxygen (Vishnevsky and Raitala, 1998). The spontaneous graphitisation of diamond occurs at > 2000 K forming a stable diamond-graphite interface at 1000 K (De Vita et al., 1996). Therefore cooling of high-temperature diamond-bearing impactites to below 1000 K

would inhibit further graphitisation and preserve diamonds within a graphite core. Spontaneous graphitisation and explosive disintegration of diamond at > 2000 K forming diamond fragments with graphite coatings was observed by Andreev (1999) where the temperature of reaction was dependent on the density of defect structures. A similar process may explain the fragmented diamond structures often seen in the suevite samples, where a hexagonal structure is only party preserved (e.g. figure 3. 4).

Removal of the graphite coatings revealed diamond within previously black, sooty grains and clusters of grains. This may also expose the detailed structure of a diamond surface with etched pits and margins where preferential graphitisation may have occurred in areas with high concentrations of defect structures. Ma et al. (1991) found that during polytype transformations the nucleation of the second phase tended to occur along defect structures.

As mentioned in the introduction to this chapter the samples from the core sections provided all fell within the second unit of the core as classified by Von Englehardt and Graup, (1984). Comparison of the results obtained for these samples with samples from the other units of fall-back suevite would be an interesting study. Schmitt et al. (1999) found diamond in a single section of core from a suite of 25 core samples. The evidence suggests that diamonds are preserved in this unit of high temperature suevite and it would be interesting to compare this with samples from the low temperature material, together with detailed information concerning the cooling histories.

4.7. IMPACT DIAMOND FORMATION.

The range of mechanisms used experimentally to produce diamonds from a variety of different types of carbon has greatly expanded the field of knowledge concerning diamond formation. Correspondingly the mechanisms proposed to produce diamonds during meteorite impacts has increased (table 4.12). These mechanisms operate in a variety of ways and at variable pressures and temperatures. The aim of this section is to consider whether differences in these formational conditions, the observed

structures found within natural impact diamonds and the types of associated carbon polymorphs can be used to indicate which mechanisms are the most likely to have occurred. The predominant carbon source which has been considered is graphite, whether through direct transformation or via a vapour growth model. In addition, some of the proposed mechanisms and natural observations are suggestive that other carbon forms may be important for example, coal (Ezersky, 1982; 1986) and carbynes (Whittaker, 1978; Heimann, 1994).

Each of the proposed mechanisms may be expected to produce diamonds with, to some extent, characteristic structural features and/or mineralogical associations. For example, inherited structures or diamond associated with SiC or carbynes. The pressure and temperature requirements for these mechanisms are varied but in addition some of the mechanisms require specific carbon precursor structures, e.g. porosity, crystallinity and orientation, or the addition of other elements such as silicon.

Table 4.12. Possible mechanisms for the graphite-diamond transformation.

Mechanism	Ref	Pressure and temperature
Ultrafast annealing of glassy carbon.	[1]	>35 Gpa, > 2000 K
Martensitic shear transformation of 3-R graphite.	[2]	>35 Gpa, > 2000 K
Hot spot transformation of disordered carbon.	[3]	> 35 Gpa, > 3000 K
Shock-transformation of well-crystallised graphite (quasi-martensitic).	[4]	~ 5 Gpa, ~ 1000 K
Carbon self diffusion.	[5]	Anomalous diffusion rates
Synthesis from carbyne intermediates.	[6]	< 5 Gpa, > 2600 K
Chemical vapour deposition on 4H-α–SiC.	[7]	Ambient, ~ 1200 K
Homogenous nucleation CVD.	[8]	Ambient, 2000 K

[1]. De Carli (1967); [2]. De Carli and Jamieson (1961); [3]. De Carli (1979, 1998); [4]. Chomenko et al. (1975); [5]. Heimann (1999); [6] Stoner et al. (1992) [7]. Frencklach et al. (1989), Buerki and Leutwyler (199a; 1991b) and Howard et al. (1990).

The pressure and temperature phase diagram for the carbon polymorphs diamond, graphite and carbyne is shown in figure 4.17 alongside the line for the onset of irreversible shock metamorphic effects in granitic rocks (Grieve et al., 1996) and the line for the shock synthesis of cubic diamond.

The stability fields for the various polymorphs do not exclude the persistence of different polymorphs outside their fields of stability due to the kinetic inhibition imposed by the high activation energies required for reactions (Bundy et al., 1996). Thus, diamond can persist metastably outside its stability field and similarly graphite and carbyne could exist outside their stability fields.

4.7.1. Morphological requirements of diamond formation mechanism.

The structures which have been observed in the diamonds from the Ries crater during this study are detailed in table 4.13. together with an interpretation of the structures with regards to possible formational mechanisms.

Table 4.13. Transformation mechanism requirements for observed structures.

Structure	Primary	Secondary	Mechanism requirements
Stacking faults	X	X	Direct transformation or growth mechanism
Polycrystalline	X	X	Direct transformation or growth mechanism
Layered		X	Direct non-destructive transformation
Twinning	X		Direct transformation or growth mechanism
Skeletal		X	Growth structure or partial transformation/ growth mechanism
Etched		X	Partial transformation, re-graphitisation or exposure to hot reactive gases

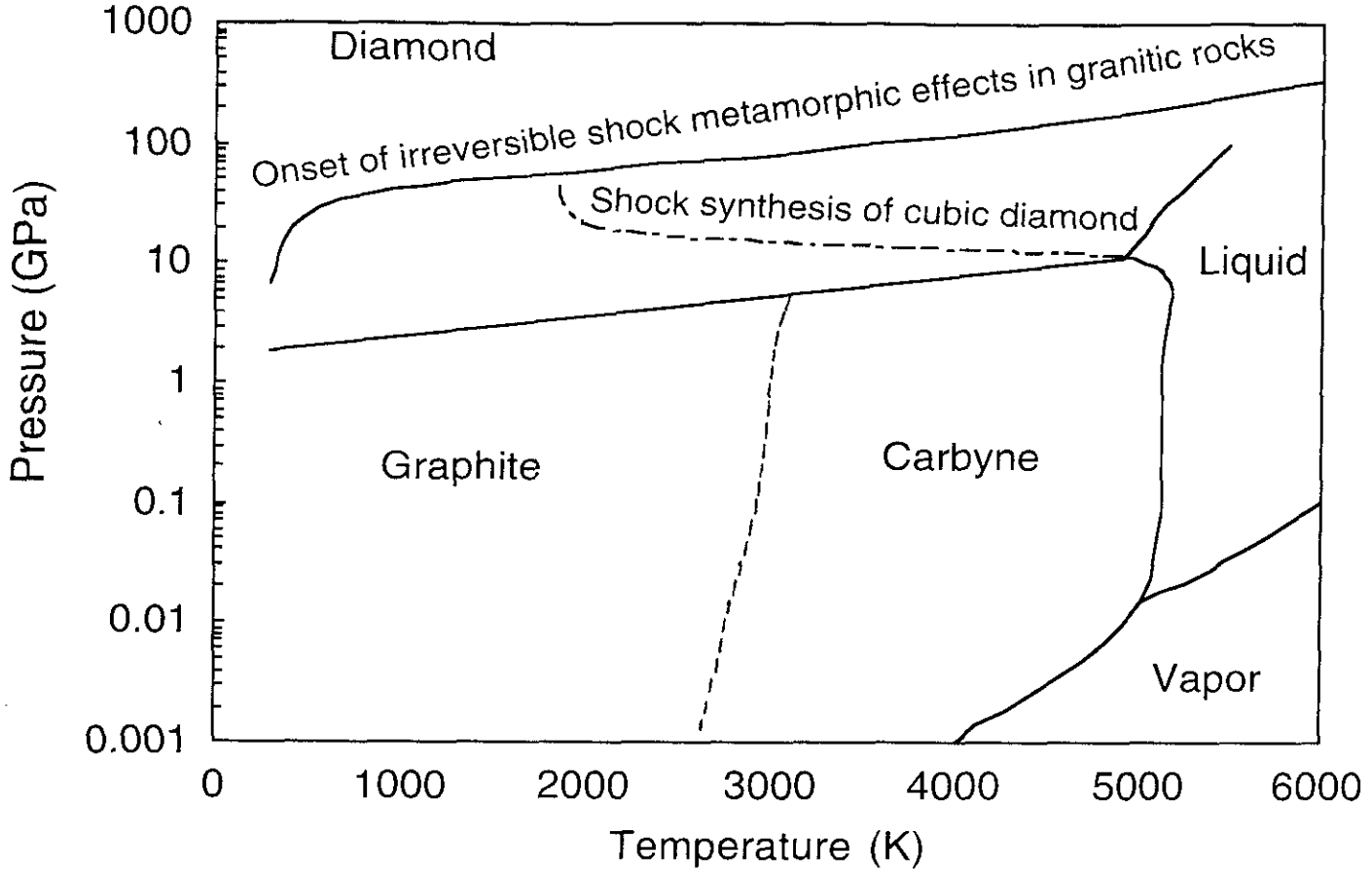

Figure 4.16. Carbon phase diagram showing graphite, carbyne, diamond, vapour and liquid fields. Also shows the pressure temperature conditions for the shock synthesis of diamond and the onset of irreversible shock metamorphic effects in granitic rocks. From Bundy, (1989) and Whittaker, (1978).

Layered structures in these diamonds are most likely to be inherited features from the precursor graphite, whilst skeletal and etching structures are secondary structures not inherited from the precursor. The remaining structures are less conclusive without detailed HRTEM.

Stacking faults are generally considered to be a secondary feature formed either during direct polytype transformations (Sebastian and Krishna, 1984), behind a shock front (Pujols and Boissard, 1970) or during rapid crystal growth (Saha et al., 1998). Thus these features may be detected in diamonds which preserve the precursor carbon polymorph morphology and within phases where the precursor and precursor structure have been destroyed either by vapourisation or diffusion. Polycrystalline structures may form from the direct transformation of a polycrystalline precursor whether through pre-impact processes or shock comminution of a single crystal (Rietmeijer, 1995) or from the nucleation of numerous individual crystallites within a precursor grain or independent substrate (Hough et al., 1995c). Twinning may be an inherited feature preserved by direct transformation or formed during the formation of a new crystal structure during a reconstructive mechanism as growth or deformation twins (Tamor and Everson, 1994; Mao et al., 1979).

Skeletal structures with a preferred orientation to the individual crystallites appear to be the result of the removal of graphite or other substrate material, crystal growth from a limited carbon feedstock (Shrafranovsky, 1964) or within a orientated stress field. Etching appears to be a predominantly secondary structure although graphite grains with etched structures were observed using the SEM. The etching of diamond grains appears to show two forms, the removal of graphite or poorly crystalline material from the diamond structure forming needle-like structures and surface etching forming pits and vugs. The formation of graphitic carbon appears to be pervasive throughout the grains whereas the surface features may represent corrosion of diamond by reactive gases (Vishnevsky and Raitala, 1998), or hot silicate melts (Langenhorst et al., 1999).

4.7.2. Polytype and mineralogical associations.

The type of diamonds found in the Ries crater impactites together with other carbon polymorphs and carbide minerals (SiC) must be taken into account when considering the possible formational mechanisms and conditions which may have occurred during the impact. Table 4.14 summarises the forms of carbon that have been detected at the Ries crater and in some instances at other impact craters.

The various polytypes and mineral associations such as diamond/SiC intergrowths are formed at different pressure and temperature conditions and require certain conditions for their formation. Large diamond plates found within the impactites are generally platy and apographitic preserving graphite morphologies. The conditions experienced by the Ries crater impactites lie within the field of diamond formation at the expense of graphite whilst still preserving graphite structures (De Carli, 1998). Single crystals of the 4 H α-SiC polytype indicate that pressures and temperatures must have been in the range of 2000-2500 K (Jepps and Page, 1983) with a mechanism for formation that must have involved either a liquid or vapour phase, or the rapid diffusion of carbon and silicon. This may have occurred during the impact event using carbon derived from graphite or possibly as a back reaction between diamond and/or graphite and silicate vapour. Silicate glass and chaoite within the impactites indicates that temperatures 2500-3000 K occurred which is sufficient to produce a liquid or vapour phase. The aggregates of α–SiC and β-SiC indicate that the conditions must lie or have passed through those suitable for the formation of both polytypes. Alternatively, conditions may have been such that one formed at the expense of the other and preserved a remnant of the parent polytype.

Table 4.14. Carbon in the Ries impact rocks.

Component	Ref	Form	Size (μm)	Morphology
Large diamond plates.	[1]	Cubic	< 300	White, platy, graphite-like pseudomorphs
Large SiC.	[1]	Hexagonal α-SiC 4H polytype	<100	Blue/green crystals
SiC aggregates.	[1]	β-SiC and α-SiC including 4H	< 1	Single crystals within SiC aggregates
Skeletal diamonds.	[1]	Cubic	0.01-2	lath shape polycrystalline aggregates
Diamond/SiC.	[1]	Epitaxial intergrowths	<1	Nanometre-scale intergrowths
Graphite.	[1]	hexagonal	< 1	Euhedral and Anhedral graphite crystals
Carbyne	[2]			Flakes within shocked graphite

[1]. Hough et al. (1995c). [2]. El Goresy and Donnay, (1968).

Skeletal diamonds do not preserve graphitic morphologies and appear to have formed (a) within an orientated pressure field produced by the passage of the shock front. (b) from a vapour as a condensate or (c) within a substrate material. It is possible that the skeletal diamonds represent remnant diamond-graphite intergrowths where the graphite has been etched away. However, as discussed in sections 3.4.2 these grains do not appear to preserve graphite morphologies and are distinct from etched grains which do. Intergrowths of diamond with silicon carbide support the idea of a vapour phase in order to incorporate Si into the diamond structure. Alternatively, the diffusion of Si into carbon may occur at high temperatures and this may be enhanced by defect structures (Morris, 1980). The existence of graphite indicates that the distribution of shock conditions was insufficient to result in wholesale diamond formation and the majority of graphite (section 4.6.2) was preserved. However, graphite in the Ries crater impactites (which has not been transformed to diamond) could represent re-graphitisation of impact diamonds or the shock-graphitisation of poorly crystalline pre-graphitic carbon.

Hirai et al. (1995) simultaneously formed diamond and crystalline graphite from poorly crystalline graphite.

The evidence for carbynes at the Ries crater is limited to one documented occurrence (El Goresy and Donnay, 1967). The formation conditions for carbyne involve temperatures > 2600 K and, depending on the polytype, relatively low pressures. The existence of this white coloured mineral within shocked graphite indicates that localised temperatures were sufficient to produce carbynes yet pressures were insufficient to produce diamond. The distribution of shock pressures and temperatures has been shown to be heterogeneous within the impactites (section 4.6.3). The carbynes may actually pre-date the impact event since they have been found in graphite from around the world (Whittaker, 1979; Whittaker and Kintner, 1985), Alternatively they may be formed during the impact by the vapourisation (Whittaker and Kintner, 1985) or high pressure transformation of graphite (Kleimann et al., 1984). The existence of carbyne at the Ries has been questioned due to the ready transformation of carbyne to diamond at high pressure (Whittaker, 1978; 1979). It has already been determined that the distribution of shock pressures and temperatures was highly heterogeneous and the majority of material experienced only low grade shock metamorphism, suggesting that pre-existing carbynes may not have experienced conditions sufficient to produce diamond. The slow kinetics of the carbyne-diamond transformation also produce a transformation ratio of 500:1 (Whittaker, 1978; 1979), further evidence that not all carbyne would form diamond.

4.8. MECHANISMS OF IMPACT DIAMOND FORMATION.

The association of impact diamonds with various proportions of lonsdaleite, (the high pressure hexagonal polymorph of diamond) led to the suggestion that these diamonds could be produced by impact shock waves (Masaitis et al., 1972). These shock waves would transform pre-existing graphite in the target rocks into diamond. Diamond found in-situ in graphite bearing gneissose basement rocks has been used to support this theory (Masaitis, 1994; El Goresy et al., 1999). There are several potential

mechanisms for this transformation, derived from experimental diamond synthesis through shock loading experiments (De Carli, 1967; De Carli and Jamieson, 1961; De Carli, 1998; Chomenko et al., 1975).

An alternative theory for the formation of these impact derived diamonds is via a mechanism of chemical vapour deposition (CVD). This process may involve the condensation of SiC in a reducing environment which is followed by the formation of intergrown diamond and silicon carbide and, finally, diamond (Hough et al., 1995c) as observed in CVD deposition of diamond on silicate substrates (Zang et al., 1991; Stoner et al., 1992).

The experimental investigation of the shock, explosion and vapour synthesis of diamond from a variety of precursor materials has indicated that the possible formational mechanisms for impact diamonds may be significantly more complex and involve intermediate phases such as carbyne (Whittaker, 1979; Heimann, 1998) or SiC (Zang et al., 1991; Stoner et al., 1992; Lannon et al., 1995).

4.8.1. Direct transformation.

The direct transformation of diamond by fast diffusionless kinetics is supported by the observations of inherited morphological features from the precursor carbon, such as kink bands and twinning (Masaitis, 1974) and hexagonal morphologies from graphite. During a dissolution and nucleation phase transformation or formation mechanism these inherited structural characteristics would be lost, whereas solid state transformations maintain the size and shape of the parent phase (Baronnet, 1992). Martensitic transformations are correctly applied to the formation of a martensite from the quench cooling of metals, which form the polymorph phase as a result of cooling. A less rigorous definition may be applied to direct-transformation polymorphism as a result of shock loading if this mechanism is fast, irreversible and non-diffusive. If sufficient activation energy is provided by high pressures and temperatures associated with an impact shock wave or shear stress from an impact shock wave then the phase transformation can occur. Contributions to produce the required activation energy may

be provided by high defect densities allowing the transformation to occur outside the required stability field and therefore enhance the growth kinetics of the new phase (Green, 1992).

One of the first reported diamond syntheses by dynamic shock pressure was by De Carli and Jamieson (1961) producing small (<10 μm), black diamonds from simple lattice compression of 3R (rhombohedral) graphite along the c-axis. Pure hexagonal graphite did not yield diamonds (De Carli and Jamieson, 1961). However no correlation was seen between the amount of 3R graphite used and diamond yields (Morris, 1980). As natural graphite is composed of only 5-15 % rhombohedral graphite (Fahy et al., 1986) this would also limit the amount of diamond that could be formed in a natural impact event. Fast martensitic graphite to diamond transformations were observed by Erskine and Nellis (1991) who reported transformation times of 1 ns at 30 Gpa when shocked along the c-axis. Their results suggested that the orientation of pyrolytic graphite greatly affected the phase change behaviour and ease of transformation. This has been shown to form lonsdaleite if shocked along the c-axis (Tielens, 1990), suggesting that only correctly orientated graphite would transform to diamond and should generally be associated with londsdaleite. The lack of correlation between graphite orientation and diamond yields together with the observation that yields were strongly dependent on temperature led to the development of other theories for the mechanism of transformation.

4.8.2. Ultrafast annealing.

Firstly ultrafast annealing of glassy carbon by high shock temperatures was suggested by De Carli (1967) following an initial collapse of the graphite lattice at high pressures. This forms a glass like structure with short range order of the carbon atoms in the diamond configuration. This is similar to the mechanism proposed by Pujols and Boisard (1970) where stacking faults are formed behind a shock front producing a defect saturated solid with the structural characteristics of a glassy phase. Such a mechanism, which involves the total destruction of the graphite lattice and formation of a

glassy intermediate phase, would result in the total destruction of any pre-existing structural characteristics and result in no inherited features. The majority of shock synthesised diamonds are cubic, polycrystalline and display no inherited structural or morphological features (De Carli, 1995). Hirai and Kondo (1991) produced cubic diamond from shock quenched 3R graphite shocked along the c-axis that occasionally displayed hexagonal morphologies.

4.8.3. Hot spot formation.

A correlation was noted between the degree of crystallinity of precursor graphite and diamond yield prompting the suggestion of a hot spot mechanism (De Carli, 1967; 1998).When porous material is shock compressed the material immediately around the collapsed pores is shock-heated to much higher temperatures than material further from pores (Williamson, 1990). Diamonds <5 μm in size have been found in-situ associated with biotite and graphite in shocked gneisses from the Ries crater (De Carli et al., 1999). As less than 5% of the available graphite contained diamond the transformation was not complete and transient hot spots at >10, 000 k and ≤ 30 Gpa were proposed to explain the observed distribution. Vapourised carbon gas can also be formed inside heterogeneously heated porous material, these pore spaces are collapsed by high pressure increasing the vapour pressure and resulting in nucleation of diamonds associated with carbynes indicating that the temperatures reached within the hotspots must have exceeded 3200 K (Kleiman et al., 1984; Kleiman 1990). This mechanism provides thermodynamic self-cooling due to adiabatic expansion and the admixture of cooler surrounding material (De Carli, 1995).

Compression of porous material could result in the orientation of pore spaces perpendicular to the direction of principal compression. This orientation of pore spaces combined with hot spots associated with pore collapse may result in the nucleation of diamond crystallites parallel to the compressed pores producing a crystallites with a preferred orientation.

4.8.4. Carbon self-diffusion.

In contrast to hot spot formation a mechanism involving carbon self-diffusion was proposed whereby anomalously high diffusion rates can be achieved by the formation of extremely high densities of defect structures following the passage of the shock front (Chomenko et al., 1970). As pressure is increased the graphite becomes increasingly unstable forming transitional states, vacancies and allowing increased atomic migration. Diffusion assisted diamond nucleation and growth was also suggested by Morris, (1980) after consideration of the shock hugoniots of diamond and graphite. No correlation is seen between shock pressures and diamond yield which appears to be controlled by temperature, suggesting a thermal diffusional reconstructive mechanism (Morris, 1980). There is a correlation between high defect structure densities in nano-crystalline and shock produced diamonds which indicate that density defects may contribute to the energy required to overcome the activation energy barrier of diamond formation and so reduce the temperatures and pressures required.

Recent data indicates that two processes occur at pressures greater than 20 Gpa: (1) a relatively slow graphite to diamond transformation which is localised in defect structure zones and (2) highly orientated graphite transformation to a diamond-like phase with fast (μs) martensitic kinetics and is reversible (Zhuk et al., 1997). Thus different pressure and temperature regimes can be identified, high pressure/low temperature (HP/LT) conditions without quenching forming diamond flakes and HP/HT hot-spot conditions with quenching by surrounding material (De Carli, 1979; 1998).

The main problem appears to be the lack of experimentally shocked diamonds displaying morphologies and structures inherited from the precursor carbon material. This may be because greater diamond yields are achieved using poorly crystallised graphite and carbonaceous material or because natural conditions have not been successfully reproduced. Highly ordered graphite shocked to ≥ 15 Gpa, ≥ 1300 K forms polycrystalline, apographitic diamond (De Carli, 1998) whereas porous disordered carbon formed ≥ 3000 K in hotspot conditions (De Carli, 1979; 1998) do

not preserve precursor structures. Indicating that the clearly apographitic coarse grained diamonds found in impact craters formed from highly ordered graphite at or around 15 GPa.

4.8.5. Carbynes.

The field of material sciences has given rise to a further model for the transformation of graphite to diamond. Unlike the direct transformation model it is suggested that linear carbon allotropes, carbynes, could form intermediary stages in the transformation (Whittaker, 1978; Heimann, 1994).

Carbyne (chaoite) was identified within shocked graphite in the basement gneisses at the Ries crater (El Goresby and Donnay, 1968). Carbynes are the thermodynamically stable allotropes of carbon at very high temperatures and can be formed by bond splitting within the planar graphite layers (Heimann, 1994). This suggests that carbynes or carbyne-like carbons may form precursor phases during the transformation of graphite to diamond, with the collapse of the carbyne structure to diamond after the shock front passes (Whittaker, 1978; Heimann, 1994). The persistence of carbynes within shocked graphite which has not been transformed to diamond may be explained by the fact that the conversion rate of carbyne to diamond is approximately 500:1 (Whittaker, 1978). This would mean that only a single carbyne grain out of 500 would be converted to diamond. Alternatively the persistence of carbynes may be a result of localised hot-spot conditions due to the heterogeneity of shock and only a proportion of the grains experiencing the required conditions for transformation. The transformation of graphite to carbynes requires high temperatures $\geq$ 2600 K due to a shift to triple bonding and graphite dissociation into chains (Whittaker, 1978). If this is followed by a high pressure pulse, carbynes may be transformed to diamond (Kleiman et al., 1984; Heimann et al., 1994).

This mechanism requires approximately a 100 μs period of high temperature, followed by a 10 ns period of high pressure. In a natural meteorite impact event the shock-induced pressure increase is associated with, and followed by, a temperature

pulse which is in contrast to the conditions required for carbyne formation. High fore-wave shock temperatures from the approaching bolide may result in the vapourisation of surficial sediments and ground cover (depending on the age of the impact) which could potentially provide carbon for carbyne condensation. This would again have to be complete and available for shock compression in a very short time.

In contrast Borodina et al. (1996) found that the carbyne to diamond transformation involves two stages: fast martensitic compression and cross-linking at the shock front to produce carbyne crystals followed by a longer period at high temperatures to form diamond. With low diamond yields due to the low rate of transformation (Whittaker, 1978) and/or subsequent graphitisation. Such a mechanism is more readily envisaged within a natural impact event where the high pressure pulse of the shock front is followed by a period of relatively high temperatures. Rapid quenching to < 1000 °C is required if the diamonds are to survive the pressure pulse. Rapid quenching is required for all the mechanisms of impact diamond formation. Masaitis, (1998) suggests the admixture of relatively cool unshocked target material during transportation leading to the preservation of diamond in the central parts of large melt sheets. Carbynes produced by pressure synthesis (≤ 56 Gpa) form platy single crystals which are commonly apographitic (Kleimann et al., 1984; Kleimann, 1999). Whether or not the transformation of graphite to diamond proceeds via high temperatures and then shock compression or shock compression, or vice versa will affect the potential for the preservation of relict precursor morphologies. A mechanism involving the vapourisation of graphite forming carbynes between 2700-3000 °C (Whittaker, 1978) is unlikely to preserve relict textures. This suggests that apographitic diamonds may be formed from graphite via an intermediary carbyne phase.

4.8.6. Fullerenes.

Although attempts to detect fullerenes within Ries crater impactites have yet to be successful they have been found associated with the K-T boundary layers (Heymann et al., 1994), the Sudbury impact crater (Becker et al., 1994), Permo-Triassic boundary

sections (Chijiwa et al., 1999) and meteorites (Becker et al., 1994; Becker and Bunch, 1997). Fullerenes may be transformed to diamond under experimental conditions by shock compression and rapid quenching (Sekine, 1992; Hirai et al., 1995). Although it is unlikely that fullerenes could be generated by vapour combustion processes and subsequently converted to diamond by high pressure during a single impact event. The association of diamond with SiC (Hough et al., 1995c) indicates that gas-phase reactions may be important in the formation of diamond (the discovery of fullerenes may substantiate this).

4.8.7. Catalysts.

Impact experiments using carbonates (Rietmeijer, 1999) have produced graphite from high temperature reducing vapours, and chaoite/hexagonal diamond (londsdaleite) from oxidising vapours, indicating a complex interrelationship between the spatial, temporal and compositional structure of the vapour plume. The carbonates may also act as catalysts for diamond formation. However this mechanism can be discounted for some of the Ries diamonds where the carbon isotopic composition indicated that the carbon source was primarily graphite.

Diamonds can be spontaneously crystallised from carbon solutions in alkaline carbonate melts i.e. $(Na_2Mg(CO_3)_2$-graphite and $NaKMg(CO_3)_2$-graphite at 8-10 Gpa and 1700-1800 °C (Litvin et al., 1999). Wang et al. (1996) found that the addition of particles of β-SiC, crystalline graphite and C_{60} to carbon/solvent alloys resulted in the heterogeneous nucleation of diamond on the surfaces of the particles. Similar processes could occur during an impact event where all the necessary elements are available including carbonate melts. Carbonate melt glasses have recently been found alongside silicate melt glass in suevites to the south and west side of the Ries crater, formed from the shock vapourisation and melting of carbonate rocks (Graup, 1999). This indicates that there was more shock melting of the sedimentary cover sequence than previously reported. However, impact diamonds are found in suevites that do not contain a lot of

carbonate melt, e.g. OQS. This suggests a carbonate catalysis mechanism is not the sole mechanism responsible for the formation of impact diamonds.

Molten transition metals (group VIII) are used commercially as solvents and catalysts for diamond growth (Burns and Davies, 1992). This suggests that the pressures and temperatures required for impact diamond formation may vary depending on the chemical composition of the trace elements within the carbon feedstock.

4.8.8. Vapour deposition related mechanism.

Natural associations of diamond and silicon carbide have been noted for the Ries crater suevite (Hough et al., 1995.c) and it was proposed that a mechanism similar to CVD operated in the impact-generated fireball and led to the condensation of nm to μm diamond crystallites. A similar mechanism has also been proposed for the formation of some interstellar diamonds, formed by stellar condensation as a metastable phase where the first solid phase to condense would be carbon and although graphite is stable and diamond metastable the energy differences are very minor (Lewis et al., 1987). Fullerenes in the Sudbury impact crater and K/T boundary layers indicate that vapour phase reactions may be important (Becker et al. 1994; Heymann et al. 1994).

The SiC found in the Ries crater impactites occurred as hexagonal α-SiC 4H aggregates with β-SiC and intergrown diamond and SiC (Hough et al., 1995c) indicating an intimate co-relationship. Diamond can be produced by CVD using a silicon substrate and this also results in the formation of SiC as an intermediary layer which is gradually replaced by diamond (Zang et al., 1991; Stoner et al., 1992; Lannon et al., 1992). β-SiC has a lattice constant between those of Si and diamond which may promote the crystallisation of diamond by forming a buffer layer between the two lattice structures (Von Munch and Wiebach, 1994).

The two different SiC polytypes have different stability fields which indicate different formational conditions (figure 4.18). This is additionally complicated by the effect of impurities which may stabilise certain polytypes (Jepps and Page, 1983). Cubic β-SiC and 2H-SiC are formed between 1, 500-2, 000 °C whereas hexagonal α-SiC (4H,

6H and 8H) are higher temperature polytypes (Yamanda and Tobisawa, 1990). This suggests that a range of temperatures must have operated during diamond and SiC condensation which would be expected from a heterogeneous ionised gas plume that has insufficient time to homogenise by mixing. Alternatively cubic SiC shows a marked preference for metastable formation and will be the first polytype to condense from a vapour or melt; this may subsequently convert to hexagonal 4H or 6H by phase transformations (Heine et al., 1991). The phase transformations are observed to be accompanied by increased densities of stacking faults and twinning (Jepps and Page, 1983).

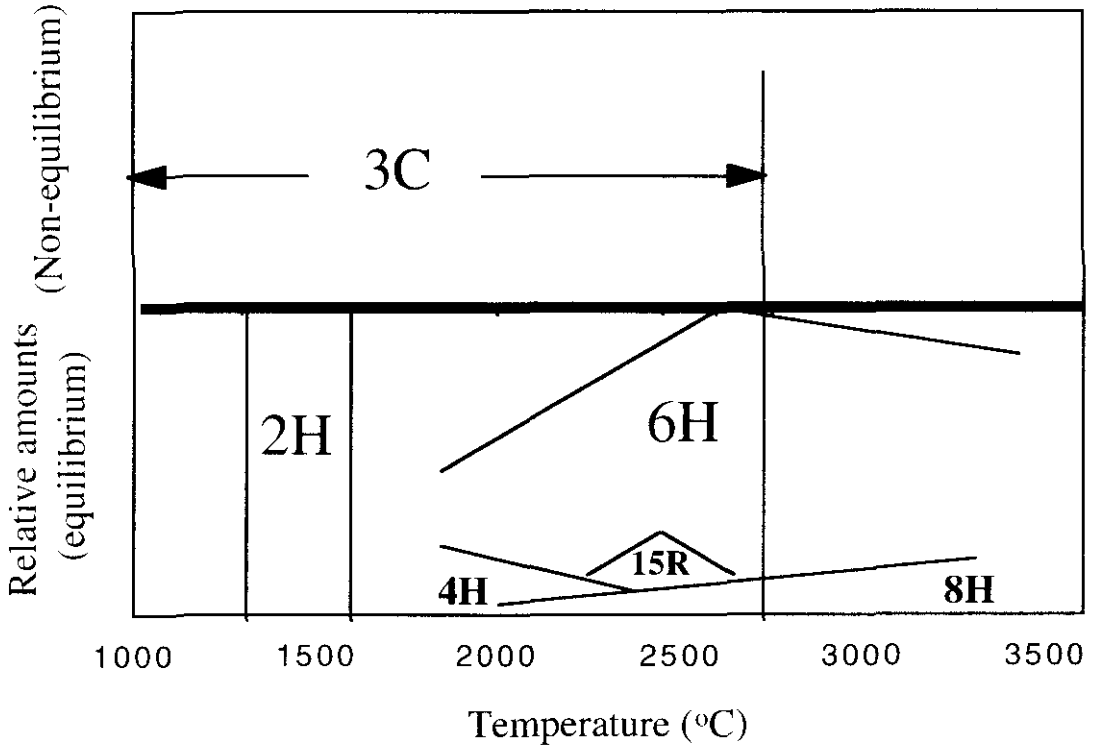

Figure 4.17. Stability diagram for the SiC polytypes showing β-SiC (3C and 2H) and α-SiC (4H, 6H, 8H and 15R) with temperature [adapted from Jepps and Page, (1983)].

Diamonds associated with silicon carbide imply that diamond and SiC formed either from a vapour phase onto a silicon-rich substrate, or diamond was deposited onto SiC which formed due to the reaction of vapourised silicon with carbon in an ionised

vapour. During CVD the gas phase is commonly 2000 °C with a cooler substrate 1000 °C to encourage condensation (Klages, 1995). SiC and Si metal can also be formed directly from shock vapourised SiH_4-CH_4 through homogenous nucleation, forming Si at 1100-1600 °C and β-SiC at 1600 °C (Carmer and Frenklach, 1989).

Langenhorst et al. (1999) suggest that extensive corrosion and graphitisation seen in diamonds from Lappijärvi (Finland) could produce skeletal diamond structures. They also suggest that SiC could be formed by the carbothermic reduction of SiC at >1550-1750 °C or through the reaction of silica rich impact melts with apographitic diamonds. The temperature range suggested falls within the field for the 3C and 2H β-SiC polymorphs and towards the field of 4H and 6H α-SiC (figure 4.17). At the suggested temperatures or the temperatures at which silicates exist as a melt (≥ 2000 °C), apographitic diamonds would be subjected to rapid graphitisation. In addition the discussion of the structure of skeletal diamonds (sections 3.4.4. and 4.4.4) emphasised the distinct structural differences between apographitic and skeletal diamonds. Etched and corroded apographitic diamonds were seen but still preserve remnant graphitic structures. The skeletal diamonds described in this study and by Hough et al. (1995c) display no apographitic structures.

Small grain-sized, defect-rich SiC can also be made by annealing C_{60} fullerene films on Si for 25 minutes at 900 °C and 100 minutes at 800 °C (Moro et al., 1997). In addition diamonds can be made from C_{60} at 12.5 Gpa and 900 °C (Brazhkin et al., 1997). This indicates that whilst SiC could be produced from fullerenes (formed by the vapour combustion of carbonaceous material) by post deposition annealing during the cooling of impactites whereas the formation of diamond requires high pressures.

Diamonds can also form via substrate-free homogenous nucleation in the vapour phase (Frencklach et al., 1989; Buerki and Leutwyler, 1991a; 1991b; Howard et al., 1990). Conditions must be such that the formation of graphite at the expense of diamond is inhibited; in experimental conditions this is generally achieved by the gasification of graphite by hydrogen (Derjaguin et al., 1994).

4.9. CONCLUDING DISCUSSION.

4.9.1. Diamonds in fallout and fallback suevite.

Suevite impactites from the Ries crater are found to contain diamonds in the rangeof 0.5-300 μm. These were found in the OQS and SBS and 3 sections of fallback suevite from the N-73 core (Abbott et al., 1998b). Diamonds were also found in glass separates from the OQS (Abbott et al., 1996; 1998a) as well as in the PIMR (high temperature suevite) and AQG. These additional discoveries substantiate the previous identification of diamond in fallout suevite from the Ötting quarry (Rost et al., 1978; Hough et al., 1995c) and glass separates (Rost et al., 1978; Siebenschock et al., 1998; Schmitt et al., 1999)

These diamonds showed morphologies and structures common to impact diamonds from the Ries crater (Rost et al., 1978) and other impact craters (Ezersky, 1982; 1986; Masaitis and Shafranovsky, 1994; Gurov et al., 1995). These structures and mineralogical associations may indicate whether or not they are formed by direct shock transformations or a mechanism similar to CVD.

Variations in the distribution of the diamonds within the N-73 core relative to the variations between the different suevite units in the core, cannot be determined from this limited set of samples. Investigations by Schmitt et al. (1999) using a much larger sample suite detected diamonds in only one section of the N-73 core and suggest that the core suevites contain a lower concentration of diamond than the fallout suevites. However it was not made clear how many of the 25 samples selected for analysis had been investigated. The three fall-back suevite samples investigated in this study contained diamond.

4.9.2. Morphological structures of Ries crater diamonds from fallout and fallback impactites.

The features observed indicate that there are a possible three distinct formational mechanisms: (1) a direct transformation preserving palimpsest structures, (2) vapour phase mechanism resulting in skeletal structures with strong preferred orientations and

(3) the incomplete transformation of a mixture of amorphous and graphitic carbon. Evidence for each of these transformation mechanisms can be observed in the diamonds. The large (≤ 300 μm) diamonds detected using optical microscopy observations of samples generally show structural characteristics suggestive of direct transformation of graphite, whereas the diamonds observed using TEM show structural features suggestive of direct transformation, vapour phase growth and incomplete transformation.

4.9.3. Mineralogical associations and heterogeneity.

The carbon polymorphs graphite, carbyne, diamond and the mineral SiC are all found in the Ries crater impactites, the varied formation and stability conditions for these phases could be seen as contradictory. The inherent heterogeneity of impactites due to the interaction of shock waves with structural boundaries and porosity (Stöffler, 1977) together with the variation in shock conditions away from the point of impact may be used to explain these apparently contradictory formational conditions.

Impact experiments can yield several carbon polymorphs such as carbyne (chaoite), graphite, diamonds (Derjaguin et al., 1994), disordered carbon and soot. Carbonates and a variety of different elements may have a catalytic effect on the growth of diamond

4.9.4. Carbon stable isotopic compositions.

The carbon stable isotopic compositions of the fallback suevite residues and extracted diamonds and graphite lie within the fields found for fallout samples.

The fallback suevite residues, graphites and diamond show a distinct cluster of values around $\delta^{13}C$ -25 to -26.5 ‰. The main exception being the residue from the 494 m sample with a $\delta^{13}C$ of -17.8 ‰. This value is more comparable to those from the Seelbronn quarry suevite samples (discussed in chapter 3) and the results by Hough et al. (1995c). The graphite samples from the N-73 core have similar isotopic values to the graphite samples taken from the fallout suevites, indicating a degree of homogeneity in

the carbon isotopic compositions of basement graphite. The graphite from the 494 m section is also comparable to those from the fallout suevites ($\delta^{13}C$ = -26 ‰) suggesting that the residue contains a ^{13}C-enriched component probably representing diamond. This indicates the possible admixture of carbonate-derived material as suggested by Hough et al. (1995c).

The $\delta^{13}C$ of the graphite and residues is also comparable to that of the diamond sample analysed as well as the diamonds from fall-out suevites. Indicating that it is not inconsistent that the carbon source for these diamonds was graphite in composition.

4.9.5. Carbon sources, mechanisms and processes.

The primary carbon source identified during detailed investigation of the individual components within the Ries crater impactites (principally suevites) is graphite. A ^{13}C-enriched component derived from the admixture of vapourised of molten carbonates is also suggested by the $\delta^{13}C$ composition of samples from the SBS and NC494.

The morphology of the diamonds identified using optical microscopy suggest inherited apographitic features. The martensitic transformation of graphite to diamond at high pressures (≤ 60 Gpa) has been suggested to account for inherited graphite morphologies (Masaitis et al., 1972). However, there are additional mechanisms which can produce apographitic features which cannot be discounted, e.g. intermediary carbynes (Kleimann et al., 1984; Kleimann, 1999).

The grains investigated using TEM include apographitic and skeletal orientated morphologies together with etching and corrosion. This indicates that vapour phase mechanisms and the partial transformation of carbonaceous material possibly within shock induced hot spots in a porous medium may have occurred.

The etching features indicate that diamond grains were exposed to corrosion by hot reactive gases or melts. The formation of amorphous carbon and graphite coatings prior to quenching could also produce these etched features. Incomplete transformation

of graphitic carbon to diamond could produce the skeletal grains which preserve graphitic morphologies.

The heterogeneous distribution of shock metamorphism and impactites found associated with impact craters highlights the heterogeneous distribution of pressures and temperatures which must exist during an impact event. The shock pressures experienced may vary on the mm to cm scale (Melosh, 1984). Providing the necessary pressure and temperature conditions for a range of diamond formation mechanisms.

The main conclusion from the investigation of the morphology and features of the impact diamonds found during this study together with an appraisal of the potential mechanisms for transformation indicate that there is evidence for a range of possible mechanisms that could have a role in the nucleation and growth of impact diamonds forming from intermediary allotropes. Restricting the formation of impact diamonds in terrestrial impact craters to a single mechanism of transformation ignores the complexity of the phase transformations and reactivity of the different allotropes of carbon. A particular example might be the experimental conversion of organic compounds and carbon-hydrocarbon mixtures which may be converted to fine grained (≤ 1 μm) diamond at high pressures (9.5 to 15 Gpa) and temperatures (1300-3000 °C). Including peanut butter which was converted to diamond at 15 Gpa and 2000 °C (Wentorf, 1965). Highlighting the fact that diamond can be formed from almost any carbonaceous precursor and at widely varying pressures and temperatures.

CHAPTER 5. GARDNOS IMPACT CRATER: A PRELIMINARY INVESTIGATION OF ITS CARBON CHEMISTRY.

5.1. INTRODUCTION.

The Gardnos impact structure (900-400 Ma) is located in Norway 125 km Northwest of Oslo and 9 km north of Nesbyen, Buskerud (Dons and Naterstad, 1992; Naterstad and Dons, 1994). The structure is 5 km in diameter, roughly circular in outline, exposes the original crater floor and crater-fill breccias and has been described in detail (Dons and Naterstad, 1992; French et al., 1995; 1997).

The Gardnos structure is intriguing in that the impactites contain anomalously high amounts of carbon averaging 0.5 to 1.0 wt %, which is 5-10 times higher than that of the metamorphic target rocks and higher than typical carbon levels in impactites from other craters (French et al., 1995; 1997). The $\delta^{13}C$ of the impactites range from -28.1 to -31.1 ‰, plus the possible presence of a carbon-rich shale overlying the metamorphic target sequence suggests that the carbon source may have been biologically derived organic matter (Dons and Naterstad, 1992; French et al., 1997). However the unshocked metamorphic target rocks contain significantly less carbon than the shocked metamorphic target rocks and impactites suggesting the introduction of carbon material during the impact event (French et al., 1997). Mechanisms for the introduction of carbon include the pervasive admixture of carbon-rich shale (Dons and Naterstad, 1992; French et al., 1995) or hydrothermal mobilisation of carbon followed by emplacement (French et al., 1997). Black shale fragments are found within the impact breccias (Anderson and Burke, 1995). The nature of the carbon material, which was presumed to be amorphous was not determined by French et al. (1997). Carbonaceous material in shocked quartzites from the Gardnos structure was determined to be poorly crystalline with graphitic inclusions (Anderson and Burke, 1995).

The inpactites are complicated by post-impact greenschist facies Caledonian metamorphic over-printing (400 Ma) and although graphite inclusions and carbon-rich

fractures are found in the shocked quartzite breccias (Anderson and Burke, 1996) this graphite may have been produced by metamorphism.

This thesis has identified graphite within the shocked impactites and two possible carbon source rocks, the Biri and Alum shales. As well as diamond within two suevite breccias and a black matrix lithic impact breccia. The shale samples were investigated in order to determine if these lithologies could account for the increase in carbon content documented for the impactites compared to the unshocked target rocks (French et al., 1997). The samples were demineralised using HF:HCl to remove silicate and carbonate minerals and allow the identification of amorphous, organic and graphitic carbon using gas chromatography mass spectrometry (GC-MS). Splits of these residues were further treated using chromic and fuming perchloric acids in order to investigate the resistant carbon phases using transmission electron microscopy (TEM) and stepped combustion combined with static mass spectrometry for carbon isotopic analysis.

A suite of Gardnos samples were investigated for soot as well as their carbon content (W. Wolbach and S. Widicus. IWU. unpublished data), the full list is contained in appendix 7.

5.2. GEOLOGICAL BACKGROUND AND STRATIGRAPHY.

The age of the Gardnos crater is poorly constrained to between 900 and 400 Ma on the basis of pegmatites dated to 900 Ma and Caledonian metamorphic overprinting from 400 Ma (Naterstad and Dons, 1994). French et al. (1995) suggest a formation date around 650 Ma. The 1.7 Ga target rocks were metamorphosed between 1500-1700 Ma (Proterozoic) and again at 400 Ma during the Caledonian orogeny (French et al., 1997).

5.2.1. Target rocks.

The basement rocks are composed of fine- to medium-grained granitic gneisses with minor amphibolites and quartzites (Dons and Naterstad, 1992; French et al., 1995) which have been brecciated and fractured by the impact event.

The off-structure shales which have been suggested as a potential carbon source are the Biri shale (late Proterozoic) (French et al., 1997) and Alum shale (Cambro-Ordovician). The Biri shale was obtained 2 km south of Biri, approximately 50 km from the Gardnos structure and the Alum shale from 5 km east of Bjorgo. The Biri shale is part of the Late Precambrian Biri Formation which comprises organic-rich limestones and shales deposited in a shallow marine basin in Southern Norway (Tucker, 1983). These shales do not outcrop at the Gardnos structure at the present day but are believed to have overlain the metamorphic sequence at the time of impact (French et al., 1997).

5.2.2. Impactites.

The crater was investigated by drilling a 400 m core in the northwest side of the crater (Naterstad and Dons, 1994) which penetrated sedimentary clastic rocks, melt bearing breccias and highly brecciated basement rocks including Gardnos breccia. The core did not reach unshocked basement rocks.The impactites comprise shocked and crushed quartzites, lithic breccias, melt-bearing breccias (suevite) and melt matrix breccias (impact melt rock) forming small irregular bodies within the suevite (Dons and Naterstad, 1992; French et al., 1995; 1998). A geological cross-section through the crater showing the location of the Banden drill core, central uplift and extent of impactites is shown in figure 5.1a, the structure of the drill core is illustrated in figure 5.1b. The lithic breccias include the Gardnos breccia which forms discontinuous bodies within the fractured basement and black matrix lithic breccias.

5.2.3. Shock metamorphism.

Shock metamorphic effects are limited in the basement rocks and are mainly confined to the impactites. The central uplift (figure 5.1a) forms an exception as it experienced maximum shock pressures from 20-35 Gpa (Robertson and Grieve, 1977; Grieve et al., 1981). Diagnostic shock effects are mainly observed in the crater fill breccias such as the melt-bearing suevites, black matrix breccias and melt-bearing

(a)

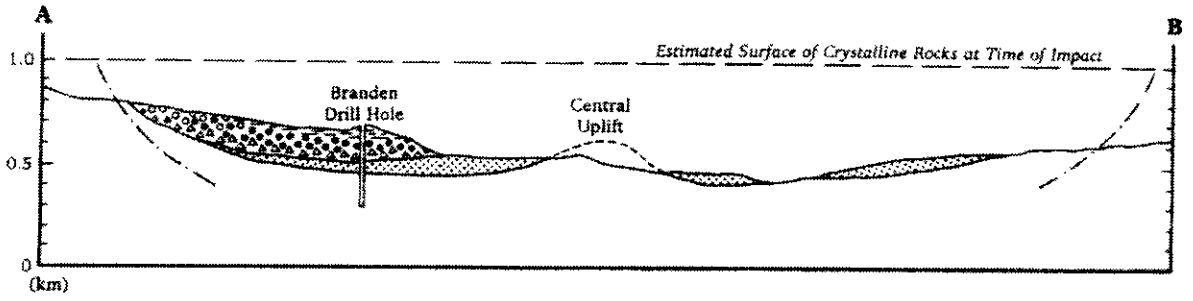

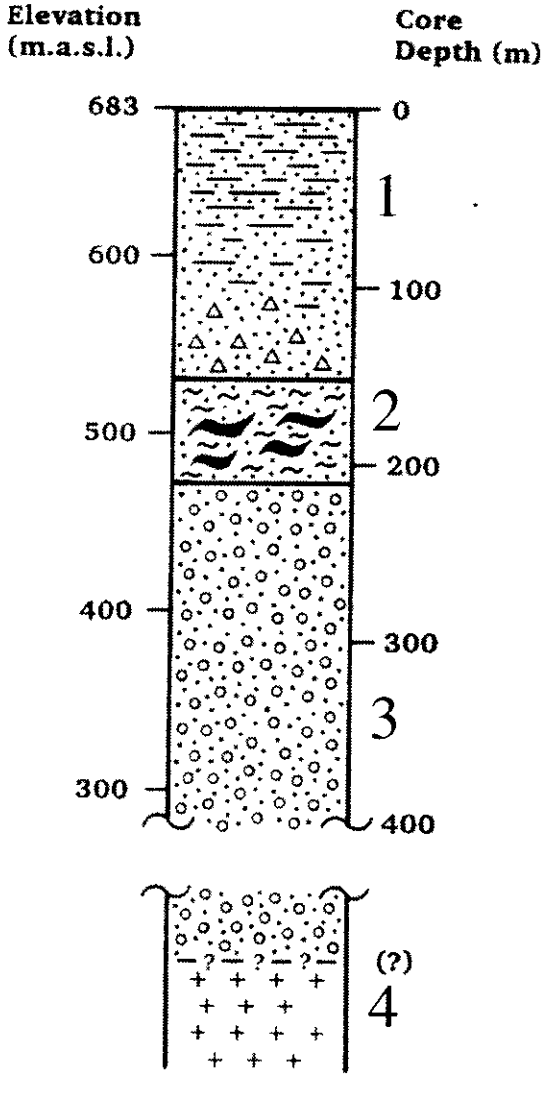

(b)

Figure 5.1. (a) Schematic cross-section through the Gardnos impact crater. (b) Schematic stratigraphic section through the Branden drill core. (1) Crater-fill sediments, mainly grey-black sandstones, large fragment breccia. (2) Suevite with impact melt breccia (large wave symbols). (3) Gardnos breccia. (4) Basement rocks. [Adapted from French et al. (1997)].

breccias. These comprise planar deformation features in quartz and feldspar, glassy fragments, melted feldspars (French et al., 1997), kink bands in biotite, melted biotite (Naterstad and Dons, 1992; French et al., 1995) and maskelynite (French et al., 1995). Planar deformation features in quartz are seen in <1 % of clasts and have a {1013} (ω) orientation diagnostic of shock (French et al., 1995; 1998). The planar deformation features and fractures may include methane-bearing fluid inclusions (Dons and Naterstad, 1992) which were formed during Caledonian (400 Ma) metamorphism (Anderson and Burke, 1995). These shock metamorphism structures indicate that the degree of shock metamorphism ranges from stage I to IV (table 5.1). The degree of shock metamorphism decreases with depth from silicate melt in impact melt rocks and suevites to fracturing and brecciation in the underlying basement rocks.

Table 5.1. Range of shock metamorphism features from the Gardnos impact crater. From Naterstad and Dons (1992); French et al. (1995; 1997) and Graup, (1990).

Structure	Pressure (Gpa)	Temperature (°C)	Stage
Fracturing and granulation	1-10	0-100	O
Kink bands in biotite	1-10	0-100	O
Planar deformation features in quartz	10-45	100-900	I-II
Melted feldspars and biotite	45-60	900-1700	III
Silicate melt glass	45-80	900-3000	III-IV

5.2.4. Samples.

Eight samples each averaging 150 g, from the Gardnos structure were provided by Professor B. French and are described in table 2.1. These samples are part of a larger collection from the Gardnos structure and surrounding area which comprise basement gneisses, black quartzites, local black shales and impact deposits such as lithic and suevite breccias.

The samples were ground to a powder using an agate pestle and mortar, 4 g of each sample was treated using microwave assisted dissolution in HF:HCl, following the procedure described in section 2.6.3 to obtain an acid-demineralised residue. Following dissolution, the samples were treated with HF:HCl to remove any residual zircons and HCl to remove neo-formed fluorites. Approximately a third of each sample was treated with chromic acid at 70 °C to remove amorphous carbon and then a further third of this sample was treated with fuming perchloric acid at ≥ 110 °C to remove crystalline graphite. Aliquots of the original demineralised samples were retained for GC-MS analysis and the perchloric and chromic acid-residue aliquots for transmission electron microscopy (TEM) and carbon stable isotope analysis using stepped combustion combined with static mass spectrometry.

5.3. CARBONACEOUS COMPONENTS INCLUDING DIAMOND IN GARDNOS CRATER IMPACTITES.

The demineralised samples were studied using a petrographic microscope as detailed in chapter 2. The high carbon content of these samples and overall black colour made the identification of minerals particularly difficult. This was compounded by the overall fine-grained nature of the samples (typically 5-50 μm). Individual zircons within the residues were considerably smaller (10-50 μm) than those observed in the Ries crater samples (150-500 μm). Diamonds were observed in the G133 suevite residue but due to their extremely small size (<30 μm) they could not be extracted.

Table 5.2. Mineralogical composition of carbon phases in Gardnos crater samples.

Sample no	Lithology	Graphite	Diamond
G164	Alum shale	X	-
G169	Biri shale	X	-
G137	Suevite	X	X
G133	Suevite	X	X
G178	Black lithic breccia	X	X
G120	Lithic breccia	X	-

The samples were analysed using the TEM following the HF/HCl stage of the acid demineralisation (table 5.2). This initial analysis indicated that the suevite and black lithic breccia samples (G137, G133 and G178) contained diamond as well as highly crystalline graphite. The grains identified as graphite produced SAED patterns with strong spots and no diffuse rings or streaking. The SAED pattern suggests that the graphite was crystalline or highly crystalline. Studies of graphite maturity have shown that SAED patterns can be used to distinguish between poorly crystalline and highly crystalline graphite as graphite maturity increases (Buseck and Huang, 1985). Electron diffraction patterns show increasing numbers of rings, decreased diffuseness and in well crystallised graphite, discrete spots (Buseck and Huang, 1985). Many of the grains identified as cubic diamond showed clear apographitic, platy morphologies, the SAED patterns of these grains however showed no indication of graphite or londsdaleite.

Diamond was identified within the G137 and G133 demineralised residues as well as the black matrix lithic impact breccia G178 and graphite was detected within all of the samples. Following perchloric acid oxidation at 120°C the presence of diamond and highly crystalline graphite was confirmed by TEM/SAED. This distribution is in contrast to that found at the Ries crater where diamonds are found in suevite and suevite components but not within lithic breccias (Schmitt et al., 1999). The shales represent unshocked potential carbon sources in the pre-impact stratigraphy of the Gardnos structure and do not outcrop in the vicinity of the impact crater at the present day.

5.4. MORPHOLOGICAL FEATURES OF GRAPHITE FROM GARDNOS IMPACTITES.

The range of morphological structures observed in the graphite grains was limited when compared with those found in carbon grains at the Ries crater impactites. The majority of the grains had strong hexagonal, platy structures and were typically very small in size (0.4 to 5 μm), confirming the characteristics noted from the optical analysis of the residues which were < 5-50 μm in size compared to <150-500 μm in the Ries

crater residues. The SAED patterns of graphite varied from clear spot patterns indicating a high degree of crystallinity to more diffuse ring patterns suggesting less crystalline or polycrystalline material. The degree of crystallinity in graphite can be estimated from the SAED patterns with clear spot patterns indicating high crystallinity and diffuse ring patterns less crystalline (Buseck and Huang, 1985).

5.4.1. Hexagonal, platy structures.

Hexagonal and platy structures were the most common morphology observed in these graphite grains. The individual layers are stacked parallel to the basal plane and rarely appear to show rotation of the layers. Figure 5.2 shows a very small (400 nm) hexagonal graphite crystal from the G137 suevite residue which appears to be composed of 2-3 individual layers.

From the SAED patterns of many of these samples the graphite spots are clear and distinct indicating a high degree of crystallinity. In contrast, some graphitic samples observed were less crystalline and had diffuse ring patterns rather than spots.

The morphologies of these hexagonal and platy graphite grains are very similar to those of the apographitic diamonds identified within the Ries crater samples (this study) and those reported from other impact craters such as Popigai (Koeberl et al., 1997) and Lappajärvi (Langenhorst et al., 1999).

5.4.2. Stacking faults.

Stacking faults were detected in the graphite grains observed in all the Gardnos samples. Figure 5.3b shows a platy, layered carbon grain from the G169 shale sample which was identified as graphite (inset SAED). The SAED pattern shows double reflections indicating several overlapping thin plates. Information concerning stacking faults in graphite is limited within the available literature, as this sample has not been subjected to impact-related shock these stacking faults are likely to be the result of growth or metamorphic deformation.

(a)

(b)

Figure 5.2. (a) BFTEM image of 400 nm hexagonal, layered graphite crystal from G137 suevite. Inset SAED shows diamond 2.06 Å. [x 40 k, 200 kV, scalebar 200 nm]. (b) BFTEM image of stacking faults in platy graphite grain from G169 shale. Inset SAED shows diamond 2.06 Å and graphite 3.35 Å. [x 40 k, 200 kV, scalebar 200 nm].

These stacking faults are similar to those observed in impact diamond from the Ries crater samples suggesting that stacking faults may be inherited structures. However, there are a number of different stacking fault configurations which can occur which cannot be distinguished without the use of HRTEM.

5.5. MORPHOLOGICAL FEATURES OF DIAMOND FROM GARDNOS IMPACTITES.

The structures observed in the diamond grains detected in suevite G137 and a black lithic breccia G178 were similar to those observed in the graphite examples discussed above.

5.5.1. Hexagonal, platy structures.

The diamond grains observed using the TEM generally had platy, horizontal graphitic layering structures representing stacked plates (figure 5.3a) inherited from the precursor graphite. Double reflections on the SAED patterns support this observation. These layers occasionally show rotation around the axis of the basal plane and fractured margins representing either the breakage of the diamond crystals or the removal of graphite coatings. The sample shown in figure 5.3b shows two distinct layers with a horizontal offset between them; the grain is rounded in form although an elongate hexagonal structure is suggested possibly indicating corrosion of the grain.

Again these hexagonal apographitic morphologies are similar to those seen in the Ries crater samples (this study) and other impact craters.

5.5.2. Etching.

Etching was not well developed in these samples although the margins of some of the platy layered samples may be the result of corrosion or fracturing. The highly irregular margins of a platy diamond grain from the G137 suevite (figure 5.4) appear to show evidence of some etching. The lack of etched structures compared to the Ries

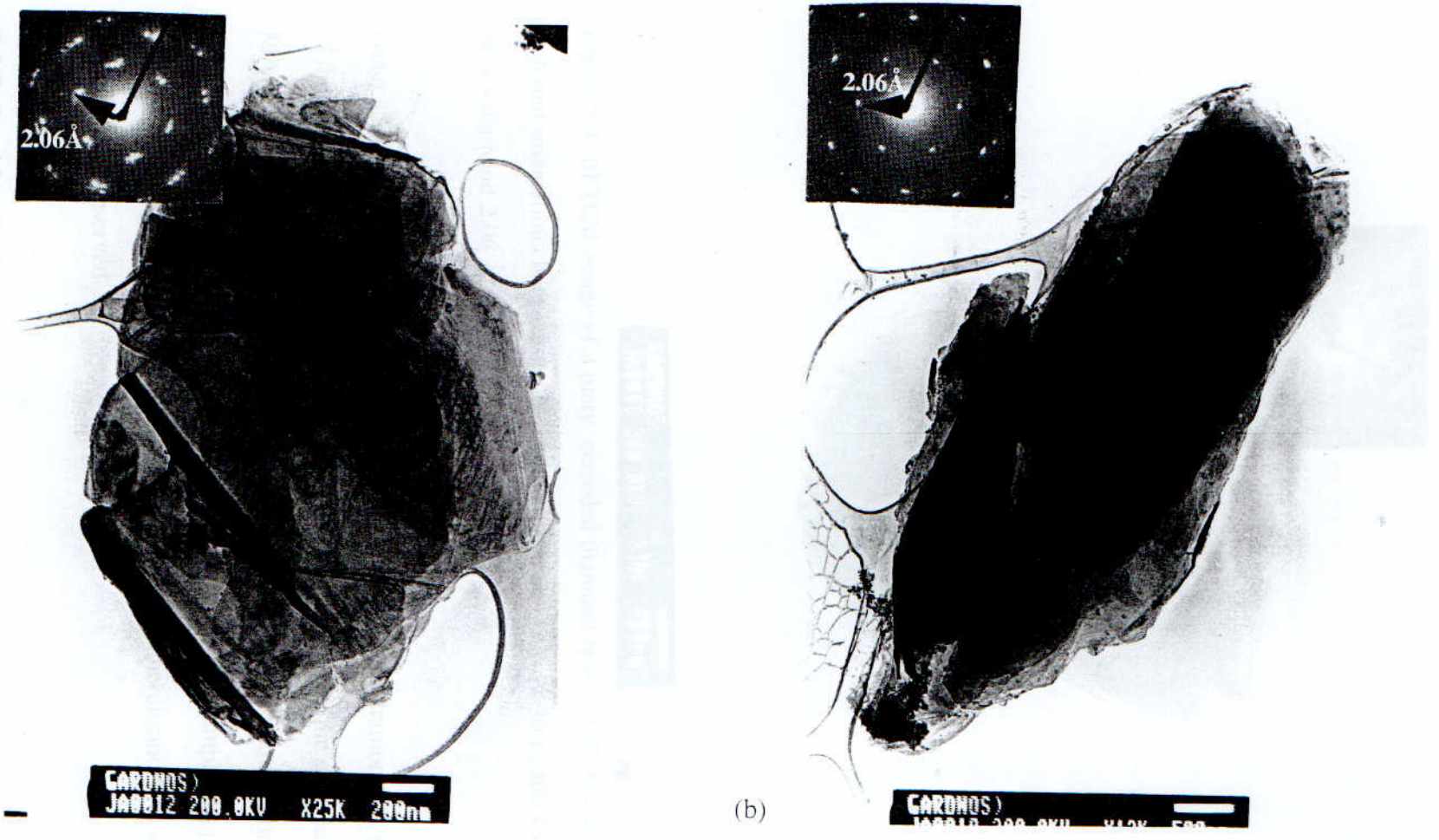

(a) (b)

Figure 5.3. (a) BFTEM image of layered, pseudo-hexagonal diamond grain from G137. Inset SAED shows diamond 2.06 Å. [x 25 k, 200 kV, scalebar 200 nm]. b. BFTEM image of platy, fractured diamond from G133. Inset SAED shows diamond 2.06 Å. [x 12 k, 200 kV, scalebar 500 nm].

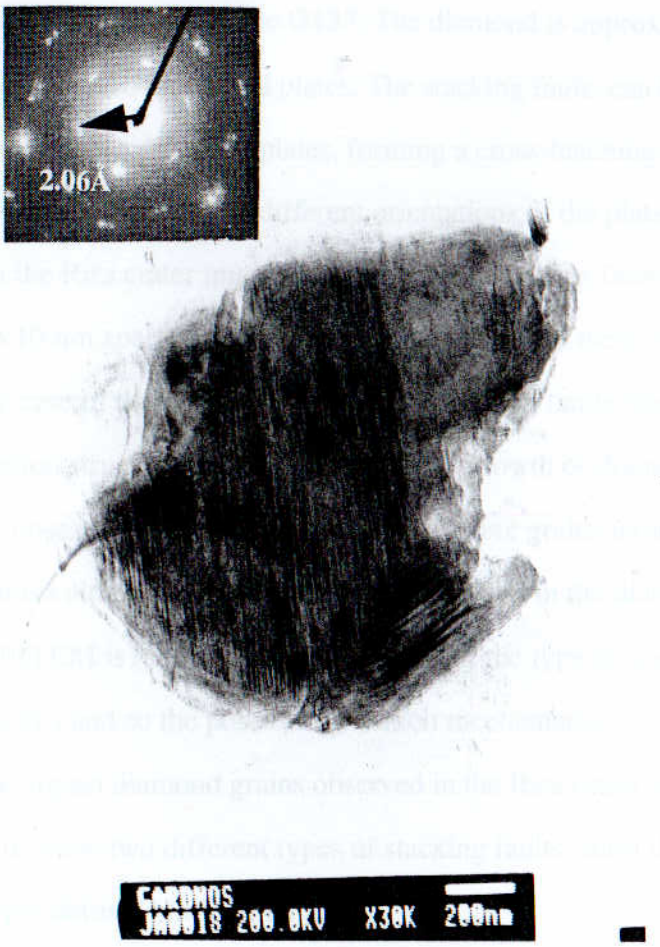

Figure 5.4. BFTEM image of a platy, corroded diamond from G137. Stacking faults show different orientations between the individual diamond plates [x 30 k, 200 kV]. Inset SAED shows diamond 2.06 Å.

crater samples suggests that the corrosion of the Ries impact diamonds is not the result of the acid treatments as both sets of samples were treated with the same acids. The MARS5™ system used to demineralise these samples achieves temperatures of ≤ 300 °C which is 150-200 °C more than the temperatures that the Ries samples were exposed to. This should be more corrosive than the conventional demineralisation yet less etching features were observed.

5.5.3. Stacking faults.

Stacking faults were well developed in the samples and were similar to those observed in the Ries crater impactites comprising numerous thin black lamellae. Figure

5.4 shows a diamond from the suevite G137. The diamond is approximately 1.5 μm in size, composed of atleast 6 individual plates. The stacking faults can be seen in both the surface plate and several subsurface plates, forming a cross-hatching pattern intersecting at approximately 60°, indicating the different orientations of the plates. This feature was also observed in the Ries crater impact diamonds. The stacking faults in figure 5.4a and 5.5 are less than 10 nm apart emphasising the high density of these defect structures.

As in the case of the Ries crater impactites stacking faults may be inherited growth, deformation structures or the result from the growth of diamond at the expense of graphite. The observation of stacking faults in graphite grains indicates that these may be inherited features although the stacking faults observed in the diamond grains were more defined. HRTEM is required in order to identify the type of stacking faults that occur in these grains and so the possible formation mechanisms.

As in the impact diamond grains observed in the Ries crater samples these samples appear to show two different types of stacking faults: short thick black lamellae and narrow sharply defined black lamellae.

5.5.4. Polycrystalline textures.

None of the diamond grains observed under the TEM showed polycrystalline morphological structures similar to those observed in the Ries crater samples. The SAED pattern for the diamond shown in figure 5.4 has diffuse diamond spots indicating a degree of polycrystallinity. The lack of obvious surface polycrystalline structures suggests that the diamonds may have annealed surfaces although the obvious stacking fault structures suggest that this is unlikely. As these diamonds are 0.4-1.5 μm in size they are likely to be composed of only a few crystallites. The crystallites in polycrystalline diamond are reported to be 0.1-1 μm in size (Langenhorst et al., 1998) whilst individual diamonds from the K/T boundary layers are ≥ 6 nm (Gilmour et al., 1992). This suggests that the Gardnos diamonds may be composed of around <1-100 crystallites hence the lack of clear polycrystalline SAED patterns.

5.5.5. Summary of morphological features.

The diamonds from these samples (suevite G133, G137 and black matrix lithic breccia G178) are predominantly platy, layered grains with apographitic to graphitic hexagonal morphologies. Skeletal structures observed in the Ries crater impactites (Hough et al., 1995c; this study) and preferred orientation structures were not seen in these residues. This suggests that the primary mechanism for diamond formation was the direct shock transformation of graphite. However, the carbon source within the pre-impact stratigraphy is difficult to determine due to post-impact metamorphism (400 Ma) to the greenschist facies (Naterstad and Dons, 1994) which may have increased the degree of crystallinity in the graphite samples. As a significant proportion of the carbon in the samples is composed of poorly graphitised or amorphous carbon the contribution towards diamond formation from this carbon source must be considered.

5.6. CARBON STABLE ISOTOPIC COMPOSITIONS OF GARDNOS IMPACTITES AND ACID DEMINERALISED RESIDUES.

Acid demineralised residues from this study were analysed for carbon stable isotopic compositions using stepped combustion combined with static mass spectrometry in order to identify individual components and variations in the isotopic composition of these components. Bulk whole-rock carbon stable isotopic compositions were obtained from French et al. (1997).

5.6.1. Bulk whole-rock carbon stable isotopic compositions.

Whole-rock stable carbon isotopic analyses of the Gardnos samples indicated a relatively narrow range from $\delta^{13}C$ = -28.1 to -31.5 ‰ (French et al., 1997). On the basis of the isotopic composition of the impactites (depleted in ^{13}C by 3 ‰ relative to the basement rocks), Tucker (1983) suggested that biologically fixed carbon derived from local shales may have provided the carbon for the observed concentration increases.

5.6.2. Carbon stable isotopic composition of acid demineralised residues.

Two of the demineralised residues were analysed by stepped combustion combined with static mass spectrometry. One prior to perchloric acid (G137) and one following perchloric demineralisation (G178-P)
(Appendix 5).

Transmission electron microscope analysis of both samples indicate the presence of diamond and highly graphitised carbon. Using stepped combustion two components were detected in the G137 suevite residue with markedly different isotopic compositions (figure 5.5).

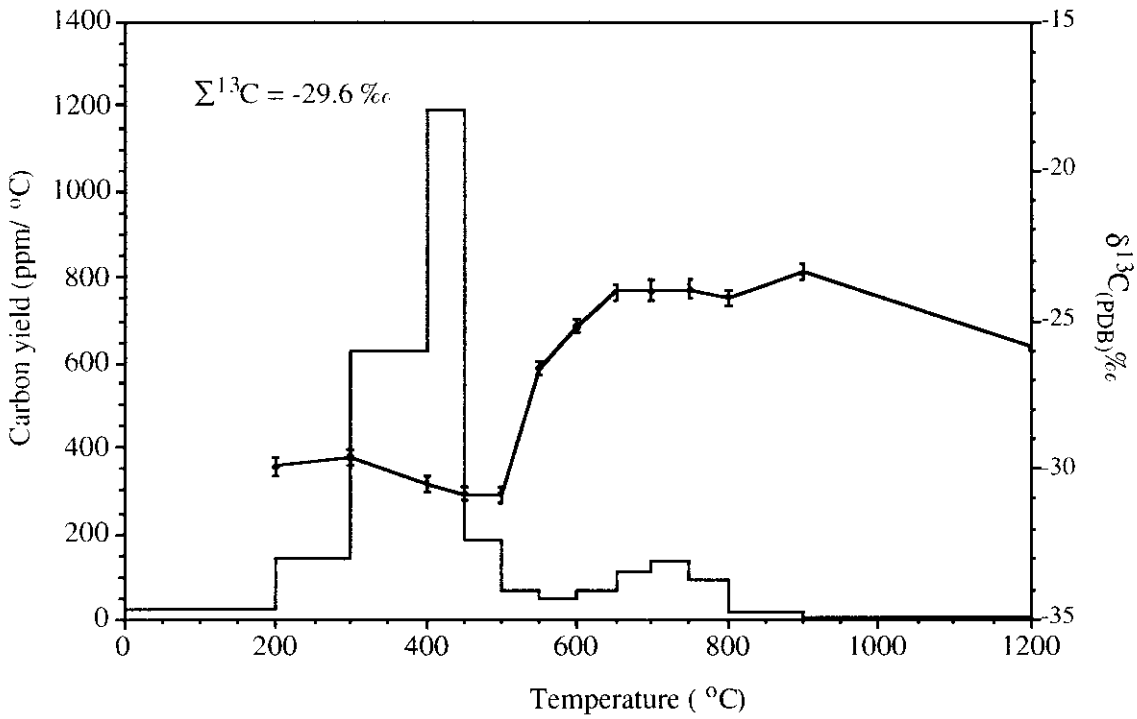

Figure 5.5. Stepped combustion analysis of G137 suevite acid-demineralised residue (sample weight = 14.3 µg). $\Sigma\ \delta^{13}C$ = -29.6 ‰ and Σ carbon yield 17.8 wt%.

The low temperature release from 300-500 °C has a $\delta^{13}C$ of -30.5 ‰ which is in the same range as the bulk isotopic compositions (French et al., 1997). The high temperature release from 650-800 °C had a $\delta^{13}C$ of -24 ‰ which is enriched in ^{13}C by 3.9 ‰ relative to the bulk compositions. The minor high temperature (> 600 °C)

component released by the residue would effectively be swamped by the greater low temperature yield in a bulk experiment. In addition the bulk experiment samples were not demineralised and may contain carbonate or amorphous carbon material which has been removed by the acid digestion process and chromic acid treatment in this study. The low total carbon yield (17.8 %) indicates that the sample was not pure and probably contained resistant zircons.

Following fuming perchloric acid oxidation at 110 °C for 4 days to remove more resistant carbonaceous components such as graphitic carbon, a sample of a black lithic breccia G178-P was analysed by stepped combustion. The results (figure 5.6) show 2-3 carbon releases and markedly variable $\delta^{13}C$ ranging from -27 to -32 ‰. The low temperature release from 300-400 °C ranges in $\delta^{13}C$ from -27.6 to -31.2 ‰ whereas the high temperature release at 650 °C has a $\delta^{13}C$ of -32.5 ‰. The averaged $\delta^{13}C$ composition was for the sample -28.8 ‰. These values are again within the range of those determined for the whole-rock samples (French et al, 1997).

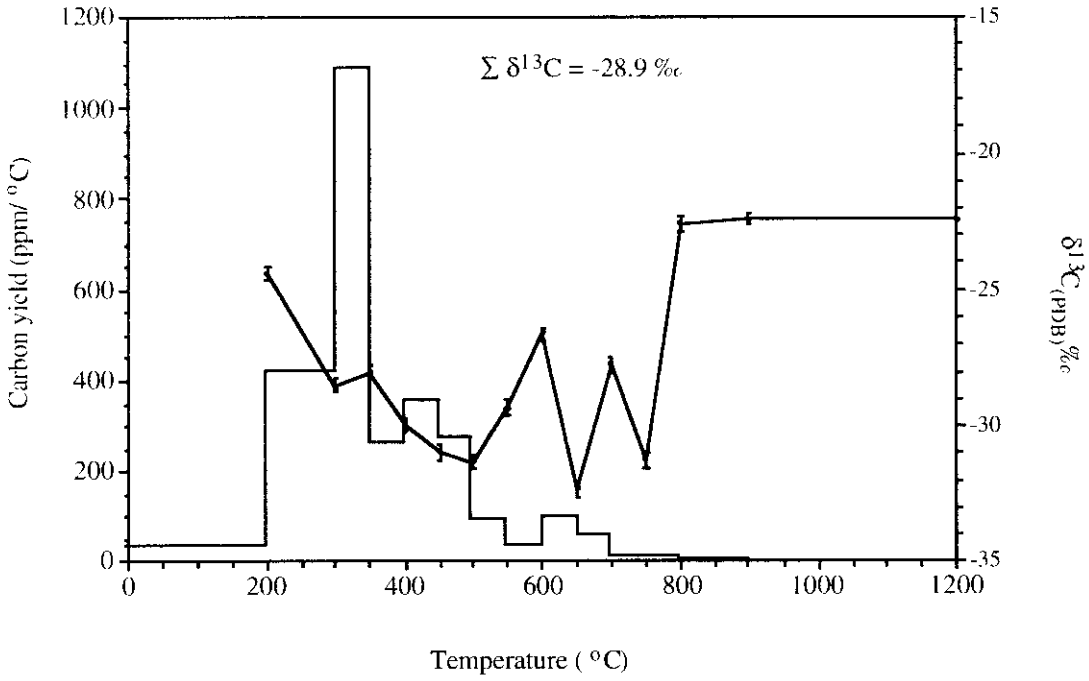

Figure 5.6. Stepped combustion analysis of G178-P acid-demineralised residue following perchloric acid treatment (sample weight = 17.6 µg). Σ $\delta^{13}C$ = -28.9 ‰ and Σ carbon yield = 16.4 wt%.

The carbon stable isotopic compositions ($\delta^{13}C$) of the small high temperature releases range from -24 to -32.5 ‰. Again the total carbon yield was low (16.4 %) indicating an impure sample. The difference in carbon yield between G137 and G178-P (18.6 to 16.4 %) is relatively small suggesting that amorphous carbon (which would be removed by perchloric acid) was not a significant component in the G137 sample.

The average carbon stable isotopic compositions of these two samples (G137 and G178) are relatively similar, $\delta^{13}C$ -29.6 to -28.9 ‰ but variations of over 7 ‰ exist within each residue.

The two-stage releases (low temperature and high temperature) possibly suggest that the sample is composed of two main carbonaceous components, graphite or poorly crystalline graphite (low termperature) and diamond (high temperature). This is complicated by the low temperatures of the two releases. The graphite samples from the Ries crater combusted at between 450 and 550 °C and the diamonds at 650-900 °C. These Ries crater samples were between 150 and 300 μm in size. It has already been noted that the grain size of the Gardnos residues (graphite, zircon and diamond) was distinctly finer than that of the Ries crater residues. The influence of grain size on combustion temperatures was investigated by Ash et al. (1990) whose results indicate that 1-10 nm diamonds combust at around 500 °C and 1 mm diamonds at 800-850 °C. Distinguishing between crystalline graphite and diamond can be difficult using stepped combustion plots.

Therefore, although the TEM/SAED analysis indicates that diamond and graphite are present in these samples and the 178 sample was vigorously oxidised using fuming perchloric acid the two releases may represent mixtures of poorly crystalline graphite and amorphous carbon (low temperature release) and crystalline graphite and ≤ 1 μm diamonds (high temperature release). The stepped combustions do suggest two different carbonaceous components and further demineralisation, TEM and stepped combustion investigations are required in order to clearly identify the components.

5.7. DISCUSSIONS.

Crystalline graphite and poorly crystalline amorphous carbon material was found in all of the Gardnos samples studied. Diamond has been identified in the two suevite samples and a black matrix lithic breccia. These diamonds occur at low concentrations and are predominantly fine-grained and apographitic in structure.

5.7.1. Carbon composition and sources.

The Gardnos impact structure has experienced post-formation Caledonian greenschist facies metamorphic overprinting (Naterstad and Dons, 1994). The temperatures and pressures (350-550 °C, 0.2-1 Gpa) were sufficient to convert some organic carbon to graphite.

During prograde metamorphism, oxygen, hydrogen and nitrogen are released from organic matter and the residual carbon atoms become increasingly ordered (Grew, 1974; Itaya, 1981; Buseck and Huang, 1985). The transformation of organic matter to graphite can occur between 300-500 °C (Ruland, 1968) and the degree of crystallinity and size of crystallites increases with metamorphic grade, but graphite can form in the chlorite zone (Buseck and Huang, 1985). The nature of the precursor carbon for example, aromatic structures with hexagonal benzene ring structures greatly affects the ease of graphitisation and degree of structural order (Buseck and Huang, 1985). Small scale structural and chemical heterogeneity including rotational layer disorder persists at relatively low degrees of graphitisation (Rietmeijer, 1991).

Graphite inclusions and carbon-rich fractures found in shocked quartzite breccias from the Gardnos structure (Anderson and Burke, 1996) indicate that a proportion of the carbon content is graphitic and crystalline. The metamorphic overprinting makes it difficult to determine the structure of the precursor carbon material which would have been available for the shock transformation to diamond. The metamorphic overprinting occurred within the Caledonian orogeny (400 Ma) (Naterstad and Dons, 1992; French et al., 1998) which would have affected the shales to an equivalent degree. Therefore

graphitic carbonaceous material would also have been produced from organic material within the shales.

The stable carbon isotopic composition of graphite depends on the isotopic composition of the precursor organic matter and the extent of fractionation during metamorphism. Several mechanisms may fractionate graphite during metamorphism including approximately 3 ‰ due to the removal of ^{12}C from the dehydrogenation loss of CH_4 (Peters et al., 1981a; 1981b). Methane-bearing fluid inclusions found in PDF within the blackened quartzites (Naterstad and Dons, 1992; Anderson and Burke, 1995) formed by reaction between solid carbonaceous material and aqueous metamorphic fluids (Anderson and Burke, 1995). This suggests that the carbon stable isotopic composition of the graphite and carbonaceous material within the Gardnos impactites may have been enriched in ^{13}C up to 3 ‰ compared to any impact diamonds formed prior to the Caledonian metamorphism.

The metamorphic overprinting makes it difficult to determine whether the shales contained graphite at the time of the impact. The impact diamonds may therefore, be derived from either amorphous carbonaceous material or graphite derived from the basement rocks underlying the shales.

The discovery of sub-micron impact diamonds within suevites and lithic breccias from the Gardnos impact crater confirms the suggestion by Vishnevsky and Raitala, (1998) that impact diamonds can survive greenschist facies metamorphism.

The Gardnos impactites show a broad range of whole-rock carbon contents. Figure 5.7 shows the average carbon contents (wt %) for the different impactites and potential carbon sources (basement rocks). The carbon content is variable between the different lithologies and indicates a clear 10-fold variation in carbon contents (French et al., 1995; 1998).

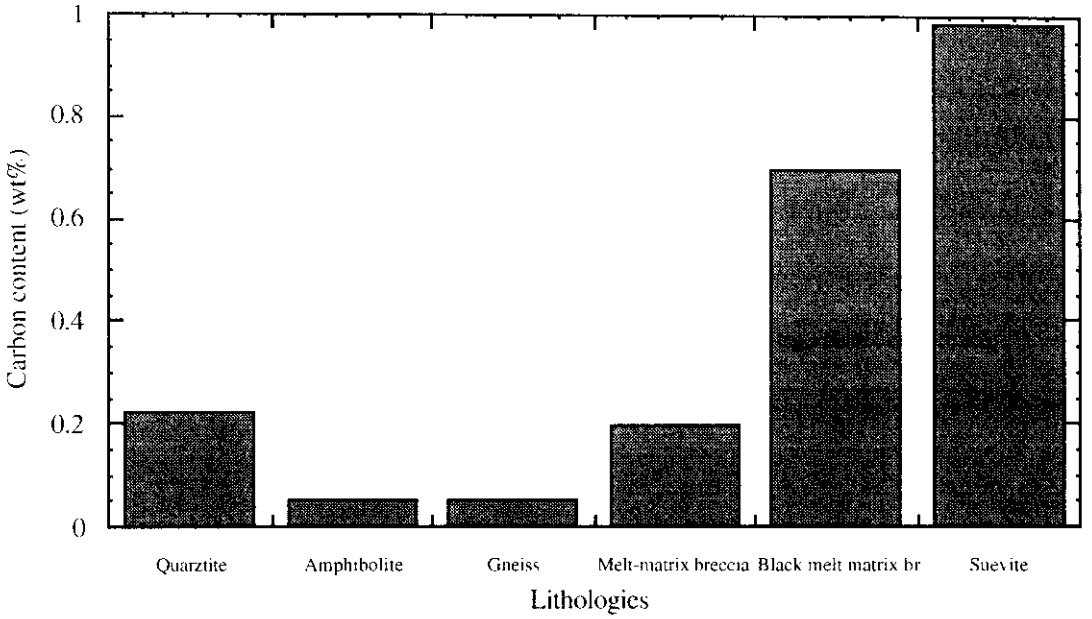

Figure 5.7. Average carbon contents (wt %) for Gardnos impactites and target rocks. [Data from French et al., 1997].

The total carbon and soot contents of the sample suite were provided by W. Wolbach and S. Widicus, IWU (unpublished data) and those results for the samples used in this study are shown in table 5.3.

Table 5.3. Carbon content and soot for Gardnos structure samples. Data from W. Wolbach and S. Widicus, IWU. (unpublished data).

Sample no	Original mass (g)	Total C (ppm)	Error (±ppm)	Soot (ppm)	Error (±ppm)
Basement rocks: black shales, off structure.					
164	2.56444	55000	1000	5100	800
169	2.25117	7200	700	5400	700
Melt-bearing suevite breccia.					
133	2.37714	2100	100	30	40
137	2.26706	16000	1000	1100	100
Black matrix lithic breccia.					
178	2.46650	26000	1000	200	600
Gardnos lithic breccia, subcrater rocks.					
120	2.45246	3200	200	8	9

The high errors for some of the samples (178, 120 and 133) indicates that soot cannot be confirmed in all the samples. The presence of soot in the melt-bearing suevite 137 could indicate that fires and combustion of carbon material may have been an important process during the impact event. The existence of soot in the unshocked shales 164 Alum shale (Cambro-Ordovician) and 169 Biri (Proterozoic) is problematic unless these rocks accumulated carbon from fires during their deposition and formation. The material identified as soot may be poorly crystalline carbonaceous material or kerogen.

5.7.2. Diamond yield and carbon-diamond transformation ratios.

Assuming the carbon yield for stepped combustion steps ≥ 600 °C to be from diamond in the two samples analysed (G137 and G178, then the diamond yield from G137 was 0.02 % and for the G178 0.009 %. The amount of graphite in the samples is harder to calculate, although again the carbon yield for the stepped analyses may be used as a rough measure and give graphite:diamond ratios of 8:1 and 17:1 respectively. This is clearly an overestimate as a great deal of the carbon in the samples would have been removed by the chromic and fuming perchloric acid treatments. In addition many of the whole-rock samples have very high carbon contents composed of organic and amorphous carbon as well as graphite. The original carbon prior to metamorphic overprinting may well have been predominantly amorphous and poorly crystalline, subsequently matured to graphite.

5.7.3. Morphological features of diamond.

The predominant feature of the diamonds found in these samples is a strong apo-graphitic morphology with numerous individual plates often associated with dense distributions of stacking faults. These stacking faults may represent inherited features or represent pre-transformation deformation as suggested to explain kink bands in apo-graphitic diamonds (Valter, 1986; Valter and Yerjomenko, 1996). Alternatively these stacking faults may represent growth or deformation structures during the diamond

formation. The relative lack of structural features in the diamonds from these samples may indicate that post-formation annealing has taken place or simply be a reflection of the limited number of samples observed.

5.7.4. Graphite formation: shock metamorphism or greenschist regional metamorphism.

This study has identified graphitic carbon within the shocked Gardnos impactites as well as within off-structure unshocked shales (this study) which were proposed as potential carbon sources (French et al., 1997). These shales are located off-structure in that the do not occur at the crater at the present day but are believed to have overlain the metamorphic target rocks at the time of impact. The target rocks have experienced two episodes of metamorphism, firstly between 1500-1700 Ma and secondly following the impact at 380-400 Ma (Naterstad and Dons, 1994). Both of these episodes could have resulted in the formation of crystalline graphite from pre-existing organic matter. Raman spectra of this carbonaceous material indicates formation from metamorphic recrystallisation of biogenetic carbon in the greenschist facies (Anderson and Burke, 1995). The concentration of carbon within the unshocked target rocks is low (figure 5.7) ranging from 0.22 to 0.05 wt % (French et al., 1997) indicating that only small percentages of carbon were introduced at the time of formation (pre-1100 ma). The shales which are suggested to have provided the observed increase in carbon concentrations in the impactites (French et al, 1997) are Proterozoic (Biri) to Cambro-Ordovician (Alum) in age (590-505 Ma). Indicating that the Alum shale experienced a single metamorphic event (400 Ma) and may not have existed at the time of the impact which is poorly dated (900-400 Ma).

Graphitisation of poorly crystalline and amorphous carbonaceous material can also be achieved during shock metamorphism, as shock experiments producing diamond and crystalline graphite indicate (Hirai et al., 1995). Shock graphitisation should produce material inheriting the structure of the precursor carbon or very fine-grained material. Graphitisation during metamorphism proceeds through the development of increasingly

large crystallites, crystal lengths and crystalline perfection over time (Buseck and Huang, 1985). During a brief shock event the formation of large, highly orientated crystals is unlikely. Polycrystalline material with diffuse ring patterns on the SAED were observed in the graphite samples as well as material with spot patterns indicating a range in crystallinity or a mixture of single crystal graphite and polycrystalline shock comminuted material. Progressive comminution of pre-graphitic carbon subjected to experimental shock pressures up to 59.6 Gpa, produced characteristic polycrystalline ring patterns (Rietmeijer, 1995). The observation of dense distributions of stacking faults within the graphite and impact diamonds could suggest disordered shock formation. However the stacking fault structures were also observed in graphite from the unshocked off-structure shales, indicating that their formation is the result of growth or regional metamorphism. HRTEM is required in order to distinguish the type of stacking faults involved.

The evidence suggests that graphite was produced from organic material during both periods of regional metamorphism and polycrystalline textures due to shock comminution may have been produced by the impact and preserved in crystalline graphite. The degree of crystallinity within the graphite was probably increased by the impact event and subsequent Caledonian metamorphism.

5.7.5. Diamond formation mechanisms.

The shock conditions (P/T) experienced by the Gardnos impactites during the impact event range from 1-80 Gpa and 0-3000 °C (table 5.1) with the majority of the impactites experiencing low degrees of shock. The suevite samples contain impact melt glass indicating peak pressures and temperatures of 60-80 Gpa and 900-3000 °C respectively. The black matrix lithic breccia contains quartz and feldspar crystals displaying PDF indicating peak shock conditions of 10-45 Gpa and 100-900 °C. These conditions lie within the field for diamond stability (figure 4.16) as well as those required for the suggested diamond formation processes (Table 4.8).

From the TEM/SAED analysis the graphite within these samples is on average well crystallised. This crystalline maturity may have been enhanced by greenschist facies

metamorphism during the Caledonian (400 Ma) and it is difficult to determine the original carbon composition at the time of impact. The structures of the diamonds that were seen under the TEM were strongly apographitic, displaying layering parallel to the basal plane and pseudo-hexagonal to hexagonal morphologies. This indicates that the carbon available for shock transformation was graphitic. In addition shock metamorphism by the impact event may have resulted in the graphitisation of poorly crystalline amorphous carbon material. Shock transformation experiments using amorphous and poorly crystalline carbon resulted in the formation of diamond and graphite (Hirai et al, 1995). Shock metamorphism of pre-existing graphitic carbon may also produce structural features such as polycrystallinity.

5.7.6. Preservation of diamond.

As in the case of the Ries and other impact craters the preservation of diamond formed by shock transformations (≥35 Gpa and ≥3000 K) requires rapid cooling to ≤ 1000 K in order to inhibit re-graphitisation (De Carli, 1995). The small size (0.4-5 μm) of these diamonds may be due to the size of the pre-existing graphite crystals within the target rocks or represent relict cores from re-graphitisation processes. The regional metamorphism had a maximum of 400-500 °C and 4-7 kbar representing greenschist facies conditions. Vishnevsky and Raitala, (1998) determined that impact diamonds can survive regional metamorphism.

5.8. CONCLUSIONS.

5.8.1. Carbon compositions.

Graphitic carbon has been identified using optical observations and TEM/SAED in four samples of shocked impactites from the Gardnos impact structure as well as within two shale samples (this study) proposed as potential carbon sources for a documented increase in carbon content between the unshocked metamorphic target rocks and shocked impactites (French et al., 1997). In addition 0.4-5 μm diamonds have been identified using TEM in two suevite samples and a black matrix lithic impact breccia.

The concentration of diamond within the suevite and black matrix lithic impact breccia was estimated at between 0.02 and 0.009 % respectively.

5.8.2. Carbon stable isotopic compositions.

The bulk whole-rock isotopic compositions $\delta^{13}C$ range from -28.1 to -31.5 ‰ (French et al., 1997) indicating that these samples contain a ^{13}C-enriched component, which appears to be the diamond grains. The $\delta^{13}C$ the high temperature release (possibly diamond) found within these samples was -24 ‰ in G137 suevite and between -26 to -32.3 ‰ in G178-P black matrix lithic breccia. The isotopic composition $\delta^{13}C$ of the low temperature release (possibly graphite) was -30.8 ‰ in G137 suevite and -29.9 to -31.3 ‰ in G178-P black matrix lithic breccia.

The overall carbon stable isotopic compositions are within the range for marine organic material as suggested by French et al. (1997). The $\delta^{13}C$ of diamonds from the Ries crater impactites (this study) are ^{13}C-depleted compared to those used to suggest that the $\delta^{13}C$ of carbon in the Gardnos samples was not derived from diamond (French et al., 1997). The results of this study indicate a wider range of carbon stable isotopic compositions in impact diamonds as well as the presence of diamond within the Gardnos impactites.

5.8.3. Diamond formation mechanisms.

The shock pressures and temperatures experienced by the Gardnos impactites which contained diamond were within the field of diamond stability and formation. The structural characteristics of the diamonds indicated that the primary mechanism of formation was one of direct transformation with the preservation of inherited graphite morphologies. Diamonds displaying characteristics suggestive of a vapour growth formation or formation from amorphous carbon material were not observed.

CHAPTER 6. CONCLUDING REMARKS AND FURTHER WORK.

6.1. DIAMOND FROM THE RIES CRATER.

1. Diamonds were found in glass bombs from the Ötting quarry suevite (Abbott et al., 1996; 1998a), as well as in whole-rock suevites from the Ötting quarry, Seelbronn quarry and Polsingen quarry and gneiss from Aumühle. These discoveries of impact diamonds have been subsequently confirmed in other localities of the Ries crater (Siebenschock et al., 1998). Three sections of suevite from the N-73 drill core were found to contain diamond (Abbott et al., 1998b) and have been subsequently confirmed in a further section of the core (Schmitt et al., 1999).

2. Following acid demineralisation the residues were found to contain 50-300 μm size diamonds visible under the petrological microscope, this was confirmed using transmission electron microscopy (TEM) and selected area electron diffraction (SAED) and where possible stepped combustion in order to distinguish individual carbonaceous components. The hexagonal polymorph of diamond, londsdaleite was not detected using TEM and SAED. TEM allowed examination of the grains at a much higher resolution than bulk x-ray analyses that have been used previously to estimate londsdaleite contents within impact diamonds. The lack of londsdaleite in the SAED from the impact diamonds in this study suggest that stacking faults may contribute to the occurrence of londsdaleite using x-ray analysis.

3. The diamonds from the Ries crater identified during this study were of two distinct morphologies:- apographitic displaying inherited structural features and skeletal polycrystalline diamonds with preferred orientations. Morphologically they displayed characteristics common to previously described impact diamonds (Vishnevsky et al.,

1989). Apographitic diamonds were found in the OQS, OQGB, SBS and N-73 core sections NC343, NC384 and NC494.

5. The apographitic diamonds were observed under the petrological microscope (50-300 μm) and TEM (5-20 μm). They were predominantly platy and composed of numerous (2-7) individual plates with hexagonal morphologies. Many of the examples observed using the petrological microscope displayed high birefringence (second to third order interference colours) indicative of internal stress and strain (Masaitis, 1995). Other examples were coated with black soot-like deposits. Surface structures included parallel and cross-hatched lineations that may represent twinning (Masaitis et al., 1990; Valter et al., 1992; Koeberl et al., 1997; Langenhorst et al., 1999) or stacking faults on the individual plates.

Under the TEM the samples showed well developed stacking faults, evidence of twinning and polycrystallinity. The individual plates were often offset with fractured or corroded margins. Fine scaled etching of grain surfaces (<1 μm) could represent the removal of individual crystallites (Langenhorst et al., 1999) or the expression of polycrystalline textures.

6. Skeletal structure diamonds were only observed under the TEM and were smaller in size (<5-20 μm) than the apographitic diamonds. Structurally these diamonds were predominantly polycrystalline aggregates of cubic diamond with pronounced preferred orientations. The preferred orientation of individual crystallites along the long axis of the grains suggests growth in a preferred direction possibly perpendicular to the principal stress direction. Individual needle-like protrusions from these grains were < 10 nm thick, suggesting individual crystallites of < 10 nm thickness. Skeletal diamonds were observed in the OQS, OQGB, SBS and NC384.

7. Skeletal structures observed in NC384 were distinct in morphology from skeletal grains with a preferred orientation. These skeletal grains appear to represent layered apo-graphitic diamond-graphite intergrowths.

It has been suggested that extensive corrosion and etching of apographitic diamonds within melts could produce diamonds with skeletal morphologies from apographitic diamond (Langenhorst et al., 1999). This appears to be the case for the skeletal structures observed in NC384 but not the distinctive skeletal diamonds from the fallout suevites and glass. These skeletal grains do not show any apparent remnant graphitic structures or morphologies, rather they represent fine-grained (1-20 nm) crystallites with a pronounced preferred orientation. Preferred orientations have been observed in impact diamond, lonsdaleite and graphite in the ALHA77283 and Canon Diablo meteorites (Clarke et al., 1981) and impact diamonds from Kara (Gurov et al., 1995).

The conditions suggested for the production of skeletal diamonds as a result of extensive corrosion and etching within impact melts (Langenhorst et al., 1999) can be estimated to be between 1700-3000 °C, at shock stage IV -V. Diamond rapidly graphitises at temperatures 1000-2000 K and the preservation of impact diamonds requires rapid cooling to ≤ 1000 K (De Carli, 1995). Graphitisation and the removal of these graphite or amorphous carbon coatings is suggested to result in skeletal structures. As indicated the skeletal grains preserve no apographitic structures unlike the heavily etched grains from the 384 m section of the N-73 core.

8. The morphology of the diamond found in the Ries crater samples suggests that at least three possible mechanisms have been involved in the formation of the observed diamonds. The larger (≤ 300 mm) platy, apographitic diamonds most likely formed from a direct phase transformation from graphite. With the rarer skeletal diamonds forming from either a vapour phase deposition mechanism or the incomplete transformation of a mixture of poorly graphitised and graphitic carbon within an orientated stress field.

These morphological observations support the idea that the very complexity of carbon chemistry and impact related chemistry is such that a single mechanism for diamond formation is unlikely. The readiness with which carbon materials of all types can be converted into diamond supports this idea. The distribution of shock metamorphic conditions within the Ries crater that have been documented in detail in the literature indicate that the conditions for the various mechanisms of diamond formation clearly exist. The formation of other allotropes of carbon such as graphite, carbynes, fullerenes and carbon minerals such as silicon carbide are also possible. Restricting the formation of impact diamonds to a purely martensitic solid-state transformation (Langenhorst et al., 1999) ignores the various mechanisms by which diamonds have been produced (De Carli, 1967; 1979; De Carli and Jamieson, 1961) as well as suggested mechanisms, intermediary phases (Chomenko et al., 1975; Heimann, 1999) and chemical vapour deposition (Frencklach et al., 1989; Buerki and Leutwyler, 1991a; 1991b; Howard et al., 1990).

9. The whole-rock bulk stable carbon isotopic compositions of the fallout and fallback suevites, shocked gneiss, basement rocks and individual components extracted from these lithologies suggest compositions derived from the admixture of different proportions of carbonate and graphitic carbon. The correlation between ^{13}C enrichment and carbon contents indicates that between 500 and 2000 ppm of carbon in the impactites is composed of graphite. Additional carbon is derived from carbonate-bearing sedimentary cover rocks. The SBS is enriched in ^{13}C compared to the OQS and this is attributed to a higher proportion of sedimentary and carbonate rocks derived from shallow levels in the target stratigraphy.

The N-1973 drill core samples are depleted in ^{13}C compared to the fallout suevites and contain a lower concentration of carbon suggesting that the carbon within these suevites was predominantly derived from graphite-bearing basement rocks. Variations in the carbon content and $\delta^{13}C$ can be attributed to pervasive calcite cements.

10. Stepped combustion combined with static mass spectrometry analyses of acid demineralised residues and extracted graphite, diamonds and SiC indicate that the primary carbon source for the diamonds was graphite. The $\delta^{13}C$ composition of graphite from these samples is depleted in ^{13}C compared to graphite analyses from Popigai impact crater (Masaitis, 1992; Shelkov, 1997), indicating that the graphite in the Ries is either less mature and therefore possibly less crystalline or has undergone less isotopic exchange with carbonate minerals within the basement rocks.

The $\delta^{13}C$ values of individual diamonds extracted from the residues range from -26.6 to -26.9 ‰. These compositions lie to the ^{13}C-depleted end of the range of graphite $\delta^{13}C$ compositions (-19.9 to -26.6‰). The bulk residue analyses encompass a $\delta^{13}C$ range from -17.0 to -26.5 ‰ again lying within and slightly beyond the range of graphite $\delta^{13}C$ compositions. The ^{13}C-enriched graphite analyses (-19.9 ‰) was from the SBS which also yields ^{13}C-enriched bulk measurements suggesting a greater carbonate component and a contribution from ^{13}C-enriched graphite relative to the other samples. This is complicated by the ^{13}C-enriched bulk $\delta^{13}C$ results for NC494 (-17.9 ‰). Graphite extracted from NC494 is ^{13}C-depleted suggesting that this suevite contains either a higher proportion of carbonate material derived from shallow levels in the basement or a greater proportion of post formation calcite cement. This section of the core (NC494) is part of a unit of suevite believed to comprise a fallout deposit that settled directly into the crater cavity in contrast to slumped material (NC343 and NC384) from the inner crater rim (Stöffler, 1977).

11. The concentration of diamond in the Ries crater impactites can be estimated from the carbon yield of the residues and original sample mass. The concentrations range from 0.1-1.7 ppm, with graphite-diamond transformation ratios varying between 500:1 and 1000:1. This can be attributed to the heterogeneous distribution of shock metamorphic pressures and temperatures experienced by the target rocks. In addition these ratios suggest that the mechanisms involved do not result in complete graphite transformation.

6.2. THE GARDNOS CRATER.

1. Impactites from the Gardnos structure are characterised by elevated carbon contents relative to the pre-impact target rocks (French et al., 1997). The mineralogic composition of this amorphous carbon was not determined by French et al., (1997) and was therefore investigated during this study. All of the samples investigated were found to contain graphitic carbon distinguished under the TEM by characteristic SAED patterns. In addition the evidence strongly suggests that the two suevite samples and one black matrix breccia contain small (0.4-5 μm) apographitic diamonds.

2. The diamonds were detected within suevite and a black matrix lithic breccia using transmission electron microscopy and selected area electron diffraction. The small size of these diamonds (≤ 0.7-5 μm) when observed under the TEM and the fine-grained nature of the residues under the petrological microscope was distinctive when compared to residues from the Ries crater which were much coarser.

3. The diamonds displayed strong hexagonal, platy morphologies and stacking faults. The small grain size prevented clear observation of the structures.

4. The $\delta^{13}C$ isotopic composition of the whole-rock Gardnos samples ranges from -28.1 to -31.5 ‰ (Koeberl et al., 1997) a slightly wider range than observed in the residues used in this study -28.9 to -29.6 ‰. The diamond fractions from the stepped combustion profiles (> 600 °C) have $\delta^{13}C$ values ranging from -24 to -32.5 ‰ which lie outside the range of compositions for the whole-rock analyses. This apparently suggests the incorporation of both ^{13}C-enriched and ^{13}C-depleted components that have not yet been identified.

5. This study has identified graphitic carbon within the shocked Gardnos impactites as well as within off structure unshocked shales (this study) which were proposed as potential carbon sources by French et al. (1997). The target rocks have experienced two

episodes of metamorphism, firstly between 1500-1700 Ma and secondly following the impact at 380-400 Ma (Naterstad and Dons, 1994). Both of these episodes could have resulted in the formation of crystalline graphite from pre-existing organic matter. It is known that certain forms of organic material, e.g. aromatic structures with hexagonal benzene ring structures, greatly affect the ease of graphitisation and degree of structural order attained compared to other forms (Buseck and Huang, 1985).

Graphitisation of poorly crystalline and amorphous carbonaceous material can also be achieved during shock metamorphism, as shock experiments producing diamond and crystalline graphite indicate (Hirai et al., 1995). Shock graphitisation should produce material inheriting the structure of the precursor carbon or very fine grained material.

The evidence suggests that graphite was produced from organic material during both periods of regional metamorphism. The polycrystalline textures due to shock comminution may have been produced by the impact and preserved in crystalline graphite. The degree of crystallinity within the graphite was probably increased by the impact event and subsequent Caledonian metamorphism.

6. The shock conditions (P/T) experienced by the Gardnos impactites during the impact event range from 1-80 Gpa and 0-3000 °C with the majority of the impactites experiencing low degrees of shock. These conditions lie within the field for diamond stability as well as those required for the suggested diamond formation processes.

From the TEM/SAED analysis the graphite within these samples is well crystallised. This crystalline maturity may have been enhanced by greenschist facies metamorphism during the Caledonian orogeny (400 Ma) and it is difficult to determine the original carbon composition at the time of impact. The structures of the diamonds that were seen under the TEM were strongly apographitic, displaying layering parallel to the basal plane and pseudo-hexagonal to hexagonal morphologies. This indicates that the carbon available for shock transformation was graphitic. In addition, shock metamorphism by the impact event may have resulted in the graphitisation of poorly

crystalline, almost amorphous, carbon material. Shock metamorphism of pre-existing graphitic carbon may also produce structural features such as polycrystallinity.

7. When compared with the Ries crater samples, the Gardnos impactites contain significantly more black amorphous and graphitic carbon. The concentration of diamond appears to be significantly less than that of the Ries crater, which may be a reflection of the fine grained nature of the material or connected with the size of the crater itself. Though there is no clear correlation between the distribution and size of impact diamonds and the size of the crater that they are associated with.

6.3. FURTHER WORK.

1. High resolution transmission electron microscope (HRTEM) analyses of the diamonds from the Ries and Gardnos impact craters is required in order to determine the nature of the observed stacking fault and twinning structures. Identification of structures characteristic of graphite, growth or deformation would enable the determination of the predominant formation mechanisms.

2. Further transmission electron microscope analyses of Ries crater impactites with the aim of identifying carbynes and other carbon polymorphs including the diamond polymorphs such as 4H and 6H.

3. Transmission electron microscope analyses of graphitic carbon to identify the degree of crystalline maturity.

4. The selection of further diamonds and if possible SiC from the Ries crater impactites for analysis using SEM and stepped combustion combined with static mass spectrometry.

5. In-situ observation of impact diamonds in shocked graphite bearing basement samples.

6. Gas chromatography mass spectrometry and solvent extraction analyses of HF:HCl demineralised Gardnos impactites is required in order to identify the composition of amorphous and organic carbon material. Although graphitic carbon has been identified using the TEM the majority of the carbon material is poorly crystalline and amorphous.

7. Further stepped combustion combined with static mass spectrometry analyses of Gardnos impactites in order to confirm the results presented here and characterise the remaining samples.

APPENDIX. 1. SOLUTIONS.

1. Preparation of dilute hydrocloric acid for carbonate digestion.

Reagents. Hydrochloric acid 37%.

Apparatus. 2 x 250 ml glass measuring cylinders.

- 500 ml glass reagent bottle or 250 ml polyproylene wash bottle.

Procedure for the preparation of 250ml of desired molarity.

In a fume cupboard.

1. Measure out required amount of HCl, see table into a glass measuring cyclinder (Table1.1)
2. Measure out required ammount of distilled water into a separate cylinder.
3. Pour the water into a reagent bottle.
4. Add the HCl to the water.

Table 1.1. Dilution measurements for HCl.

Molarity	ml HCl	ml H_2O
1	21	229
2	42	208
3	63	187
4	83	167
5	104	146
6	125	125
7	146	104
8	167	83
9	187	63
10	208	42
11	229	21

2. Preparation of hydrofloric acid/hydrochloric acid for silicate digestion.

Reagents. Hydrofluoric acid (48 %).

Hydrochloric acid (37 %).

Apparatus. 500 ml polypropylene measuring cylinder.

50 ml glass measuring cylinder.

500 ml non-drip polypropylene reagent bottle.

Procedure to make 500 ml of 10M HF/1M HCl.

Prepare in fumecupboard.

1. Measure 173 ml of HF into a 500 ml polypropylene measuring cylinder.

2. Measure 42 ml of HCl into a glass measuring cylinder.

3. Add the HCl to the HF.

4. Pour 285 ml of distilled water into a polypropylene reagent bottle with a non-drip dispensing system.

5. Add the HF/HCl mixture to the water in the reagent bottle, replace the cap and swirl gently to mix. Allow to cool.

3. Preparation of chromic acid.

Reagents. Sulphuric acid (conc).

Sodium dichromate.

Apparatus. 500 ml beaker.

50 ml glass measuring cylinder.

500 ml polypropylene measuring cylinder.

Teflon rod.

Procedure to make 500 ml of chromic acid.

In a fume cupboard.

1. Measure 49 ml of sulphuric acid into a 50 ml glass measuring cylinder.

2. Measure 451 ml of distilled water into a 500 ml polypropylene measuring cylinder.

3. Pour water into 500ml glass beaker and add 49 ml of sulphuric acid.

4. Weigh 19.5 g of sodium dichromate and slowly add to acid mixture in beaker whilst stiring constantly. Mixture will generate heat.

5. Allow to cool, do not use hot.

4. Preparation of pentane slush.

Reagents. Pentane

Liquid nitrogen

Apparatus. 250 ml dewar.

500 ml dewar.

Glass stirring rod.

Procedure.

In fume cupboard.

1. Add 15-20 ml of pentane to a 250 ml dewar.

2. Slowly add liquid nitrogen and stir with glass rod.

3. Continue until white fuming ceases and mixture begins to freeze. Mix well to form a stiff mush.

4. Cover with aluminum foil and store in fume cupboard when not required, add more liquid nitrogen when required.

APPENDIX 2. EXAMPLE ACID DIGESTION - ÖTTING QUARRY GLASS BOMB.

14/12/1995	Glass crushed to a granular powder using clean, baked agate mortar and pestle. Care taken to remove cream/white suevite coating on margin of bomb. Weighed out approximately 150 g. Average of 4 = 149.745 g using electronic balance. Transferred quantitatively to Teflon bomb. Dilute HCl (0.2 M) added slowly, until bubbling subsides and filled. Bomb placed on hotplate at 70 °C.
15/12/1995	Drained, filled 6M HCl and placed on hotplate. Poor reaction to dilute acid, indicates low carbonate content.
8/01/1996	HCl drained, replaced with distilled water (H_2O). Allowed to settle and fresh H_2O added.
9/01/1996	H_20 drained. HF:HCl added. Placed on hotplate (70 °C).
11/01/1996	Samples checked and agitated. After reaction HF:HCl samples drained and replaced with fresh HF:HCl.
12/01/1996	Sample agitated. Placed on Hotplate (70 °C).
15/01/1996	Sample drained after cooled. H_20 added. Allowed to settle. Drained. HF:HCl added and placed on hotplate (70 °C). No evidence grey fluorites.
16/01/1996	Drained. H_20 added. Gel-like deposit forming between glass and acid - silica?. Sample allowed to settle. Drained refilled with H_20. Acid was becoming yellow = reacted.
17/01/1996	Sample drained, filled H_20 and allowed to settle. Drained again. Gel-like substance gone. Re-filled with HF/HCl, placed on hotplate.
18/01/1996	Acid yellow in colour with gel-like substance on surface of sample. Drained and washed with H_20 twice. Drained and filled with 6M HCl, placed on hotplate (70 °C) overnight.
19/01/1996	Drained, filled fresh 6 M HCL, placed on hotplate.
22/01/1996	Drained. filled H_20. Allowed to settle and drained. Replaced with HF:HCl, placed on hotplate.
25/01/1996	Sample drained, filled H_20, allowed to settle. Drained and filled 6 M HCl, placed on hotplate.
26/01/1996	Drained, filled 6 M HCl, placed on hotplate.
29/01/1996	Drained, filled H_20, repeated.
30/01/1996	Drained, filled 6M HCl, placed on hotplate.
31/01/1996	Drained, filled d.H_20. Drained filled HF:HCl, placed on hotplate.
01/02/1996	Agitated, left on hotplate.
02/02/1996	Drained, filled H_20, placed on hotplate.
05/02/1996	Drained, filled H_20. Gel-like "silica" precipitate present at base of bomb. All black

	powdered sample gone, very little sample remains, hard to establish through cloudy precipitate. Drained, filled 6 M HCl and placed on hotplate. Developed strong yellow colour.
06/02/1996	Drained, filled H_20. Very little residue remains, No strong colour (i.e.: organics). Some colloidal Gel. Once settled drained and filled 6 M HCl and placed on hotplate.
07/02/1996	Drained, filled H_20,. Drained filled HF/HCl, placed on hotplate.
08/02/1996	Drained, filled H_20.
12/02/1996	Drained, transferred to glass petri-dish, evaporated dry.
13/02/1996.	Samples washed with H2O, x2, left to dry.
14/02/1996	When dried, studied under petrological microscope. Sample consists of zircon, graphite, and at least 2 diamonds c. 100-300 µm.
15/02/1996	Transferred to disposable plastic petri-dish, left to dry.
16/02/1996	Dry weight petri-dish (z=8) = 16.0973±0.0002 g. Petri-dish + residue (z=6) = 16.10842 g Residue = 11.12 mg Left over weekend to dry = 3.2 mg
17/06/1996	Residue washed with H_20, transferred to centrifuge vials. Centrifuged with H_20 repeatedly. Centrifuged with 6 M HCl, 2,500 rpm and drained. Washed with H_20 x2. Transferred to glass petri-dish. Checked under petrographic microscope.
	Chromic acid stage.
09/09/1996	Transferred to 15 ml Teflon bomb for chromic acid stage.
10/9/1996	Made up chromic acid, as per protocol sheet.
17/09/1996	Filled chromic acid, placed on hotplate.
02/10/1996	Acid changed.
06/11/1996	Drained, washed. After several weeks at 70-80 °C in chromic acid, sample appears unchanged, no change in acid colour.
	Fuming Perchloric acid stage
20/01/1997	Sample studied under petrographic microscope, cleaner, still a lot of zircon grains and possibly polycrystalline graphite/graphite coated diamond clusters. Photographed. Samples transferred from glass petri-dish to 15 ml Teflon bomb for fuming perchloric and Conc HF (150 °C) stages, along with a number of other samples.
21/01/1997	Samples drained of H_20, left damp and a few drops of $HClO_4$ added. Following protocol outlined in chapter 2 section samples were heated at 100-150 °C until fumed dry. 4-5 hours. [power cut].
22/01/1997	Re- application of $HClO_4$, fumed 5-6 hours.

23/01/1997	Samples drained and washed with H_20.
27/01/1997	Samples washed H_20.
Conc HF stage- High pressure bombs.	
01/09/1997	Several samples were transferred to high pressure metal bombs. Ötting Quarry Glass bomb sample 2 was treated and sample 1 retained in case of problems. The samples were covered in Conc HF, 6 M HCl and a few drops of HNO_3.
05/09/1997	Samples in oven at 180 °C.
12/0901997	3 samples removed, including Ötting quarry glass bomb. Allowed to cool.
19/09/1997	Removed from bomb casings, drained and transferred to washed 15 ml Teflon bombs.
22/09/1997	Samples drained and filled with H2O, repeated x4.
26/09/1997	Samples transferred to clean, dry glass petri-dishes and left to dry in fume cupboard. Pipettes flushed with H_2O into matching sample petri-dish.
01/10/1997	Samples observed under petrological microscope.

APPENDIX 3. TRANSMISSION ELECTRON MICROSCOPE BRIGHTFIELD AND SELECTED AREA ELECTRON DIFFRACTION IMAGES.

27/06/97 Ötting quarry glass bomb residue.

Number	Comments noted
1	Carbon grain.
2	SAED 4 sec.
3	SAED 8 sec.
4	Large carbon crystal with needle like extensions.
5	Large carbon crystal showing constructive interference.
6	
7	SAED
8	SAED
9	SAED
10	SAED
11	SAED
12	Constructive interference near thin margins, centre too thick
13	Constructive interference near thin margins, centre too thick
14	Constructive interference near thin margins, centre too thick
15	Constructive interference near thin margins, centre too thick
16	Bottom right of crystal - cross-hatched stacking faults
17	SAED 4 sec
18	SAED 8 sec
19	Needle like projection left side
20	Pic
21	SAED - polycrystalline
22	SAED
23	Needle-like crystals
24	SAED 4 sec
25	SAED 8 sec
26	SAED 4 sec
27	SAED 8 sec
28	Pic
29	Large crystal with constructive interference
30	SAED 2 sec
31	SAED 4 sec
32	SAED 8 sec
33	Platy layered carbon grain
34	SAED 4 sec
35	SAED 8 sec
36	SAED 4 sec
37	SAED 8 sec
38	Top right side of small layered carbon crystal
39	SAED 4 sec
40	SAED 8sec
41	SAED 4 sec
42	SAED 8 sec
43	Pic
44	SAED 4 sec

45	SAED 8 sec
46	Platy carbon crystal
47	Platy carbon crystal
48	SAED 2 sec polycrystalline

03/11/97. Nördlingen core 384 m section residue.

Number	Comments noted
1-14	large fibrous carbon grain
15	Skeletal needle like grain
16	Skeletal needle like grain
17	Skeletal needle like grain
18	SAED 2 sec
19	SAED 4 sec
20	SAED 8 sec
21	Large fibrous carbon grain
22	Large fibrous carbon grain
23	SAED 4 sec
24	Large fibrous and fractured carbon grain
25	SAED 4 sec
26	SAED 8 sec
27	
28	Needle like crystal layrs
29	SAED tip of needle
30	SAED
31	Large carbon grain
32	Large carbon grain
33	Large carbon grain
34	Needle like crystal
35	Rectangular fibrous crystal
36	Pic
37	SAED
38	SAED
39	Thinner carbon crystal with constructive interference
40	Pic of same
41	SAED
42	Pic of whole crystal
43	Skeletal polycrystalline crystal
44	SAED - skeletal area
45	SAED
46	SAED - Polycrystalline area
47	SAED
48	layered and fractured carbon grain
49	SAED
50	SAED
51	Pic needle like elongate grain
52	SAED
53	SAED
54	SAED
55	SAED

05/12/97. Seelbronn suevite residue.

Number	Comments noted
1	SAED
2	Polycrystalline carbon grain
	Carbon grain with short fat stacking faults
3	SAED 2 sec
4	SAED 4 sec
5	SAED 8 sec
6	Thin large playty grain- constructive interference, and SF
7	
8	Pic
9	
10	SAED 8 sec
11	SAED 4 sec
12	SAED 2 sec
13	Irregular layered grain, SF. SAED 2 sec
14	SAED 4 sec
15	Elongate fractured grain. SAED 4 sec
16	Platy elongate carbon grain, SF. SAED 4 sec
17	SAED 2 sec
18	
19	
20	Pic
21	Long thin fibrous carbon grain, SF
22	SAED 2 sec
23	SAED 4 sec - faint inner spots (graphite)
24	SAED 2 sec
25	Pic
26	Needle like carbon grains. SAED 2 sec
27	SAED 4 sec
28	Pic
29	Thin irregular carbon grain SAED 4 sec
30	SAED 2 sec
31	Pic
32	large fractured layered carbon grain. SAED 8 sec
33	SAED 4 sec
34	Pic
35	Pic

05/12/97. Nördlingen core 384 m section residue.

Number	Comments noted
37	large layered crystal, some SF. SAED 4 sec
38	Fibrous and fractured
39	layered grain with SF. SAED 4 sec - graphite
40	SAED 2 sec
41	Fractured carbon grain with SF
42	SAED 2 sec - diamond
43	SAED 4 sec
44	Pic
45	Large carbon grain strong SF
46	Sf
47	SAED 2 sec
48	SAED 2 sec
49	SAED 2 sec
50	Pic

10/12/97. Nördlingen core 494 m section residue.

Number	Comments noted (mislabled 1 = 16)
1 (16)	large opaque carbon grain SAED 2 sec
2 (17)	SAED 2 sec
3	Overall pic
4	Closeup pic
5	SAED 2 sec
6	Smaller opaque carbon grain SAED 2 sec
7	Pic
8	Pic
9	SAED 2 sec
10	Small carbon grain SAED 2 sec
11	Pic layered, platy needle like extensions
18	SAED 2 sec
19	Elongate carbon grain fractured
20	Elongate metal silicate grain
21	SAED 2 sec
22	Rectangular carbon grain SAED 2 sec
23	Close-up pic
24	Pic
25	Large carbon grain
26	SAED
27	Pic
28	Large carbon grain SAED 2 sec
29	Pic etched opqaque carbon grain
30	SAED 2 sec
31	SAED 2 sec
32	Small carbon grain SAED 2 sec
33	SAED 2 sec
34	Closeup pic etched platy carbon grain with SF
35	SAED 2 sec - faint graphite - diamond
36	Irregular carbon grain SAED 2 sec - diamond
37	Pic etched blocky
38	Large carbon grain (no. 28). SAED 2 sec

39	Pic
40	SAED 2 sec

10/12/97. Nördlingen core 384 m section residue.

Number	Comments noted
12	Elongate carbon grain with SF
13	Pic
14	SAED 2 sec
15	Pic
16	SAED 2 sec
17	Pic
41 (52)	Small elongate irregular grain, SF SAED 2 sec
42	Pic elongate fractured carbon grain
43	Close-up pic SF
44	SAED 2 sec
45	Small cluster of lath like crystals Pic
46	Pic
47	SAED 2 sec
48	SAED 2 sec
49	Elongate carbon lath SAED 2 sec
50	Pic
51	large carbon grain similar to 494 m layered, etched faint SF SAED 2 sec
52	SAED 2 sec
53	Pic
54	PIc

12/12/98. Seelbronn suevite residue.

Number	Comments noted
1	Etched carbon grain
2	Poor resolution carbon grain
3	SAED 2 sec polycrystalline faint graphite
4	Better focus pic (2) SF
5	Overall grain
6	Platy carbon grain, needle like extensions, SF
7	SAED 2 sec - overexposed
8	SAED 2 sec
9	Polycrystalline cluster
10	SAED 2 sec
11	SAED 2 sec
12	SAED 2 sec
13 (14)	Skeletal blocky grain
14 (15)	Closeup pic
15 (16)	SAED 2 sec
16 (17)	Skeletal grain SAED 2 sec

15/01/98. Ötting quarry glass bomb residue.

Number	Comments noted
1	Large graphitic carbon grain
2	SAED 2 sec - graphite
3	Pic
4	Pic
5	SAED
6	Irregular carbon grain needle like areas, SF
7	SAED mainly diamond very faint graphite
8	Close-up SF
9	Pic
10	SAED
11	Pic
12	Small hexagonal layered grain. SAED - kikuchi like lines
13	Pic o/all grain
14	SAED
15	large crystal, SF and needle-like extensions
16	Close-up SF
17	SAED
18	Cluster fine grained needles (Ca + Mg)
19	Very thin carbon sheet, SF, Kikuchi. SAED
20	pic
21	Elongate layered carbon grain, SF. SAED
22	Pic
23	Overall grain
24	SAED
25	SAED
26	Thin carbon platy grain, SF
27	SAED - diamond
28	Blocky layered grain SF SAED
29	Pic
30	Closeup SF

19/03/98. Nördlingen core 343 m residue.

Number	Comments noted
1 (0)	SAED diamond
2 (1)	Rectangular platy grain, SF, multiple layers
3	Pic
4	Closeup pic
5	Skeletal grain, needle like edges, thick interior. SAED
6	Pic overall grain
7	closeup pic
8	SAED
9	large layered grain, needle like extensions pic top right
10	Pic top left
11	pic bottom left
12	pic bottom right
13	Pic closeup
14	Centre
15	SAED
16	Small skeletal carbon grain

17	SAED
18	Layered carbon grain. SAED possible twinning
19	closeup pic
20	Overall pic
21	Skeletal etched carbon grain. SAED
22	Pic
23	large skeletal grain. SAED
24	SAED
25	Pic
26	Twinned carbon grain SAED
27	Pic

24/03/98. Seelbronn suevite residue.

Number	Comments noted
1	Polycrystalline carbon cluster SAED - graphite
2	Pic
3	Pic
4	Cloudy grain some clear SF and layering
5	Overall pic
6	Closeup SF
7	SAED - diamond polycrystalline
8	large grain, kikuchi, twin (?), needle like margins
9	Close-up pic
10	SAED
11	SAED
12	Skeletal elongate etched grain
13	Skeletal grain
14	close-up
15	SAED - diamond
16	SAED
17	Skeletal grain
18	close-up
19	c;lose-up

24/03/98. Nördlingen 343 m section residue.

Number	Comments noted
20	Metallic dark opaque grain SAED
21	Pic
22	Small grain SAED - diamond
23	Pic
25	Platy grain needle like projections
25	SAED
26	Skeletal elongate grain, polycrystalline. SAED
27	Pic
28	Opaque grain SAED
29	Large layered grain, needle like fringes, fibrous. SAED
30	Pic

22/04/98. Ötting quarry suevite residue.

Number	Comments noted
1	Skeletal grain
2	SAED 2 sec
3	Pic as 1
4	SAED 4 sec
5	Overall pic of carbon grain, SF
6	SAED (on SF)
7	Closeup pic
8	SAED of 9
9	Overall pic grain
10	Close-up pic
11	SAED
12	Skeletal polycrystalline grain
13	Pic
14	SAED
15	Pic
16	Large carbon grain - SAED
17	Pic
18	Skeletal carbon grain
19	SAED
20	Pic

30/05/98. Bunte breccia residue.

Number	Comments noted
1	Hexagonal graphitic structure carbon grain
2	SAED - diamond
3	Pic
4	Pic elongate rutile?
5	Platy carbon grain SAED
6	Pic

30/05/98. Nördlingen core 384 m residue.

Number	Comments noted
7	Skeletal grain with faint SF
8	SAED - diamond
9	Blocky fractured carbon grain
10	Etched structure with SF
11	SAED
12	SAED
13	Close-up pic
14	Small grain. SAED
15	Elongate fractured grain. SF
16	Close-up image
17	SAED - diamond

Polsingen impact melt rock.

Number	Comments noted
6	Layered grain, SF. SAED
7	Pic
8	Large grain SF/skeletal
9	close-up pic SF
10	SAED
11	overall pic
12	Carbon grain with SF. SAED
13	Pic
14	pic
15	Overall- pic

Aumühle Gneiss

Number	Comments noted
16	Elongate layered grain with faint SF. SAED
17	Pic
18	Pic
19	SAED - 2 plates, diamond
20	SAED
21	Pic close-up
22	Blocky carbon grain. SAED
23	pic

11/05/99. Gardnos 137 residue.

Number	Comments noted
1	Hexagonal graphitic structure platy grain. SAED
2	Pic
3	PIc
4	Similar grain. SAED
5	pic
6	pic
7	SAED, faint kikuchi lines
8	SAED
9	SAED
10	Pic
11	SAED
12	pic

11/05/99. Gardnos 164.

Number	Comments noted
13	SAED - 2.06
14	PIc
23	SAED - 2.06
24	Pic
25	SAED - 2.06, 3.34
26	Pic
27	PIc

11/05/99. Gardnos 133.

Number	Comments noted
15	SAED - 2.06, 3.34
16	Pic
17	SAED - 2.06
18	Pic
19	SAED - 2.06
20	Pic
21	SAED - 2.06
22	Pic

13/05/99. Gardnos 178 residue.

Number	Comments noted
1	SAED - 2.06
2	Pic
3	Hexagonal platy grain. SAED - 2.06 minor graphite
4	Pic
5	SAED
6	SAED

22/06/99. Gardnos 137 residue.

Number	Comments noted
1	Irregular layered carbon grain. SAED
2	SAED
3	Pic
4	SAED
5	Layered graphitic structure grain. SAED
6	Pic
7	Very small pseudo-hexagonal grain 2-3 layers. SAED
8	Pic
9	Possible rutile. SAED
10	Pic
11	Elongate, layered grain with SF. SAED
12	SAED
13	Pic
14	Pic

22/06/99. Gardnos 169 residue.

Number	Comments noted
15	Triangular layered grain SF
16	SAED
17	SAED
18	Pic
19	SAED
20	Pic

22/06/99. Gardnos 178 residue.

Number	Comments noted
21	SAED
22	Pic
23	Elongate, SF and cross-hatching (layers)
24	SAED
25	SAED
26	SAED
27	Pic
28	Very large polycrystalline grain. SAED - diamond
29	Pic overall grain
30	Pic close-up
31	SAED - coarsely polycrystalline diamond
32	Rounded low relief grain. SAED

07/07/99. Gardnos 178 residue.

Number	Comments noted
3	Pic platy grain SF
4	Pic close-up
5	SAED
6	Pic large grain dense SF layered
7	SAED
8	Pic hexagonal platy layered grain
9	Pic etched and corroded grain
10	SAED
11	Pic elongate layered grain
12	SAED

APPENDIX 4. WHOLE ROCK CARBON STABLE ISOTOPES.

4.1. Table of bulk $\delta^{13}C$ stable isotopic ratios for whole rock Ries crater samples.

All sample bulk analyses dynamic mass spectrometer (SIRA).

Sample	$\delta^{13}C$ (PDB)	%Carbon
Otting Quarry Suevite		
Glass (bomb)	-28.072	0.038
Glass (bomb)	-27.909	0.020
Glass	-15.110	0.152
Glass	-15.089	0.117
Glass	-12.265	0.410
Glass	-13.144	0.317
Whole Rock	-11.902	1.573
Lithic (basement)	-20.945	0.368
Lithic (sedimentary)	-11.847	4.067
Lithic (sedimentary)	-11.529	1.154
Lithic (sedimentary	-10.445	3.505
Seelbronn Suevite		
Whole rock	-7.890	3.880
Whole rock	-7.752	3.630
Glass	-10.625	0.722
Lithic (basement)	-8.191	0.287
Lithic (sedimentary)	1.950	2.490
Lithic (sedimentary)	2.384	2.939
Lithic (sedimentary)	-9.198	2.944
Nördlingen Core		
Nördlingen Core 1059	-13.987	0.121
Nördlingen Core 494	-18.229	0.130
Nördlingen Core 384	-13.941	0.430
Nördlingen Core 343	-15.387	0.406
Others		
Itzingen Quarry	-25.032	0.024
Bunte Breccia	-10.066	1.893

APPENDIX 5. STEPPED COMBUSTION COMBINED WITH STATIC MASS SPECTROMETRY.

5.1. MS319. Ötting quarry suevite residue.

T (°C)	C (ng)	$\delta^{13}C$ (‰)	±s (‰)
200	118.89	-29.19	0.47
500	762.23	-25.18	0.45
600	38.87	-15.29	0.41
700	5699.35	-22.01	0.31
800	13.65	-18.09	0.39
900	41.29	-23.69	0.45
1200	8.71	-25.89	0.39

5.2. MS343. Ötting quarry suevite SiC.

T (°C)	C (ng)	$\delta^{13}C$ (‰)	±s (‰)
200	112	-28.4	0.4
400	787	-25	0.4
600	186	-24.8	0.3
800	260	-19	1.2
1000	18.1	-25	0.1
1200	21.4	-25.6	0.4
1300	32.6	-27.4	0.2

5.3. MS355. Ötting quarry glass bomb. Diamond.

T (°C)	C (ng)	$\delta^{13}C$ (‰)	±s (‰)
200	33.4	-28	1
300	30.9	-26.8	0.3
400	20.9	-24.9	0
500	10.3	-25.6	0.5
550	3.74	-25.8	0.3
600	7.2	-28.8	0.2
650	24	-26.9	0.2
700	22	-25.5	0.4
750	68.5	-26.5	0.6
800	691	-26.4	0.1
850	808	-26.7	0.1

900	10.3	-31.1	0.4
950	2.27	-27.4	0.5
1000	1.52	-26.3	0.4
1200	7.6	-28.8	0.5

5.4. Ötting quarry glass bomb. Graphite. 1.

T (°C)	C (ng)	$\delta^{13}C$ (‰)	±s (‰)
400	1002.18	-26.55	0.25
800	2605.86	-26.8	0.5
1200	2166.88	-27.95	0.15

5.5. MS344. Ötting quarry glass bomb graphite. 2.

T (°C)	C (ng)	$\delta^{13}C$ (‰)	±s (‰)
200	169	0	0
250	46.2	0	0
300	46.2	0	0
350	54.2	-26.2	0.1
400	376	-27.8	0.4
450	37	-27.1	0.3
500	19.4	-28.2	1.1
550	15.6	-24	1.1
600	10.7	-31.2	0.5
650	13.1	-28.5	0.1
700	8163	-25.1	0
800	115	-24	0
850	55.3	-23.9	1.1
900	35.9	-24.3	0.8
1000	31.7	-25.9	0.3
1100	18.3	-28.6	0.4
1200	27.6	-27	0.8

5.6. MS345. Ötting quarry Silicon carbide.

T (°C)	C (ng)	$\delta^{13}C$ (‰)	±s (‰)
200	112	-28.4	0.4
400	787	-25	0.4
600	186	-24.8	0.3
800	260	-19	1.2
1000	18.1	-25	0
1200	21.4	-25.6	0.4
1300	32.6	-27.4	0.2

5.7. MS345. Seelbronn quarry suevite graphite.

T (°C)	C (ng)	$\delta^{13}C$ (‰)	±s (‰)
200	81.58	-28.03	0.39
400	32.00	-31.73	0.39
500	106.05	-19.02	0.39
600	1127.81	-19.02	0.35
700	2.84	-25.2	0.61
800	7.57	-25.86	0.45
900	6.41	-24.39	0.43
1200	4.55	-24.14	0.45

5.8. MS318. Seelbronn quarry suevite residue.

T (°C)	C (ng)	$\delta^{13}C$ (‰)	±s (‰)
200	54	-27.6	0
300	56	-26.6	0.2
350	26.2	-26.5	0.1
400	23.2	-25.8	0.2
450	18.2	-25.4	0.4
500	12.5	-26.6	0.1
550	14.4	-21.7	0.4
600	43	-18.4	0.3
650	193	-17.8	0.5
700	368	-16.7	0.3
750	1010	-16.8	0.2

800	3260	-16.7	0.5
850	6846	-16.6	0.2
900	6893	-17.2	0.1
950	562	-17.4	0.4
1000	7.81	-21.3	0.3
1100	4.48	-22.9	0.3
1200	4.67	-23.6	0.3

5.9. MS 276. Nördlingen core 343. Residue.

T (°C)	C (ng)	$\delta^{13}C$ (‰)	±s (‰)
200	181.2	-27.46	0.14
600	1601.7	-26.6	0.16
650	3155.34	-26.96	0.17
700	3911	-26.2	0.17
800	251.63	-26.23	0.18
900	3.9	-12.26	0.25
1200	3.8	-24.66	0.20

5.10. MS267. Nördlingen core residue 384.

T (°C)	C (ng)	$\delta^{13}C$ (‰)	±s (‰)
200	94.69	-26.08	0.21
300	109.2	-25.6	0.23
400	1.34	-27.87	0.25
500	98.81	-25.2	0.2
600	429.24	-25.7	0.18
700	4053.2	-25.14	0.18
800	935.12	-26.25	0.21
900	10.51	-24.58	0.21
1000	2.48	-26.02	0.23
1200	4.23	-25.62	0.21

5.11. MS293. Nördlingen core 384. Diamond.

T (°C)	C (ng)	$\delta^{13}C$ (‰)	±s (‰)
200	71.82	-27.99	0.17
400	117.3	-23.46	0.2
500	26.67	-22.5	0.22
550	8.19	-24.24	0.21
600	28.23	-23.1	0.22
625	81.08	-24.67	0.22
650	126.43	-26.98	0.19
675	95.85	-26.62	0.18
700	874.7	-26.78	0.19
800	1177.3	-26.44	0.23
900	4129	-27.29	0.21
1200	1.55	-30.68	0.34

5.12. Nördlingen core 494 residue.

T (°C)	C (ng)	$\delta^{13}C$ (‰)	±s (‰)
200	3.604	-21.87	0.51
400	70.82	-29.68	0.48
500	10.84	-21.71	0.46
600	369.67	-19.23	0.48
700	2.86	-14.74	0.52
800	434.51	-22.64	0.68
900	577.10	-11.9	0.52
1000	819.0	-17.92	0.5
1200	0.02	-48.07	2.75

5.13. MS346. Nördlingen core 494 graphite. 1.

T (°C)	C (ng)	$\delta^{13}C$ (‰)	±s (‰)
400	84.6	-26.6	0.3
600	11535	-26.2	0.6
700	471	-25.4	0.4
800	233	-26	0.5
1000	149	-26	0.6
1200	142	-26.2	0.4

5.14. MS347. Nördlingen core 494 graphite. 2.

T (°C)	C (ng)	$\delta^{13}C$ (‰)	±s (‰)
400	2746	-27.4	0.6
500	4371	-25.4	0.4
600	2961	-25.4	0.4
800	160	-26.2	0.6
1200	130	-26.4	0.3

Non Ries samples.

5.15. MS323. Lappijarvi graphite.

T (°C)	C (ng)	δ (‰)	±s (‰)
200	223.39	-24.73	0.49
1000	787.72	-18.62	0.46
1200	9.79	-15.35	0.489

5.16. MS396. Gardnos 137. Pre-perchloric.

T (°C)	C (ng)	δ (‰)	±s (‰)
200	72	-29.91	0.5
300	202	-29.59	0.26
400	928	-30.50	0.28
450	881	-30.80	0.25
500	138	-30.81	0.26
550	47.46	-26.63	0.26
600	36.93	-25.22	0.25
650	46.07	-24.06	0.26
700	79.58	-24.01	0.3
750	100.15	-23.96	0.26
800	65.16	-24.23	0.28
900	28.4	-23.41	0.26
1200	20.13	-25.92	0.29

5.17. MS398. Gardnos 178. Perchloric.

T (°C)	C (ng)	δ (‰)	±s (‰)
200	119.17	-29.4	0.27
300	742	-28.55	0.26
350	955	-27.98	0.26
400	231.5	-29.94	0.27
450	312.35	-30.99	0.28
500	239.69	-31.32	0.27
550	78.10	-29.34	0.27
600	29.29	-26.61	0.26
650	87.32	-32.33	0.29
700	47.06	-27.71	0.28
750	6.61	-31.24	0.28
800	7.78	-22.53	0.28
900	7.33	-22.39	0.25
1200	9.24	-22.76	0.26

APPENDIX 6. GARDNOS CARBON AND SOOT CONCENTRATIONS.

Data from W. Wolbach and S. Widicus, IWU, 1997. (unpublished data).

Sample	Original rock mass (g)	Total C (ppm)	Error (ppm)	Soot (ppm)	Error (ppm)
Basement rocks (quartzites, shocked, fractured, black and carbon-bearing)					
129	2.35474	1200	500	550	520
143	2.03032	600	700	80	700
Basement rocks: Black shales (off structure, potential carbon sources, target rocks)					
164	2.56444	55000	1000	5100	800
169	2.25117	7200	700	5400	700
170	2.24192	4800	600	2900	600
171	2.42848	27000	2000	16000	2000
Gardnos crater: Gardnos lithic breccia (subcrater rocks)					
120	2.45246	3200	200	8	9
121	2.54749	1500	200	8	9
Gardnos crater: Black matrix lithic breccias.					
126	2.52514	21000	1000	1000	600
176	2.45272	930	470	30	430
178	2.46650	26000	1000	200	600
Gardnos crater: melt-bearing suevite breccias.					
133	2.37714	2100	100	30	40
137	2.26706	16000	1000	1100	100
175	2.50408	100	500	70	500
Gardnos crater: Melt matrix (impact melt) breccias.					
179	2.48521	480	30	140	20
Gardnos crater: Sedimentary fill above glassy breccias (black, carbon-bearing)					
160	2.38759	32000	2000	22000	2000

REFERENCES.

Abbott J. I., Hough R. M., Gilmour I. and Pillinger C. T. (1996). Impact diamonds in glass from Ötting quarry, Ries crater, Germany. *Meteoritics and Planetary Science*, **31**, A5.

Abbott J. I., Hough R. M, Gilmour I. and Pillinger C. T. (1998a). Carbon chemistry of suevites and target rocks at the Ries crater, Germany. *Meteoritics and Planetary Science*, **33**, A7.

Abbott J. I., Hough R. M., Gilmour I. and Pillinger C. T. (1998b). Nördlingen drill core 1973 - Diamonds and stable carbon isotopes from a selection of crater suevite samples. In: *Impacts and the Early Earth. European Space Foundation. 1st International Workshop of the Scientific Programme on Response of the Earth System to Impact Processes, December 13-15, Cambridge*, London.

Akizuki M. (1981). Investigation of phase-transition of natural ZnS minerals by high resolution electron-microscopy. *American Mineralogist*, **66**, 9-10, 1006-1012.

Alvarez L., Alvarez W., Asaro F. and Michel H. (1980). Extraterrestrial cause for the Cretaceous-Tertiary extinction. *Science*, **208**, 1095-1108.

Alvarez W., Smit J., Lowrie W., Asaro F., Margolis S. V., Claeys P., Kastner M. and Hildebrand. A. R. (1992). Proximal impact deposits at the Cretaceous-Tertiary boundary in the Gulf of Mexico - A restudy of DSDP Leg 77 sites 536 and 540. *Geology*, **20**, 8, 697-700.

Amari S., Lewis R. S. and Anders E. (1990). Interstellar graphite in meteorites: growing complexity implied by its noble-gas components. *Lunar and Planetary Science*, **XXI**, 19-20.

Anders E. and Zinner E. (1993). Interstellar grains in primitive meteorites, Diamond, Silicon carbide and Graphite. *Meteoritics and Planetary Science*, **28**, 490-514.

Andersen T. and Burke E. A. J. (1996). Methane inclusions in shocked quartz from the Gardnos impact breccia, south Norway. *European Journal of Mineralogy*, **8**, 5, 927-936.

Andreev V. D. (1999). Spontaneous graphitization and thermal disintegration of diamond at T>2000 K. *Physics Of The Solid State*, **41**, 4, 627-632

Andrews K. W. Dyson D. J. and Keown S. R. (1971). Interpretation of electron diffraction patterns. Hilger. 239 pp.

Anthony T. R. (1999). Inclusions in diamonds with solubility changes and phase transformations. *Diamond and Related Materials*, **8**, 78-88.

Arneth J. D., Schidlowski M., Sarbas B., Goerg U. and Amstutz G. C. (1985). Graphite content and isotopic fractionation between calcite-graphite pairs in metasediments from the Mgama Hills, Southern Kenya. *Geochimica et Cosmochimica Acta*, **49**, 1553-1560.

Ash R. D., Wright I. P., Grady M. M., Pillinger C. T., Lewis R. S. and Anders. E. (1987). An investigation of carbon and nitrogen isotopes in Cδ and the effects of grain size on combustion temperatures. *Meteoritics*, **22**, 319.

Badzian A. and Badzian T. (1996). Defects in CVD diamond. *Ceramics International*, **22**, 3, 223-228.

Bales G. S. and Gooding R. J. (1991). Interfacial dynamics at a 1st order phase transition involving strain-dynamic twin formation. *Physical Review Letters*, **67**, 24, 3412-3415.

Baronnet A. (1992). Polytypism and stacking disorder. in Minerals and reactions at the atomic scale: Transmission electron microscopy. *Reviews in Mineralogy*, **27**. 231-282.

Barrat J. A., Jahn B. M., Amosse J., Rocchia R., Keller F., Poupeau G. R. and Diemer E. (1997). Geochemistry and origin of Libyan Desert glasses. *Geochimica et Cosmochimica Acta*, **61**, 9, 1953-1959.

Bauberger W., Mielke H., Schmeer D. and Stettner G. (1974). Petrographische Profildarstellung der Forschungsbohrung Nördlingen 1973 (von Meter 263 an bis zur Endteufe im Masstab 1: 200). *Geologica Bavarica*, **72**, 33-34.

Becker L., Bada J. L., Winans R. E. and Bunch T. E. (1994). Fullerenes in Allende meteorite. *Nature*, **372**, 507.

Becker L., Poreda R. J. and Bada J. L. (1996). Extraterrestrial helium trapped in fullerenes in the Sudbury impact structure. *Science*, **272**, 5259, 249-252.

Becker L. and Bunch T. E. (1997). Fullerenes, fulleranes and polycyclic aromatic hydrocarbons in the Allende meteorite. *Meteoritics and Planetary Science*, **32**, 479-487.

Becker L., Glavin D. P. and Bada J. L. (1997). Polycyclic aromatic hydrocarbons (PAHs) in Antarctic Martian meteorites, carbonaceous chondrites and polar ice. *Geochimica et Cosmochimica Acta*, **61**, 2, 475-481.

Bergfeld D., Nabeleck P. I. and Labotka T. C. (1996). Carbon isotopic exchange during polymetamorphism in the Panamint Mountains, California. *Journal of Metamorphic Geology*, **14**, 199-212.

Blank E., Bürgi H. B., Restori R., Schwarzenbach D. and Ochsenbein P. H. (1996). X-ray diffraction study of stacking faults in hexagonal C_{70} single crystals. *Europhysics Letters*, **33**, 205-210.

Blank V. D., Buga S. G., Dubitsky G. A., Serebryanaya N. R., Popov M. Yu. and Sundqvist B. (1998). High-pressure polymerized phases of C-60. *Carbon*, **36**, 4, 319-343.

Bogdanov S. V., Moroz E. M. and Korobov Yu. A. (1995). Substructural features of ultrafine-particle diamonds prepared by explosion synthesis. *Inorganic Materials*, **31**, 6, 742-744.

Bohor B. F., Foord E. E., Modreski P. and Triplehorn. D. M. (1984). Mineralogic evidence for an impact event at the Cretaceous-Tertiary boundary. *Science*, **224**, 4651, 867-869.

Bohor B. F., Betterton W. J. and Krogh T. E. (1993). Impact-shocked zircons: discovery of shock induced textures reflecting increasing degrees of shock metamorphism. *Earth and Planetary Science Letters*, **119**, 419-424.

Boland J. N. and Liebermann R. C. (1983). Mechanism of the olivine to spinel phase transformation in Ni2SiO4. *Geophysical Research Letters*, **10**, 87-90.

Borg I. Y. (1972). Some shock effects in granodiorite to 270 kilobars at the Pile Driver site. In *Flow and fracture of rocks, AGU Monograph*, **16**, 293-311.

Bottinga Y. (1969). Carbon isotope fractionation between graphite, diamond and carbon dioxide. *Earth and Planetary Science Letters*, **5**, 301-307.

Bottomly R., Grieve R., York D. and Masaitis V. (1997). The age of the Popigai impact event and its relation to events at the Eocene/Oligocene boundary. *Nature*, **388**, 365-368.

Bouska V., Povondra P., Florenskij P. V. and Randa Z. (1981). Irghizites and Zamanshinites - Zamanshin Crater, USSR. *Meteoritics*, **16**, 2, 171-184.

Bouska V. (1994). Moldavites: The Czech Tektites. Prague.

Bratkovsky A. M., Heine V. and Salje E. K. H. (1996). Strain effects, particularly in phase transitions. *Philosophical Transactions of the Royal Society of London Series A-Mathematical Physical and Engineering Sciences*, **354**, 1720, 2875-2896.

Bazhkin V. V., Lyapin A. G., Popova S. V., Voloshin R. N., Antonov Y. V., Lyapin S. G., Kluev Y. A., Naletov A. M. and Melnik N. N. (1997). Metastable crystalline and amorphous carbon phases obtained from fullerite C-60 by high pressure-temprature treatment. *Physical Review B- Condensed Matter*, **56**, 18, 11465-11472.

Bringemeier D. (1994). Petrofabric examination of the main suevite of the Ötting Quarry, Nördlinger Ries, Germany. Meteoritics and Planetary Science, 29, 3, 417-422.

Brozolo F. R. Di., Bunch T. E., Fleming R. H. and Macklin J. (1994). Fullerenes in an impact on the LDEF spacecraft. *Nature*, **369**, 37-40.

Buerki P. R. (1996). Low-pressure formation routes for interstellar microdiamonds: chemical vapour deposition vs. homogenous nucleation. *Meteoritics and Planetary Science*, **31**, A24-25.

Buerki P. R. and Leutwyler S. (1991a). Homogenous nucleation of diamond powder by CO2-laser-driven gas-phase reactions. *Journal of Applied Physics*, **69**, 6, 3739-3744.

Buerki P. R. and Leutwyler S. (1991b). Substrate-free gas-phase synthesis of diamond powder by CO_2 laser pyrolysis of C_2H_4. *Surface and Coatings Technology*, **47**, 22, 28.

Buerki P. R. and Leutwyler S. (1993). CO2-laser-induced gas-phase synthesis of micron-sized diamond powders: recent results and future developments. *Diamond and Related Materials*, **2**, 174-182.

Buerki. P. R. and Leutwyler. S. (1994). CO2-laser-induced vapour-phase synthesis of HN-diamond nanoparticles at 0.6-2bar. *Nanostructured Materials*, **4**, 5, 577-582.

Bundy F. P. (1989). Pressure-temperature phase-diagram of elemental carbon. *Physica A*, **156**, 1, 169-178.

Bundy F. P., Bassett W. A., Weathers M. S., Hemley R. J., Mao H. K. and Goncharov A. F. (1996). The pressure-temperature phase and transformation diagram for carbon: updated through 1994. *Carbon*, **34**, 2, 141-153.

Burns R. C. and Davies. G. J. (1998). Growth of synthetic diamond. In: *The properties of natural and synthetic diamond*. 395-422. Ed. J. E. Field. Academic Press. pp.710.

Buseck. P. R. and Huang. B. (1985). Conversion of carbonaceous material to graphite during metamorphism. *Geochimica et Cosmochimica Acta*, **49**, 2003-2016.

Carlise D. B. (1992). Knudsen Farm "Diamonds at the K/T boundary". *Nature*, **357**, 119-120.

Carlise D. B. and Braman D. R. (1991). Nanometre-size diamonds in K/T boundary clay of Alberta. *Nature*, 352, 708-709.

Carmer C. S. amd Frenklach M. (1989). Formation of silicon carbide particles behind shock waves. *Applied Physics Letters*, **54**, 15, 1430-1432.

Claeys P., Smit J., Montanari A. and Alvarez W. (1998). The Chicxulub impact crater and the Cretaceous-Tertiary boundary in the Gulf of Mexico region. *Bulletin de la Societe Geologique de France*, **169**, 1, 3-9.

Clark C. D., Collins A. T. and Woods G. S. (1996). Absorption and luminescence spectroscopy. 35-80. in *The properties of natural and synthetic diamond*. Ed: J. E. Field. Academin Press. 710 pp.

Clarke R. S., Appelman D. E. and Ross P. B. (1981). An Antarctic iron meteorite contains pre-terrestrial impact-produced diamonds and londsdaleite. *Nature*, **352**, 708-709.

Clarke R. S., Jarosewich E., Ross. D. R., Wasson J. T. and English M. (1994). The Chuckwalla. CA, IAB Iron contains preterrestrial impact-produced diamonds with sphalerite. *Meteoritics*, **29**, 4, 457.

Chao E. C. T. (1967). Shock effects in certain rock forming minerals. *Science*, **156**, 192-202.

Chao E. C. T. (1977). Preliminary interpretation of the 1973 Ries research deep drill core and a new Ries cratering model. *Geologica Bavarica*, **75**, 421-442.

Chao E. C. T., Hüttner R. and Schmidt-Kaler H. (1978). Principal Exposures of the Ries meteorite Crater in Southern Germany: Description, petrographic documentation and interpretation. *Bayerisches Geologisches Landesamt*. 84 pp.

Chijiwa. T., Arai T., Sugai T., Shinohara H., Kumazawa M., Takano M. and Kawakami S. (1999). Fullerenes found in the Permo-Triassic mass extinction period. *Geophysical Research Letters*, **26**, 6, 767-770.

Chen J. H. and Van Tendeloo G. (1999). Microstructure of tough polycrystalline natural diamond. *Journal of Electron Microscopy*, **48**, 2, 121-129.

Chomenko A. A., Gankevich L. T., Kotonosov A. S. and Futeinikov A. F. (1975). *Sint. Almazy*, **3**, 3.

Coes L. (1953). A new dense crystalline silica. *Science*, **118**, 131.

Cordier P. and Gratz A. J. (1995). TEM study of shock metamorphism in quartz from the Sedan nuclear test site. *Earth and Planetary Science letters*, **129**, 163-170.

Cottrell A. H. (1964). Theory of crystal dislocations. Documents on modern physics. Blackie.

Crawford D. and Schultz P. H. (1991). Laboratory investigations of impact-generated plasma. *Journal of Geophysical Research*, **96**, E3, 18807-18817.

Daly T. K., Buseck P. R., Williams P. and Lewis C. F. (1993). Fullerenes from a Fulgurite. *Science*, **259**, 5101, 1599-1601.

Daulton T. L. and Ozima M. (1996). Diamond formation in Uranium-rich carbonaceous materials. *Science*, **271**, 1260-1262

David E. J. H. (1972). The tektite production process. *Forstehr Mineralogische*, **49**, 154-182.

Davis D. R. and Farinella P. (1997). Collisional evolution of Edgeworth-Kuiper Belt objects. *Icarus*, **125**, 1, 50-60.

De S., Heaney P. J., Hargreaves R. B., Vicenzi E. P. and Taylor P. T. (1998). Microstructural observations of polycrystalline diamond: a contribution to the carbonado conundrum. *Earth and Planetary Science Letters*, **164**, 421-433.

De Carli P. S. (1967). in Science and Technology of Industrial Diamonds, **1**, 49. (Industrial Diamond Information Bureau, London).

De Carli P. S. (1979). Nucleation and growth of cubic diamond in shock wave experiments. in: *High Pressure Science and Technology*, ed K. D. Timmerhaus and M. S. Barber, 6th AIRAPT Conference, Boulder, Colorado, 1977, **1**, 940-943, Plenum, New York.

De Carli P. S. (1995). Shock wave synthesis of diamond and other phases. *Materials Research Society Symposium Proceedings*, **383**, 21-31.

De Carli P. S. (1998). Direct synthesis of diamond in the laboratory and in impact craters. *Meteoritics and Planetary Science*, **33**, 4, A39.

De Carli P. S. and Jamieson J. C. (1961). Formation of diamond by explosive shock. *Science*, **133**, 1821.

Derjaguin R. V. and Fedoseev D. V. (1994). Physio-chemical synthesis of diamond in metastable range. *Progress in Surface Science*, **45**, 1-4, 71-94.

De Vita A., Galli G., Canning A. and Car R. (1996). A microscopic model for surface-induced diamond-to-graphite transitions. *Nature*, **379**, 523-526.

Dietz R. S. (1947). Meteorite impact suggested by the orientation of shatter cones at the Kentland structure, Indiana, disturbance. *Science*, **105**, 76

Dietz R. S. (1959). Shatter cones in cryptoexplosion structures (meteorite impact). *Journal of Geology*, **67**, 496-505.

Dikov P. Yu. Gerasimov M. V., Yakovlev O. I. and Wlotzka F. (1996). High temperature vaporisation of Mg-Ca-carbonate-sulphate-quartz-alumina targets. *Lunar and Planetary Science*, **XXVII**, 311.

Donnet J. B., Lemoigne C., Wang T. K., Peng C-M., Samirant M. and Eckhardt. S. (1997). Detonation and shock synthesis of nanodiamonds. *Bulletin de la Societe Chimique de France*, **134**, 10-11, 875-890.

Dons J. and Naterstad J. (1992). The Gardnos impact structure, Norway. *Meteoritics*, **27**, A215.

Duke E. F. and Rumble D. (1983). Textural and isotopic variation of graphite in the New Hampshire Plutonic series. *Carnegie Institute of Washington Yearbook*, 82, 270-273.

Duvall G. E. and Graham R. A. (1977). Phase transitions under shock-wave loading. *Reviews in Modern Physics*, **49**, 523-579.

El Goresy A. and Donnay G. (1968). A new allotropic form of carbon from the Ries crater. *Science*, **161**, 3839, 363-364.

El Goresy A., Chen M., Gillet P., Künstler F. and Stähle V. (1999). In situ discovery of shock-induced graphite-diamond phase transformations in polished thin sections of shocked gneiss from the Ries crater, Germany. *Meteoritics and Planetary Science*, **34**, 4, A125.

Elo S., Jokinen T. and Sonininen H. (1992). Geophysical investigations of the Lake Lappajarvi impact structure, Western Finland. *Tectonophysics*, **216**, 1-2, 99-109.

Epanchintsev O. G., Korneev A. E., Dityat'ev A. A., Nesterenko V. F., Simonov V. A. and Luk'yanov Ya. L. (1995). Shock wave synthesis of diamond from fullerenes C60 to C100. *Combustion explosion and shock waves*, **31**, 2, 241-246

Epanchintsev O. G., Zubchenko A. S., Korneyev A. E. and Simonov V. A. (1997). Highly-efficient shock-wave diamond synthesis from fullerenes. *Journal of Physics and Chemistry of Solids*, **58**, 11, 1785-1788.

Er'omenko G. K. and Polkanov Ju. A. (1978). The modern ideas about the carbon minerals. in *The basic conceptions in mineralogy*. Kiev: Naukova Dumka Press, 103-106.

Erskine D. J. and Nellis W. J. (1991). Shock-induced martensitic phase transformation of oriented graphite to diamond. *Nature*, **349**, 317-318.

Evance T. and Santer D. H. (1961). Etching of diamond surfaces by gases. *Philadelphia Magazine*, **6**. 429-440.

Ezersky V. A. (1986). The high-pressure polymorphs originated by shock transformations of coal. *Zapiski Vseouznogo Mineralogicheskogo Obstchestva*, **115**, 1, 26-33.

Ezersky V. A. (1982). The shock metamorphosed carbon matter in impactites. *Meteoritika*, **41**, 143-140.

Fahy S., Louie S. G. and Cohen M. L (1986). Pseudopotential total-energy study of the transition from rhombohedral graphite to diamond. *Physical Review B- Condensed Matter*, **34**, 2, 1191-1199.

Farinella P. and Davies D. R. (1996). Short-period comets: Primordial bodies or collisional fragments?. *Science*, **273**, 5277, 938-941.

Farley K. A., Montanari A., Shoemaker E. M. and Shoemaker C. S. (1998). Geochemical evidence for a comet shower in the Late Eocene. *Science*, **280**, 5367, 1250-1253.

Field J. E. (1992). Appendix: Tables of properties. 668-699. in The properties of natural and synthetic diamond. ed. J. E. Field. Academinc press. 710 pp.

Fisenko A. V., Kashkarov L. L., Semenova L. F. and Pillinger C. T. (1995). Thermoluminescence of meteoritic diamonds of the interstellar and solar origin. *Geokhimiya*, **5**, 677-686.

French B. M., Koeberl C., Gilmour I., Shirey S. B., Dons J. A. and Naterstad J. (1995). Petrology and geochemistry of target rocks and breccias from the Gardnos impact structure, Norway. *Lunar And Planetary Science*, **XXVI**, 423-424.

French B. M., Koeberl C., Gilmour I., Shirey S. B., Dons J. A. and Naterstad J. (1997). The Gardnos impact structure, Norway: Petrology and geochemistry of target rocks and impactites. *Geochimica et Cosmochimica Acta.*, **61**, 4, 873-904.

Frondel C. and Marvin U. B. (1967). Lonsdaleite, a hexagonal polymorph of diamond. *Nature*, **214**, 587-589.

Foote A. E. (1891). A new locality for meteorite iron with a preliminary notice of the discovery of diamond in the iron. *Proceedings of the Association of Advanced Science*, **40**. 279 pp.

Galimov E. M. (1991). Kimberlite magmatism and diamond formation. *Geochimica et Cosmochimica Acta*, **6**, 55, 1697-1708.

Garvin J. B. and Fawley J. J. (1998). Geometric properties of Martian impact craters: Preliminary results from the Mars Orbiter Laser Altimeter. *Geophysical Research Letters*, **25**, 24, 4405-4408.

Gentner W. and Wagner A. W. (1969). Cogenesis of the Ries crater and Moldavites and the origin of tektites. *Geologica Bavarica*, **61**, 296-303.

Gi R. A., Mizumasa T., Akiba Y., Hirose Y., Kurosu T. and Iida M. (1995). Formation mechanism of p-type surface conductive layer on deposited diamonds films. *Japanese Journal of Applied Physics Part 1 - Regular Papers Short Notes And Review Papers*, **34**, 10, 5550-5555.

Giblin I. (1998). New data on the velocity-mass relation in catastrophic disruption. *Planetary and Space Science*, **46**, 8, 921-928.

Gilkes K. W. R. and Pillinger C. T. (1999). Carbon: How many allotropes associated with meteorites and impact phenomena. 17-30. in *Carbyne and Carbynoid Structures*. eds. R. B. Heimann., S. E. Evsyukov and L. Kavan. Kluwer Press. 444 pp.

Gilmour I. (1999). Carbon allotropes in impact-produced rocks. *Meteoritics and Planetary Science*, **34**, A43.

Gilmour I., Russell S. S., Arden J. W., 'Lee M. R., Franchi I. A. and Pillinger C. T. (1992). Terrestrial carbon and nitrogen isotopic ratios from K/T boundary nanodiamonds. *Science*, **258**, 1624-1626.

Gilmour. I. and Wolbach W. S. (1994). Diamonds, soot and molecules: The geochemistry of carbon at the K/T boundary. *Lunar and Planetary Institute Contributions*, **825**, 43.

Girdler R. W., Taylor P. T. and Frawley J. J. (1992). A possible impact origin for the Bangui magnetic anomaly (Central Africa). *Tectonophysics*, **212**, 1-2, 45-58.

Glass B. P., Koeberl C., Blum J. D. and McHugh C. M. G. (1998). Upper Eocene tektite and impact ejecta layer on the continental slope off New Jersey. *Meteoritics and Planetary Science*, **33**, 2, 229-241.

Glass B. P. and Koeberl C. (1999). Ocean Drilling Project Hole 689B spherules and upper Eocene microtektite and clinopyroxene-bearing spherule strewn fields. *Meteoritics and Planetary Science*, **34**, 2, 197-208.

Goltrant O., Leroux H., Doukhan J-C. and Cordier P. (1992). Formation mechanisms of PDF in naturally shocked quartz. *Physics of earth and Planetary Interiors*, **74**, 219-240.

Gratz A. J., Fisler D. K. and Bohor B. F. (1996). Distinguishing shocked from tectonically deformed quartz by the use of the SEM and chemical etching. *Earth and Planetary Science Letters*, **142**, 3-4, 513-521.

Graup G. (1977). Die Petrographie der Kristallinen Gesteine der Forschungsbohrung Nördlingen 1973. *Geologica Bavarica*, **75**, 219-229.

Graup G. (1978). Das Kristallin im Nördlinger Ries: Petrographische Zusammensetzung und Auswurfmechanismus der Kristallinen Trümmermassen, Struktur des Kristallinen Untergrundes und Beziehungen zum Moldanubikum: Stuttgart, Enke. 190 pp.

Graup G. (1981). Terrestrial chondrules, glass spherules and accretionary lapilli from the suevite, Ries crater, Germany. *Earth and Planetary Science Letters*, **55**, 407-418.

Graup G. (1999). Carbonate-silicate liquid immiscibility upon impact melting: Ries crater, Germany. *Meteoritics and Planetary Science*, **34**, 3, 425-438.

Green H. W. (1991). Petrology - High temperature and deformation-induced reactions. in Minerals and reactions at the atomic scale - Transmission electron microscopy. *Reviews in Mineralogy*, **27**, 425-452.

Greiner N. R. (1990). Diamonds in detonation soot. *NASA Conference Proceedings*, 3061.

Grier J. A., Swindle T. D., Kring D. A. and Melosh H. J. (1995). Investigation of the Gardnos impact structure - Ar40 AR39 results. *Meteoritics*, **30**, 5, 513-514.

Grew E. S. (1974). Carbonaceous material in some metamorphic rocks of New England and other areas. *Journal of Geology*, **82**, 50-73.

Grieve R. A. F. (1987). Terrestrial impact structures. *Annual Reviews of Earth and Planetary Science*, **15**, 245-270.

Grieve R. A. F. (1995). The Ries - still giving up its secrets. *Meteoritics*, **30**, 3, 241.

Grieve R. A. F. (1997). Target Earth: Evidence for large-scale impact events. *Annals of the New York Academy of Sciences*, **822**, 319-352.

Grieve R. A. F., Robertson P. B. and Dence M. R. (1981). Constraints on the formation of ring impact structures, based on terrestrial data. In *Multi-ring basins, Proceedings of Lunar and Planetary Science*, **12B**, 1607-1621.

Grieve R. A. F., Stöffler D. and Deutsch A. (1991). The Sudbury structure - Controversial or misunderstood. *Journal of Geophysical Research - Planets*, **96**, E5, 22753-22764.

Grieve R. A. F. and Cintala M. J. (1992). An analysis of differential impact melt-crater scaling and implications for the terrestrial impact record. *Meteoritcs*, **27**, 526-538.

Grieve R. A. F. and Masaitis V. L. (1994). The economic potential of terrestrial impact craters. *International Geology Review*, **36**, 105-151.

Grieve R. A. F., Langenhorst F. and Stöffler D. (1996). Shock metamorphism of quartz in nature and experiment: II. Significance in geosciences. *Meteoritics and Planetary Science*, **31**, 6-35.

Grieve R. A. F. and Pesonen L. J. (1996). Terrestrial impact craters: Their spatial and temporal distribution and impacting bodies. *Earth Moon and Planets*, **72**, 1-3, 357-376.

Gurov E. P., Gurova E. P. and Rakitskaya R. B. (1995). Impact diamonds in the craters of the Ukrainian shield. *Meteoritics*, **30**, 5, 515-516.

Gurov E. P., Gurova E. P. and Rakitskaya R. B. (1996). Impact diamonds of Zapadnaya crater: phase composition and some properties. *Meteorites and Planetary Science*, **31**, A56.

Gurov E. P., Koeberl C. and Reimold W. U. (1998). Petrography and geochemistry of target rocks and impactites from the Ilyinets crater, Ukraine. *Meteoritics and Planetary Science*, **33**, 6, 1317-1333.

Haggerty S. E. (1996). *Eos Transactions AGU, supplement., 1996 spring meeting*, S143.

Hannemann R. J., Strong H. M. and Bundy F. P. (1967). Hexagonal diamond in meteorites: implications. *Science*, **155**, 995-997.

Harris S. J. and Weiner A. M. (1985). Chemical kinetics of soot particle growth. *Annual Review of Physical Chemistry*, **36**, 31-52.

Heimann R. B. (1994). Linear finite carbon chains (carbynes) - their role during dynamine transformation of graphite to diamond, and their geometric and electronic-structure. *Diamond and related materials*, **3**, 1151-1157.

Heimann R. B. (1999). Diamond synthesis from carbyne. 409-426. in *Carbynes and Carbynoid Structures*. eds. R. B. Heimann., S. E. Evsyukov. and L. Kavan.. Kluwer. 444 pp.

Heimann R. B., Evsyukov S. E. and Koga Y. (1997). Carbon allotropes: a suggested classification scheme based on valence orbital hybidization. *Carbon*, **35**, 10-11, 1654-1658.

Heine V., Cheng. C. and Needs R. J. (1991). The preference of silicon-carbide for growth in the metastable cubic form. *Journal of the American Ceramic Society*, **74**, 10, 2630-2633.
Henkel H. and Pesonen L. J. (1992). Impact craters and craterform structures in Fennoscandia.*Tectonophysics*, **216**,1-2, 31-40.

Heymann D., Chibante L. D. F., Brooks R. R., Wolbach W. S. and Smalley R. E. (1994). Fullerenes in the Cretaceous-Tertiary boundary-layer. *Science*, **265**, 5172, 645-647.

Heymann D., Korochantsev A., Nazarov M. A. and Smit J. (1996). Search for fullerenes C-60 and C-70 in Cretaceous-Tertiary boundary sediments from Turkmenistan, Kazakhstan, Georgia, Austria and Denmark. *Cretaceous Research*, **17**, 3, 367-380.

Heyman D., Yancey T. E., Wolbach W. S., Thiemens M. H., Johnson E. A., Roach D. and Moecker S. (1998). Geochemical markers of the Cretaceous-Tertiary boundary event at Brazos River, Texas, USA. *Geochimica et Cosmochimica Acta*, 62, 1, 173-181.

Hildebrand A. R. (1993). The Cretaceous-Tertiary boundary impact (or the dinosaurs didnt have a chance). *Journal of the Royal Astronomical Society of Canada*. **87**, 2, 77-118.

Hildebrand A. R., Penfield G. T., Kring D. A., Pilkington M., Camargo A. Z., Jacobsen S. B. and Boynton W. V. (1991). Chicxulub Crater: A possible cretaceous/ Tertiary boundary impact crater on the Yucatan Peninsula, Mexico. *Geology*, **19**, 9, 867-871.

Hirai H., Kondo K. and Ohwada T. (1995a). Diamond synthesis by shock compression from a thin graphite plate with suppressed regraphitisation. *Carbon*, **33**, 2, 203-208.

Hirai H., Tabira Y., Kondo K., Okiawa T. and Ishizawa N. (1995b). Radial distribution function of a new form of amorphous diamond shock induced from C_{60} fullerene. *Physical Review B*, **52**, 9, 6162-6165.

Hörz F. (1982). Ejecta of the Ries crater, Germany. *Geological Society of America Special Paper*, **190**, 39-55.

Hörz F., Ostertag R. and Rainey D. A. (1983). Bunte breccia of the Ries: Continuous deposits of large impact craters. *Reviews of Geophysics and Space Physics*. **21**, 8, 1667-1725.

Hough R. M. (1996). Diamonds, soot, C60 and gas bubbles: carbon and impacts. Phd Thesis, Open University.

Hough R. M., Gilmour I. and Pillinger C. T. (1995a). Diamond and silicon carbide in suevite from the Nördlinger Ries impact crater. In *4th int. workshop of the ESF Scientific Network on "Impact cratering and Evolution of Planet Earth" Ancona, May 12-17, 1995. The Role of the impacts in the evolution of atmosphere and biosphere with regards to short- and long-term changes. Abstracts and Field trip volume.* (A. Montanari and R. Coccioni eds.), 93-94.

Hough R. M., Wright I. P., Pillinger C. T. and Gilmour I. (1995b). Diamonds from the K/T iridium rich horizons of the Arroyo El Mimbral (Mexico), Brownie Butte (Montana) and Berwind Canyon (Colorado). In *4th int. workshop of the ESF Scientific Network on "Impact cratering and Evolution of Planet Earth" Ancona, May 12-17, 1995. The Role of the impacts in the evolution of atmosphere and biosphere with regards to short- and long-term changes. Abstracts and Field trip volume* (A. Montanari and R. Coccioni eds.), 95-96.

Hough R. M., Gilmour I., Pillinger C. T., Arden J. W. Gilkes. K. W. R., Yuan J. and Milledge H. J. (1995c). Diamond and silicon carbide in impact melt rocks from the Ries crater. *Nature*, **378**, 41-44.

Hough R. M., Gilmour I., Newton J., Arden J. W. and Pillinger C. T. (1995d). Chemically-robust carbon particles in peat from the Tunguska impact site. *Meteoritics and Planetary Science*, **30**, 5, 521.

Hough R. M., Gilmour. I., Pillinger C. T., Langenhorst F. and Montanari A. (1997). Diamonds from the iridium-rich K-T boundary layer at Arroyo el Mimbral, Tamaulipas, Mexico. *Geology*, **25**, 11, 1019-1022.

Huffman A. R., Brown J. M., Carter N. L. and Reimold W. U. (1993). The microstructural response of quartz and feldspar under shock loading at variable temperatures. *Journal of Geophysical Research - Solid Earth*, **98**, B12, 22171-22197.

Hutt P., Alvarez W., Elder W. P., Hansen T., Kauffman, E. G., Keller G., Shoemaker E. and Weissman P. R. (1987). Comet showers as a cause of mass extinctions. *Nature*, **329**, 118-126.

Hwang N. M. (1999). Crystal growth by charged cluster focused on CVD diamond process. *Journal of Crystal Growth*, **198/199**, 945-950.

Itaya T. (1981). Carbonaceous material in pelitic schists of the Sanbagawa metamorphic belt in central Shikoku, Japan. *Lithos*, **14**, 215-224.

Izokh E. P. (1996). Origin of tektites: An alternative to terrestrial impact theory. *Chemie der Earde-Geochemistry*, **56**, 4, 458-474.

Jankowski B. (1977). Die gradierte Einheit oberhalb der Suevites der Forschungsbohrung Nördlingen 1973. *Geologica Bavarica*. **75**, 155-162.

Jepps N. W. and Page T. F. (1983). Polytypic transformations in silicon carbide. *Progress in Crystal Growth and Characterisation*, **7**, 259-307.

Jones B. W. (1999). Discovering the solar system. Wiley. 416 pp.

Jones E. M. and Kodis J. W. (1982). Atmospheric effects of large body impacts: The first few minutes. in Geological implications of large asteroids and comets on the Earth. *Geological Society of America Special Paper*, **190**, 175-186. eds. L. T. Silver, and P. H. Schultz.

Kadono T. and Fujiwara A. (1996). Observation of expanding vapour cloud generated by hypervelocity impact. *Journal of Geophysical Research, IDI, EII*, **26**, 097-26, 169.

Kaminsky S. V. (1987). Genesis of diamond-carbonado polycrystalline aggregates. *Doklady Akademii Nauk SSR*, **294,** 2, 439-440.

Kaminsky S. V., Klyuyer Y. A., Prostopchuk B. I., Shcheka S. A., Smirnov V. I. and Ivanovskaya S. A. (1978). First carbonado and new Ballas finds in the Soviet Union. *Doklady*, **242**, 153-

Kamo S. L., Reimold W. U., Krogh T. E. and Collinston W. P. (1996). A 2.023 Ga age for the Vredefort impact event and a first report of shock metamorphosed zircons in pseudotachylitic breccias and Granophyre. *Earth and Planetary Science Letters*, **144**, 369-387.

Kelly A. and Groves G. W. (1970). Crystallography and crystal defects. Longman.

Kieffer S. W. and Simmonds C. H. (1980). The role of volatiles and lithology in the impact cratering process. *Reviews of Geophysics and Space Physics*, **18**, 1, 143-181.

Kim G. H. (1997). Transmission electron microscope observation of diamond/WC interface. *Journal of Crystal Growth*, **178,** 4, 634-638.

Klages C-P. (1993). Chemical Vapour deposition of diamond. *Applied Physics*, **A56**, 513-526.

Klages C-P. (1995). Metastable diamond synthesis- Principles and applications. *European Journal of Mineralogy*, **7**, 767-774.

Kleiman J., Heimann R. B., Hawken D. and Salansky N. M. (1984). Shock compression and flash heating of graphite/metal mixtures at temperatures up to 3200 K and pressures up to 25 Gpa. *Journal of Applied Physics*, **56**, 5, 1440-1454.

Koeberl C. (1994). African meteorite impact craters: Characteristics and geological importance. *Journal of African Earth Science*, **18**, 4, 263-295.

Koeberl C. Sharpton V. L., Harrison T. M, Sandwell D., Muraki A. V. and Burke K. (1990). The Kara/Ust-Kara twin impact structure; a large scale impact event in the late Cretaceous. *Geological Society of America Special Paper*, **247**, 233-

Koeberl C., Masaitis V. L., Langenhorst F., Stöffler D., Schrauder M., Lengauer C., Gilmour I and Hough R. M. (1995). Diamonds from the Popigai impact structure, Russia. *Lunar and Planetary Science*, **XXVI**, 777-778.

Koeberl C., Poag C. W., Reimold W. U. and Brandt D. (1996). Impact origin of the Chesapeake bay structure and the source of the N. American tektites. *Science*, **271**, 1263-1266.

Koeberl C., Masaitis V. L., Shafranovsky G. I., Gilmour I., Langenhorst F. and Schrauder M. (1997). Diamonds from the Popigai impact structure, Russia. *Geology*, **25**, 967-970.

Koeberl C., Reimold W. U., Blum J. D. and Chamberlain C. P. (1998). Petrology and geochemistry of target rocks from the Bosumtwi impact structure, Ghana and comparison with Ivory Coast tektites, *Geochimica et Cosmochimica Acta*, **62**, 12, 2179-2196.

KohseHoinghaus K. (1998). Diamond films and rust particles: Reactive atmospheres in fuel-rich flames. *Chemie in Unserer Zeit*, **32**, 5, 242-250.

Koval'sky V. V. and Cherskiy N. V. (1973). Possible sources and isotopic composition of carbon in diamond. *International Geology Review*, **15**, 1, 1224-1228.

Kring D. A., Melosh H. J. and Hunten D. H. (1996). Impact induced perturbations of atmospheric sulphur. *Earth and Planetary Science Letters*, **140**, 1-4, 201-212.

Kroto H. W., Heath J. R., O'Brien S. C., Curl R. F. and Smalley R. E. (1985). C_{60}: Buckminsterfullerene. *Nature*, **318**, 162-163.

Kudryavtsev Yu. P. (1999). The discovery of Carbyne. 1-6. in *Carbyne and Carbynoid structures*, eds. R. B. Heimann., S. Evsyukov. and L. Kavan. Kluwer Academic. 444 pp.

Kudryatsev Yu. P. and Bystrova. N. A. (1998). Polyadamantane as a source of diamond-like carbon. *Russian Chemical Bulletin*, **47**, 7, 1399-1340.

Kukkonen I. T., Kivekäs L. and Paananen M. (1992). Physical properties of Kärnäite (impact melt), suevite and impact breccia in the Lappijarvi meteorite crater, Finland. *Tectonophysics*, **216**, 111-122.

Kurdumov A. V. and Pilankevitch A. N. (1979). The phase transformations in Carbon and Boron Nitride, Kiev: Naukova Press, 188 pp.

Langenhorst F. (1994). Shock experiments on pre-heated α- and β- quartz: II. X-ray and TEM investigations. *Earth and Planetary Science Letters*, **128**, 683-698.

Langenhorst F. and Masaitis V. L. (1996). Microstructural characteristics of impact diamonds from the Popigai crater (Russia). *Meteoritics and Planetary Science*, **31**, A77.

Langenhorst F., Shafranovsky G. and Masaitis V. L (1998). A comparative study of impact diamonds from the Popigai, Ries, Sudbury, and Lappajarvi craters. *Meteoritics and Planetary Science*, **33**, 4, A90-A91.

Langenhorst F., Shafranovsky G. I., Masaitis V. and Koivisto M. (1999). Discovery of impact diamonds in a Fennoscandian crater and evidence for their genesis by solid-state transformation. *Geology*, 27, 8, 747-750.

Lannon J. M., Gold J. S. and Stinespring C. D.,(1995). Hydrogen-ion interactions with silicon-carbide and the nucleation of diamond thin-films. *Journal of Applied Physics*, **77**, 8, 3823-3830.

Lawes G. (1987). Scanning electron microscopy and x-ray microanalysis. Analytical chemistry through open learning. Eds. James. A. M. J. Wiley and Sons.

Lewis R. S., Srinivasan B. and Anders E. (1975). Host phase of a strange xenon component in Allende. *Science*, **190**, 1, 47-74.

Lewis R. S., Ming T., Wacher J. F., Anders E. and Steel E. (1987). Interstellar nanodiamonds in meteorites. *Nature*, **326**, 160-162.

Litvin Y. A., Chudinovskikh L. T., Saparin G. V., Obyden S. K., Chukichev M. V. and Vavilov V. S. (1999). Diamonds of new alkaline carbonate-graphite HP syntheses: SEM morphology, CCL_SEM and CL spectroscopy studies. *Diamond and Related Materials*, **8**, 2-5, 267-272.

Lupishko D. F. and Dimartino M. (1998). Physical properties of near-Earth asteroids. *Planetary and Space Science*, **46**, 1, 47-74.

Luque F. J. Pasteres J. D. Wopenka B. Rodas M. and Barrenechea J. F. (1998). Natural fluid-deposited graphite: Mineralogical characteristics and mechanisms of formation. *American Journal of Science*, **298**, 6, 471-498.

Ma J. S., Yagyu H., Hiraki A., Kawarada H. and Yonehara T. (1991). Large area diamond selective nucleation based epitaxy. *Thin Solid Films*, **206**, 1-2, 192-197.

Mao H. K., Bell P. M., Duna K. J., Cherenko R. M. and DeVries R. C. (1979). *Reviews in Science. Instrum*, **50**, 1002.

Marakushev A. A., Bogatyrev O. S., Fenogenov A. D., Paneyakh N. A. and Fedosava. S. P. (1993). Impactogenesis and volcanism. *Petrology*, **1**, 6, 517-595.

Martinez I., Scharer U. and Guyot F. (1993). Impact-induced phase transformations at 50-60 Gpa in continental crust - An EPMA and ATEM study. *Earth and Planetary Science Letteres*, **119**, 1-2, 207-223.

Martinez I., Agrinier P., Schärer U. and Javoy M. (1994). A SEM-ATEM and stable isotopic study of carbonates from the Haughton impact crater. *Earth and Planetary Science Letters*, **121**, 559-574.

Martinez I., Deutsch A., Scharer U., Ildefonse P., Guyot F. and Agrinier P. (1995). Shock recovery experiments on Dolomite and thermodynamical calculations of impact-induced decarbonation. *Journal of Geophysical Research - Solid Earth*, **100**, B8, 15465-15476.

Martinez I. and Agrinier P. (1998). Meteorite impact craters on Earth: major shock-induced effects inrocks and minerals. *Comptes Rendus De L Academie Des Sciences Serie II Fascicule A-Sciences De La Terre Et Des Planetes*, **327**, 2, 75-86.

Martini E. J. (1978). Coesite and stishovite at the Vredefort Dome, South Africa. *Nature*, **272**, 715-717.

Marques L., Hodeau J. L. Nunez-Regueiro M. and Perroûx M. (1996). Pressure and temperature diagram of polymerised fullerite. *Physical review B*, **54**, 18, 12633-12636.

Marzari F., Farinella P., Davis D. R., Scholl H. and Bagatin A. C. (1997). Collisonal evolution of Trojan asteroids. *Icarus*, 125, 1, 39-49.

Masaitis V. L. (1992). Impact craters: are they useful. *Meteoritics and Planetary Science.*, **27**, 21-27.

Masaitis V. L. (1993). Diamond bearing impactites, their distribution and petrogenesis. *Regionalaia geologia I Metallogenia.*, **1**, 121-134.

Masaitis V. L. (1994). Impactites from the Popigai Crater. *Geological Society of America Special Paper*, **293**, 153-162.

Masaitis V. L. (1995). The origin and distribution of diamond bearing impactites. *Meteoritics*, **30**, 5, 541.

Masaitis V. L. (1996). Impact diamonds in astroblemes. In: *Mineralogical Society of America 1996 Spring Meeting, May 20-24, Baltimore, Maryland. Abstract supplement to Eos Transactions.* Washington: AGU press, S142-S143.

Masaitis V. L. (1998). Popigai crater: Origin and distribution of diamond-bearing impactites. *Meteoritics and Planetary Science*, **33**, 349-359.

Masaitis V. L. and Shafranovsky G. I. (1994). Comparative study of impact diamonds from the Ries and Popigai craters. In: *3rd int. Workshop of the ESF Scientific Network on "Impact cratering and the Evolution of Planet Earth", Limoges, 18-21 sept, 1994. Shock-wave behaviour of solids in nature and experiments. Guide for field trip, Program and abstracts.* organised by U. Scharer, J-C. Doukhan and P. Agrinier, 47.

Masaitis V. L., Shafranovsky G. I., Ezersky V. A. and Reshetnyak N. B. (1990). Impact diamonds in ureilites and Impactites. *Meteoritika*, 49, 180-196.

Masaitis V. L. (1989). The economic geology of impact craters. *International Geology Review*, **31**, 922-933.

Masaitis V. L., Futergendler S. I. and Gnevyshev M. A. (1972). The diamonds in the impactites of the Popigai meteoritic crater. *Zapiski Vsesouznogo Mineralogicheskogo Obstchestva*, **101**, 108-113.

Masaitis V. L., Shafranovsky G. I., Yezersky V. A. and Reshetnyak N. B. (1990). Impact diamonds in urelites and impactites. *Meteoritica*, **8**, 180-195.

Master S. (1998). The Kogo structure (Equatorial Guinea) as a possible source crater for the origin of carbonado diamonds from Brazil and the Central African Republic. *Meteoritics and Planetary Science*, **33**, 4, A98.

Matese J. J., Whitman P. G., Innanen K. A. and Valtonen M. J. (1995). Periodic modulation of the Oort cloud comet flux by the adiabatically changing galactic disc. *Icarus*, **116**, 2, 255-268.

Matsuda J-I., Fukunaga K. and Ito K. (1991). Noble gas studies in vapour-growth diamonds: Comparison with shock-produced diamonds and the origin of diamonds in ureilites. *Geochimica et Cosmochimica Acta*, **55**, 2011-2023.

Matsuda J-I., Kusumi A., Yajima H. and Syono Y. (1995). Noble gas studies in diamonds synthezed by shock loading in the laboratory and their implications on the origins of diamonds in ureilites. *Geochimica et Cosmochimica Acta*, **59**, 23, 4939-4949.

Matsumoto S., Sato Y., Tsutsumi M. and Setaka N. (1982). Growth of diamond particles from methane-hydrogen gas. *Journal of Materials Science*, **17**, 3106-3112.

McEwan A. S., Moore J. M. and Shoemaker E. M. (1997). The Phanerozoic impact cratering rate: Evidence from the farside of the Moon. *Journal of Geophysical Research-Planets*, **102**, E4, 9231-9242.

McHugh C. M. G., Snyder S. W. and Miller K. G. (1998). Upper Eocene ejecta of the New Jersey continental margin reveal dynamics of Chesapeake Bay impact. *Earth and Planetary Science Letters*, **160**, 3-4, 353-367.

Melosh H. J. (1989). Impact cratering: a geologic process. *Oxford monographs on geology and geophysics:*, **11**. Oxford University Press, 245 pp.

Melosh H. J. (1998). Impact physics constraints on the origin of tektites. *Meteoritics and Planetary Science*, **33**, 4SS, A104.

Melosh H. J., Schneider N. M., Zahnle K. J. and Latham D. (1990). Ignition of global wildfires at the Cretaceous-Tertiary boundary. *Science*, **33**, 4, A104.

Meisel T., Lange J-M. and Krähenbühl U. (1997). The chemical variation of Moldavite tektites: Simple mixing of terrestrial sediments. *Meteoritics and Planetary Science*, **32**, 493-502.

Michler J., Von Kaenel., Stiegler J. and Blank E. (1998). Complementary application of electron microscopy and micr-Raman spectroscopy for microstructure, stress and bonding defect investigation of heteroepitaxial chemical vapour deposited diamond films. *Journal of Applied Physics*, **83**, 1, 187-197.

Miura Y. (1995). New shocked calcite and iron grains from Nördlingen Ries impact crater. *Meteoritics*, **30**, 5, 550-551.

Montanari A., Bagatin A. C. and Farinella P. (1998). Earth cratering record and impact energy flux in the last 150 Ma. *Planetary and Space Science*, **46**, 2-3, 271-281.

Morbidelli A. and Gladman B. (1998). Orbital and temporal distributions of meteorites originating in the asteroid belt. *Meteoritics and Planetary Science*, **33**, 5, 999-1016.

Moro L., Paul A., Lorents D. C., Malhotra R., Ruoff R. S., Jiang L., Stupian G. W., Wu K. J. and Subramoney S. (1997). Growth of patterned SiC by ion modification and annealing of C-60 films on silicon. *Applied Surface Science*, **119**, 1-2, 76-82.

Morris D. G. (1980). An investigation of the shock-induced transformation of graphite to diamond. *Journal of Applied Physics*, **51**, 4, 2059-2065.

Nakazawa S., Watanabe S., Kato. M., Lijima Y., Kobayashi T. and Sekine T. (1997). Hugoniot equation of state of basalt. *Planetary and Space Science*, **45**, 11, 1489-1492.

Napier W. M. and Clube S. V. M. (1997). Our cometary environment. *Reports on progress in physics*, **60**, 3, 293-343.

Naterstad J. and Dons J. (1994). Unpublished notes and geologic map for excursion to Gardnos impact structure, Norway, in connection with European Science Foundation Workshop on " The identification and characterisation of impacts, Östersund, Sweden, May 31-June 5, 1994.
Newman W. I., Symbalisty E. M. D., Ahrens T. J. and Jones E. M. (1999). Impact erosion of planetary atmospheres: Some suprising results. *Icarus*, **138**, 2, 224-240.

Newsom H. E. and Taylor S. R. (1989). Geochemical implications of the formation of the Moon by a single giant impact. *Nature*, **338**, 6210, 29-34.

Newsom H. E., Graup G., Iseri D. A., Geissman J. W. and Keil K. (1990). The formation of the Ries crater, West Germany; Evidence of atmospheric interactions during a larger cratering event. *Geological Society of America Special Paper*, **247**, 195-206.

Nistor L. C., Vanlanduyt J., Ralchenko V. G., Smolin A. A., Korotushenko K. G. and Obraztsova E. D. (1997). Structural studies of diamond thin films grown from DC-arc plasma. *Journal of Materials Research*, **12**, 10, 2533-2542.

O'Keefe J. A. (1976). Tektites and their origin. Elsevier, New York.

O'Keefe J. A. (1985). The coming revolution in planetology. *EOS*, **66**, 89-90.

O'Keefe J. A. (1994). Origin of tektites. *Meteoritics*, **29**, 1, 73-78.

O'Keefe J. A. and Ahrens T. J. (1982). The interaction of the K/T extinction bolide with the atmosphere, ocean and solid earth. *Geological Socierty of America Special Paper*, **190**, 103-120.

O'Keefe J. A., Alterescu S. and Thorpe A. N. (1982). Foaming of natural glasses. *American Ceramic Society Bulletion*, **61**, 8, 820.

Oleinik G. A. and Danilenko N. V. (1997). Polytypeformation in nonmetallic substances. *Uspekhi Khimii*, **66**, 7, 615-640.

Ozima M. and Tatsumoto M. (1997). Radiation-induced crystallisation: Origin of carbonados and its implications on meteorite nan-diamonds. *Geochimica et Cosmochimica Acta*, **61**, 2, 369-376.

Pearson D. G., Davies G. R. and Nixon P. H. (1995). Orogenic ultramafic rocks of UHP (diamond facies) origin. in *Ultrahigh pressure metamorphism*. eds: R. G. Coleman and X. Wang. Cambridge University Press, 456-510.

Perniche E., Horn P. and Pohl J. (1987). Chemical record of the projectile in the graded fall back sedimentary unit, Ries crater. *Earth and Planetary Science letters*, **86**, 113-121.

Peters K. E., Rohrback B. G. and Kaplan I. R. (1981). Carbon and hydrogen stable isotopic variations in kerogen during laboratory-simulated thermal maturation. *AAPG Bulletin- American Association of Petroleum Geologists*, **65**, 501-508.

Phelps A. W., Howard W. and Smith D. K. (1993). Space groups of the diamond polytypes. *Journal of Material Research*, **8**, 11, 2835-2839.

Pierrard O., Robin E., Roccia R. and Montanari A. (1998). Extraterrestrial Ni-rich spinel in upper Eocene sediments from Massignano, Italy. *Geology*, **26**, 4, 307-310.

Pierazzo E., Kring D. A. and Melosh H. J. (1998). Hydrocode simulation of the Chicxulub impact event and the production of climatically active gases. *Journal of Geophysical Research-Planets*, **103**, E12, 28607-28625.

Pierazzo E. and Melosh H. J. (1999). Hydrocode modeling of Chicxulub as an oblique impact event. *Earth and Planetary Science Letters*, **165**, 2, 163-176.

Pipping F. and Lehtinen M. (1992). Geology, stratigraphy and structure of the Lappajarvi meteorite crater, Western Finland - preliminary results of deep drilling. *Tectonophysics*, **216**, 1-2, 91-97.

Poag C. W. (1997). The Chesapeake Bay bolide impact: A convulsive event in the Atlantic Coastal Plain evolution. *Sedimentary Geology*, **108**, 1-4, 45..

Poag C. W., Powars D. S., Poppe L. J. and Mixon R. B. (1994). Meteoroid mayhem in Ole-Virginny - Source of the North-American tektite strewn field. *Geology*, **22**, 8, 691-694.

Pohl J., Bader K., Berktold A., Blohm E. K., Bram K., Ernston K., Friedrich H., Haak V., Hänel R., Homilius J., Knödel K., Schmidt-Kaler H., Rodemann H., Wagner G. A. and Weisner. H. (1974). The research drillhole Nördlingen 1973 in the Ries crater a summary of geophysical investigations. *Geologica Bavarica*, **75**, 323-328.

Pohl J., Stöffler D., Gall H. and Ernstson K. (1977). The Ries impact crater. in Impact and explosion cratering. eds: Roddy. D. J., Pepin. R. O. and Merril. R. B. 343-404. Pergamon, New York.

Polansky C. A. and Ahrens T. J. (1994). Scaling craters in carbonates - Electron-Paramagnetic-Resonance analysis of shock damage. *Journal of Geophysical Research-Planets*, **99**, E3, 5621-5638.

Polyakov V. B. and Kharlashina N. N. (1994). Effect of pressure on equilibrium isotopic fractionation. *Geochimica et Cosmochimica Acta*, **58**, 4739-4750.

Prosser S. J., Wright I. P. and Pillinger C. T. (1990). A preliminary investigation into the isotopic measurement of carbon at the picomole level using static vacuum mass spectrometry. *Chemical Geology*, **83**, 71-88.

Pujols H. and Boisard F. (1970). Effects of an intense shock wave on graphite. *Carbon*, **8**, 781-783.

Rampino M. R. (1997). The galactic theory of mass extinctions: An update. *Celestial mechanics and Dynamical Astronomy*, **69**, 1-2, 49-58.

Rampino M. R. and Haggerty B. M. (1996). The "Shiva Hypothesis". Impacts, mass extinctions and the galaxy. *Earth Moon and Planets*, **72**, 1-3, 441-460.

Rao N., Girshick S., Heberlein J., McMurry P., Jones S., Hansen D. and Micheel B. (1995). Nano particle formation using a plasma expansion process. *Plasma Chemistry and Plasma Processing*, **15**, 4, 581-584.

Reimold W. U., Leroux H., Koeberl C., Hornemann U. and Armstrong R. A. (1998). Optical and transmission electron microscopy analysis of experimentally shock-deformed zircon. *Meteoritics*, **33**, 4, A128.

Riedel M. R. and Karato S. (1997). Grain-size evolution in subducted oceanic lithosphere associated with the olivine-spinel transformation and its effects on rheology. *Earth and Planetary Science letters*, **148**, 27-43.

Rietmeijer F. J. M. (1991). Mixed layering in disordered Sri Lanka graphite. *Carbon*, **29**, 4-5, 669-675.

Rietmeijer F. J. M. (1995). A transmission electron microscope study of experimentally shocked pregraphitic carbon. *Carbon*, **33**, 6, 827-831.

Robertson D. H., Brenner D. W. and White C. T. (1992). On the way to fullerenes - Molecular-dynamics study of the curling and closure of graphitic ribbons. *Journal of Physical Chemistry*, **96**, 15, 6133-6135.

Robertson P. B. and Grieve R. A. F. (1977). Shock attenuation at terrestrial impact structures. *in Impact and Explosion Cratering*. Ed: D. J. Roddy. 687-702. Pergamon.

Rochow T. G. and Rochow E. G. (1978). An introduction to microscopy by means of light, electrons, x-rays or ultrasound. Plenum press, New York.

Roddy D. J. and Shoemaker E. M. (1995). Meteor crater (Barringer Meteorite crater), Arizona - summary of impact conditions. *Meteoritics*, 30, 5, A567.

Rodonot J. (1994). Recognition of eroded astroblemes. *Earth Science Reviews*, **35**, 331-365.

Rost R., Dolgov Yu. A. V. and Shnevshiy S. A. (1978). Gases in inclusions of impact glass in the Ries crater, West Germany, and finds of high pressure carbon polymorphs. *Dokladi AN SSSR*, **241**, 695-698.

Rowan L. R. and Ahrens T. J. (1994). Observations of Impact-Induced Molten-Metal Silicate Partitioning. *Earth and Planetary Science Letters*, **122**, 1-2, 71-88.

Rubie D. C. and Champness P. E. (1987). The evolution of microstructure during the transformation of Mg_2GeO_4 olivine to spinel. *Bulletin de Mineralogie*, **110**, 5, 471-480.

Ruland W. (1968). X-ray diffraction studies on carbon and graphite. in *Chemistry and Physics of Carbon*, ed P. L. Walker, Jnr, 4, 1-84, Dekker, New York.

Russell S. (1992). A carbon and nitrogen isotope study of chondritic diamond and silicon carbide. Phd Theis, Department of Earth Sciences, The Open University.

Russell S. S., Ash R. D., Pillinger C. T. and Arden J. W. (1990). On the existence of occluded isotopically light carbon in Allende. *Lunar and Planetary Science*, **XXI**, 1049-1050.

Saha D. K., Koga K. and Takeo H. (1998). Structural properties of diamond fine particles and clusters prepared by detonation and decomposition of TNT. *Surface Science*, **400**, 134-139.

Salje E. (1985). Thermodynamics of sodium-feldspar. I. Order parameter treatment and strain induced coupling effects. *Physics and Chemistry of Minerals*, **12**, 2, 93-98.

Scheele N. and Hoefs J. (1992). Carbon isotope fractionation between calcite, graphite and CO_2: an experimental study. *Contributions to Mineralogy and Petrology*, **112**, 35-45.

Schmitt R. T., Siebenschock M. and Stöffler D. (1999). Distribution of impact diamonds in the Ries crater, Germany. *Meteoritics and Planetary Science*, **34**, 4, A102.

Schultz P. H. and Gault D. E. (1982). Impact ejecta dynamics in an atmosphere: Experimental results and extrapolations. *Geological Society of America Special Paper*, **190**, 153-

Schultz P. H. and Gault D. E. (1979). *Journal of Geophysical Research*, **84**, 7669-7687.

Sebastian M. T. and Krishna P. (1984). Stacking faults and structural transformations in ZnxMn1-xS single crystals grown from vapour. *Journal of crystal growth*, **66**, 586-592

Sebastian M. T. and Krishna P. (1987). Stacking faults in close-packed structures. in *Recent advances in X-ray characterisation of materials. Progress in Crystal Growth and Characterisation*. **14**. ed. B. R. Pamplin. Pergamon Press. 103-183.
Sekine T. (1992). Diamond recovered from shocked fullerites. *Proceedings of the Japan Academy Series B- Physical and Biological Sciences*, **68**, 7, 95-99.

Shafranovsky I. I. (1964). Almazy (Diamonds). Nauka Press, Moscow.

Sharpton V. L. and Grieve R. A. F. (1990). Meteorite impact, cryptoexplosion and shock metamorphism: A perspective on the evidence at the K/T boundary. *Geological Society of America Special Paper*, **147**, eds: V. L. Sharpton and P. D. Ward. 301-318.

Shelkov D. (1997). N and C isotopic composition of different varieties of terrestrial diamonds and carbonado. PhD Open University.

Shelkov D., Verchovsky A. B., Pillinger C. T., Hutchison R. and Milledge H. J. (1995). Carbonado: more clues to a common impact origin for samples from Brazil and the Central African Republic. *Lunar and Planetary Science*. **XXVI**, 1281-1282.

Shelkov D. A., Verchovsky A. B., Milledge H. J., Kaminsky F. V. and Pillinger. C. T. (1998). Carbon, nitrogen, argon and helium study of impact diamonds from Ebeliakh alluvial deposits and Popigai crater. *Meteoritics and Planetary Science*, **33**, 985-992.

Shi H., Barker J., Saïdei M. Y. and Koksbang R. (1996). Structure and lithium intercalation properties of synthetic and natural graphite. *Journal of the Electrochemical Society*, **143**, 11, 3466-3472. (1996)

Shoemaker E. M. (1960). Penetration mechanics of high velocity meteorites, illustrated by Meteor crater, Arizona. In: *Report of the International Geology Congress*, XXI Session, Norden. **XVIII**, 418-434, Copenhagen.

Shoemaker E. M. (1963). Impact Mechanics at Meteor Crater, Arizona. In *The Moon, meteorites and comets*. eds. B. M. Middlehurst, G. P. Kuiper, 301-336. The Solar System, **1**, University of Chicago Press.

Shoemaker E. M. and Chao E. C. T. (1961). New evidence for the impact origin of the Ries basin, Bavaria, Germany. *Journal of Geophysical Research*, **66**, 3371.

Shoemaker E. M., Wolfe R. F. and Shoemaker C. S. (1990). Asteroid and comet flux in the neighborhood of Earth. In: *Geological Society of America Special Paper*, **247**, Eds: V. L. Sharpton. and P. D. Ward. 155-170.

Siebenschock M. Schmitt R. T. and Stöffler D. (1998). Impact diamonds in glass bombs from suevite of the Ries crater, germany: new observations. *Meteoritics*, **33**, 4, A145.

Simmonds C. H., Warner J. L. and Phinney W. C. (1976). Thermal regimes in cratered terrain with emphasis on the role of impact melt. *Americal Mineralogist*, **61**, 569-

Simonson B. M., Davies D., Wallace M., Reeves S. and Hassler S. W. (1998). Iridium anomaly but no shocked quartz from late archean microkrystite layer: Oceanic impact ejecta?. *Geology*, **26**, 3, 195-198.

Skala A. R. and Bouska V. J. (1992). Characteristics of impact diamonds. *Meteoritics*, **27**, 3, 290.

Smit J., Alvarez W., Montanari A., Swinburne N., Vankempen T. M., Klaver G. T. and Lustenhouwer W. J. (1992). Tektites and microkrystites at the Cretaceous-Tertiary boundary - 2 strewn fields, one crater. *Proceedings of Lunar and Planetary Science*, **22**, 87-100.

Smith E. D., Zuber M. T., Solomon S., Phillips R. J., Head J. W., Garvin J. B., Barnerdt W. B., Muhleman D. O., Pettengill G. H., Neumann G. A., Lemoine F. G., Abshire J. B., Ahronson O., Brown C. D., Hauck S. A., Ivanov A. B., McGovern P. J., Zwally H. J. and Duxbury T. C. (1999). The global topography of Mars and implications for surface evolution. *Science*, **284**, 1495-1503.

Smith J. V. and Dawson J. B. (1985). Carbonado: Diamond aggregates from early impact of crustal rocks. *Geology*, **13**, 342-343.

Spitsyn B. V., Bouilov L. L. and Derjaguin B. V. (1981). Vapour growth of diamond on diamond and other surfaces. *Journal of Crystal Growth*, **52**, 219-226.

Spear K. E., Phelps A. W. and White W. B. (1990). Diamond polytypes and their vibrational spectra. *Journal of Material Research*, **5**, 11, 2277-2285.

Stahle V. and Ottemann J. (1977). Ries-Forschungsbohrung 1973; Zeolithisierung der gläser im Suevite und petrographie der Beckensuevite und Gangbrecccien. *Geologica Bavarica.*, **75**, 191-218.

Stammeier M., Stockel R., Ley L., Albrecht M. and Strunk H. P. (1997). Diamond nucleation on silicon during bias treatment in chemical vapour deposition as analysed by electron microscopy. *Diamond and Related Materials*, **6**, 5-7, 747-751.

Staudacher T. H. Jessberger E. K. Dominik B. Kirsten T. and Schaeffer O. A. (1982). Ar40-Ar39 ages of rocks and glasses from the Nördlinger Ries crater and the temperature history of impact breccias. *Journal of Geophysics-Zeitschrift Fur Geophysik*, **51**, 1, 1-11.

Steel D. (1998). Distributions and moments of asteroid and comet impact speeds upon the Earth and Mars. *Planetary and Space Science*, **46**, 5, 473-478.

Stöffler D. (1972). Deformation and transformation of rock forming minerals by natural and experimental shock processes. I. behavious of minerals under shock compression. *Fortschr Mineralogische*, **49**, 50-113.

Stöffler D. (1977). Research drilling Nördlingen 1973: Polymict breccias, crater basement and cratering model of the Ries impact structure. *Geologica Bavarica*, **75**, 443-458.

Stöffler D., Gault D. E., Wedekind J. and Polkowski G. (1975). Experimental hypervelocity impact into quartz sand: Distribution and shock metamorphism of ejecta. *Journal of Geophysical Research*, **80**, 29, 4063.

Stöffler D., Ewald U., Ostertag. R. and Reimold. W. U. (1977). Research drilling Nördlingen 1973: Composition and texture of polymict impact breccias. *Geologica Bavarica*, **75**, 163-189.

Stöffler D. and Grieve R. A. F. (1996). IUGS Classification and Nomenclature of Impact Metamorphic Rocks: Towards a final proposal. International Workshop Postojna '96: *The Role of Impact Processes in the Geological and Biological Evolution of the Planet Earth*. Eds: K. Drobne, B. Kotnik. Ljubljana, 1996.

Stoneham A. M. (1992). Theoretical status of diamond and its defects, excited states and atomic motion. *Materials Science and Engineering B-solid state materials for advanced technology*, **11**, 1-4, 211-218.

Stoner B. R. and Glass J. T. (1992). Textured diamond growth on (100) beta-SiC via microwave plasma. *Applied Physics Letters*, **60**, 6, 698-700.

Stothers R. B. (1998). Galactic disc dark matter, terrestrial impact cratering and the law of large numbers. *Monthly notices of the Royal Astronomical Society*, **300**, 4, 1098-1104.

Tamor M. A. and Everson M. P. (1994). On the role of penetration twins in the morphological development of vapour-growth diamond films. *Journal of Materials Research*, **9**, 7, 1839-1848.

Taylor E. A., Kay L and Shrine N. R. G. (1997). Hypervelocity impact on brittle materials of semi-infinite thickness: Fracture morphology related to projectile diameter. *Advances in Space Research*, **20**, 8, 1437-1440.

Taylor H. P. and Epstein S. (1966). Oxygen isotope studies of Ivory Coast tektites and impactite glass fom the Botsumtwi Crater, Ghana. *Science*, **153**, 173-175.

Taylor R., Hare J. P., Abdul-Sada A. and Kroto H. W. (1990). Isolation, separation and characterisation of the Fullerenes C60 and C70: The third form of carbon. *Journal of Chemical Society. Chemical Communications.*, **20**, 1423-1425.

Tedesci W. J., Remo J. L., Schulze J. F. and Young R. P. (1995). Experimental hypervelocity impact effects on simulated planetisimal materials. international *Journal of Impact Engineering*, **17**, 4-6. 837-848.

Tielens A. G. G. M. (1990). Carbon stardust: from soot to diamonds. *NASA Conference Publication*, **3061**, 59-60.

Tucker M. E. (1983). Sedimentation of Organic-rich limestsones in the Late Precambrian of Southern Norway. *Precambrian Research*, **22**, 295-315.

Ugarte D. (1992). Curling and closure of graphitic networks under electron-beam irradiation. *Nature*, **359**, 6397, 707-709.

Urey H. C., Mele A. and Mayeda T. (1957). Diamonds in stone meteorites. *Geochimica et Cosmochimica Acta*, **13**, 1, 1-4.

Valley J. W. and O'Neil J. R. (1981). $^{13}C/^{12}C$ exchange between calcite and graphite: a possible thermometer in Grenville marbles. *Geochimica et Cosmochimica Acta*, **45**, 411-419.

Val'ter A. A., Yeremenko G. K., Kwasnitsa V. N. and Polkanov Yu. A. (1992). The shock metamorphic minerals of carbon. Kiev, 172 pp.

Val'ter A. A. and Yeremenko G. K. (1996). Carbon minerals in rocks of astroblemes. *Meteoritics and Planetary Science*, **31**, A144.

Valtonen M. J., Zheng J. Q., Matese J. J. and Whitman P. G. (1995). Near-earth populations of bodies coming from the Oort cloud and their impacts with planets. *Earth Moon and Planets*, **71**, 3, 219-223.

Van Tendeloo G., Amelinckx S., De Boer J. L., Van Smaalen S., Verheijen M. A., Meekes H. and Meijer G. (1993). Structural phase transitions in C_{70}. *Europhysics Letters*, **21**, 329-334.

Varshavskii A. V. and Shul'pyakov Y. F. (1967). Orientated crystallisation of α-SiC on diamond. *Soviet Physics-Doklady*, **12**, 3, 202-

Verchovsky A. B., Ott U. and Bergemann F. (1993). Implanted radiogenic and other noble gases in crustal diamonds from N. Khazakhstan. *Earth and Planetary Science Letters*, **120**, 87-102.

Vdovykin G. P. (1972). Forms of carbon in the new Haverö ureleite of Finland. *Meteoritics*, **7**, 547-552.

Vilotijevic M., Dimitrijevic S. T. and Randjelovic I. (1993). Deposition of polycrystalline diamonds in a DC plasma jet of Ar, H_2 and CH_4. *Journal of Material Science Letters*, **12**, 1261-

Vishnevsky S. A. and Palchik N. A. (1975). The carbon in the rocks of the Popigai: the destruction and transformation to another phases of the carbon system. *Geologia I Geophyzika*, **1**, 67-75.

Vlodarchik E. and Trebinski R. (1997). Transformations of graphite and boron nitride in shock wavers. *Shock Waves*, **7**, 4, 231-248.

Vishnevsky S. A., Afanas'ev V. P., Koptil' V. I. and Montanari A. (1995). Popigai distal ejecta deposits: evidence by the strewn field of impact diamonds. In: *4th int. workshop of the ESF Scientific Network on "Impact cratering and Evolution of Planet Earth" Ancona, May 12-17, 1995. The Role of the impacts in the evolution of atmosphere and biosphere with regards to short- and long-term changes. Abstracts and Field trip volume* (A. Montanari and R. Coccioni eds.), 160-162.

Vishnevsky S. A., Afanas'ev V. P. Argunov K. P. and Pal'chik N. A. (1997). Impact diamonds: their features, origin and significance. United inst. of Geology, Geophysics and Mineralogy (UIGGM), Siberian branch, Russian Academy of Sciences. Novosibirsk:SB RAS Press, SPC UIGGM, pp. 53.

Vishnevsy S and Raitala J. (1998). Impact diamonds: The only possible evidence of shock metamorphism in hardly re-worked Pre-Cambrian impactites. in: *Impacts and the Early Earth, European Space Foundation, 1st International Workshop of the Scientific Programme on Response of the Earth System to Impact Processes, December 13-15, Cambridge*, London. 39.

Von Englehardt W. (1967). Chemical composition of Ries glass bombs. *Geochimica et Cosmochimica Acta*, **31**, 1677-1689.

Von Englehardt W. (1971). Detrital impact formations. *Journal of geophysical Research*, **76**, 5566-5574.

Von Englehardt W. (1972). Shock produced glasses from the Ries crater. *Contributions to Mineralogy and Petrology*, **36**, 265-292.

Von Englehardt W. (1990). Distribution, petrography and shock metamorphism of the ejecta of the Ries crater in germany - a review. *Tectonophysics*, **171**, 259-273.

Von Englehardt W. (1997). Suevite breccia of the Ries impact crater, Germany: Petrography, chemisty and shock metamorphism of crystalline rock clasts. *Meteorites and Planetary Science*, **32**, 545-554.

Von Englehardt W. and Stöffler D. (1968). Stages of shock metamorphism in crystalline rocks of the Ries basin, Germany. in *Shock Metamorphism of Natural Materials*. Eds: B. M. French and N. M. Short. 159-168. Mono Book Corp, Baltimore.

Von Englehardt W. and Graup G. (1977). Shock metamorphism in crystalline rocks from the borehole Nördlingen 1973. *Geologica Bavarica*. **75**, 225-272.

Von Englehardt. W. and Graup. G. (1980). Origin and Transport of Suevite, Ries crater. Germany. *Meteoritics*, **15**, 4, 287.

Von Englehardt W. and Graup G. (1984). Suevite of the Ries crater. Germany. *Geologische-Rundschau*, **73**, 2, 447-481.

Von Englehardt W. and Luft E. (1987). Origin of Moldavites. *Geochimica et Cosmochimica Acta*, **51**, 1425-1443.

Von Englehardt W., Arndt J, Fecher B. and Pankau H. G. (1995). Suevite breccia from the Ries crater, Germany. Origin, cooling and devitrification of impact glasses. *Meteoritics*, **30**, 279-293.

Von Huttner R. (1977). Makroskopische Beobachtungen zur deformation des Kristallins in der Forschungsbohrung Nördlingen 1973. *Geologica Bavarica.*, **75**, 273-283.

Von Munch W. and Wiebach S. (1994). Production of β-SiC buffer layers for CVD diamond thin-films by ion-implantation. *Diamond and Related Materials*, **3**, 4-6, 500-505.

Wang S. Q., Lu H. B., Ma F. K. and Mu Y. F. (1996). Heterogeneous nucleation of diamond under high static pressure and high temperature. *Journal of Crystal Growth*, **162**, 1-2, 69-72.

Wasson J. T. and Moore K. (1998). Possible formation of Libyan Desert glass by a Tunguska-like aerial burst. *Meteoritics and Planetary Science*, **33**, 4, A 163-164.

Weissman P. R. (1996). Star passages through the Oort cloud. *Earth Moon and Planets*, **72**, 1-2, 25-30.

Weissman P. R. and Levison H. F. (1997). Origin and evolution of the unusual object 1996 PW: Asteroids from the Oort cloud?. *Astrophysical Journal*, **488**, 2, 2, L133-L136.

Wentorf. R. H. (1965). *Journal of Physical Chemistry*, **75**, 1833-1837.

Wiegert P. and Tremaine S. (1999). The evolution of the long-period comets. *Icarus*, **137**, 1, 84-121.

Williamson R. L. (1990). Parametric studies of dynamic powder consolodation using a particle-level numerical model. *Journal of Applied Physics*, **68**, 1287-1296.

Whittaker G. A. (1978). Carbon: a new view of its high-temperature behaviour. *Science*, **200**, 763-764.

Whittaker G. A. (1979). Carbon: Occurrence of carybne forms of carbon in natural graphite. *Carbon*, **17**, 21-24.

Whittaker G. A. and Kintner P. L. (1985). Carbon: Observations on the new allotropic form. *Science*, **165**, 589-591.

Wolbach W. S., Anders E. and Nazarov M. A. (1990a). Fires at the K/T boundary - carbon at the Sumbar, Turkmenia site. *Geochimica et Cosmochimica Acta*, **54**, 4, 1133-1146.

Wolbach W. S., Gilmour I. and Anders E. (1990b). Major wildfires at the Cretaceous/Tertiary boundary. in Global catastrophes in Earth history. *Geological Society of America Special Paper*, **247**, 391-400.

Wright I. P. and Pillinger C. T. (1989). Carbon isotopic analysis of small samples by use of stepped-heating extraction and static mass spectrometry. In: *New Frontiers in Stable Isotopic Research: laser probes, ion probes and small-sample analysis*, 9-34. Eds: W. C. Shanks, and R. E. Criss.

Yamada K. and Tobisawa S. (1990). Crystal growth of radiating filaments of α-SiC formed by the conically converging shock wave technique. *Philosophical magazine*, **89**, 2297-2304.

Yang W. B. and Ahrens T. J. (1998). Shock vaporization of anhydrite and global effects of the K/T bolide. *Earth and Planetary Science Letters*, **156**, 3-4, 125-140.

Yerofeev M. V. and Lachinov P. A. (1888). About the Novo Urei meteorite. *Zhurnal Russkogo Physiko-Khimicheskogo Obstchestva*, **XX**, 185-213.

Yusa H., Takemura K., Matsui Y., Morishima H., Watanabe K., Yamawaki H. and Aoki K. (1998). Direct transformation of graphite to cubic diamond observed in a laser-heated diamond anvil cell. *Applied Physics Letters.*, **72**, 15, 1843-1845.

Zahnle K. J. (1990). Atmospheric chemisty by large impacts. *Geological Society of America Special Paper*, **247**, 271.

Zang F. Q., Song Z. Z., Li J. Q., Chen G. G., Jiang X. L. and Cong Q. Z. (1991). Structure studies of synthetic diamond thin-films by x-ray. *Thin Solid Films*, **199**, 1, 123-128.

Zhang Q. L., O'Brien S. C., Heath J. R., Liu Y., Curl R. F., Kroto H. W. and Smalley R. E. (1986). Reactivity of large carbon clusters - spheroidal carbon shells and their possible relevance to the formation and morphology of soot. *Journal of physical chemistry*, **90**, 525-528.

Zhuk A. Z., Borodina T. I., Fortov V. E., Lash A. A. and Val'iano G. E. (1997). Shock metamorphism of the graphite quasimonocrystal. *High Pressure Research*, **15**, 245-254.